Evaluation of structural changes in protein therapeutics by HX-MS

By

Juan Pablo Rincon Pabon

Submitted to the graduate degree program in Chemistry and the Graduate Faculty of the University of Kansas in partial fulfillment of the requirements for the degree of Doctor of Philosophy.

Chairperson: David D. Weis, Ph.D.

Timothy Jackson, Ph.D.

Krzysztof Kuczera, Ph.D.

John Karanicolas, Ph.D.

Michael J. Hageman, Ph.D.

Date Defended: 31 August 2021

The dissertation committee for Juan Pablo Rincon Pabon certifies that this is the approved version of the following dissertation:

Evaluation of structural changes in protein therapeutics by HX-MS

Chairperson: David D. Weis, Ph.D

Date Approved: 31 August 2021

Abstract

Function of protein therapeutics is governed by its high order structure (HOS). Changes in HOS can provoke changes in protein structure, stability, safety, and protein activity among others. Thus, monitoring HOS of protein therapeutics and identification of conformational changes is essential for development, production, and usage of protein therapeutics. Hydrogen exchange-mass spectrometry (HX-MS) is a well-established technique to probe HOS of proteins and is considered an intermediate resolution technique capable to point structural changes at a peptide level. Here we described experiments to: (1) probe conformational changes in a scFv used as a protein switch, (2) recognize allosteric effects in an IgG1 during interaction with a commercially available protein A ligand and (3) identify structural changes in the NIST mAb after a change in the pH formulation buffer.

We used HX-MS experiments to identify conformational changes in a single chain variable fragment used as a protein switch. Previous results showed that introducing a cavity forming mutation into the scFv (W-to-G) decreased the protein activity. Later, by the addition of indole to the solution the protein activity is partially restored. Our results support the model of chemical rescue of the structure, whereby introducing a cavity forming mutation, the activity of the protein gets reduced due to critical conformation changes and later by the addition of a small molecule, the structure and activity of the protein is restored. Statistical analysis of HDX data showed that WT and rescued scFv protein (after the addition of indole) have a very similar structure, with minor differences that could explain why the rescued protein does not have the same binding affinity as the wild-type.

To identify allosteric effects in the NIST mAb during interaction with a commercially available protein A ligand (ProA), we used ProA ligand both free in solution and attached onto a resin. When in-solution protein A was used at a 2:1 ProA:mAb ratio, allosteric effects in the Fab region were identified. However, at lower concentrations (1:1 ratio) or when ProA resin was employed, only peptides right at the binding site showed strong protection against hydrogen exchange. With these experiments, we were

able to rule out all reversible allosteric effects in the interaction between the NIST mAb and protein A attached to a resin.

Finally, we used HX-MS to identify conformational changes in a model IgG1 mAb after changing the formulation pH. Results showed that decreasing the pH of the solution induce a general increase in flexibility across the whole mAb, and stronger effects were seen in the C_H2 domain and parts of the C_H2-C_H3 interface of the model mAb, most probably due to introduction of protonated histidine residues in the C_H2-C_H3 interface that induce new and affect critical electrostatic interactions in the region. An increase in pH showed the contrary, strong rigidity in the C_H2 domain close to the hinge region and in the C_H3 domain close to the C_H2-C_H3 interface. Additionally, changes in the pH caused changes in flexibility in the F_{ab} domain of the antibody, involving CDRH3 when the pH is decreased and CDRL2 when the pH is increased. These effects are in critical regions for monoclonal antibodies that could affect effector functions or antigen binding.

Acknowledgments

I would like to thank my advisor, Dr. David D. Weis, for his mentorship and incredible support throughout my graduate studies at the University of Kansas. He not only supported me academically but also financially during the whole PhD program. I thank him for all the time and energy he spent educating and helping me to become the scientist I am today. He shared with me his love for research, invaluable knowledge, and scientific integrity every day during my studies. Dr. Weis was always open to discussion and provided a pleasant work environment that help me to finish my degree. He is a remarkable scientist with incredible human values.

I thank my dissertation committee members, Dr. Timothy Jackson, Dr. Krzysztof Kuczera, Dr. Michael Hageman, Dr. John Karanicolas, and Dr. David Weis, for their support and time evaluating my dissertation. I thank past and current members of the Weis research group for their friendship and support during these years. They were always happy to help and provided priceless discussions. Also, I would like to thank Jennifer Zhang for her training and support during my internship.

I am tremendously thankful for the support from my parents, Pilar and Edgar, and my brothers, David and Felipe. They all took care of me while I was battling cancer and have unconditionally supported me in many ways during my whole life. I thank Gloria Ortiz for her love, support, and patience during all the amazing years we have spent together. Additionally, I need to thank all the incredible friends I was able to make during my stay in Lawrence. Without their support, company, and advice I wouldn't have finished my studies.

Finally, I would like to thank the University of Kansas, the Chemistry department, the Fulbright organization, and the Colombian government for providing me with the opportunity to pursue a PhD program.

Table of Contents

1. Chapter one: Introduction 1

1.1. Proteins and protein therapeutics 2

1.1.1. Overview 2

1.1.2. Importance 3

1.1.3. Primary structure 4

1.1.4. Secondary structure 5

1.1.5. Tertiary structure 6

1.1.6. Quaternary structure 8

1.1.7. Structure of antibodies 8

1.1.8. Importance of high order structure characterization 10

1.2. Characterization of protein structure 11

1.2.1. Determination of the primary structure 11

1.2.2. Characterization of high order structure 12

1.2.3. Mass spectrometry methods for high order structure characterization 15

1.2.4. Cross-linking methods 16

1.2.5. Covalent labeling methods 17

1.3. Hydrogen exchange mass spectrometry 19

1.3.1. Fundamentals 19

1.3.2. Mechanism of exchange 20

1.3.3. pH effects 21

1.3.4. Temperature effects 22

1.3.5. Other effects 23

1.3.6. Linderstrøm-Lang mechanism 25

1.3.7. In-solution experimental workflow 27

1.3.8. Data analysis 29

1.4. LC-ESI-QTOF analysis 32
1.4.1. Liquid chromatography separation 32
1.4.2. ESI-QTOF 33
1.4.3. MS-CID-MS 36
1.5. Overview of the dissertation 37
1.6. References 40
2. Chapter two: Structural changes of a scFv after chemical rescue 50
2.1. Introduction 51
2.2. Materials and methods 53
2.2.1. Materials 53
2.2.2. Hydrogen exchange-mass spectrometry 54
2.3. Results 56
2.3.1. FITC-E2 WT and VH W118G variant are structurally different 57
2.3.2. Comparison of FITC-E2 WT scFv with and without indole and fluorescein 59
2.3.3. Comparison of FITC-E2 VH W118G scFv with and without indole and fluorescein 60
2.3.4. Comparison of FITC-E2 VH W118G and WT with indole and fluorescein 62
2.4. Discussion 64
2.5. Appendix A 68
2.6. References 70
3. Chapter three: Protein A does not induce allosteric structural changes in an IgG1 antibody during binding 72
3.1. Introduction 73
3.2. Materials and methods 75
3.2.1. Materials 75
3.2.2. Sample preparation 76

3.2.3. Hydrogen exchange-mass spectrometry 77
3.3. Results 79
3.3.1. ProA binding induces a decrease in backbone flexibility in the CH2 and CH3 regions 79
3.3.2. All peptides with decreased backbone flexibility contained residues located on the proA:Fc interface 83
3.4. Discussion 86
3.5. Appendix B 89
3.6. References 94
4. Chapter four: Evaluation of structural changes in a monoclonal antibody at different pHs 100
4.1. Introduction 101
4.2. Materials and methods 102
4.2.1. Materials 102
4.2.2. Sample preparation 103
4.2.3. Hydrogen exchange-mass spectrometry 103
4.3. Results 107
4.3.1. Evaluation of the time point conversion using IER compounds 107
4.3.2. Changes in mAb conformation and dynamics at pH below 7 111
4.3.3. Changes in mAb conformation and dynamics at pH 8 115
4.4. Discussion 119
4.5. Appendix C 125
4.6. References 161
5. Chapter five: Summary and future directions 167
5.1. Summary 168
5.2. Future directions 169

List of Figures

Figure 1.1 Peptide bond schematic representation. 5

Figure 1.2 Protein ribbon representation. 7

Figure 1.3 Schematic layout of an IgG1 antibody. 9

Figure 1.4 Exchangeable hydrogen atoms for peptide Lys-Gly-Ser-Asn. 20

Figure 1.5 Base-catalyzed amide hydrogen exchange mechanism. 21

Figure 1.6 Calculated chemical exchange rate constant for a poly-DL-alanine peptide as a function of pH. 22

Figure 1.7 Theoretical chemical exchange rate constant as a function of temperature. 23

Figure 1.8 Linderstrøm-Lang mechanism for amide hydrogen exchange in a folded protein 25

Figure 1.9 General workflow for in-solution bottom-up hydrogen exchange experiments. 29

Figure 1.10 Theoretical spectral peaks for a model peptide (RVVSVL) 31

Figure 1.11 Positive electrospray ionization mechanisms for ion formation. 34

Figure 1.12 Schematic diagram for a Q-TOF mass spectrometer. 35

Figure 1.13 Possible CID fragments for GluLysGlySerAsn peptide. 37

Figure 2.1. Deuterium uptake plots for scFv WT and W118G variant at an intact level 57

Figure 2.2 Peptides with increased deprotection in VH W118G compared to the wild-type as revealed by HX-MS experiments.. 58

Figure 2.3. Peptides with increased protection in WT scFv in the presence of indole and fluorescein as revealed by HX-MS experiments 60

Figure 2.4. Peptides with increased protection in W118G scFv in the presence of indole and fluorescein as revealed by HX-MS experiments. 62

Figure 2.5 . Peptides with increased deprotection in W118G scFv in the presence of indole and fluorescein compared to WT with indole and fluorescein as revealed by HX-MS experiments. 63

Figure 2.6. HX-MS differences mapped onto the homology model (2A9N). 65

Figure 3.1 Representative uptake plots showing the effect of ProA binding to the NIST mAb. 80

Figure 3.2 Statistical analysis for the MabSelect SuRe in solution (1:1 ratio) experiment. 82
Figure 3.3 Statistical analysis for the MabSelect SuRe resin experiment..... 83
Figure 3.4 HX-MS differences provoked by binding to (a) MabSelect SuRe in solution (1:1 ratio) (b) MabSelect SuRe in solution (2:1 ratio) and (c) MabSelect SuRe resin mapped onto the NIST mAb homology model.. 85
Figure 3.5 Correlation between HX protection in the NIST mAb heavy chain for the resin experiment with the SpA B domain interface. 87
Figure 4.1 NIST mAb peptic peptides coverage map for the hydrogen exchange experiments. 105
Figure 4.2. Deuterium uptake plot for synthetic peptide YPI measured at different pH. 108
Figure 4.3 Deuterium uptake plots for IER compounds TM-68 and TM-65 measured at different pH values. 109
Figure 4.4 Statistical analysis for the NIST mAb at pH 6 and 5 compared to the reference state. 112
Figure 4.5 Representative uptake plots of the HC peptides showing the effect of lower pH (pH 5) compared to the reference state..... 113
Figure 4.6 Bar plot showing the classification and magnitude of the effects in the peptides measured at pH 5 compared to the reference state..... 114
Figure 4.7 Representative uptake plots for HC peptides at pH 8 and pH 7 after the empirical labeling time correction. 116
Figure 4.8 Bar plot showing the classification and magnitude of the effects in the peptides measured at pH 8 compared to the reference state..... 117
Figure 4.9 HX-MS differences provoked by changing the formulation pH compared to the reference state 118

List of Tables

Table 4.1 HX experiment labeling times 104

Table 4.2.Mass balance for ionic species and total ionic strength values for the McIlvaine buffer used in the HX experiments at different pH values..... 110

1. CHAPTER ONE: INTRODUCTION

1.1. PROTEINS AND PROTEIN THERAPEUTICS

1.1.1. Overview

Proteins are large complex biomolecules composed of one or more polypeptide chains, each with a specific sequence of amino acids joined by peptide bonds.[1] These macromolecules are essential structural components of cells, and they play crucial roles in performing and monitoring regulatory processes, cell signaling, transporting other molecules, and generating mechanical and electrical forces, among many other functions.[2] A complete list with all known protein functions will have thousands of entries yet will still be incomplete since we do not fully understand the function of thousands of other proteins.

Many human diseases are related to a lack of specific proteins or protein concentration, structure, and function changes.[3] Protein therapeutics are proteins that possess therapeutic properties to treat a disease. They have many advantages compared to small drug molecules: mainly highly specific functions that small compounds cannot achieve. Hence, they are less likely to interfere with normal biological processes.

Since the human body naturally produces many proteins used as therapeutics (e.g., insulin and endogenous antibodies), bioengineered therapeutics are usually well-tolerated and less prone to provoke immune responses.[4] However, there are also drawbacks to using protein therapeutics, such as low solubility, short half-life, instability, and degradation, making the application of these therapeutics more complicated.[5] Additionally, high molecular weights and charged species can decrease their bioavailability, presenting additional challenges.

The use of proteins as therapeutics to treat various diseases is not new. The first protein vaccine (cowpox) was introduced in 1796,[6] and the first protein pharmaceutical (insulin) was introduced in 1922.[7] However, the extraction and production of these proteins were difficult with low yields. It was

not until much later that the production of protein therapeutics became easier when recombinant DNA technology was developed, and the human genome project was completed.

Therapeutic proteins are produced by using living organisms such as mammalian cells, bacteria (e.g., *E. coli*), and yeast.[3,7] Post-translational modifications, glycosylation profile, protein complexity, general structure, and the amount needed must be carefully considered before selecting the production organism. Therapeutic proteins have more complex pharmacokinetics, pharmacodynamics, and mechanisms of action compared to small drug molecules. Nevertheless, with the help of new technologies and increasing knowledge of protein structure and function, the production and development of protein therapeutics is expanding daily.

1.1.2. Importance

Since 1978, when the first recombinant protein (insulin) was introduced to the market,[8] the number of protein therapeutics has skyrocketed. Currently, over 380 biotherapeutics (peptides and proteins) are approved by the FDA.[5] Among these, over 80 are monoclonal antibodies[9] (the fastest-growing group of protein therapeutics), with approximately 570 more protein therapeutics in different clinical stages. The biopharmaceutical market is expected to reach >380 billion USD by 2024.[10]

Although the production of protein therapeutics is a very expensive and complex process (it is estimated that a typical protein product goes through 5000 critical process steps),[11] the high specificity and potential therapeutic advantages to treating many high-incidence diseases are critical to the pharmaceutical industry. Among the approved protein therapeutics on the market, 24% are designed to treat metabolic disorders, 18% immunological disorders, 13% different types of cancers, and 13% hormonal disorders.[5] Thus, an understanding of protein structure can help address certain challenges faced during the production and development of a protein therapeutic. Generally, protein structure is divided into primary, secondary, tertiary, and quaternary structures.

1.1.3. Primary structure

Amino acids are α-amino-substituted carboxylic acid compounds. All proteins are composed of a specific combination of 20 common amino acids with different side chains, each of which is unique and has specific physical and chemical properties. Amino acids are *zwitterions* since they can hold positive and negative charges simultaneously.

The primary structure of a protein is the linear sequence of amino acids that compose the protein. Depending on the organic group attached to the α-carbon, an amino acid could have non-polar, uncharged polar, or charged polar sidechains. The amino acids within the polypeptide chain are joined through peptide bonds, and the chemistry of these bonds is somewhat special. The atoms involved in the peptide bond, C', the oxygen, the nitrogen, and the hydrogen atom form a single plane (see red lines, **Figure 1.1**). The bond between C' and nitrogen is shorter (1.32 Å) than a normal C-N bond (1.49 Å) due to the resonance of the double bond between the oxygen and the nitrogen atom.[12,13] There is no rotation around the C'-N bond; hence, amino acids can be in a *cis* or *trans* configuration.

However, due to steric hindrance, the *trans* configuration is more probable (99.95%) and stable for all amino acids except proline. The other C-N and C-C bonds are single bonds with possible rotation. Dihedral angles, around the C-N and C-C bonds, are named Φ and ψ, respectively (see **Figure 1.1**). Rotation angles can have values between -180° and +180° that do not result in steric clashes. Bond angles, size, and side chains of amino acids make some conformations more stable than others. All the different structures of proteins come from the combinations of these variables: amino acid sequences, backbone bond angles, and dihedral side-chain angles.[13]

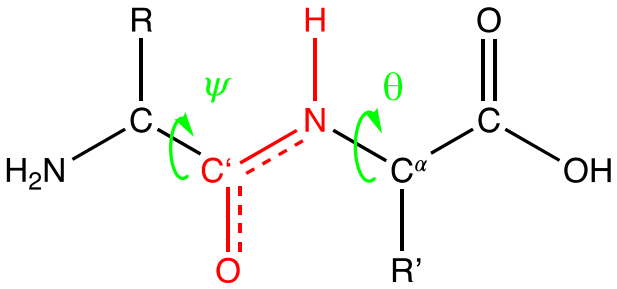

1.1.4. Secondary structure

A polypeptide chain is a single series of amino acids joined by peptide bonds. Each single amino acid in the polypeptide chain is called a residue. The secondary structure of a protein represents the local conformation of the polypeptide chain. Protein secondary structure is mainly stabilized by hydrogen bonds between the amide hydrogens and the carbonyl groups and can be further divided into four structural motifs common in proteins.

α-helix motifs (see red motifs in **Figure 1.2**) are found when the polypeptide chain is rolled around an imaginary axis. Notably, α-helixes have 3.6 amino acids per turn, and the distance the helix rises along the helical axis is approximately 5.4 Å.[13] The bond angles between amino acids are approximately $\Phi \approx -57°$ and $\psi \approx -47°$. These helixes are stabilized by intramolecular hydrogen bonds between the peptide C=O bond of the *nth* residue and the peptide N-H bond of the (*n*+4) *th* residue along the helix axis. All helixes turn with a counterclockwise rotation (clockwise rotation is theoretically possible but not observed in nature). Amino acid side chains in α-helixes always point away from the helix (perpendicular to the helical axis), avoiding possible steric interferences.

β-sheets (see yellow motifs in **Figure 1.2**) are found when the polypeptide chain is extended, and no hydrogen bonds are present between the C=O and N-H groups of neighboring amino acids. Instead,

several strands lay next to each other forming interstrand hydrogen bonds. These strands can be parallel or antiparallel depending on whether the terminal ends of the chain face the same side or not. Amino acid side chains point above or below the plane of the β-sheet. These sheets are unlikely to be completely flat and sometimes exhibit a right-handed twist forming a β-barrel.

Amino acid chains with secondary structure are usually joined by short segments of the polypeptide chain that abruptly change direction. These segments are called turns (see **Figure 1.2**). Turns can contain three or four residues (usually glycine or proline) commonly stabilized by an intramolecular hydrogen bond between the peptide N-H bond of the *nth* residue and the peptide C=O bond of the *(n-3) th* residue along the turn.[13] Finally, coils or random coils (see **Figure 1.2**) are any segments of the polypeptide chain that do not have a distinct secondary structure motif. These coils have defined positions and help with the general protein structure.

1.1.5. Tertiary structure

The tertiary structure of a protein (see **Figure 1.2**) represents the global conformation of the protein and describes how the secondary structure elements are organized in a three-dimensional space. There are several forces involved in keeping the tertiary structure together. Electrostatic interactions between charged amino acids, dispersion forces, hydrogen bonds, van der Waals forces, and disulfide bonds (covalent bonds between cysteine residues) create a combination of forces that stabilize the protein. The hydrophobic effect (water's tendency to minimize contact with hydrophobic molecules) also plays an important role in protein structure since many large molecules assume their shapes at least partially in response to this effect. Apart from disulfide bonds, all these forces are non-covalent, weak interactions, but their cumulative effect gives proteins unique shapes. It is important to note that the primary structure determines the tertiary structure of a protein.

Christian Anfinsen's experiments, showing protein refolding after a denaturation process, prove that the tertiary structure can be stored in the primary structure of proteins[14]. While the tertiary structure

information might be stored in the primary structure, many proteins need help from chaperones to fold the polypeptide chain into a functional protein properly.[15] Proteins likely go through several intermediate structures until reaching their native conformation.

The folding process begins with forming local segments of secondary structure, forming a molten globule state. Then, the secondary structure becomes stabilized, and the tertiary structure starts to form. Later, the protein undergoes a series of rearrangements that form hydrogen bonds and expel water molecules from its hydrophobic core. Finally, multiple domains assemble to produce the proteins' native state.[2]

Hence, proteins appear to fold hierarchically, starting with small secondary structure fragments, followed by larger elements until reaching the native structure. Predicting protein structure based on the primary structure is very challenging because the number of atoms and all the forces involved in the protein make the prediction challenging. Nevertheless, modeling protein structure is an active research topic that has shown huge progress and exiting results.[16,17]

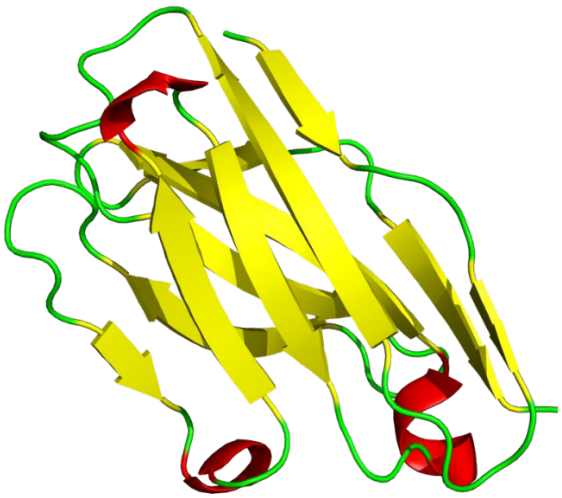

Figure 1.2 Protein ribbon representation showing the tertiary structure colored by secondary structure motifs. In red alpha helixes, yellow beta sheets, and in green turns and random coils. PBD: 5YD3

1.1.6. Quaternary structure

Some proteins are formed by more than one polypeptide chain. The quaternary structure of a protein represents how those polypeptide chains combine to form a unique functional protein. It shows the spatial arrangement of tertiary structural elements tied together by weak interactions.

Both tertiary and quaternary structures of proteins determine their function:[18] a loss of structure will generate a loss of function. Thus, it is crucial to understand and characterize protein structures to ensure quality, performance, and safety but also to design and improve protein therapeutics. Together, secondary, tertiary, and quaternary structures are known as the high order structure (HOS) of a protein.

1.1.7. Structure of antibodies

Antibodies are the largest subclass of immunoglobulins (Ig). Antibodies are further divided into five large groups: IgM, IgD, IgA, IgE, and IgG, depending on the general structure. Notably, IgG is one of the most abundant proteins in the human serum (approximately 20% of plasma proteins).[19] Subsequently, IgG proteins can be divided into four classes: IgG1, IgG2, IgG3, and IgG4 based on abundance.[19] All four IgG subclasses are surprisingly similar. Although IgG subclasses share ~90% identical amino acid sequences in the heavy chain, differences in the light chain and the hinge region make each subclass unique.[19]; IgG subclasses have different antigen-binding profiles, half-lives, reactions on effector cells, responses to triggers, and many more.[19]

IgG antibodies consist of two identical heavy (H) and two light (L) chains (see **Figure 1.3**) bound together by disulfide bonds and a linker (hinge region). Each heavy chain consists of a variable domain (VH) and three constant domains (CH1, CH2, and CH3). Likewise, light chains consist of a variable domain (VL) and a constant domain (CL). Light chain is bound to VH and CH1 domains by disulfide bonds to form the Fab (fraction antigen binding) fragment of the antibody. Variable (V) domains in the antibody form the paratope, which differs greatly between different antibodies and is responsible for the

antigen-binding of the protein. Constant domains of the antibody have identical sequences among immunoglobulins of the same isotype and species (see **Figure 1.3**).

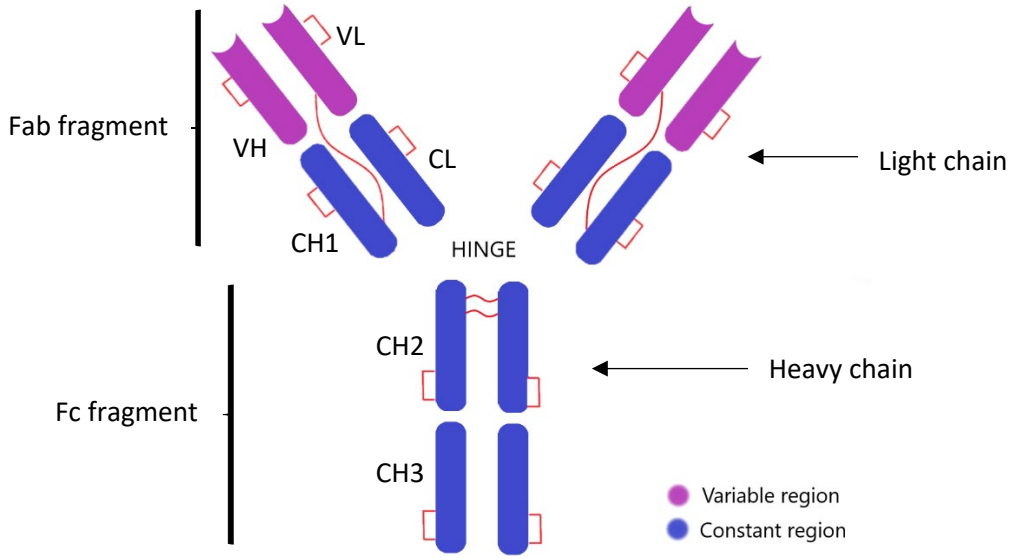

Figure 1.3 Schematic layout of an IgG1 antibody. IgG1 molecules are composed of two heavy chains and two light chains. Blue represents constant regions, purple represents variable regions, and red lines represent disulfide bonds.

Moreover, IgG1 antibodies have a relative abundance of 65% among all IgG proteins in human serum, making them the predominant class of antibodies and the most extensively studied subclass of immunoglobulins.[20] Notably, IgG1 proteins have a molecular mass of ~149 kDa, 15 residues in the hinge region, and 16 disulfide bonds across the antibody.[20] The interface between CH2 and CH3 domains has a conserved N-linked glycosylation site (asparagine 297) responsible for small changes in the HOS of the protein.[19]

The general structure of IgG glycans starts with N-acetylglucosamine (GlcNAc) and mannose residues; however, variations containing galactose, sialic acid, fucose, and more are also possible. While most IgG molecules have glycans attached to asparagine 297, experiments have shown that the variable region (V) is also glycosylated in ~10-15% of IgG antibodies isolated from human serum.[21] Several glycoforms have been found in human serum. However, only a few are the dominant and most abundant ones.[22]

Glycans attached to the Fc (fraction crystallizable) fragment influence the antibodies' HOS and directly participate in many receptor functions (e.g., FcγR, FcRn binding).[23]. Hence, removing the glycan in an antibody can alter the Fc structure and reduce or completely stop effector functions.

1.1.8. Importance of high order structure characterization

As established above, the biological function of a protein and its potential therapeutic properties are governed by its HOS. Understanding the relationship between the structure and function of a protein is fundamental. Changes in the primary structure or HOS of a protein might induce many wanted or unwanted changes.

Changes in primary structure by alanine scanning mutagenesis on the Fc region of an antibody showed an increase in the binding affinity of specific FcγR or FcRn receptors. The combination of Ser298Ala, Glu333Ala, and Lys334Ala mutation had a substantial improvement (50-100x fold) in the affinity of an IgG1 to a FcγRIII receptor, which mediates the antibody-dependent cellular cytotoxicity.[24] Additional changes in the primary structure and HOS, such as modification of glycan profiles,[25,26] exchanging of Fc domains among isotypes,[27] modification of hinge region length,[28] the use of cross-type antibodies,[29] points mutations,[30] and many others[31] have also been used to optimize activity, half-life, solubility, and antibody stability. Likewise, changes in the HOS can also cause unwanted effects in protein therapeutics. Common post-translational modifications, such as oxidation[32] and deamidation,[33] can induce protein aggregation and decrease stability.

Furthermore, several studies have shown that changes in temperature,[34,35] light,[36] pH,[37,38] buffer species,[39] ionic strength,[40] protein concentration,[35] excipients or additives,[41,42] mechanical stress,[43] and many more[44,45] can cause HOS changes and induce protein aggregation, impacting function and possibly creating immunogenicity.[46,47] Therefore, it is imperative to monitor protein structure during the whole production process to ensure product quality, performance, and safety of protein therapeutics.

1.2. CHARACTERIZATION OF PROTEIN STRUCTURE

A highly purified protein is needed to characterize and examine protein properties and functions. Purification of a specific protein is challenging and might require a combination of different purification techniques, which can be divided into two large groups: selective precipitation techniques and chromatographic techniques. Selective precipitation takes advantage of differences in relative solubility of proteins as a function of polarity (using organic solvents), salt concentration (salting out), and pH (isoelectric precipitation). Chromatographic techniques separate proteins based on their charge (ion-exchange chromatography), size (size exclusion chromatography), hydrophobicity (hydrophobic interaction chromatography), and binding affinity (affinity chromatography).[48] Once the protein is highly pure, different techniques can be used to characterize the primary, secondary, tertiary, and quaternary structures.

1.2.1. Determination of the primary structure

Only a few methods can determine the primary structure (sequence) of a protein. The first and most common method is the Sanger method. Disulfide bonds must be reduced to determine the protein sequence with the Sanger method, and the protein is digested into peptides. Peptides are later separated and purified.

Next, each peptide is treated with 1-fluoro-2,4-dinitrobenzene (Sangers reagent), which reacts with the N-terminal amino group. It is possible to determine the sequence of a protein using hydrolysis to break the peptide bond and comparing the obtained residue with standards.[48] The Sanger method is nowadays optimized by using a different reagent (Edman reagent) and better proteases to obtain more and smaller peptides. Although the process is mostly automated, it still requires large amounts of purified protein to provide reliable results.

Prediction of the primary structure of a protein by using recombinant DNA is fast and inexpensive. Modern techniques enable us to get large amounts of DNA, and automated sequencers (using DNA

sequencing methods like the Sanger method) can determine very long deoxyribonucleotide chains in a timely manner. Later, the protein sequence is predicted by translating the nucleotide triplets into amino acids.[48]

Additionally, de novo peptide sequencing can be used to determine the sequence of peptides.[49] Often, there is interest in determining small changes in the primary structure (e.g., post-translational modifications) of a protein when most of the sequence is still intact. In these cases, sequencing the whole protein is a waste of time and resources.

De novo peptide sequencing uses mass spectrometry and tandem mass spectrometry to determine peptide sequences. High sensitivity, ease of use, and speed have made mass spectrometry (MS) ideal for these cases because MS is more sensitive than the Sanger or Edman method, does not need large amounts of protein, and can be applied to all sorts of proteins. Therefore, it is possible to predict or determine parts of the protein sequence using DNA sequencing or mass spectrometry, however, full protein sequencing can only be accomplished by the Edman or Sanger method.

1.2.2. Characterization of high order structure

Many techniques are used for protein structure characterization, depending on the protein, the information needed, and the desired resolution. Generally, characterization techniques are classified into three groups depending on the obtained resolution: low-resolution, medium-resolution, and high- or atomic-resolution techniques.

Low-resolution techniques can provide basic protein structure information without any atomic coordinates. Dynamic light scattering (DLS) is very common among low-resolution techniques, which uses scattered light angles and intensities to provide hydrodynamic radius and size information. Other common low-resolution techniques are size exclusion chromatography (SEC) that uses an inert resin to separate protein by size, and atomic force microscopy (AFM) that uses a very small tip (on the nanometer scale) to scan the surface of the protein and provide a topographic image. Nevertheless, the

most common techniques are circular dichroism (CD), differential scanning calorimetry (DSC), and Fourier transform infrared spectroscopy (FTIR).

CD is a nondestructive technique that measures the difference between left- and right-handed circularly polarized light absorbance of the proteins as a function of wavelength.[50] Notably, CD can be used to characterize and quantify secondary structure motifs in the protein (α-helixes, β-sheets, and random coils), playing an important role in the analysis of biotherapeutic agents. Moreover, CD is used to examine the structural integrity of proteins, proper folding, and secondary structural changes due to binding activity or in response to pH or ionic strength changes.[50,51]

In contrast, DSC measures the heat capacity and excess heat associated with transitions induced by a temperature change. This method heats both a sample cell (containing the protein) and a reference cell while increasing both cells' temperatures as a function of time.[52] Different amounts of energy will be required to increase the temperature of the reference and sample cells, which can be measured and correlated to the sample's thermodynamic properties. Thus, DSC can provide information on protein thermal stability, conformational states, and solution conditions directly related to intra- and inter-molecular interactions within the protein.

The use of FTIR in protein characterization is based on the interaction of infrared radiation and protein samples. Protein samples absorb specific wavelengths of infrared radiation depending on the type and amount of bonds present in the sample. Characteristic bands are found in the infrared spectrum of proteins, mainly stretching vibrations and bending motions of the C=O, C-O, and the N-H bonds in the COOH, COO^-, NH_3^+, and NH_2 groups.[53] Since these bonds are involved in the hydrogen bonds of the protein, these bands are useful to characterize the secondary structure motifs in the protein.

Experiments using proteins with known structure have been used to correlate the shape and intensities of the bands with specific secondary structure content,[54] making possible the use of FTIR to provide an accurate way to quantify the amount of secondary structural motifs in a protein. However, if more

information is needed, the use of high-resolution techniques is mandatory. To date, X-ray crystallography, nuclear magnetic resonance (NMR), and, more recently, cryogenic electron microscopy (cryo-EM) are considered the gold standards for HOS characterization.

In X-ray crystallography, X-ray radiation interacts with a protein crystal. That interaction makes the incident rays diffract.[55] Measurements of diffraction angles and intensities of diffracted rays make constructing a three-dimensional (3D) electron density map of the protein crystal possible. The electron density map is later used to construct a 3D protein structure with atomic resolution. X-ray crystallography can provide atomic-level resolution of proteins of different sizes; however, it has some disadvantages. The production of protein crystals is challenging[56] and, for many proteins, impossible to date. Additionally, since X-ray crystallography uses a protein crystal to determine the structure, the structure will depict the solid-state protein, which might not have the same structure found in solution or *in vivo* environments.[57]

NMR measurements can be used to determine protein structure by measuring nuclear resonance frequencies in the protein. In NMR, proteins are placed in an external magnetic field, which induces nuclei to produce local currents and, hence, an alternative field (as opposed to the external magnetic field). The effective magnetic field on each nucleus will therefore be reduced by the local alternative fields. Experimentally, chemical shifts are measured relative to a reference signal. Since each NMR active nucleus will be exposed to different local alternative fields, each nucleus will have a different value that will depend on protein structure.

An NMR experiment will produce a spectrum with signals for each different type of active nuclei within the molecule. The development of multidimensional NMR, in-solution NMR, and the use of structural restraints now allows for the determination of protein structures at near-atomic resolution.[55,58] Although NMR is mainly applicable to small proteins, it has been used on proteins up to 1 MDa.[59] The drawback of NMR is that it needs large amounts of protein (on the order of mg) which is usually expensive and difficult to produce in early stages of development. Moreover, only odd mass nuclei are NMR active,

making ^{12}C, ^{14}N, and ^{16}O unsuitable for NMR, which often leads to the production of proteins in enriched media (in NMR-active elements), a long and expensive process. Additionally, NMR data acquisition and analysis can be very time-consuming.

Unlike X-ray crystallography and NMR, cryo-EM does not need large amounts of protein. This technique involves flash-freezing the sample and using an electron beam to produce a 3D "photograph" of the molecules by detecting scattered electrons.[60,61] The use of cryogenic temperatures minimizes distortion in protein structure with water molecules and reduces sample damage to the sample by the electron beam.[55] High-resolution protein structures are obtained by averaging multiple randomly aligned EM pictures, resulting in protein structures with atomic resolutions <1.8Å.[62] The use of cryo-EM is straightforward and requires small amounts of sample but usually only works with proteins with high molecular weights (>100 kDa).

As discussed above, low-resolution techniques, such as CD, FTIR, and DSC, have high throughput but lack spatial resolution information. However, obtaining protein crystals for some proteins is very difficult, making X-ray crystallography problematic. Additionally, solid-state structures might not be a good representation of in-solution structures. Similarly, NMR is limited by protein size and requires large amounts of proteins.

Hence, it seems that cryo-EM can overcome most of these problems, but high-resolution instruments have been limited to a few laboratories due to high costs. Therefore, intermediate resolution techniques have been developed primarily based on mass spectrometry (MS) approaches. These techniques balance throughput and spatial resolution of protein HOS characterization experiments.[55]

1.2.3. Mass spectrometry methods for high order structure characterization

Most MS methods for HOS characterization follow the same general procedure. Initially, the protein is labeled using different techniques. The labeling location and abundance will depend on several factors,

including the protein's HOS. Next, MS is used to locate the protein regions that were successfully labeled. This information is analyzed to give the desired structural information.

Many technological advances in mass spectrometry have been developed over the last 50 years to be able to use MS to analyze proteins' HOS, starting with suitable ionization techniques for proteins. Crucial developments were electrospray ionization (ESI) and matrix-assisted laser desorption ionization, which are soft ionization techniques. Notably, ESI is compatible with liquid chromatography (LC), creating an ideal system to separate and analyze complex protein mixtures. The development of high-resolution mass spectrometers with better detection limits and resolving powers also permits the analysis of large proteins.

Currently, most instruments are "hybrid" mass spectrometers since two or more mass analyzers are used in sequence. Hybrid mass spectrometers combine unique performance characteristics from different mass analyzers, including mass resolving power, sensitivity, and speed of analysis. Among the most common mass analyzers are time-of-flight (ToF), orbitrap, and ion trap, usually combined with quadrupole mass filters. Additionally, the development of suitable fragmentation techniques, such as collision-induced dissociation (CID), electron transfer dissociation (ETD), and electron capture dissociation (ECD), permits the correct identification of peptides, and locating specific features within the protein that make MS methods for HOS characterization complete and versatile techniques. MS methods for HOS characterization can be divided into two large groups: covalent labeling and cross-linking methods.

1.2.4. Cross-linking methods

Protein cross-linking occurs when a covalent bond is formed between two proteins or adjacent regions of the same protein via a bifunctional reagent (cross-linker). Generally, the cross-linker reacts with the exposed amino acid sidechains on the protein's surface and binds together adjoining regions via covalent bonds that link both regions. The nature of the chemical cross-linker reagent used varies depending on

the desired length and the linker's chemistry. N-hydroxysuccinimide esters (NHS-ester) and imidoesters are the most common linkers used for protein HOS characterization.[55,63] The reaction mechanism is simple, nucleophilic groups within the protein (primary amines, hydroxyl, or sulfhydryl groups in residues sidechains) attack the ester groups on the cross-linker reagent to form a covalent bond. The reactivity of these nucleophilic groups depends on the nature of the nucleophilic group, pH, and solution temperature. Optimization of these parameters can greatly improve the efficiency of the cross-linking reaction.

Next, proteases are used to obtain peptides and cross-linked peptides. Subsequent MS and MS/MS measurements on the peptides to locate the cross-linker within the protein give abundant structural information, such as location of protein/protein interfaces and protein/protein interactions. One disadvantage of traditional NHS-esters reagents is that fragmentation of cross-linked peptides is complex, making the analysis tedious. Thus, cleavable linkers have been developed, where part of the label can be cleaved first, making the analysis simpler.[55]

1.2.5. Covalent labeling methods

All covalent labeling methods have similar approaches. Generally, solvent-accessible surface regions of a protein are exposed to various reagents that provoke a reaction that chemically labels the protein in those regions. Labels used in these experiments are varied, from replacing a hydrogen for a deuterium to adding big tags such as isotope-coded affinity tag reagents (ICATs) to a protein.[64] The reagent choice depends greatly on the protein, region of interest, and information needed. The protein is digested to produce peptides that are later separated and analyzed by MS to check where the reagent labeled the protein.

Interpretation of the mass measurements and comparison of mass differences between two states can give plentiful information about the protein, protein interactions, protein dynamics, and much more. Secondary and tertiary structure changes can be monitored using covalent labeling methods by labeling

solvent-accessible surface areas. Later identification using MS/MS experiments can pinpoint the location of the labeling giving structural information. Quaternary structures can also be probed with covalent labeling methods by labeling two protein states where solvent-accessible regions change (e.g., apo and holo protein states).[55]

Labeling methods can be specific or non-specific depending on the site of action. Since each amino acid has a different side chain, and most have a functional group, it is possible to use a specific reagent that reacts, and label only target amino acids in a protein. For example, to label cysteine residues, α-haloketo compounds such as iodoacetamide (IAM)[65] (also used to prevent disulfide bonds reformation after reduction) and N-alkylmaleimide compounds (such as N-ethylmaleimide) can be used. Each compound reacts with exposed cysteine residues and increases the peptide mass (+57 Da for IAM and +125 Da for N-ethylmaleimide). Similarly, 2-hydroxy-5-nitrobenzyl-bromide (HNB) and HNB derivatives can be used to label tryptophan residues,[66] tetranitromethane (TNM) to label tyrosine residues,[67] phenylglyoxal for arginine residues,[68] and many more compounds that are specific for each residue.[55]

On the other hand, non-specific covalent labeling methods do not label specific amino acids in the protein but label all exposed surface areas. Hydrogen exchange mass spectrometry (HDX) and fast photochemical oxidation of proteins (FPOP) are the most common non-specific covalent labeling methods. Notably, FPOP uses very reactive radicals (hydroxyl radicals, OH•) to covalently label all surface exposed areas. OH• radicals are produced from laser photolysis of hydrogen peroxide and can react with 14 out of 20 amino acids with a preference for aromatic, heterocyclic, and sulfur-containing sidechains.[69]

Generally, the labeling reaction takes place in the sub-millisecond time range.[63] Such labeling speeds guarantee a "snapshot" of the conformation of protein. As with all other covalent labeling methods, after labeling the protein, a subsequent proteolysis step or fragmentation from tandem MS is followed, and MS measurements of the peptides/fragments give the necessary HOS information. Thus, FPOP can be

used for epitope mapping,[70] aggregation propensity studies,[71] characterization of protein folding intermediates,[72] and many more[63] as FPOP is a simple technique that provides useful information.

Most FPOP limitations are related to laser availability, setup, and maintenance.[63] Its application is also limited to proteins rich in aromatic, heterocyclic, and sulfur-containing amino acids. Most limitations can be solved using orthogonal labeling reagents such as trifluoromethyl radical[73] or carbene diradicals,[74] among others. Additionally, since oxidation is a common post-translational modification (PTM) in downstream processes, FPOP analysis and interpretation of the data could be challenging since distinguishing between PTM and FPOP oxidization is quite difficult.[75,76]

Hydrogen-deuterium exchange (HDX) labels the protein using deuterium. In a normal experiment, the protein is placed in a D_2O buffer, and the deuterium from the buffer replaces hydrogen atoms on the backbone amides of the protein. Generally, HDX is the least disruptive covalent labeling technique and labels all exposed amino acids except proline (which does not have a backbone amide). Moreover, HDX has many uses, from epitope mapping[77] to offering mechanistic insights of antibody action against dengue viruses.[78] Contrary to other covalent labeling approaches, HDX's major drawback is that the labeling reaction is reversible, forcing to run the analysis at low pH and temperature. This reversibility often results in HDX being classified as a non-covalent labeling technique. However, since N-H and N-D bonds are covalent bonds (despite being reversible), HDX is technically a covalent labeling technique. The next section will describe hydrogen exchange MS fundamentals in more detail, along with the experimental workflow and additional information.

1.3. HYDROGEN EXCHANGE MASS SPECTROMETRY

1.3.1. Fundamentals

Labile hydrogen atoms in proteins (in aqueous solutions) continuously exchange with hydrogen atoms in the solvent.[79] Labile hydrogen atoms are hydrogen atoms that are bonded directly to heteroatoms in

the protein (see blue atoms in **Figure 1.4**). When the aqueous buffer is replaced by a deuterium oxide (D_2O) buffer, labile hydrogens can naturally exchange with deuterium atoms in the solvent. The amount of exchange (labeling) primarily depends on protein structure.[80] Since deuterium is a heavier isotope of hydrogen, MS measures the increase in mass of the protein and peptides to identify the amount and location of the labeling. Although all labile hydrogen atoms exchange with deuterium in the buffer, only the exchange on amide hydrogens in the backbone of the protein (see hydrogens circled in red in **Figure 1.4**) can be experimentally measured using in-solution HDX.

The exchange rate for labile hydrogen atoms in the amino acid side chains is so fast that they back-exchange (deuterium to hydrogen) immediately during LC separation. The exchange rate for amide hydrogen goes from milliseconds to months depending on several factors such as hydrogen bonding, protein structure, pH, and temperature. They back-exchange slowly during LC separation if appropriate conditions are employed (low pH and temperature).[80,81]

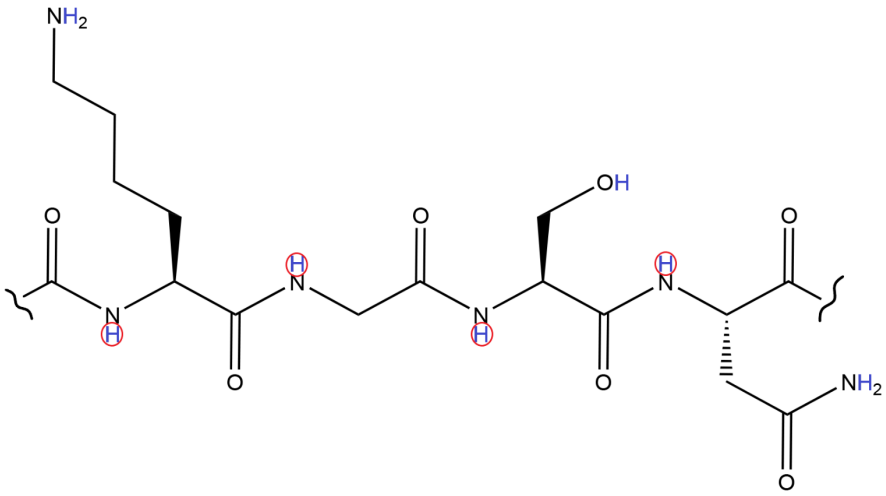

Figure 1.4 Exchangeable hydrogen atoms for peptide Lys-Gly-Ser-Asn. In blue are labile hydrogen atoms. Circled in red are amide hydrogen atoms.

1.3.2. Mechanism of exchange

Amide hydrogen exchange mechanism in folded proteins is still under debate[82,83] but it can be acid-, base-, or water-catalyzed. Acid-catalyzed can be either by N-protonation or O-protonation.[84,85] The

chemical exchange rate constant (k_{ch}) for any given amide in an unstructured peptide is given by equation 1.1[86]

$$k_{ch} = k_{int,H}[H^+] + k_{int,OH}[OH^-] + k_{int,H_2O}[H_2O] \quad (1.1)$$

Where $k_{int,H}$, $k_{int,OH,}$ and $k_{int,H2O}$ are the intrinsic rate constants for the acid-, base-, and water-catalyzed reactions. Experimental measurements for these constants using poly-DL-alanine are 41.67, $1.51x10^{10}$, and $3.16x10^{-2}$ M^{-1} min^{-1} for the acid, base, and water-catalyzed reactions, respectively, at 20°C with low salt concentrations.[87,88] Clearly, the intrinsic exchange rate constant for the base-catalyzed reaction is much bigger than the others. Hence, contributions from the acid- and water-catalyzed exchange are often omitted under physiologic conditions,[80] and only contributions from a base-catalyzed hydrogen exchange mechanism are considered (see **Figure 1.5**).

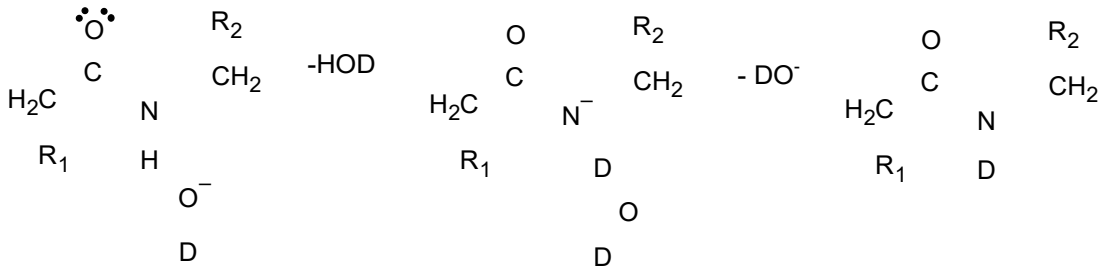

Figure 1.5 Base-catalyzed amide hydrogen exchange mechanism. First, the amide proton is abstracted by a nucleophilic attack from an OD^- molecule forming an amidate anion. Secondly, the amidate anion is re-protonated by taking a proton from the deuterium oxide. The final product has a deuterium replacing the amide hydrogen.

1.3.3. pH effects

Amide hydrogen exchange is highly dependent on the pH of the solution. Smith *et al.* used equation 1.1 and the experimental values for the intrinsic rate constants to calculate the chemical exchange rate constant for amide hydrogens in a poly-DL-alanine peptide as a function of pH (see **Figure 1.6**).[89]

Figure 1.6 shows that the chemical exchange rate constant has a minimal value when the pH is approximately 2.5-3.0. This behavior is the basis for using low pH to quench the labeling reaction and

keep the deuterium in place during the LC-MS analysis (the calculated exchange half-life for poly-DL-alanine peptide at 0°C at this pH is approximately 25 min, which is enough time to complete the LC-MS analysis).[86] At pH values below or above the k_{ch} valley (pH ≈ 2.5), the exchange reaction follows a pseudo-first-order reaction and will only depend on either the base- or acid-catalyzed contributions. Most hydrogen exchange experiments are done at pH values above 5, so the k_{ch} will mostly depend on the base-catalyzed contribution as stated in the mechanism of exchange section above.

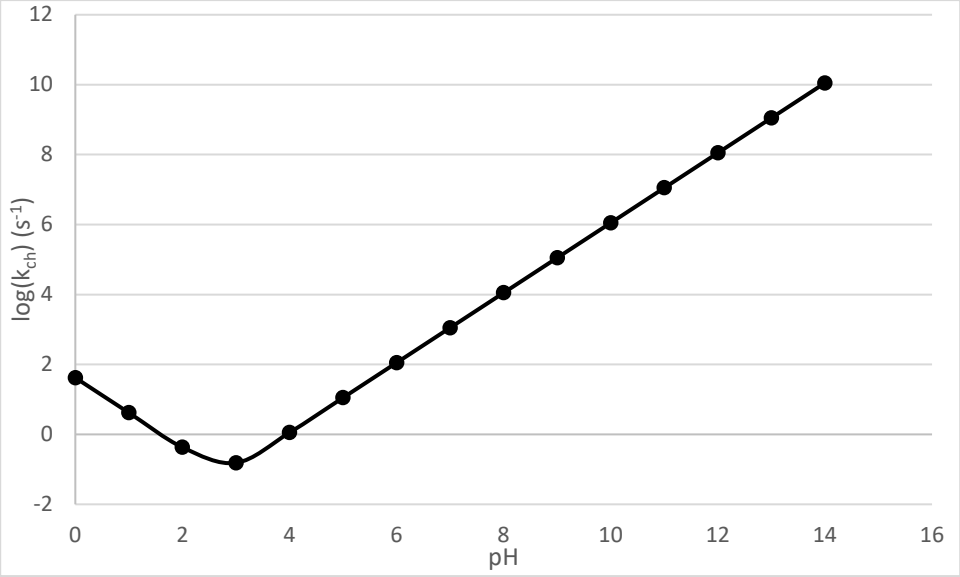

Figure 1.6 Calculated chemical exchange rate constant for a poly-DL-alanine peptide as a function of pH. Data calculated using equation 1.1.

1.3.4. Temperature effects

Chemical exchange rate constant is highly dependent on the solution temperature. Temperature changes affect the water ionization constant (K_w) and thus the concentration of hydroxide anions in solution (OH^-), affecting k_{ch} as seen in equation 1.1.[86] A modified version of the Arrhenius equation (equation 1.2) expresses the chemical exchange rate constant as a function of temperature:[87]

$$k_{ch}(T) = k_{ref}e^{\left(-\frac{E_a}{R}\left[\frac{1}{T}-\frac{1}{293}\right]\right)} \quad (1.2)$$

Where k_{ref} is an experimental reference rate constant at 20°C, E_a is the activation energy for the reaction, and R is the gas constant. **Figure 1.7** shows the effect on the chemical exchange rate constant as a function of temperature by plotting equation 1.2. By decreasing the reaction temperature, the chemical exchange rate constant can be decreased up to 20-fold (for a change of 30°C to 0°C). Low temperatures are used during quench and LC-MS analysis steps to decrease back-exchange (deuterium to hydrogen) in the experiment and keep the label in place.

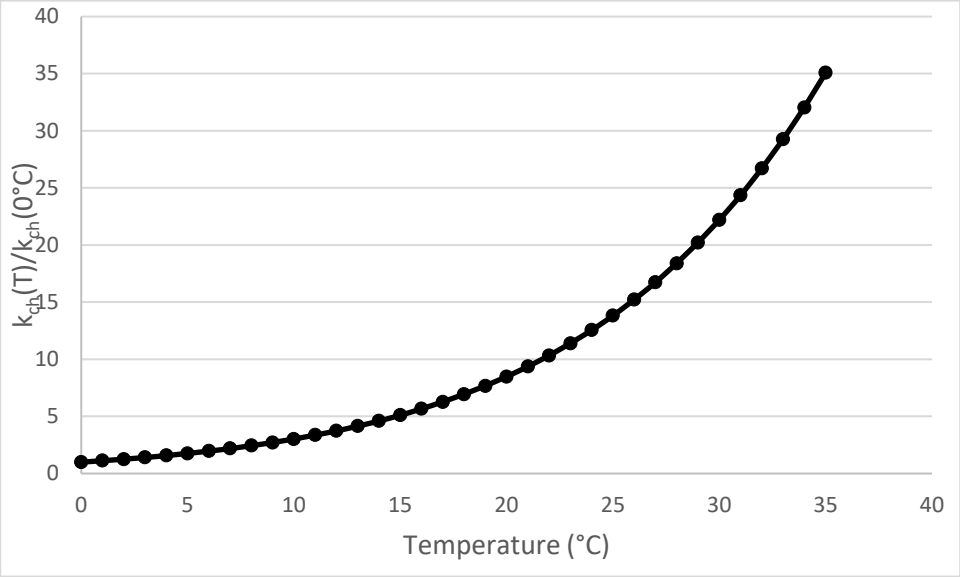

Figure 1.7 Theoretical chemical exchange rate constant as a function of temperature where k_{ch} was calculated using equation 1.2 for a base-catalyzed only reaction and normalized to the chemical exchange rate constant at 0°C.

1.3.5. Other effects

Changes in ionic strength also impact chemical exchange rates. It was found that the presence of 0.5 M KCl in solution changed the chemical exchange rate by approximately 30% for charged residues compared to solutions at lower salt concentrations.[87,90] Similarly, chemical exchange rates for uncharged

residues when exposed to 0.5 M KCl increased by a factor of 1.2 for the acid-catalyzed reaction and decreased by a factor of 1.07 for the base-catalyzed reaction using a poly-DL-alanine peptide as a model system. Although these effects can significantly change the chemical exchange constant in a hydrogen exchange experiment, most protein applications use low salt concentrations where these effects are minimum.[86] Most importantly, most HX experiments use the same labeling conditions for all protein states. Hence, the influence in the chemical exchange constant will be the same for both states.

Neighboring side chains in the peptide sequence also affect the chemical exchange rate constant, mostly due to inductive and steric effects. Polar side chains withdraw electron density from the amide hydrogen, making it more acidic and facilitating the base-catalyzed removal of the proton but decreasing the nucleophilic attack strength in the acid-catalyzed reaction.[87] Bulky side chains can have steric effects that slow the chemical exchange process for both acid- and base-catalyzed reactions. Generally, the influence of side chains in the chemical exchange rate of amide hydrogen varies with location. Effects are different when located immediately right or left of the amide hydrogen. A complete list of the effects of amino acid side chains by position on the chemical exchange rate constant of neighboring amides was published in 1993[87] and was recently corrected in 2018.[88]

Varying the solvent composition can also influence the chemical exchange rate, mainly because of changes in the water ionization constant (K_w) and concentration of the OH^- and H_3O^+ ions. The use of 50:50 aqueous-organic buffers shows a reduction in the base-catalyzed chemical exchange rate constant for poly-DL-alanine compared to fully aqueous buffers.[91] As with high salt concentrations, the use of organic solvents in protein sciences is not common, and thus, these effects are rarely seen in hydrogen exchange experiments.

Finally, pressure can also influence the chemical exchange rate. Experimental data using poly-DL-lysine and native-folded lysozyme and ribonuclease A demonstrated that the use of higher pressure increases the chemical exchange rate.[92] The effect was more prominent in the native proteins than in the unfolded

polypeptide. When the pressure is increased, the water ionization constant and concentration of OH^- ions increases, and thus, the chemical exchange rate constant.[86]

1.3.6. Linderstrøm-Lang mechanism

Chemical exchange rate constants state how fast a hydrogen atom would exchange for deuterium in the solution in an unstructured polypeptide. However, when working with native or folded proteins, a few additional steps should be considered. Amides in unstructured peptides undergo fast hydrogen exchange at pH ≈7 (half-life of milliseconds to seconds), but, as previously stated, hydrogen atoms in native proteins have an exchange rate that goes from seconds to months.[80] This sizable difference is because of the high-order structure of the protein, primarily due to the presence of hydrogen bonding.[86] In a normal experiment, the rate-limiting step for amide hydrogen exchange is the abstraction of the proton (see **Figure 1.5**). If the proton is participating in a hydrogen bond, the OD^- molecule will take more time to remove the proton; hence, the exchange rate is greatly decreased.

The Linderstrøm-Lang model[93] (see **Figure 1.8**) describes the amide hydrogen exchange mechanism in folded proteins:

$$N\text{-}H_{closed} \underset{k_{cl}}{\overset{k_{op}}{\rightleftharpoons}} N\text{-}H_{open} \xrightarrow[+D_2O]{k_{ch}} N\text{-}D_{open} \underset{k_{cl}}{\overset{k_{op}}{\rightleftharpoons}} N\text{-}D_{closed}$$

Figure 1.8 Linderstrøm-Lang mechanism for amide hydrogen exchange in a folded protein

The model states that proteins are not static entities but complex structures that are always in motion. Proteins have a "breathing" motion: backbone amides fluctuate between a closed ($N\text{-}H_{closed}$) and open ($N\text{-}H_{open}$) state. When the backbone amide fluctuates to an open state, the hydrogen bonds are momentarily disrupted, and the amide is exposed to the solvent. The equilibrium between the rate of N-H opening (k_{op}) and the rate of N-H closing (k_{cl}) determines the frequency of amide open ($N\text{-}H_{open}$)

states. Then, with an excess of D_2O in solution, the exchange occurs ($N\text{-}H_{open}$ to $N\text{-}D_{open}$) following the mechanism explained in Section 1.3.2 (see **Figure 1.5**) at an exchange rate k_{ch} (the chemical exchange rate constant defined at the beginning of the chapter). As explained before, the chemical exchange rate constant depends on the pH, temperature, and sequence, among others. Finally, the backbone amide fluctuates again to a closed state ($N\text{-}D_{closed}$) and returns to its native conformation.[80,86,87]

The observed hydrogen exchange rate (k_{HX}) in a folded protein is then related to k_{op}, k_{cl}, and $k_{ch,}$ as shown in equation 1.3:

$$k_{HX} = \frac{k_{op}k_{ch}}{k_{op} + k_{cl} + k_{ch}} \tag{1.3}$$

Under native state conditions, proteins return to the folded state quickly after unfolding (the folded state is favored). Hence, $k_{cl} >> k_{op}$ and equation 1.3 can be approximated to

$$k_{HX} \approx \frac{k_{op}k_{ch}}{k_{cl} + k_{ch}} \tag{1.4}$$

Thus, two kinetic scenarios are possible: the EX1 and EX2 scenarios.[86,94] In an EX1 kinetics scenario, the closing rate is much slower compared to the chemical exchange rate ($k_{cl}<<k_{ch}$), simplifying equation 1.4 into

$$k_{HX,EX1} \approx k_{op} \tag{1.5}$$

According to equation 1.5, for EX1 kinetics, the observed hydrogen exchange rate will depend only on the rate of opening events. Any unfolding event will result in a complete exchange, generating two populations, one with no exchange and another fully exchanged, resulting in a bimodal distribution with separated isotopic profiles after LC-MS analysis. Nevertheless, most proteins (under native conditions)

are quite stable, and closing event rates are much faster than chemical exchange rates ($k_{cl}>>k_{ch}$), which is the base of the EX2 kinetics scenario. For EX2 kinetics, equation 4 can be simplified to

$$k_{HX,EX2} \approx \frac{k_{op}}{k_{cl}} k_{ch} = K_{op} k_{ch} \quad (1.6)$$

where the equilibrium constant is K_{op} is k_{op}/k_{cl}. In EX2 kinetics, the observed hydrogen exchange depends on both the folding equilibrium and the chemical exchange rate. Since $k_{cl}>>k_{ch}$, many unfolding-folding events occur before the amide is deuterated, and contrary to EX1 kinetics, after LC-MS analysis, a single isotopic profile is seen with a shift in the mass center compared to the undeuterated profile.[86] For EX2 kinetics, it is possible to calculate the free energy for the opening of the backbone amide (ΔG_{op}) as shown in equation 1.7:

$$\Delta G_{op} = -RT \ln K_{op} = -RT \ln \frac{k_{HX,EX2}}{k_{ch}} = RT \ln \frac{k_{ch}}{k_{HX,EX2}} = RT \ln PF \quad (1.7)$$

where R is the gas constant, T is the temperature, and PF is the protection factor ($k_{ch}/k_{HX,EX2}$). A PF=1 is an unprotected, unstructured, and completely solvated amide, and PF >1 are amides with increased protection from exchange.[86]

The Linderstrøm-Lang mechanism is the most common and widely accepted mechanism for hydrogen exchange. However, this model is strictly kinetic and does not depend on protein structure.[83] Hydrogen exchange experiments using a double mutant *Staphylococcal* nuclease protein with enhanced stability have shown that the Linderstrøm-Lang model cannot explain all the experimental data, and this data set has been used to propose alternative models.[83,95] Factors considered to explain HX data are solvent accessibility,[96] electrostatic fields,[97,98] and local fluctuations,[99] among others.[83] At present, there is no HX mechanism able to explain every single hydrogen amide exchange.

1.3.7. In-solution experimental workflow

The general workflow for in-solution bottom-up hydrogen exchange experiments is divided into five steps (see **Figure 1.9**). Protein samples start in their native buffer to preserve HOS during the whole

process. Protein samples are then diluted into a D_2O buffer that mimics the composition of the native buffer (pH is corrected for isotopic effects.)[100] Next, protein is labeled for various time amounts at constant temperature (steps 1 and 2). At short labeling times, only unstructured regions will exchange (step 1), but at longer labeling times, structured regions will exchange as well (step 2).

After labeling, the reaction is quenched, and the protein is denatured by decreasing the pH and temperature in the presence of a chaotropic agent (step 3). The use of low pH and temperature reduces back-exchange during subsequent steps. Depending on the protein, the quench step might also involve reducing agents such as tris(2-carboxyethyl) phosphine (TCEP) to reduce disulfide bonds present in the protein.

After denaturation, protein is digested (step 4) using different kinds of proteases, often pepsin, at low temperatures. Finally, the resulting peptides are desalted, separated in a chromatography column, and analyzed by MS (step 5). The use of robots to improve the throughput of the experiments is common and provides more precise labeling times to help reduce variability in replicate measurements.[101]

There are many variations to the general workflow exposed here. Some applications omit proteolysis and denaturing (step 3 in **Figure 1.9**), instead analyzing the exchange at the intact protein level. Intact protein analysis can give information on protein binding but cannot point to the binding location within the protein. Moreover, there are middle-down and top-down approaches as well. Both approaches identify the labeling location by using MS/MS experiments at a different degree.

Step 4 involves partial digestion of the protein for a middle-down workflow, dividing the protein into big chunks or long peptides later fragmented in the MS analysis. The top-down approach does not have any digestion steps but instead fragments the whole protein in the mass spectrometer. Although both middle-down and top-down approaches can locate the labeling at a single amino acid resolution level (ideal for most applications), there are many caveats in the experimental procedure.[102] Mass analyzers capable of fragmenting whole proteins are expensive, and the data is usually much harder to interpret.

Deuterium scrambling can occur during gas-phase fragmentation of proteins and peptides (if collision-induced fragmentation is used), resulting in randomization of the backbone hydrogen and deuterium atoms in the protein/peptide.[102,103]

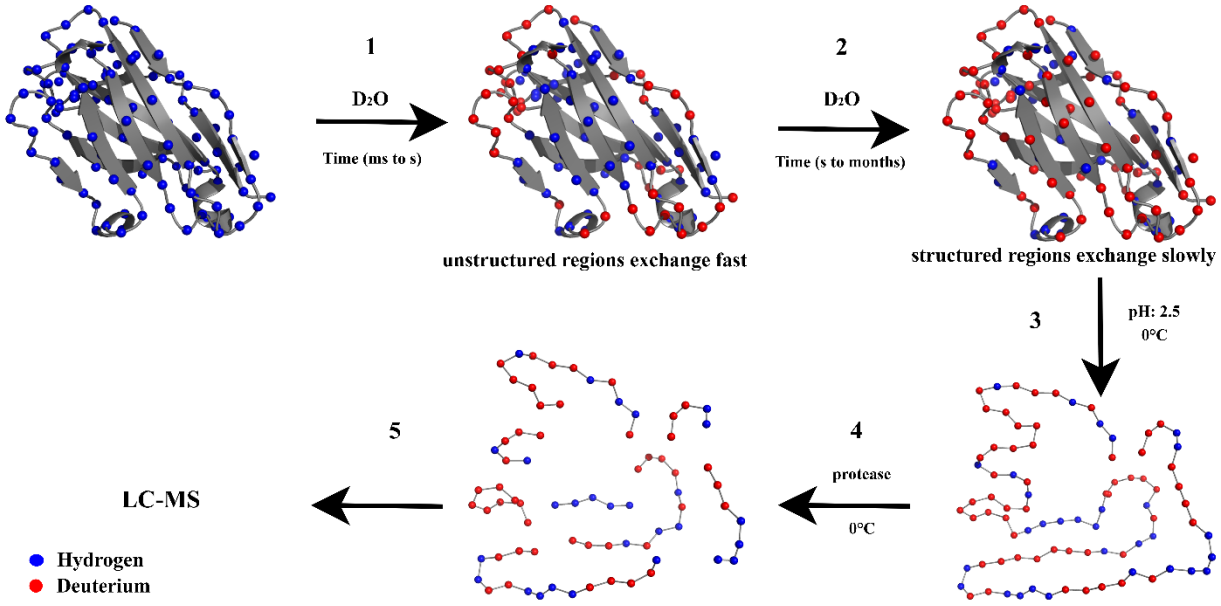

Figure 1.9 General workflow for in-solution bottom-up hydrogen exchange experiments. First, the protein is labeled by diluting it into a D_2O buffer for specific amounts of time. After labeling, the reaction is quenched, and the protein is denatured by reducing pH and temperature. The protein is then digested using a protease, and the resulting peptides are subject to LC-MS analysis. Blue and red spheres represent backbone amide hydrogen and deuterium atoms. PBD: 5YD3

There are many other hydrogen exchange workflows, such as gas-phase HX,[104] solid-phase HX,[105] pulse-labeling HX,[106] and many more[107] that are not within the scope of this dissertation. All HX-MS experiments presented in Chapters 2, 3, and 4 were obtained using the general in-solution bottom-up workflow (**Figure 1.9**) described above.

1.3.8. Data analysis

A database containing all peptides obtained from protein digestion with retention time (RT) is needed to start analyzing the HX-MS data. Thus, an independent experiment is performed where D_2O buffers are not employed (no labeling). Instead, a traditional H_2O buffer is used, and the HX experiment is mimicked using the same quench, temperature, and protease. This experiment will result in a set of

unlabeled peptides coming from the protein of interest. Similar to the HX workflow (**Figure 1.9**), the peptides are then separated using liquid chromatography and measured by MS. Furthermore, MS/MS data is also collected to provide an accurate database and confirm the identity (sequence) of the peptides. The database is then created with the sequence and RT of the peptides in the experiment.

An extracted ion chromatogram (EIC) is obtained using experimental or theoretical m/z values for the unlabeled peptides. The centroid of the spectral envelope is then calculated using equation 1.8:[108]

$$centroid = \frac{\sum m_i I_i}{\sum I_i} \tag{1.8}$$

where m_i is the m/z value of a specific spectral peak (i) in the spectral envelope and I_i is the intensity of that specific spectral peak. Summation of the product of all m/z values and intensities of the peaks that form the spectral envelope divided by the total magnitude gives the centroid mass of the unlabeled peptide (**Figure 1.10a**). Both labeled and unlabeled peptides behave similarly in the chromatography column resulting in subtle or minor changes in the RT.

Thus, a centroid mass is calculated (equation 1.8) for all labeled peptides (all replicates at different labeling times). The extent of HX (in Da) is then calculated by subtracting the centroid mass of the unlabeled peptide from the centroid mass of the labeled one (**Figure 1.10b**). With these values, a peptide HX plot is then constructed by plotting the change in centroid mass at each labeling time.

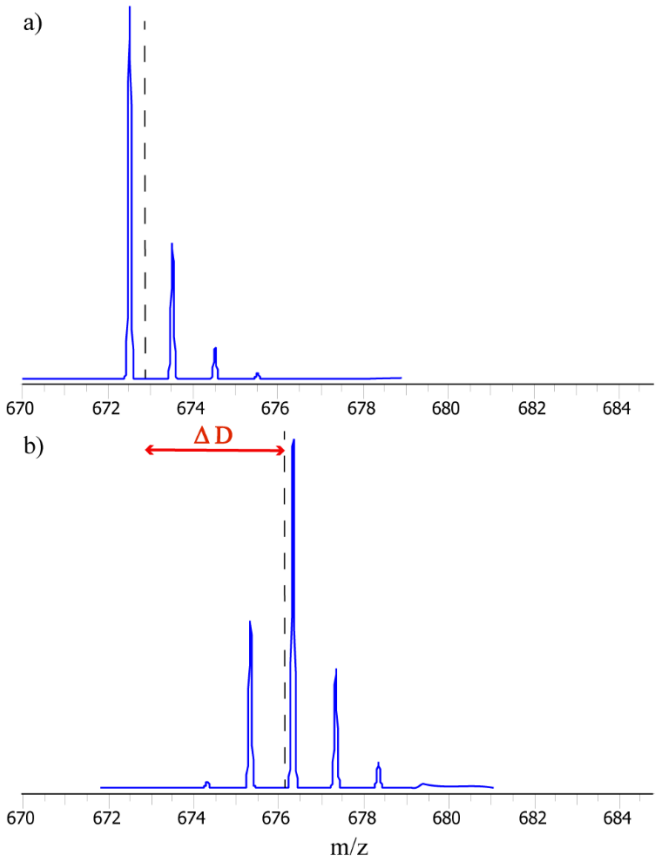

Figure 1.10 Theoretical spectral peaks for a model peptide (RVVSVL) where (a) shows the spectra for the unlabeled state and (b) after labeling. Black dashed lines represent centroid mass values calculated with equation 1.8. In red, the extent of hydrogen exchange is calculated by subtracting the centroid mass value of the unlabeled peptide to the centroid mass value of the labeled one.

Statistical analysis of HX measurements is crucial for correct data interpretation and identification of changes in the protein HOS. A good statistical analysis eliminates subjectivity and control type I and II errors while considering experimental errors during measurements. Generally, a confidence interval for the observed differences of centroid masses is calculated using a Student's t-distribution.[109] Confidence intervals are then used to reject or not a null hypothesis, which usually occurs if the HX difference is not statistically significant.

Individual (for each HX difference) and global (for all HX differences) confidence intervals have been used to analyze HX data; [110,111] however, the rate of type I and II errors is higher when these approaches are taken separately. Hageman *et al.* developed a hybrid significance test that considers the strengths of both individual and global significance testing to overcome most drawbacks seen before.[112] This hybrid

approach considers the magnitude of the difference and its significance to identify HOS differences. Statistical analysis of HX-MS experiments presented in Chapters 2, 3, and 4 of this dissertation use the hybrid approach mentioned above.

1.4. LC-ESI-QTOF ANALYSIS

1.4.1. Liquid chromatography separation

Notably, LC is a technique to separate molecules in solution, where a mobile phase is used to pass the molecules through a stationary phase. Molecules interact differently with the mobile and stationary phases causing them to separate and elute at different times. Moreover, LC has many variations that serve numerous applications. Combinations of stationary and mobile phases can separate molecules based on shape, charge, polarity, affinity, size, or a combination of these characteristics. The most popular method is reversed-phase LC, which separates the molecules based on their hydrophobic interactions with the stationary phase, employing a non-polar stationary phase (usually hydrophobic alkyl chains bonded to silica particles) and an aqueous polar mobile phase.

When separating proteins and peptides, hydrophobic regions will strongly interact with the alkyl groups in the stationary phase, resulting in the molecules being partitioned to different degrees in the stationary phase. Proteins are separated and eluted by changing the polarity of the aqueous mobile phase by increasing the concentration of a less polar organic solvent (e.g., acetonitrile or methanol). By adding an organic solvent, the molecules partition to the less polar mobile phase and elute from the chromatography column. Generally, an increasing gradient of organic solvent is used to accommodate various peptides with different hydrophobic interactions and accelerate the separation process. The LC separation process has many variables that can be adjusted to improve the separation.

For example, increasing the column length will increase the separation efficiency, decreasing the particle size improve the resolution of the peak (at the cost of increasing system backpressures), increasing column temperature improve the resolution, and much more. All variables should be optimized for each

application to ensure a good and fast separation of the molecules in the solution. Following the separation, peptides and proteins pass through an LC-compatible detector that monitors the separation and provides the user with understandable data. There is no universal detector that can monitor all compounds, but for most protein applications, photodiode array (PDA), multiangle light scattering (MALS), fluorescence (FL), and MS are common.

1.4.2. ESI-QTOF

The first step to use MS after liquid chromatography is to transfer the molecules from the liquid phase to gas phase and ionize them. There are many ionization techniques;[113] however, in LC, the most common one is electrospray ionization (ESI), a soft ionization technique (no fragmentation involved) where the molecules in solution are transferred to a gas phase and ionized simultaneously. The exact mechanism for ESI ionization is still debated,[113] but the general process is as follows.

After chromatographic separation, the solution is mixed with a nebulizing gas passed through a small capillary at atmospheric pressure with a strong voltage difference at the tip. The applied voltage can be either positive or negative, depending on the nature of the analyte and the desired ion charge. When the mixture of liquid and gas passes through the tip of the capillary, an aerosol is formed with small, charged droplets. With the help of high temperatures and the use of an inert gas (usually nitrogen), the solvent in each droplet evaporates (desolvates).

Two mechanisms are proposed here (see **Figure 1.11**). Smaller droplets could be formed due to solvent evaporation and Coulombic fissions of the initial droplets. Then, gas-phase ions are directly released from the droplet's surface when the Rayleigh limit is reached (electrostatic repulsion of molecules within the droplet is greater than the surface tension of the droplet).[113] Additionally, gas-phase ions could be released by complete evaporation of the solvent, which is more likely to happen with large molecules such as proteins.[113]

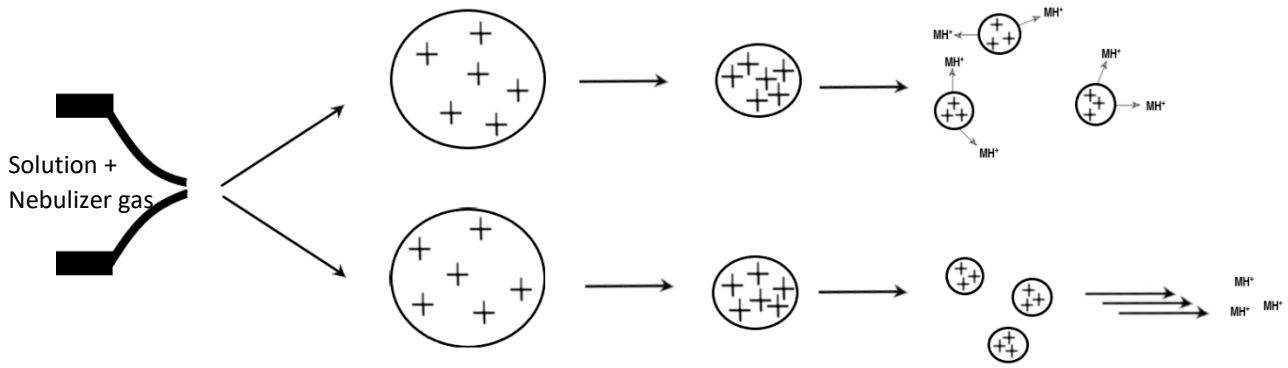

Figure 1.11 Positive electrospray ionization mechanisms for ion formation. The solution is mixed with a nebulizer gas and passed through a charged capillary to form a mist of droplets. Gas-phase ions could be formed and released directly from the surface of the droplets after the Rayleigh limit is reached or after complete desolvation has been achieved.

Solvents suitable for positive ESI must be volatile and capable of donating a proton to the analyte (for the ionization). Many additives can be added to the solvent to help the ionization or decrease matrix effects, and volatile acids are commonly used (e.g., formic acid, acetic acid, and trifluoroacetic acid). For most positive ESI ionization experiments, water, methanol, or acetonitrile are used.

After molecules have been ionized and transferred to the gas phase, the mass-to-charge ratio (m/z) is measured by using a quadrupole time of flight (Q-TOF) mass spectrometer (see **Figure 1.12**). After ions are formed in the ESI chamber (**Fig 1.12a**), ions are transferred through the sampling capillary at high temperatures (**Fig 1.12b**) to desolvate the ions further. Next, the skimmer cone (**Fig 1.12c**) removes the inert gas and solvent molecules with the help of high vacuum in the chamber. Ions coming from the skimmer cone are focused by an octopole ion guide and optic lenses (**Fig 1.12d-e**), and ions pass through the quadrupole, collision cell, and another octopole ion guide (**Fig 1.12f-h**) that act as resolution enhancers and guarantee proper ions transmission.

Ions finally reach the pulser in the flight tube (**Fig 1.12i**), where they are orthogonally accelerated using high voltage. The pulser imparts the same kinetic energy to all ions as they fly through the flight tube to the reflectron (**Fig 1.12j**). A higher vacuum is used in the flight tube to avoid molecular collisions that affect the results by increasing signal losses. The reflectron compensates for minor velocity differences, improving the resolving power of the mass spectrometer and directing the ions toward the detector.

Finally, the time of flight for the ions to fly from the pulser to the microchannel plate detector (Fig 1.12k) is measured to obtain the m/z ratio for each ion.

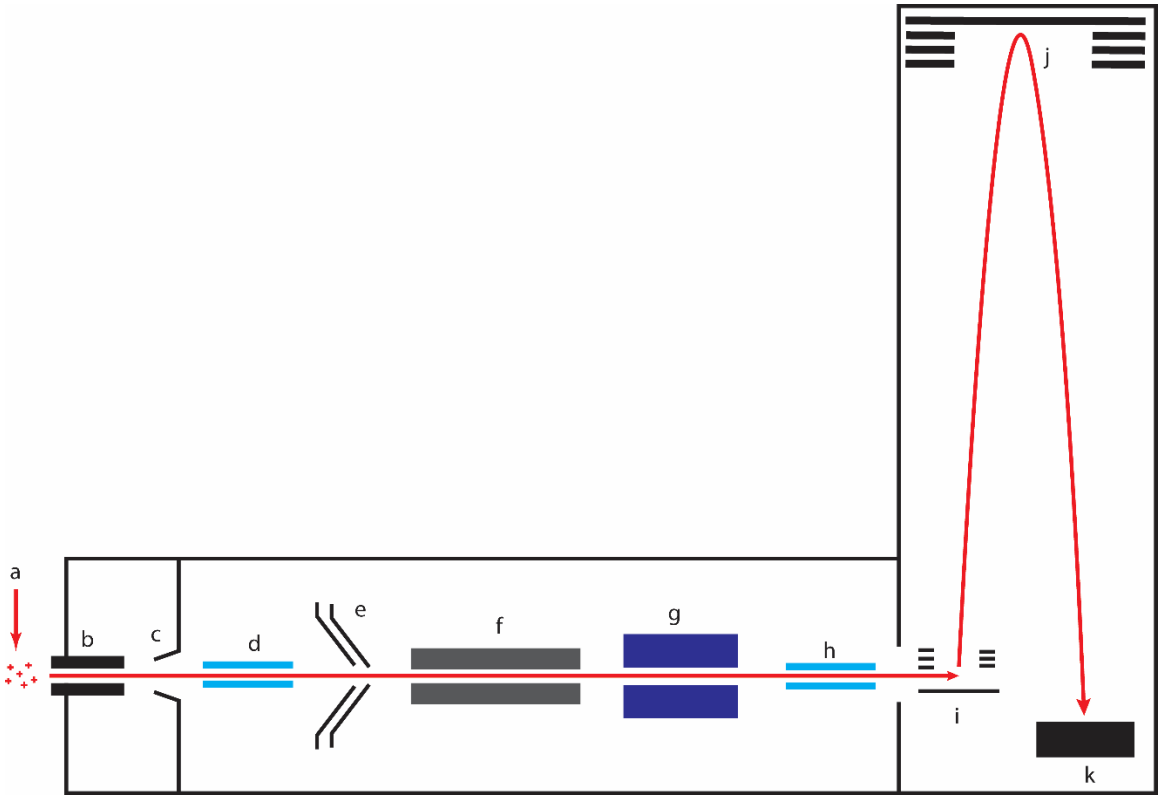

Figure 1.12 Schematic diagram for a Q-TOF mass spectrometer: ESI chamber (a), sampling capillary (b), skimmer cone (c), octopole ion guides (d,h), optic lenses (e), quadrupole (f), collision cell (g), pulser (i), reflectron (j), and microchannel plate detector (k).

Time-of-flight measurements are directly related to the m/z ratio of the ions. Kinetic energy (K_e) is related to the applied acceleration potential (V) and the charge (z) of the ions, as seen in equation 1.9:

$$K_e = zV = \frac{1}{2}mv^2 \tag{1.9}$$

Similarly, the kinetic energy of a particle in motion is related to the mass (m) and velocity (v) of the particle (equation 1.9). Thus, in the rearranging of equation 1.9, the velocity of the molecule is

$$v = \sqrt{\frac{2zV}{m}} \tag{1.10}$$

Moreover, the amount of time (t) to travel a distance (D) at a velocity (v) is shown in equation 1.11:

$$t = \frac{D}{v} = D\sqrt{\frac{1}{2V}(m/z)} \quad (1.11)$$

Hence, knowing the length of the flight tube in the mass spectrometer and measuring the time of flight for the ions to reach the detector, it is possible to calculate the m/z ratio for the ions and the mass spectrum. Modern Q-TOF mass spectrometers use an empirical approach rather than deriving m/z values directly from equation 1.11. Standard compounds with known masses are analyzed, and the resulting times of flight are used to correlate m/z and time of flight values using an empirical form of equation 1.11.[114]

1.4.3. MS-CID-MS

Q-TOF mass spectrometers are capable of many types of experiments. As explained in section 1.3.8 for hydrogen exchange mass spectrometry experiments, tandem MS is used to confirm the identity and sequence of peptic peptides.

In an MS/MS experiment, specific ions are isolated (precursors) and then fragmented to produce smaller ions (fragments). Mass measurements of fragment ions are later used to confirm a peptides' amino acid sequence. Once a precursor is identified, the quadrupole (**Fig 1.12f**) isolates the ion and directs it to the collision cell (**Fig 1.12g**). A quadrupole mass selector is composed of four circular rods. Alternating current (AC) and direct current (DC) voltages are applied to the rods creating an electric field. Ions traveling through the quadrupole are guided by the electrical field present. By carefully changing the AC and DC voltages, it is possible to isolate a specific m/z range value to travel through the quadrupole and expel other ions.

Once the precursor is isolated, it is transferred to the hexapole or collision cell (Fig 1.12g), where an inert gas is present, and a small voltage is applied to force collision induce dissociation (CID) between molecules. This CID fragmentation occurs in two steps. First, precursor ions are excited to higher energy levels by forcing collisions with the inert gas, and secondly, a unimolecular dissociation occurs, where

the excited precursor ions fragment and form a smaller ion and a neutral molecule.[115] Both precursor and ions fragments are later guided and focused again by an octopole ion guide (**Figure 1.12h**), continuing the normal process in the time of flight tube to get the mass-to-charge ratio of the ions.

For peptides, CID usually induces fragmentation at the peptide bond (**Figure 1.13**), producing N-terminal ions positively charged at the carbonyl atom of the peptide bond (b-ions) or C-terminal ions charged at the amine atom of the peptide bond (y-ions; see **Figure 1.13**). This process happens for all precursor molecules and produces several b- and y-ions later analyzed to produce an MS/MS spectrum. Automated software can identify peaks in the MS/MS spectrum, match them with the theoretical values, and confirm the peptide sequences.

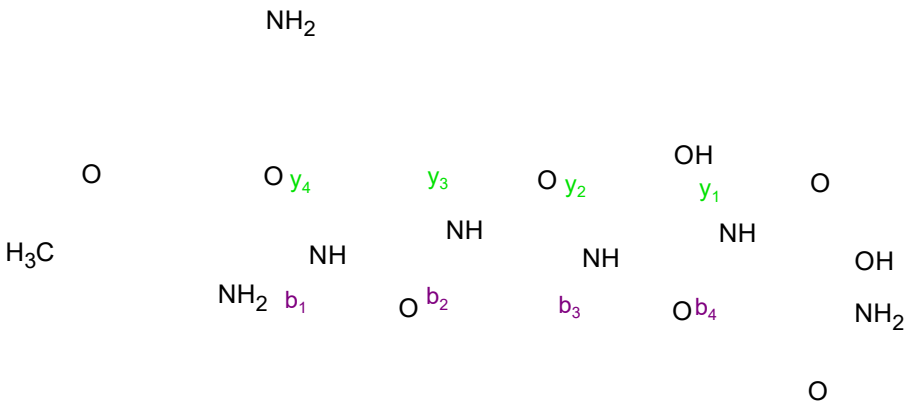

Figure 1.13 Possible CID fragments for GluLysGlySerAsn peptide. CID fragmentation can produce b-ions (purple) or y-ions (green).

1.5. OVERVIEW OF THE DISSERTATION

The production of protein therapeutics (e.g, monoclonal antibodies) has skyrocketed in the last 20 years, mainly because of high specificity and therapeutic properties. However, some protein therapeutics can still have serious secondary effects on human health.[116,117] The use of tunable therapeutics, where the molecule's activity can be closely controlled, might be a good solution to reduce secondary effects. Protein switches are proteins where the function or activity can be controlled as desired by different methods.[118]

An interesting approach to protein switches is the use of a chemical rescue of the structure. This approach uses a cavity-forming mutation in the protein to disrupt the structure and decrease the protein activity. Later, the addition of a small molecule allows for a partial or full restoration of the active structure with the desired therapeutic properties. Hence, the activity of these protein switches can be modulated by the addition of a small molecule.

In Chapter 2, hydrogen exchange MS is used to identify structural changes on an anti-fluorescein single-chain variable fragment (scFv) with and without a cavity-forming mutation. Previously obtained data showed that by adding indole into the solution, the scFv structure is rescued, and the activity is partially restored. Thus, HX-MS experiments assessed and compared the rescued scFv structure to the wild-type structure.

Affinity chromatography is widely used for antibody purification in biopharmaceutical production due to its high selectivity and ease of use. This process involves the use of affinity matrixes that bind specifically to antibodies. Although evidence suggests that some antibodies undergo allosteric structural changes upon binding, allosteric changes in the antibody structure have not been well-explored when bound to an affinity chromatography matrix.

In Chapter 3, HX-MS revealed conformational changes in the NIST reference mAb, an IgG1 antibody, upon binding with a commercially available protein A (ProA) matrix. Two experimental approaches were followed. In one approach, protein A was free in solution. In the other, protein A was covalently attached to a resin.

The stability of protein therapeutics is concerning. Small changes in protein structure could lead to aggregation, loss of activity, or immunogenic effects, among others. Notably, pH has a critical role in the stability of antibodies, and it has been shown that low pH values might cause antibody loss of tertiary structure and denaturation. Moreover, pH is crucial in controlling many degradation pathways, such as deamidation and oxidation.

It is known that pH changes in formulation buffers could lead to changes in the aggregation propensity and general molecule stability. However, there is no information on specific structural changes in antibodies at different pH values. In Chapter 4, HX-MS evaluated structural changes in the NIST reference mAb when changing the formulation pH of the antibody. Four pH values were evaluated that encompass the whole physiological range and common formulation of pH values.

1.6. REFERENCES

1. Nelson DL, Lehninger AL, Cox MM. 2008. Lehninger Principles of Biochemistry. ed.: W. H. Freeman.
2. Voet D, Voet, J., Pratt, C. 2019. Fundamentals of Biochemistry: Life at the Molecular Level. 5th ed.: Wiley.
3. Ozgur A, Tutar Y 2013. Therapeutic proteins: A to Z. Protein Pept Lett 20(12):1365-1372.
4. Leader B, Baca QJ, Golan DE 2008. Protein therapeutics: a summary and pharmacological classification. Nat Rev Drug Discov 7(1):21-39.
5. Usmani SS, Bedi G, Samuel JS, Singh S, Kalra S, Kumar P, Ahuja AA, Sharma M, Gautam A, Raghava GPS 2017. THPdb: Database of FDA-approved peptide and protein therapeutics. PLoS One 12(7):e0181748.
6. Riedel S 2005. Edward Jenner and the history of smallpox and vaccination. Proc (Bayl Univ Med Cent) 18(1):21-25.
7. Demain AL, Vaishnav P 2009. Production of recombinant proteins by microbes and higher organisms. Biotechnology Advances 27(3):297-306.
8. Goeddel DV, Kleid DG, Bolivar F, Heyneker HL, Yansura DG, Crea R, Hirose T, Kraszewski A, Itakura K, Riggs AD 1979. Expression in Escherichia coli of chemically synthesized genes for human insulin. Proceedings of the National Academy of Sciences 76(1):106-110.
9. Kaplon H, Reichert JM 2019. Antibodies to watch in 2019. MAbs 11(2):219-238.
10. Tsumoto K, Isozaki Y, Yagami H, Tomita M 2019. Future perspectives of therapeutic monoclonal antibodies. Immunotherapy 11(2):119-127.
11. Lagassé HAD, Alexaki A, Simhadri VL, Katagiri NH, Jankowski W, Sauna ZE, Kimchi-Sarfaty C 2017. Recent advances in (therapeutic protein) drug development. F1000Research 6:113-113.
12. Berg J, Tymoczko JL., Stryer, L. 2002. Biochemistry. 5th ed., New York: W H Freeman.
13. Buxbaum E. 2007. Fundamentals of Protein Structure and Function. 1st ed.: Springer.
14. Anfinsen CB 1973. Principles that Govern the Folding of Protein Chains. Science 181(4096):223-230.
15. Saibil H 2013. Chaperone machines for protein folding, unfolding and disaggregation. Nature reviews Molecular cell biology 14(10):630-642.
16. Leman JK, Weitzner BD, Lewis SM, Adolf-Bryfogle J, Alam N, Alford RF, Aprahamian M, Baker D, Barlow KA, Barth P, Basanta B, Bender BJ, Blacklock K, Bonet J, Boyken SE, Bradley P, Bystroff C, Conway P, Cooper S, Correia BE, Coventry B, Das R, De Jong RM, DiMaio F, Dsilva L, Dunbrack R, Ford AS, Frenz B, Fu DY, Geniesse C, Goldschmidt L, Gowthaman R, Gray JJ, Gront D,

Guffy S, Horowitz S, Huang P-S, Huber T, Jacobs TM, Jeliazkov JR, Johnson DK, Kappel K, Karanicolas J, Khakzad H, Khar KR, Khare SD, Khatib F, Khramushin A, King IC, Kleffner R, Koepnick B, Kortemme T, Kuenze G, Kuhlman B, Kuroda D, Labonte JW, Lai JK, Lapidoth G, Leaver-Fay A, Lindert S, Linsky T, London N, Lubin JH, Lyskov S, Maguire J, Malmström L, Marcos E, Marcu O, Marze NA, Meiler J, Moretti R, Mulligan VK, Nerli S, Norn C, Ó'Conchúir S, Ollikainen N, Ovchinnikov S, Pacella MS, Pan X, Park H, Pavlovicz RE, Pethe M, Pierce BG, Pilla KB, Raveh B, Renfrew PD, Burman SSR, Rubenstein A, Sauer MF, Scheck A, Schief W, Schueler-Furman O, Sedan Y, Sevy AM, Sgourakis NG, Shi L, Siegel JB, Silva D-A, Smith S, Song Y, Stein A, Szegedy M, Teets FD, Thyme SB, Wang RY-R, Watkins A, Zimmerman L, Bonneau R 2020. Macromolecular modeling and design in Rosetta: recent methods and frameworks. Nature Methods 17(7):665-680.

17. Senior AW, Evans R, Jumper J, Kirkpatrick J, Sifre L, Green T, Qin C, Žídek A, Nelson AWR, Bridgland A, Penedones H, Petersen S, Simonyan K, Crossan S, Kohli P, Jones DT, Silver D, Kavukcuoglu K, Hassabis D 2020. Improved protein structure prediction using potentials from deep learning. Nature 577(7792):706-710.

18. Rehman I, Kerndt CC, Botelho S. 2020. Biochemistry, Tertiary Protein Structure. StatPearls, ed., Treasure Island (FL): StatPearls Publishing.

19. Vidarsson G, Dekkers G, Rispens T 2014. IgG Subclasses and Allotypes: From Structure to Effector Functions. Frontiers in Immunology 5:520.

20. Schroeder HW, Jr., Cavacini L 2010. Structure and function of immunoglobulins. J Allergy Clin Immunol 125(2 Suppl 2):S41-S52.

21. Anumula KR 2012. Quantitative glycan profiling of normal human plasma derived immunoglobulin and its fragments Fab and Fc. Journal of Immunological Methods 382(1):167-176.

22. Zauner G, Selman MH, Bondt A, Rombouts Y, Blank D, Deelder AM, Wuhrer M 2013. Glycoproteomic analysis of antibodies. Mol Cell Proteomics 12(4):856-865.

23. Mimura Y, Katoh T, Saldova R, O'Flaherty R, Izumi T, Mimura-Kimura Y, Utsunomiya T, Mizukami Y, Yamamoto K, Matsumoto T, Rudd PM 2018. Glycosylation engineering of therapeutic IgG antibodies: challenges for the safety, functionality and efficacy. Protein & Cell 9(1):47-62.

24. Shields RL, Namenuk AK, Hong K, Meng YG, Rae J, Briggs J, Xie D, Lai J, Stadlen A, Li B 2001. High resolution mapping of the binding site on human IgG1 for FcγRI, FcγRII, FcγRIII, and FcRn and design of IgG1 variants with improved binding to the FcγR. Journal of Biological Chemistry 276(9):6591-6604.

25. Davies J, Jiang L, Pan LZ, LaBarre MJ, Anderson D, Reff M 2001. Expression of GnTIII in a recombinant anti-CD20 CHO production cell line: expression of antibodies with altered glycoforms leads

to an increase in ADCC through higher affinity for FCγRIII. Biotechnology and bioengineering 74(4):288-294.
26. Umaña P, Jean–Mairet J, Moudry R, Amstutz H, Bailey JE 1999. Engineered glycoforms of an antineuroblastoma IgG1 with optimized antibody-dependent cellular cytotoxic activity. Nature biotechnology 17(2):176-180.
27. Kelton W, Mehta N, Charab W, Lee J, Lee C-h, Kojima T, Kang TH, Georgiou G 2014. IgGA: a "cross-isotype" engineered human Fc antibody domain that displays both IgG-like and IgA-like effector functions. Chemistry & biology 21(12):1603-1609.
28. Michaelsen T, WESTBY AAC, Sandlie I 1990. Enhancement of complement activation and cytolysis of human IgG3 by deletion of hinge exons. Scandinavian journal of immunology 32(5):517-528.
29. Natsume A, In M, Takamura H, Nakagawa T, Shimizu Y, Kitajima K, Wakitani M, Ohta S, Satoh M, Shitara K 2008. Engineered antibodies of IgG1/IgG3 mixed isotype with enhanced cytotoxic activities. Cancer Research 68(10):3863-3872.
30. Lazar GA, Dang W, Karki S, Vafa O, Peng JS, Hyun L, Chan C, Chung HS, Eivazi A, Yoder SC 2006. Engineered antibody Fc variants with enhanced effector function. Proceedings of the National Academy of Sciences 103(11):4005-4010.
31. Saunders KO 2019. Conceptual Approaches to Modulating Antibody Effector Functions and Circulation Half-Life. Frontiers in Immunology 10(1296).
32. Torosantucci R, Schöneich C, Jiskoot W 2014. Oxidation of Therapeutic Proteins and Peptides: Structural and Biological Consequences. Pharmaceutical research 31(3):541-553.
33. Gamage CLD, Hageman TS, Weis DD 2019. Rapid Prediction of Deamidation Rates of Proteins to Assess Their Long-Term Stability Using Hydrogen Exchange-Mass Spectrometry. Journal of pharmaceutical sciences 108(6):1964-1972.
34. Wilkening A, Rüb C, Sylvester M, Voos W 2018. Analysis of heat-induced protein aggregation in human mitochondria. The Journal of biological chemistry 293(29):11537-11552.
35. Brange J, Andersen L, Laursen ED, Meyn G, Rasmussen E 1997. Toward understanding insulin fibrillation. Journal of pharmaceutical sciences 86(5):517-525.
36. Li DY, Borkman RF, Wang RH, Dillon J 1990. Mechanisms of photochemically produced turbidity in lens protein solutions. Exp Eye Res 51(6):663-669.
37. Roy S, Henderson I, Nayar R, Randolph TW, Carpenter JF 2008. Effect of pH on stability of recombinant botulinum serotype A vaccine in aqueous solution and during storage of freeze-dried formulations. Journal of pharmaceutical sciences 97(12):5132-5146.

38. Van Buren N, Rehder D, Gadgil H, Matsumura M, Jacob J 2009. Elucidation of two major aggregation pathways in an IgG2 antibody. Journal of pharmaceutical sciences 98(9):3013-3030.
39. Katayama DS, Nayar R, Chou DK, Valente JJ, Cooper J, Henry CS, Vander Velde DG, Villarete L, Liu CP, Manning MC 2006. Effect of buffer species on the thermally induced aggregation of interferon-tau. Journal of pharmaceutical sciences 95(6):1212-1226.
40. Tsai AM, van Zanten JH, Betenbaugh MJ 1998. II. Electrostatic effect in the aggregation of heat-denatured RNase A and implications for protein additive design. Biotechnol Bioeng 59(3):281-285.
41. Sluzky V, Klibanov AM, Langer R 1992. Mechanism of insulin aggregation and stabilization in agitated aqueous solutions. Biotechnol Bioeng 40(8):895-903.
42. Manikwar P, Majumdar R, Hickey JM, Thakkar SV, Samra HS, Sathish HA, Bishop SM, Middaugh CR, Weis DD, Volkin DB 2013. Correlating excipient effects on conformational and storage stability of an IgG1 monoclonal antibody with local dynamics as measured by hydrogen/deuterium-exchange mass spectrometry. Journal of pharmaceutical sciences 102(7):2136-2151.
43. Kiese S, Papppenberger A, Friess W, Mahler HC 2008. Shaken, not stirred: mechanical stress testing of an IgG1 antibody. Journal of pharmaceutical sciences 97(10):4347-4366.
44. Chen B, Costantino HR, Liu J, Hsu CC, Shire SJ 1999. Influence of calcium ions on the structure and stability of recombinant human deoxyribonuclease I in the aqueous and lyophilized states. Journal of Pharmaceutical Sciences 88(4):477-482.
45. 2010. External Factors Affecting Protein Aggregation. Aggregation of Therapeutic Proteins, ed. p 119-204.
46. Filipe V, Jiskoot W, Basmeleh AH, Halim A, Schellekens H, Brinks V 2012. Immunogenicity of different stressed IgG monoclonal antibody formulations in immune tolerant transgenic mice. MAbs 4(6):740-752.
47. Uchino T, Miyazaki Y, Yamazaki T, Kagawa Y 2017. Immunogenicity of protein aggregates of a monoclonal antibody generated by forced shaking stress with siliconized and nonsiliconized syringes in BALB/c mice. J Pharm Pharmacol 69(10):1341-1351.
48. Rodwell VW, Bender D, Botham KM, Kennelly PJ, Weil PA. 2018. Harper's Illustrated Biochemistry Thirty-First Edition. ed.: McGraw-Hill Education.
49. Frank AM, Savitski MM, Nielsen ML, Zubarev RA, Pevzner PA 2007. De novo peptide sequencing and identification with precision mass spectrometry. J Proteome Res 6(1):114-123.
50. Miles AJ, Wallace BA. 2015. Chapter 6 - Circular Dichroism Spectroscopy for Protein Characterization: Biopharmaceutical Applications. In Houde DJ, Berkowitz SA, editors. Biophysical Characterization of Proteins in Developing Biopharmaceuticals, ed., Amsterdam: Elsevier. p 109-137.

51. Ravi J, Hills AE, Knight AE 2009. Reproducible circular dichroism measurements for biopharmaceutical applications. Advances in Biomedical Spectroscopy 1:125-140.
52. Durowoju IB, Bhandal KS, Hu J, Carpick B, Kirkitadze M 2017. Differential Scanning Calorimetry - A Method for Assessing the Thermal Stability and Conformation of Protein Antigen. J Vis Exp (121):55262.
53. Wolpert M, Hellwig P 2006. Infrared spectra and molar absorption coefficients of the 20 alpha amino acids in aqueous solutions in the spectral range from 1800 to 500cm−1. Spectrochimica Acta Part A: Molecular and Biomolecular Spectroscopy 64(4):987-1001.
54. Surewicz WK, Mantsch HH 1988. New insight into protein secondary structure from resolution-enhanced infrared spectra. Biochimica et Biophysica Acta (BBA) - Protein Structure and Molecular Enzymology 952:115-130.
55. Liu XR, Zhang MM, Gross ML 2020. Mass Spectrometry-Based Protein Footprinting for Higher-Order Structure Analysis: Fundamentals and Applications. Chemical Reviews 120(10):4355-4454.
56. McPherson A, Gavira JA 2014. Introduction to protein crystallization. Acta Crystallogr F Struct Biol Commun 70(Pt 1):2-20.
57. Garbuzynskiy SO, Melnik BS, Lobanov MY, Finkelstein AV, Galzitskaya OV 2005. Comparison of X-ray and NMR structures: Is there a systematic difference in residue contacts between X-ray- and NMR-resolved protein structures? Proteins: Structure, Function, and Bioinformatics 60(1):139-147.
58. Bax A, Grzesiek S 1993. Methodological advances in protein NMR. Accounts of Chemical Research 26(4):131-138.
59. Mainz A, Religa TL, Sprangers R, Linser R, Kay LE, Reif B 2013. NMR Spectroscopy of Soluble Protein Complexes at One Mega-Dalton and Beyond. Angewandte Chemie International Edition 52(33):8746-8751.
60. Callaway E 2015. The revolution will not be crystallized: a new method sweeps through structural biology. Nature News 525(7568):172.
61. Milne JLS, Borgnia MJ, Bartesaghi A, Tran EEH, Earl LA, Schauder DM, Lengyel J, Pierson J, Patwardhan A, Subramaniam S 2013. Cryo-electron microscopy--a primer for the non-microscopist. FEBS J 280(1):28-45.
62. Merk A, Bartesaghi A, Banerjee S, Falconieri V, Rao P, Davis MI, Pragani R, Boxer MB, Earl LA, Milne JLS, Subramaniam S 2016. Breaking Cryo-EM Resolution Barriers to Facilitate Drug Discovery. Cell 165(7):1698-1707.
63. Liu XR, Rempel DL, Gross ML 2020. Protein higher-order-structure determination by fast photochemical oxidation of proteins and mass spectrometry analysis. Nat Protoc 15(12):3942-3970.

64. Gygi SP, Rist B, Gerber SA, Turecek F, Gelb MH, Aebersold R 1999. Quantitative analysis of complex protein mixtures using isotope-coded affinity tags. Nat Biotechnol 17(10):994-999.
65. Anson ML 1940. THE REACTIONS OF IODINE AND IODOACETAMIDE WITH NATIVE EGG ALBUMIN. Journal of General Physiology 23(3):321-331.
66. Koshland DE, Karkhanis YD, Latham HG 1964. An Environmentally-Sensitive Reagent with Selectivity for the Tryptophan Residue in Proteins. Journal of the American Chemical Society 86(7):1448-1450.
67. Riordan JF, Sokolovsky M, Vallee BL 1966. Tetranitromethane. A Reagent for the Nitration of Tyrosine and Tyrosyl Residues of Proteins1. Journal of the American Chemical Society 88(17):4104-4105.
68. Takahashi K 1968. The reaction of phenylglyoxal with arginine residues in proteins. J Biol Chem 243(23):6171-6179.
69. Xu G, Chance MR 2007. Hydroxyl Radical-Mediated Modification of Proteins as Probes for Structural Proteomics. Chemical Reviews 107(8):3514-3543.
70. Jones LM, B. Sperry J, A. Carroll J, Gross ML 2011. Fast Photochemical Oxidation of Proteins for Epitope Mapping. Analytical Chemistry 83(20):7657-7661.
71. Li KS, Rempel DL, Gross ML 2016. Conformational-Sensitive Fast Photochemical Oxidation of Proteins and Mass Spectrometry Characterize Amyloid Beta 1–42 Aggregation. Journal of the American Chemical Society 138(37):12090-12098.
72. Stocks BB, Konermann L 2009. Structural Characterization of Short-Lived Protein Unfolding Intermediates by Laser-Induced Oxidative Labeling and Mass Spectrometry. Analytical Chemistry 81(1):20-27.
73. Cheng M, Zhang B, Cui W, Gross ML 2017. Laser-Initiated Radical Trifluoromethylation of Peptides and Proteins: Application to Mass-Spectrometry-Based Protein Footprinting. Angewandte Chemie International Edition 56(45):14007-14010.
74. Zhang B, Rempel DL, Gross ML 2016. Protein Footprinting by Carbenes on a Fast Photochemical Oxidation of Proteins (FPOP) Platform. Journal of the American Society for Mass Spectrometry 27(3):552-555.
75. Xu G, Kiselar J, He Q, Chance MR 2005. Secondary Reactions and Strategies To Improve Quantitative Protein Footprinting. Analytical Chemistry 77(10):3029-3037.
76. Boys BL, Kuprowski MC, Noël JJ, Konermann L 2009. Protein Oxidative Modifications During Electrospray Ionization: Solution Phase Electrochemistry or Corona Discharge-Induced Radical Attack? Analytical Chemistry 81(10):4027-4034.

77. Toth RTt, Angalakurthi SK, Van Slyke G, Vance DJ, Hickey JM, Joshi SB, Middaugh CR, Volkin DB, Weis DD, Mantis NJ 2017. High-Definition Mapping of Four Spatially Distinct Neutralizing Epitope Clusters on RiVax, a Candidate Ricin Toxin Subunit Vaccine. Clin Vaccine Immunol 24(12):e00237-00217.
78. Lim X-X, Chandramohan A, Lim X-YE, Crowe Jr JE, Lok S-M, Anand GS 2017. Epitope and paratope mapping reveals temperature-dependent alterations in the dengue-antibody interface. Structure 25(9):1391-1402. e1393.
79. Hvidt A, LinderstrØM-Lang K 1954. Exchange of hydrogen atoms in insulin with deuterium atoms in aqueous solutions. Biochim Biophys Acta 14(4):574-575.
80. Wales TE, Engen JR 2006. Hydrogen exchange mass spectrometry for the analysis of protein dynamics. Mass Spectrometry Reviews 25(1):158-170.
81. Zhang Z, Smith DL 1993. Determination of amide hydrogen exchange by mass spectrometry: a new tool for protein structure elucidation. Protein science : a publication of the Protein Society 2(4):522-531.
82. McAllister RG, Konermann L 2015. Challenges in the Interpretation of Protein H/D Exchange Data: A Molecular Dynamics Simulation Perspective. Biochemistry 54(16):2683-2692.
83. Skinner JJ, Lim WK, Bédard S, Black BE, Englander SW 2012. Protein hydrogen exchange: testing current models. Protein science : a publication of the Protein Society 21(7):987-995.
84. Berger A, Loewenstein A, Meiboom S 1959. Nuclear Magnetic Resonance Study of the Protolysis and Ionization of N-Methylacetamide1. Journal of the American Chemical Society 81(1):62-67.
85. Perrin CL 1989. Proton exchange in amides: Surprises from simple systems. Accounts of Chemical Research 22(8):268-275.
86. Jensen PF, Rand KD. 2016. Hydrogen Exchange. Hydrogen Exchange Mass Spectrometry of Proteins, ed. p 1-17.
87. Bai Y, Milne JS, Mayne L, Englander SW 1993. Primary structure effects on peptide group hydrogen exchange. Proteins 17(1):75-86.
88. Nguyen D, Mayne L, Phillips MC, Walter Englander S 2018. Reference Parameters for Protein Hydrogen Exchange Rates. Journal of the American Society for Mass Spectrometry 29(9):1936-1939.
89. Smith DL, Deng Y, Zhang Z 1997. Probing the non-covalent structure of proteins by amide hydrogen exchange and mass spectrometry. J Mass Spectrom 32(2):135-146.
90. Molday R, Englander S, Kallen R 1972. Primary structure effects on peptide group hydrogen exchange. Biochemistry 11(2):150-158.

91. Englander SW, Kallenbach NR 1983. Hydrogen exchange and structural dynamics of proteins and nucleic acids. Quarterly Reviews of Biophysics 16(4):521-655.
92. Carter JV, Knox DG, Rosenberg A 1978. Pressure effects on folded proteins in solution. Hydrogen exchange at elevated pressures. J Biol Chem 253(6):1947-1953.
93. Hvidt A, Nielsen SO. 1966. Hydrogen Exchange in Proteins. In Anfinsen CB, Anson ML, Edsall JT, Richards FM, editors. Advances in Protein Chemistry, ed.: Academic Press. p 287-386.
94. Wales TE, Eggertson MJ, Engen JR 2013. Considerations in the analysis of hydrogen exchange mass spectrometry data. Methods Mol Biol 1007:263-288.
95. Skinner JJ, Lim WK, Bédard S, Black BE, Englander SW 2012. Protein dynamics viewed by hydrogen exchange. Protein science : a publication of the Protein Society 21(7):996-1005.
96. Truhlar SM, Croy CH, Torpey JW, Koeppe JR, Komives EA 2006. Solvent accessibility of protein surfaces by amide H/2H exchange MALDI-TOF mass spectrometry. J Am Soc Mass Spectrom 17(11):1490-1497.
97. LeMaster DM, Anderson JS, Hernández G 2009. Peptide conformer acidity analysis of protein flexibility monitored by hydrogen exchange. Biochemistry 48(39):9256-9265.
98. Anderson JS, Hernández G, Lemaster DM 2008. A billion-fold range in acidity for the solvent-exposed amides of Pyrococcus furiosus rubredoxin. Biochemistry 47(23):6178-6188.
99. Wooll JO, Wrabl JO, Hilser VJ 2000. Ensemble modulation as an origin of denaturant-independent hydrogen exchange in proteins11Edited by I. Wilson. Journal of Molecular Biology 301(2):247-256.
100. Glasoe PK, Long FA 1960. USE OF GLASS ELECTRODES TO MEASURE ACIDITIES IN DEUTERIUM OXIDE1,2. The Journal of Physical Chemistry 64(1):188-190.
101. Espada A, Haro R, Castañon J, Sayago C, Perez-Cozar F, Cano L, Redero P, Molina-Martin M, Broughton H, Stites RE, Pascal BD, Griffin PR, Dodge JA, Chalmers MJ 2019. A Decoupled Automation Platform for Hydrogen/Deuterium Exchange Mass Spectrometry Experiments. Journal of the American Society for Mass Spectrometry 30(12):2580-2583.
102. Pan J, Han J, Borchers CH, Konermann L 2009. Hydrogen/deuterium exchange mass spectrometry with top-down electron capture dissociation for characterizing structural transitions of a 17 kDa protein. J Am Chem Soc 131(35):12801-12808.
103. Hamuro Y, Tomasso JC, Coales SJ 2008. A Simple Test To Detect Hydrogen/Deuterium Scrambling during Gas-Phase Peptide Fragmentation. Analytical Chemistry 80(17):6785-6790.
104. Rand KD, Pringle SD, Murphy JP, Fadgen KE, Brown J, Engen JR 2009. Gas-Phase Hydrogen/Deuterium Exchange in a Traveling Wave Ion Guide for the Examination of Protein Conformations. Analytical Chemistry 81(24):10019-10028.

105. Kammari R, Topp EM 2019. Solid-State Hydrogen–Deuterium Exchange Mass Spectrometry (ssHDX-MS) of Lyophilized Poly-d,l-Alanine. Molecular Pharmaceutics 16(7):2935-2946.
106. Deng Y, Zhang Z, Smith DL 1999. Comparison of continuous and pulsed labeling amide hydrogen exchange/mass spectrometry for studies of protein dynamics. Journal of the American Society for Mass Spectrometry 10(8):675-684.
107. Krishna MM, Hoang L, Lin Y, Englander SW 2004. Hydrogen exchange methods to study protein folding. Methods 34(1):51-64.
108. Wang LC, Krishnamurthy S, Anand GS. 2016. Hydrogen Exchange Mass Spectrometry Experimental Design. Hydrogen Exchange Mass Spectrometry of Proteins, ed. p 19-35.
109. Hageman TS, Weis DD 2019. Reliable Identification of Significant Differences in Differential Hydrogen Exchange-Mass Spectrometry Measurements Using a Hybrid Significance Testing Approach. Analytical Chemistry 91(13):8008-8016.
110. More AS, Toth RT, Okbazghi SZ, Middaugh CR, Joshi SB, Tolbert TJ, Volkin DB, Weis DD 2018. Impact of Glycosylation on the Local Backbone Flexibility of Well-Defined IgG1-Fc Glycoforms Using Hydrogen Exchange-Mass Spectrometry. Journal of Pharmaceutical Sciences 107(9):2315-2324.
111. Arora J, Hickey JM, Majumdar R, Esfandiary R, Bishop SM, Samra HS, Middaugh CR, Weis DD, Volkin DB 2015. Hydrogen exchange mass spectrometry reveals protein interfaces and distant dynamic coupling effects during the reversible self-association of an IgG1 monoclonal antibody. MAbs 7(3):525-539.
112. Hageman TS, Weis DD 2019. Reliable Identification of Significant Differences in Differential Hydrogen Exchange-Mass Spectrometry Measurements Using a Hybrid Significance Testing Approach. Anal Chem 91(13):8008-8016.
113. Awad H, Khamis MM, El-Aneed A 2015. Mass Spectrometry, Review of the Basics: Ionization. Applied Spectroscopy Reviews 50(2):158-175.
114. Technologies A. 2011. Publication number 5990-9207EN. ed.
115. Stiving AQ, VanAernum ZL, Busch F, Harvey SR, Sarni SH, Wysocki VH 2019. Surface-Induced Dissociation: An Effective Method for Characterization of Protein Quaternary Structure. Analytical chemistry 91(1):190-209.
116. Hansel TT, Kropshofer H, Singer T, Mitchell JA, George AJ 2010. The safety and side effects of monoclonal antibodies. Nat Rev Drug Discov 9(4):325-338.
117. Sathish JG, Sethu S, Bielsky M-C, de Haan L, French NS, Govindappa K, Green J, Griffiths CEM, Holgate S, Jones D, Kimber I, Moggs J, Naisbitt DJ, Pirmohamed M, Reichmann G, Sims J, Subramanyam M, Todd MD, Van Der Laan JW, Weaver RJ, Park BK 2013. Challenges and approaches

for the development of safer immunomodulatory biologics. Nature Reviews Drug Discovery 12(4):306-324.

118. Ostermeier M 2005. Engineering allosteric protein switches by domain insertion. Protein Eng Des Sel 18(8):359-364.

2. CHAPTER TWO: STRUCTURAL CHANGES OF A SCFV AFTER CHEMICAL RESCUE

This work was adapted from Kaiser, C. E.; Rincon Pabon, J. P.; Khowsathit, J.; Castaldi, M. P.; Kazmirski, S. L.; Weis, D. D.; Zhang, A. X.; Karanicolas, J., Modulating Antibody Structure and Function through Directed Mutations and Chemical Rescue. ACS Synth Biol 2018, 7 (4), 1152-1162.

2.1. INTRODUCTION

Monoclonal antibodies are now the largest class of protein therapeutic in the market, mainly because of their ability to inhibit or activate with high specificity biological targets[1,2]. Currently, there are more than 80 therapeutic antibodies approved by the US FDA, and many more therapeutic proteins at various clinical stages[3,4]. While antibody therapeutics have many advantages, they can still have many secondary effects after administration such as anaphylaxis, cardiotoxicity or immunogenicity[5]. Some of those secondary effects are associated with suboptimal or exaggerated on-target interactions of the drug[6]. Hence, there is a need to better control antibody activity by increasing therapeutic properties while decreasing secondary effects.

Engineered protein switches are proteins where the function or activity can be controlled as desired, usually by inserting a ligand sensing domain into an output domain[7]. With this approach, one domain will display a signal recognition function and the other will have the function to be modulated. These types of protein switches are challenging to design and produce due to many challenges encountered while putting together the domains[8]. Alternatively, proteins variants with critical mutations in the binding site can be used. A mutation in the binding site could cause loss of activity of the protein that can later be restored by using a modified substrate or an exogenous ligand[9]. Similarly, a chemical rescue of the structure has been developed[10-12]. With this approach, a cavity-forming mutation is introduced in a structurally critical point for the active site and protein function is lost. Later, by the addition of an exogenous compound the structure is restored, and the protein activity is rescued. A tryptophan-to glycine mutation near the active site of a β-glycosidase caused loss of enzyme activity, that was later restored by subsequent addition of indole[10]. In this case, the rescued enzyme activity was equivalent to the corresponding wild-type. Subsequent studies suggested that a tryptophan to glycine mutation could modulate protein structure and function by a discrete conformational change or indirectly by controlling protein stability. Regardless of the mechanism that causes loss of function, the addition of indole rescued protein activity[11].

To further evaluate the chemical rescue of structure by the addition of indole after a tryptophan to glycine mutation, Kaiser *et al*. used a single chain variable fragment (scFv) that recognizes fluorescein as its antigen[13]. More specifically, using FITC-E2 scFv, a fusion protein containing immunoglobulin V_H and V_L domains connected with a linker that has been widely studied and which crystal structure is available[14]. FITC-E2 scFv has five tryptophan residues. V_H W41 and V_L W41 are in buried positions in the interior of the immunoglobulin domains. V_H W52 and V_L W107 are located in the antigen binding site and V_H W118 that is positioned at the V_H-V_L interface. Each one of those tryptophan residues were individually mutated to glycine. V_H W41G and V_L W41G mutants gave insoluble products after *E. coli* expression. Hence only FITC-E2 V_H W118G, V_H W52G and V_L W107G were expressed, purified and later evaluated for changes in activity using a fluorescence quenching assay. All three mutant variants had diminished activity compared to the wild-type scFv with V_H W52G and V_L W107G presenting a bigger effect (V_H W118G ~40%, V_H W52G ~10% and V_L W107G <10%). After the addition of 1 mM indole, all mutants had increased activity, with V_H W118G reaching almost identical activity compared to the wild-type (~90%). Moreover, titration experiments showed that rescued protein activity of V_H W118G was statistically significant at indole concentration above 50 μM with a midpoint of 220 μM and also showed clear evidence that the addition of indole induces a tighter antigen binding by the V_H W118G mutant contrary to the wild-type protein.

To confirm the direct interaction of indole with V_H W118G, an inhibition in solution assay (ISA) was employed using a fluorescein analogue[13]. As expected, increasing the concentration of free fluorescein in solution decreases the available protein to bind to the fluorescein analogue, resulting in decrease surface plasmon resonance (SPR) responses. After the addition of 150 μM indole to the incubation step, a decrease (2-fold tighter) in the half maximal inhibitory concentration (IC50) was observed, confirming that the observed rescued FITC-E2 V_H W118G activity by the addition of indole is due to enhanced binding affinity for fluorescein. Finally, knowing that changes in protein stability could be the basis of inactivation and rescue of protein activity after a tryptophan to glycine mutation[11], a differential scanning

fluorimetry (DSF) assay was employed to evaluate protein unfolding in the V_H W118G, V_H W52G and V_L W107G mutant variants[13]. In the presence of fluorescein (at a 1:1 molar ratio), all three FITC-E2 mutant variants had lower melting temperature compared to the wild-type, representative of lower thermal stability. The magnitude of the effect was higher for the V_H W118G variant. When both indole and fluorescein were added, the melting temperature of the V_H W118G variant increased by 1.4°C, indicative of higher thermal stability. Nevertheless, the presence of indole was destabilizing for the wild-type and other two mutant variants. Interestingly, that effect was not seen when only indole was present (no fluorescein). All constructs (wild-type and all three mutant variants) had a decrease in thermal stability when only indole was added. These results suggest that the V_H W118G mutant has an alternate conformation when fluorescein is present, providing the cavity needed for indole binding. Overall, the results indicate that there is a positive collaboration between fluorescein binding and indole binding, suggesting that the inactivation and later rescue of the V_H W118G variant is due to a conformational change tied to a change in protein stability.

Here, based on previous findings by Kaiser *et al*.[13], we used hydrogen exchange-mass spectrometry to evaluate possible conformational changes in the FITC-E2 WT and V_H W118G mutant variant when indole and fluorescein were added. Four constructs were compared: wild-type FITC-E2 and V_H W118G mutant (both at an intact and peptide level), wild-type FITC-E2 with and without indole and fluorescein, FITC-E2 V_H W118G mutant with and without indole and fluorescein and wild-type and V_H W118G FITC-E2 both with indole and fluorescein present.

2.2. MATERIALS AND METHODS

2.2.1. Materials

FITC-E2 WT scFv and mutant FITC-E2 V_H W118G scFv were expressed, purified, and provided by AstraZeneca (Boston, MA) as described elsewhere[13], at a concentration of 3.3 and 1.8 mg/mL,

respectively, in PBS buffer pH 7.1. Indole, fluorescein and DMSO were provided by AstraZeneca (Boston, MA). Premium grade tris (2-carboxyethyl) phosphine hydrochloride (TCEP) was purchased from ThermoScientific (Rockford, IL). Sodium phosphate dibasic (anhydrous), monosodium phosphate (anhydrous), potassium phosphate dibasic (anhydrous), sodium chloride, LC-MS grade water and LC-MS 0.1% formic acid in water were purchased from Fisher Scientific (Hampton, NH). Guanidine hydrochloride was purchased from Sigma-Aldrich (St. Louis, MO). LC-MS grade acetonitrile containing 0.1% formic acid was obtained from Burdick-Jackson (Muskegon, MI). Deuterium oxide (99+ %D) was obtained from Cambridge Isotope Laboratories (Tewksbury, MA).

2.2.2. Hydrogen exchange-mass spectrometry

FITC-E2 WT scFv and mutant FITC-E2 V_H W118G scFv stock solutions were prepared at a nominal concentration of 10 μM using a 1% (v/v) DMSO 6 mM phosphate, 135 mM sodium chloride, pD 7.11 with and without 10 μM fluorescein and 10 mM indole. All samples were incubated for at least 1 hour, stored at 4°C and used within few hours.

HX labeling was performed using a LEAP Technologies HDX PAL robot (Carrboro, NC) with a customized three-valve configuration as described previously[15]. For the intact level HX-MS experiment, deuterated samples were prepared by diluting 5 μL of the protein stock solution in 36 μL D_2O labeling buffer (1% (v/v) DMSO, 6 mM phosphate, 135 mM sodium chloride, pD 7.11 in D_2O). The pD was obtained from pH measurements with a glass electrode and corrected for deuterium isotope effect (pD = pH + 0.4)[16]. Samples were labeled for 10, 50, 100, 1000 and 10000 s at 25°C. After labeling, 40 μL of each labeled sample was quenched with 40 μL precooled quench buffer (200 mM phosphate, 4 M guanidine, 0.5 M TCEP, pH 2.5 in water) at 1°C. Non-deuterated controls were prepared identically, but using 1% (v/v) DMSO, 6 mM phosphate, 135 mM sodium chloride, pH 7.11 in H_2O. Later, 40 μL of sample was injected into an Agilent 1260 Infinity series LC system kept at 0°C. Intact protein was captured on a C12 trap (10 mm x 1 mm) (Jupiter, Phenomenex, Torrance, CA) and desalted before analysis.

For the peptide level HX-MS experiment, deuterated samples were prepared by diluting 5 µL of the protein stock solution in 36 µL D_2O labeling buffer (1% (v/v) DMSO, 6 mM phosphate, 135 mM sodium chloride, pD 6.7) with and without fluorescein and indole. Samples were labeled in triplicate for each labeling time (30, 120, 420, 1620, 6060, 22860 and 86130 s) at 25°C. After labeling, 35 µL of each labeled sample was quenched with 35 µL precooled quench buffer (200 mM phosphate, 4 M guanidine, 0.4 M TCEP, pH 2.5 in water) at 1°C. Non-deuterated controls were prepared identically, but using 1% (v/v) DMSO, 6 mM phosphate, 135 mM sodium chloride, pH 7.01 in H_2O. Immediately after, 67 µL of sample was injected into a temperature-controlled chromatography cabinet connected to an Agilent 1260 Infinity series LC system. Cabinet temperature and equipped LC solvent pre-cooler were maintained at 0°C for all experiments. Injected sample was passed over an immobilized pepsin column (2.1 × 50 mm), prepared in house, at 200 µL min^{-1} for 180 s with 0.1% formic acid in H_2O. The resulting peptic peptides were captured on a Poroshell 120 SB-C18 trap (2.1 × 5 mm, 2.7 µm particles) and washed at 200 µL min^{-1} for 60 s with 0.1% formic acid in H_2O. Desalted peptic peptides were separated on a ZORBAX RRHD C18 column (2.1 × 50 mm, 1.8 µm particles) with a linear gradient of 0.1% formic acid in acetonitrile. Peptide masses were subsequently measured with an Agilent 6530 Q-TOF mass spectrometer running in ESI-positive mode. Pepsin column washes were performed between each sample injection during the elution step to minimize peptide carry-over[15]. Undeuterated scFv peptic peptides were identified by a combination of data-dependent and targeted CID-MS2 in the QTOF using the same LC gradient. MS2 spectra were matched to the scFv sequence, with fixed modifications, using Agilent BioConfirm B.07. FITC-E2 WT scFv peptide digestion resulted in 77% sequence coverage (see **Figure 2.A-1**) and V_H W118G in 100% sequence coverage (see **Figure 2.A-2**). A total of 44 unique peptides were present for both the wild-type and the W118G mutant corresponding to a 73% sequence coverage (see **Figure 2.A-3**).

All HX-MS experiments were performed consecutively spanning 48 hours. HX-MS data was analyzed using HDExaminer (v. 2.2.0, Sierra Analytics, Modesto, CA) and results were manually reviewed and curated.

Peptide level data set comparing WT scFv and W118G scFv had a pooled standard deviation of 0.15 Da, WT scFv and WT scFv with indole and fluorescein (WT+IF) 0.18 Da, W118G and W118G with indole and fluorescein (W118G+IF) 0.12 Da and WT and W118G both with indole and fluorescein had 0.15 Da. Differential HX data were tested for significance using the hybrid significance testing criteria method[17] using an in-house Matlab script. Mean HX differences from labeling replicates were classified as significant when the mean centroid mass difference of each peptide at each labeling time point (ΔD) was higher than a critical value (0.71 Da for the WT vs W118G comparison, 0.86 Da for WT vs WT+IF comparison, 0.57 Da for the W118G vs W118G+IF and 0.70 Da for the WT+IF vs W118G+IF comparison), and a Welch's two-sample t test had $p < 0.01$. Normalized HX differences (ΔHX) for each peptide were obtained by dividing by the theoretical maximum exchange (number of backbone amide hydrogens in each peptide, excluding the N-terminal amide). The absolute values of the normalized differences were then clustered using k-means clustering with $k = 3$ to define thresholds for strong, moderate, and negligible HX differences as described previously[18,19]. For visualization of the HX observations, crystal structure of the anti-fluorescein scFv FITC-E2 was used (PBD 2A9N[14]). Peptides with strong or moderate effects as shown by the k-means clustering were mapped onto the homology model. When two overlapping peptides had different clustering, priority was given to the strongest effect.

2.3. RESULTS

Hydrogen exchange-mass spectrometry was employed to identify conformational changes in a single chain variable fragment that recognizes fluorescein as its antigen (FITC-E2) and its mutant V_H W118G variant with and without the addition of indole and fluorescein. FITC-E2 wild-type scFv and the V_H W118G mutant were compared directly at an intact level. Additionally, four states were measured at a

peptide level: FITC-E2 wild-type scFv, FITC-E2 wild-type scFv in the presence of indole and fluorescein, mutant FITC-E2 V_H W118G and mutant FITC-E2 V_H W118G in the presence of indole and fluorescein.

2.3.1. FITC-E2 WT and VH W118G variant are structurally different

HX-MS measurements at an intact protein level on FITC-E2 wild-type and V_H W118G variant show different deuterium uptake (see **Figure 2.1**). V_H W118G mutant had increased deuterium uptake compared to wild-type, demonstrating that FITC-E2 V_H W118G is more flexible and solvent exposed than the wild-type. These data suggest that V_H W118G mutant is structurally different from the wild-type, however, it is impossible to locate the structural differences. To evaluate where the differences are located, a peptide level HX experiment was developed.

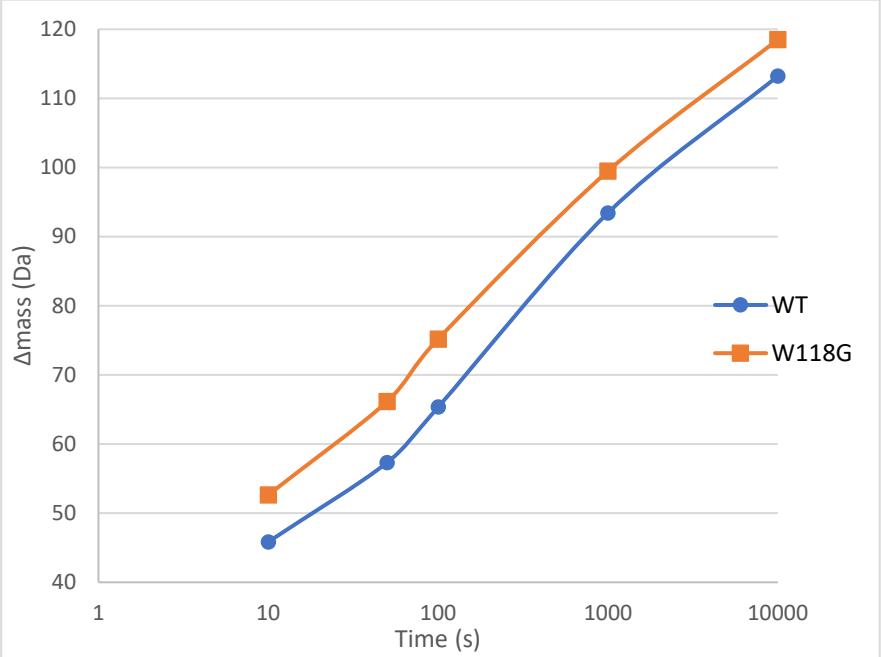

Figure 2.14. Deuterium uptake plots for scFv WT and W118G variant at an intact level

Statistical analysis of the peptide level HX experiment comparing FITC-E2 wild-type and the W118G mutant variant (see **Figure 2.2**) shows many peptides with increased flexibility in the V_H W118G variant. Residues 1-10, 18-23, 27-46, 69-93, 114-122 and 175-178 (peptide number 1, 6, 9-11, 17-18,

25, 27-29, 33-34 and 36) were strongly deprotected (blue bars and dots in Figure 2.2). These residues encompass most of the V_H domain in the FITC-E2 protein including the mutation site W118G (see **Figure 2.6A**). Residues 11-17, 24-26, 47-53, 102-107 and 155-168 (peptide numbers 2-4, 7, 12-15, 18, 30 and 35) showed intermediate increase in flexibility compared to the wild-type protein (green dots and regions). A single timepoint in peptide 22 (residues 53-68) showed increase protection in the V_H W118G compared to the wild-type. No other timepoint in the same peptide showed statistically significant differences and overlapping peptides on the same region had no significant differences either. Hence, this intermediate increase in protection can be classified as a false positive in the experiment. Poor sequence coverage in the V_L domain makes complicated to identify changes in that region. Overall, V_H W118G showed a strong increase in flexibility along the whole V_H domain and in parts of the V_L domain, consistent with a major change in protein structure compared to the wild-type.

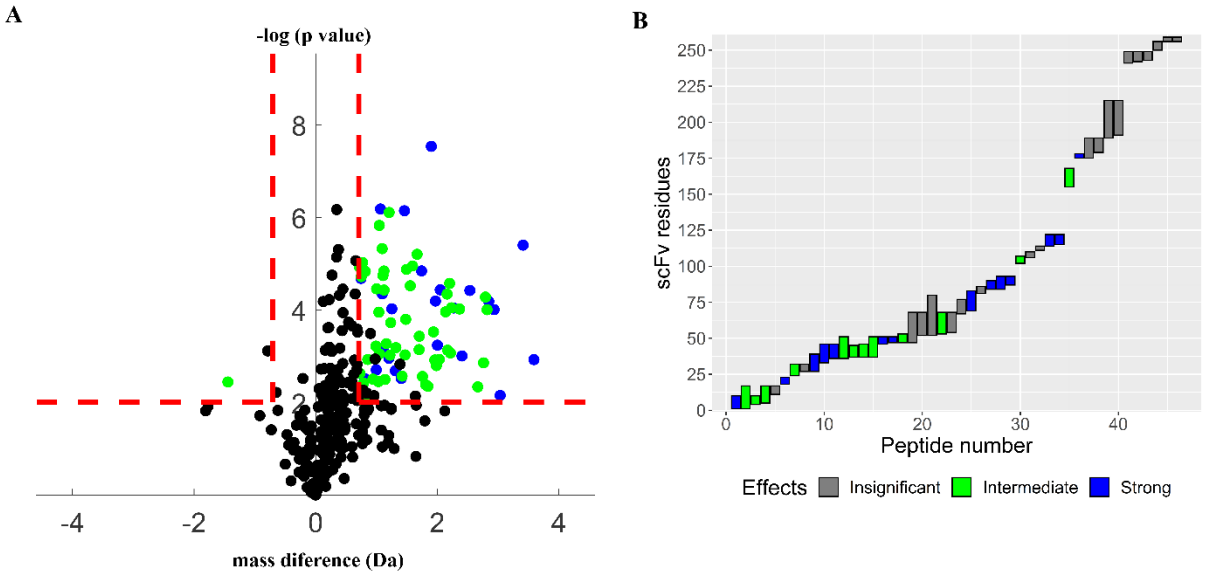

Figure 2.15 Peptides with increased deprotection in VH W118G compared to the wild-type as revealed by HX-MS experiments. (A) volcano plot for identification of peptides with significant differences and magnitude of the effects. Negligible (black), moderate (green) and strong (blue) effects as revealed by k-means clustering of the data. Red dashed lines in the volcano plot represent significance thresholds (horizontal significance threshold = 2, vertical significance threshold = ±0.7087 Da) as defined by Hageman et al.[17] Note: black dots above the threshold limits are statistically significant but considered negligible effects since the normalized magnitude is small. (b) Bar plot showing the classification and magnitude of the effects on the peptides measured by HX-MS. The vertical axis shows the protein residues numbers and the horizontal axis the peptide number.

2.3.2. Comparison of FITC-E2 WT scFv with and without indole and fluorescein

HX-MS experiments of the WT scFv in the presence of indole and fluorescein show several peptides with increased protection from hydrogen exchange compared to the WT scFv alone. WT scFv was used as the reference state for the comparison. These experiments had an unusually high pooled standard deviation (SD_{pooled}: 0.18 Da for this data set) mainly due to low MS signal intensity coming from the peptides. An increase in SD provokes an increase in the threshold significance limit for the data set. However, statistical analysis of the data (see **Figure 2.3**) identified four peptides strongly protected in the presence of indole and fluorescein (peptide number 21-22, 39 and 41; residues 46-51, 102-107, 111-114) and few more intermediately protected (peptide numbers 2-3, 11, 14, 16, 20, 23-25, 28, 42 and 44; residues 1-17, 27-46, 52-68, 155-134). Note that Figure 2.3A shows other peptides that pass the significance limit threshold (black dots on volcano plot passing red dashed lines). Those peptides were later classified as insignificant by the k-means clustering when the effects were normalized by the total number of exchangeable amides in the peptide. Fluorescein binds to the WT scFv FITC-E2 through the region between the V_H and V_L domains[14], since this experiment uses fluorescein, it is expected to see an increase protection from hydrogen exchange in peptides in or near the fluorescein binding zone. **Figure 2.6B** show the location of the protected peptides mapped onto the homology model. Peptides with increased protection (blue regions) are located next to the fluorescein binding site. Peptides with intermediate protection (green regions), are in or close to the fluorescein binding region. This increase in hydrogen exchange protection is expected in those regions since fluorescein binding to the scFv will block those residues, inducing local stabilization of the secondary structure and thus protecting them from hydrogen exchange.

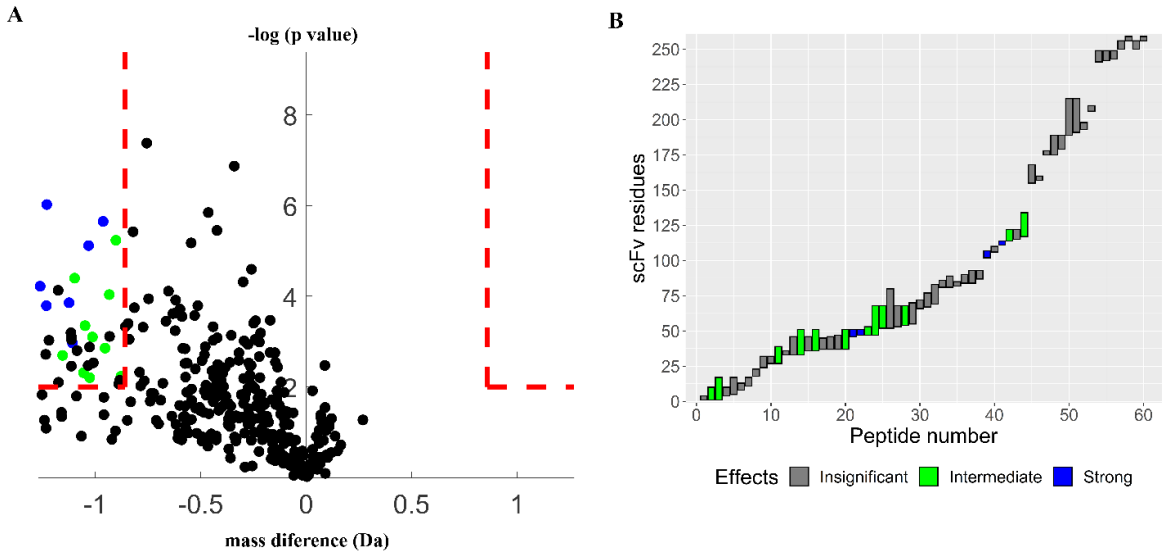

Figure 2.16. Peptides with increased protection in WT scFv in the presence of indole and fluorescein as revealed by HX-MS experiments. (A) volcano plot for identification of peptides with significant differences and magnitude of the effects. Negligible (black), moderate (green) and strong (blue) effects as revealed by k-means clustering of the data. Red dashed lines in the volcano plot represent significance thresholds (horizontal significance threshold = 2, vertical significance threshold = ±0.8581Da) as defined by Hageman et al.[17] Note: black dots above the threshold limits are statistically significant but considered negligible effects since the normalized magnitude is small. (b) Bar plot showing the classification and magnitude of the effects on the peptides measured by HX-MS. The vertical axis shows the protein residues numbers and the horizontal axis the peptide number.

2.3.3. Comparison of FITC-E2 V_H W118G scFv with and without indole and fluorescein

Introducing a tryptophan (W) to glycine (G) mutation in the interface of the two-immunoglobulin domains (W118G) leads to loss of activity of the protein[13]. This mutation seems to create a cavity in the core of the protein that alters the structure of the protein. The activity and structure of the scFv can later be restored by the addition of indole. To evaluate structural changes in the scFv W118G mutant after the addition of indole and fluorescein HX-MS was employed. For this experiment the reference state was the scFv W118G mutant without the addition of indole and fluorescein. Digestion and signal intensity for the scFv W118G was much better, resulting in 122 peptides with 100% sequence coverage (see Materials and Methods section). Statistical analysis of the data set (see **Figure 2.4**) identified many peptides strongly protected in the scFv W118G when indole and fluorescein was added (peptide number 17, 30-31, 40, 43-44, 62, 65, 68, 71-73, 80, 83, 85 and 98; residues 18-23, 34-53, 81-95, 102-107, 111-

122 and 175-178) and many more intermediately protected (peptide number 1-14, 16, 18-20, 24-25, 27-29, 32-39, 41-42, 47, 51, 55, 59-61, 63-64, 66-67, 69-70, 74-78, 84, 86-88, 90-92, 94-95, 97, 99, 105, 110-111, 113 and 115; residues 1-17, 24-33, 54-80, 96-101, 108-110, 123-174, 179-183, 189-193 and 210-257). Peptides with strong or intermediate protection on scFv W118G in the presence of indole and fluorescein encompass the whole protein sequence (except for a small number of residues in the V_L domain). **Figure 2.6C** shows the protected peptides in the scFv W118G mutant in the presence of indole and fluorescein compared to the mutant alone mapped into the homology model. It is evident that the whole protein structure changes drastically when indole and fluorescein are added into the solution. Peptides with strong hydrogen exchange protection are located immediately next to the mutation site (residue 118, red sticks in the homology model) or next to the fluorescein binding site. The rest of the protein is also intermediately affected when indole and fluorescein are added. This result strongly supports that introducing a W118G mutation in the V_H-V_L interface, creates a cavity in the protein changing the structure of the scFv WT, similarly to results obtained previously using a W-to-G mutation in a β-glucuronidase[11]. After addition of indole and fluorescein the whole structure of the scFv protein changes drastically and most of it becomes more rigid and protected from hydrogen exchange.

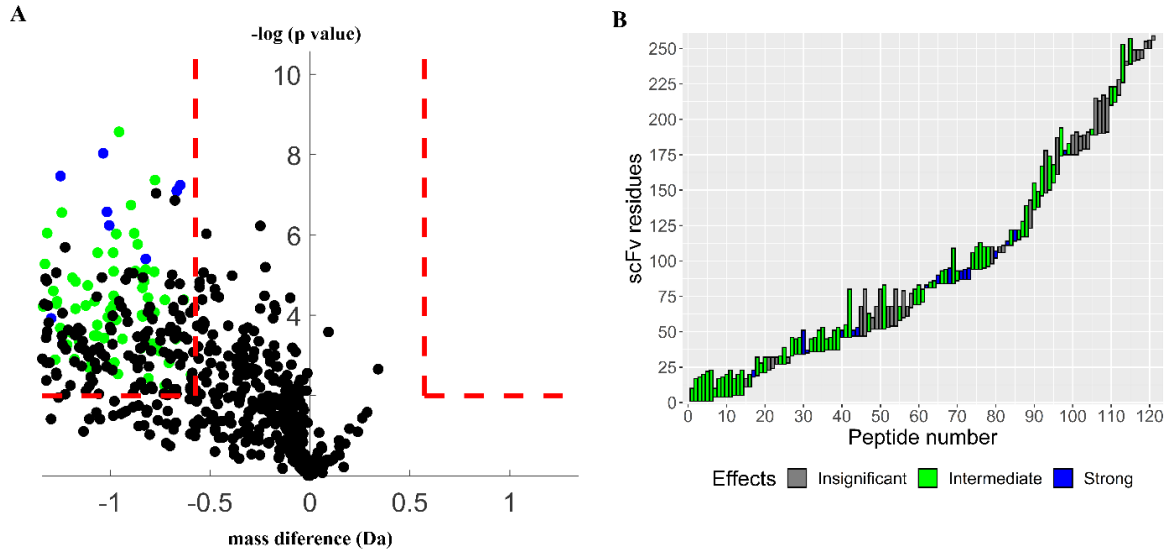

Figure 2.17. Peptides with increased protection in W118G scFv in the presence of indole and fluorescein as revealed by HX-MS experiments. (A) volcano plot for identification of peptides with significant differences and magnitude of the effects. Negligible (black), moderate (green) and strong (blue) effects as revealed by k-means clustering of the data. Red dashed lines in the volcano plot represent significance thresholds (horizontal significance. threshold = 2, vertical significance threshold = ±0.5736Da) as defined by Hageman et al.[17] Note: black dots above the threshold limits are statistically significant but considered negligible effects since the normalized magnitude is small. (b) Bar plot showing the classification and magnitude of the effects on the peptides measured by HX-MS. The vertical axis shows the protein residues numbers and the horizontal axis the peptide number.

2.3.4. Comparison of FITC-E2 V_H W118G and WT with indole and fluorescein

To determine if scFv W118G mutant recovers the initial structure of the WT after the addition of indole and fluorescein, a comparison between scFv W118G mutant and WT with indole and fluorescein was performed. For this case, the reference state was the scFv WT with indole and fluorescein added. WT scFv and its W118G mutant produce different peptic peptides after digestion. They both share 44 unique peptic peptides resulting in 75% sequence coverage, with few regions with overlapping peptides (see **Figure 2.A-3**). Statistical analysis of the data set (see **Figure 2.5**) identified one peptide (peptide number 32; residues 111-114) strongly *deprotected* in the scFv W118G construct when indole and fluorescein was added compared to the scFv WT with indole and fluorescein. An additional nine peptides showed intermediate *deprotection* in the mutant variant (peptide number 7, 9-10, 12, 15, 19, 25, 33-34; residues 24-52, 69-83, 115-122) upon the addition of indole and fluorescein. Residues 53-68 were classified both as protected and deprotected in different peptides (peptide numbers 22 and 23), suggesting a false

positive in the data set. Poor sequence coverage in that region makes it difficult to identify the false positive peptide, however, there is an additional peptide covering those residues (peptide number 19) showing increase protection in the scFv W118G construct compared to the WT, hence, most probably the protected peptide is the false positive and hence, residues 53-68 were classified as intermediately *deprotected* for this experiment. Additional experiments with improved digestion could provide more overlapping peptides in the region and clearly identify the false positive. Peptides identified as statistically significant by hydrogen exchange experiments were mapped into the homology model (see **Figure 2.6D**). The peptide with strong *deprotection* is located right at the fluorescein binding site (blue segment), and intermediately deprotected peptides (green segments) are either close to the binding region or close to the mutation site (residue 118). Most of these regions overlap with the ones previously identified in the comparison of the scFv WT and WT with the addition of indole and fluorescein (**Figure 2.6B**). Again, lack of coverage in the WT scFv could hide additional effects in the protein.

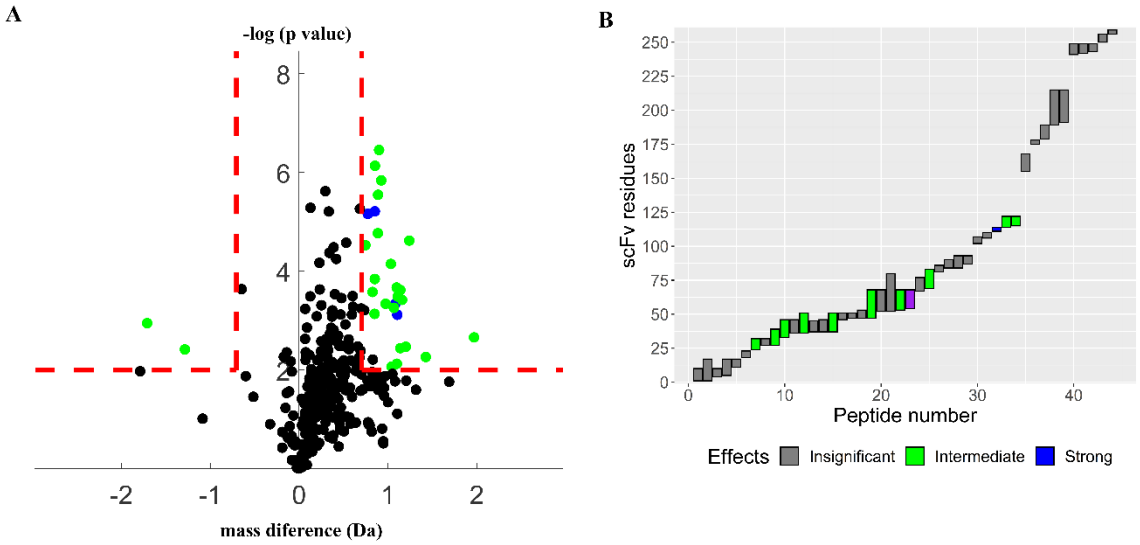

Figure 2.18 . Peptides with increased deprotection in W118G scFv in the presence of indole and fluorescein compared to WT with indole and fluorescein as revealed by HX-MS experiments. (A) volcano plot for identification of peptides with significant differences and magnitude of the effects. Negligible (black), moderate (green) and strong (blue) effects as revealed by k-means clustering of the data. Red dashed lines in the volcano plot represent significance thresholds (horizontal significance threshold = 2, vertical significance threshold = ±0.7043Da) as defined by Hageman et al.[17] Note: black dots above the threshold limits are statistically significant but considered negligible effects since the normalized magnitude is small. (b) Bar plot showing the classification and magnitude of the effects on the peptides measured by HX-MS. The vertical axis shows the protein residues numbers and the horizontal axis the peptide number. In purple, peptide identified as false positive (see main text for details).

2.4. DISCUSSION

Conformational changes in FITC-E2 single chain variable fragment used as a protein switch after a tryptophan to glycine mutation was introduced were evaluated by hydrogen exchange-mass spectrometry. While a chemical rescue of structure after a W-to-G mutation has been used before[10,11], this is the first time demonstrating this approach using a single chain variable fragment. Kaiser *et al*.[13], showed that the activity of the V_H W118G FITC-E2 can be restored by the addition of indole, restoring the activity almost to the level of the wild-type variant. The extent of the conformational changes induced trough the W-to-G cavity forming mutation is discussed here.

Hydrogen exchange experiments at an intact protein level show that introducing a W-to-G mutation in the protein provokes a change in the general structure of the protein (see **Figure 2.1**), evident by the increase in flexibility and deprotection of the V_H W118G variant. Peptide-level experiments on the V_H W118G mutant locate strong increase in flexibility all along the V_H domain of the protein, with intermediate increase in flexibility in the V_L domain as well. Hydrogen exchange experiments show that in general the V_H W118G mutant is more flexible and less structured than the wild-type consisting with a major change in protein structure.

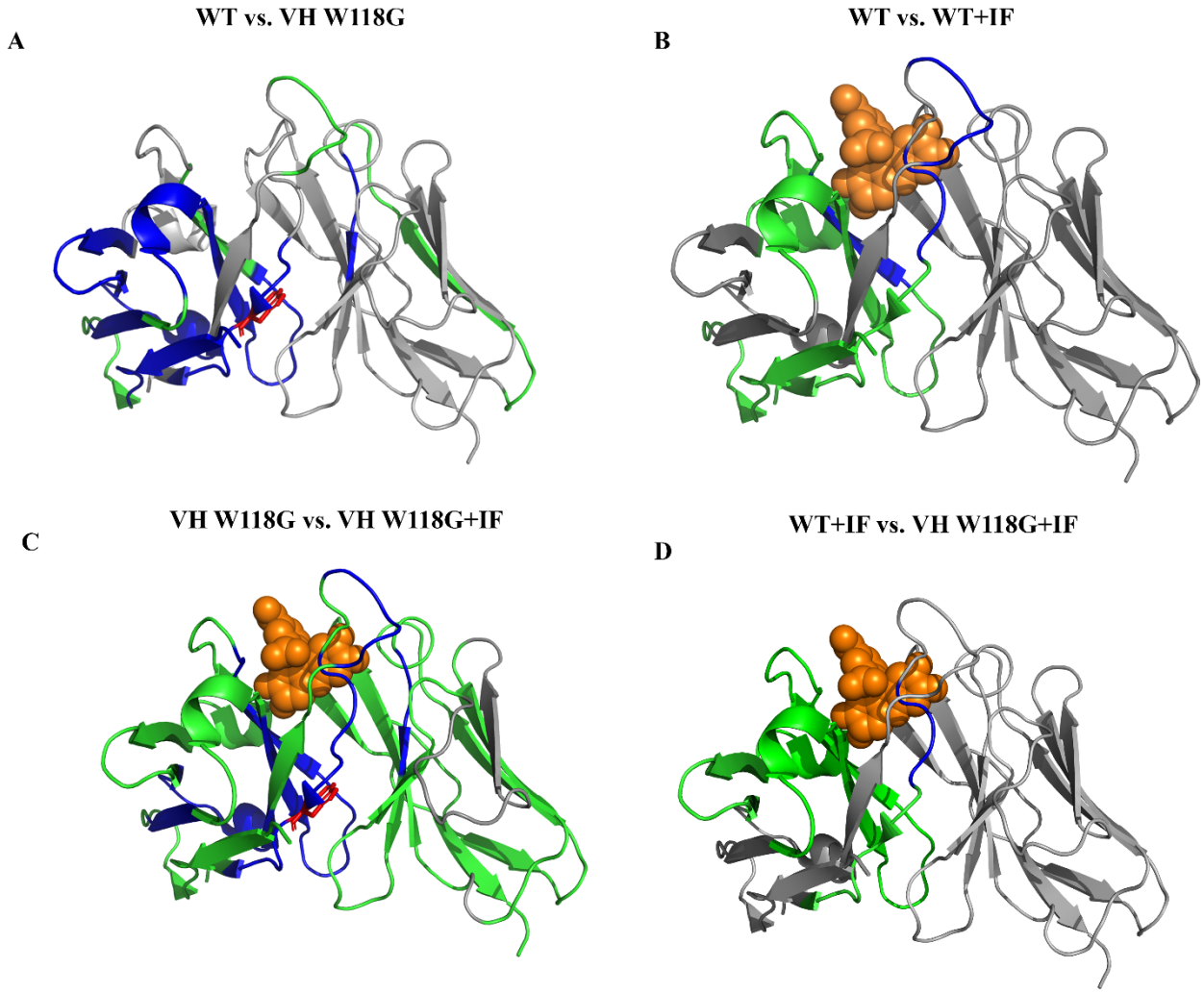

Figure 2.19. HX-MS differences mapped onto the homology model (2A9N[14]). (a) Peptides with increased deprotection in V_H W118G compared to the wild-type. (b) Peptides with increased protection in WT scFv in the presence of indole and fluorescein (WT+IF) compared to the wild-type scFv alone. (c) Peptides with increased protection in W118G scFv in the presence of indole and fluorescein (V_H W118G+IF) compared to the V_H W118G alone. (d) Peptides with increased deprotection in W118G scFv in the presence of indole and fluorescein (V_H W118G+IF) compared to WT with indole and fluorescein (WT+IF). Green regions represent intermediate effects and blue strong effects. In red site of mutation and in orange Fluorescein atoms in the crystal structure.

To locate where in the structure the differences are located, peptide-level hydrogen exchange experiments were used. As seen before[13], the restored activity is dependent on the concentration of indole in solution with a midpoint at 220 μM. Hydrogen exchange-mass spectrometry experiments used a 1:1000 molar ratio for scFv:indole to push the equilibrium to favor the bound state and be able to locate the structural changes. Additionally, DSF experiments showed an apparent cooperativity between

fluorescein binding and indole binding to restore V_H W118G structure. Hence, both components were added to all systems. **Figure 2.6B** shows that adding indole and fluorescein to the FITC-E2 WT variant induces exchange protection in the peptides nearby to the binding site of the fluorescein as seen in the crystal structure[14]. Residues right at the binding site (46-51, 102-107, 111-114) showed strong protection from hydrogen exchange, while residues nearby had intermediate protection. No peptides distal from the binding site showed any statistically significant differences compared to the free FITC-E2 WT in solution. However, not every residue located at the fluorescein binding site resulted in hydrogen exchange protection due to low sequence coverage for WT scFv experiments (see Materials and Methods section). Kaiser *el al.*'s[13] differential scanning calorimetry experiments, showed that the addition of indole and fluorescein to the FITC-E2 WT caused a decrease in thermal stability ($\Delta T_m \approx$ 0.7°C), but such effect is not detected with hydrogen exchange-mass spectrometry probably for the same reason as explained above. HX by FITC-E2 V_H W118G in the presence of indole and fluorescein showed many peptides with strong and intermediate protection along the whole protein structure (see **Figure 2.6C**). Again, strong hydrogen exchange protection was seen in peptides next to the fluorescein binding site as well as next to the mutation site (W118). On the chemical rescue of structure model, an indole molecule replaces the side chain of the tryptophan in the mutation site. Consequently, it is expected that there will be a strong increase in protection in that region as well. Intermediate protection effects were also seen at distal regions from the binding and mutation sites, implying that there is a major structural change along the whole protein (consistent with a cavity-forming mutation). Finally, **Figure 2.6D** compares the FITC-E2 WT and V_H W118G variants both after the addition of indole and fluorescein. A single peptide located at the fluorescein binding site showed increased *deprotection* in the V_H W118G mutant and a few peptides had intermediate *deprotection* in regions close to the mutation site. These differences in the WT and V_H W118G, show that the rescued FITC-E2 V_H W118G protein and WT have very similar structures. However, there are subtle differences. The difference in deuterium exchange at the fluorescein binding site show that both WT and W118G variants bind to fluorescein but the interactions are stronger in the WT. This difference could explain why the restored V_H W118G does not

bind to fluorescein with the same binding affinity as the wild-type (approximately 90%) even at high indole concentrations[13]. These subtle effects in the protein show that both proteins structures are very similar but not identical. One of the drawbacks of this chemical rescue of structure is the need for high concentrations of indole to restore the activity. These high concentrations make this model less attractive for therapeutic use. However, new approaches devising bigger cavities in the protein and different small molecules to restore the activity might overcome these problems[20].

Altogether, these results support the model of chemical rescue of structure by the addition of indole after a cavity forming mutation in the protein. This is the first time that a single chain variable fragment is used as a protein switch, using indole to restore the structure and activity. It is likely that this approach can be transferred to other full-length monoclonal antibodies with therapeutic properties and be able to modulate its activity to increase on-target activity and reduce possible secondary effects.

2.5. APPENDIX A

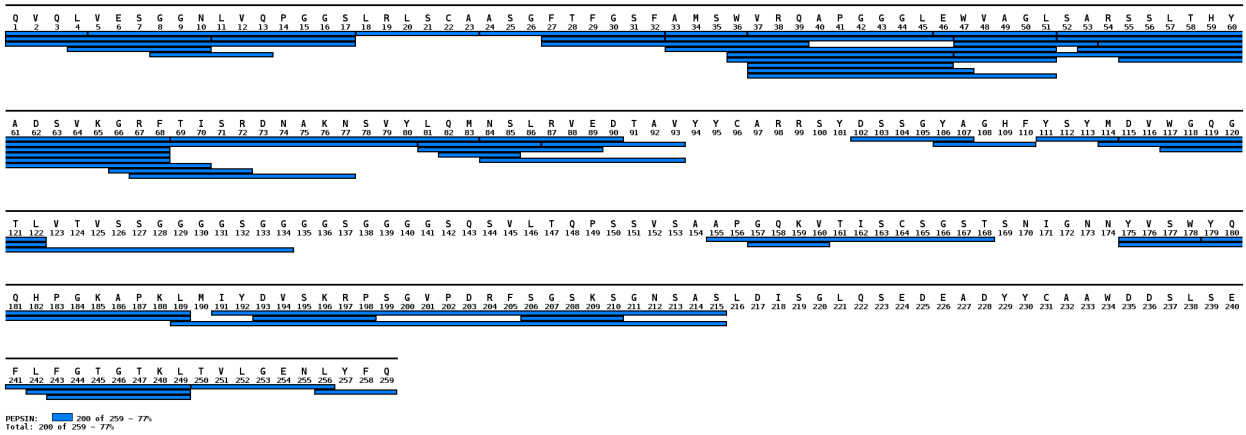

Figure 2.A-1. FITC-E2 wild-type peptic peptide coverage map.

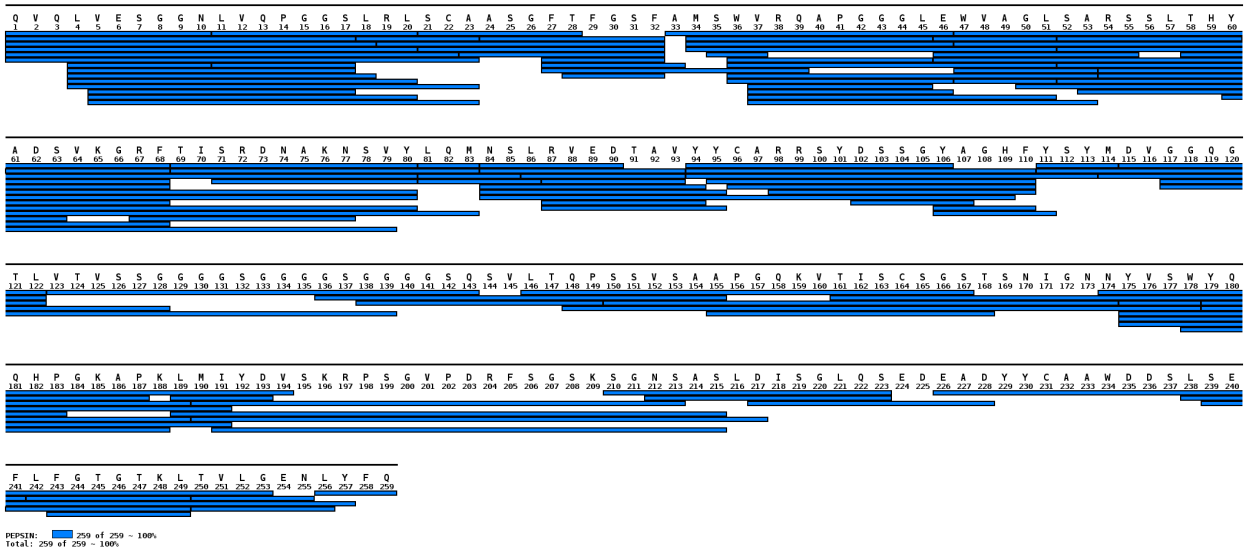

Figure 2.A-2. FITC-E2 V_H W118G mutant peptic peptide coverage map.

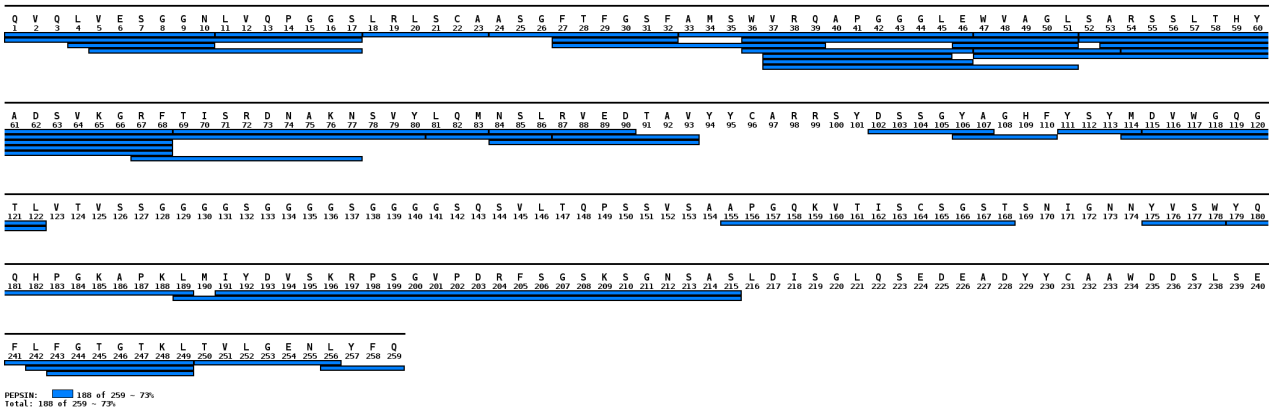

Figure 2.A-3. Common peptic peptides for both FITC-E2 wild-type and FITC-E2 V_H W118G mutant variant.

2.6. REFERENCES

1. Ecker DM, Jones SD, Levine HL 2015. The therapeutic monoclonal antibody market. MAbs 7(1):9-14.
2. Singh S, Kumar NK, Dwiwedi P, Charan J, Kaur R, Sidhu P, Chugh VK 2018. Monoclonal Antibodies: A Review. Current clinical pharmacology 13(2):85-99.
3. Kaplon H, Reichert JM 2019. Antibodies to watch in 2019. MAbs 11(2):219-238.
4. Tsumoto K, Isozaki Y, Yagami H, Tomita M 2019. Future perspectives of therapeutic monoclonal antibodies. Immunotherapy 11(2):119-127.
5. Hansel TT, Kropshofer H, Singer T, Mitchell JA, George AJ 2010. The safety and side effects of monoclonal antibodies. Nat Rev Drug Discov 9(4):325-338.
6. Sathish JG, Sethu S, Bielsky M-C, de Haan L, French NS, Govindappa K, Green J, Griffiths CEM, Holgate S, Jones D, Kimber I, Moggs J, Naisbitt DJ, Pirmohamed M, Reichmann G, Sims J, Subramanyam M, Todd MD, Van Der Laan JW, Weaver RJ, Park BK 2013. Challenges and approaches for the development of safer immunomodulatory biologics. Nature Reviews Drug Discovery 12(4):306-324.
7. Ostermeier M 2005. Engineering allosteric protein switches by domain insertion. Protein Eng Des Sel 18(8):359-364.
8. Dagliyan O, Shirvanyants D, Karginov AV, Ding F, Fee L, Chandrasekaran SN, Freisinger CM, Smolen GA, Huttenlocher A, Hahn KM, Dokholyan NV 2013. Rational design of a ligand-controlled protein conformational switch. Proc Natl Acad Sci U S A 110(17):6800-6804.
9. Carter P, Wells JA 1987. Engineering enzyme specificity by "substrate-assisted catalysis". Science 237(4813):394-399.
10. Deckert K, Budiardjo SJ, Brunner LC, Lovell S, Karanicolas J 2012. Designing Allosteric Control into Enzymes by Chemical Rescue of Structure. Journal of the American Chemical Society 134(24):10055-10060.
11. Xia Y, DiPrimio N, Keppel TR, Vo B, Fraser K, Battaile KP, Egan C, Bystroff C, Lovell S, Weis DD, Anderson JC, Karanicolas J 2013. The Designability of Protein Switches by Chemical Rescue of Structure: Mechanisms of Inactivation and Reactivation. Journal of the American Chemical Society 135(50):18840-18849.
12. Budiardjo SJ, Licknack TJ, Cory MB, Kapros D, Roy A, Lovell S, Douglas J, Karanicolas J 2016. Full and Partial Agonism of a Designed Enzyme Switch. ACS Synthetic Biology 5(12):1475-1484.

13. Kaiser CE, Rincon Pabon JP, Khowsathit J, Castaldi MP, Kazmirski SL, Weis DD, Zhang AX, Karanicolas J 2018. Modulating Antibody Structure and Function through Directed Mutations and Chemical Rescue. ACS Synth Biol 7(4):1152-1162.
14. Honegger A, Spinelli S, Cambillau C, Plückthun A 2005. A mutation designed to alter crystal packing permits structural analysis of a tight-binding fluorescein-scFv complex. Protein Sci 14(10):2537-2549.
15. Majumdar R, Manikwar P, Hickey JM, Arora J, Middaugh CR, Volkin DB, Weis DD 2012. Minimizing carry-over in an online pepsin digestion system used for the H/D exchange mass spectrometric analysis of an IgG1 monoclonal antibody. J Am Soc Mass Spectrom 23(12):2140-2148.
16. Glasoe PK, Long FA 1960. Use of Glass Electrodes to Measure Acidities in Deuterium Oxide1,2. The Journal of Physical Chemistry 64(1):188-190.
17. Hageman TS, Weis DD 2019. Reliable Identification of Significant Differences in Differential Hydrogen Exchange-Mass Spectrometry Measurements Using a Hybrid Significance Testing Approach. Analytical Chemistry 91(13):8008-8016.
18. Angalakurthi SK, Vance DJ, Rong Y, Nguyen CMT, Rudolph MJ, Volkin D, Middaugh CR, Weis DD, Mantis NJ 2018. A Collection of Single-Domain Antibodies that Crowd Ricin Toxin's Active Site. Antibodies (Basel) 7(4):45.
19. Toth RTt, Angalakurthi SK, Van Slyke G, Vance DJ, Hickey JM, Joshi SB, Middaugh CR, Volkin DB, Weis DD, Mantis NJ 2017. High-Definition Mapping of Four Spatially Distinct Neutralizing Epitope Clusters on RiVax, a Candidate Ricin Toxin Subunit Vaccine. Clin Vaccine Immunol 24(12):e00237-00217.
20. Khowsathit J, Bazzoli A, Cheng H, Karanicolas J 2020. Computational Design of an Allosteric Antibody Switch by Deletion and Rescue of a Complex Structural Constellation. ACS Central Science 6(3):390-403.

3. CHAPTER THREE: PROTEIN A DOES NOT INDUCE ALLOSTERIC STRUCTURAL CHANGES IN AN IGG1 ANTIBODY DURING BINDING

3.1. INTRODUCTION

Monoclonal antibodies (mAbs) are the fastest growing category of therapeutic agents due to their high specificity, efficacy, and safety.[1-5] They are used to treat many disorders such as cancers, cardiovascular, infectious and autoimmune.[6] Currently, there are more than 80 therapeutic antibodies approved by the US FDA, and more than 570 therapeutic proteins at various clinical stages.[7,8] As part of the normal manufacturing process, all of these therapeutic agents need to be purified. Impurities such as media, host cell proteins, DNA, and aggregates must be removed to ensure the quality of the therapeutic agent and to yield a product that is suitable for use in humans.[2,9] The appropriate process for the purification of an antibody varies and depends on its specific case. However, the most common technique used during downstream processing is affinity chromatography.[11] Affinity chromatography is based on the ability of an affinity ligand that has been immobilized on a matrix or resin to recognize the antibody. The most common affinity ligands suitable for antibody purification are protein A, protein G, and protein L.[12]

Staphylococcal protein A (SpA) is a 42 kDa protein located on the surface of the *Staphylococcus aureus* bacterium.[13] SpA consists of five IgG-Fc binding domains called E, D, A, B, and C. Each of these domains consist of a three α-helical motif that has high binding specificity for the Fc-region of most immunoglobulins.[14] As an example, each of these domains are capable of binding to human IgG1, IgG2, and IgG4 with an affinity constant (K_A) of ~10^8.[14,15] SpA is stable over a wide range of pH (2-11) and is able to refold after treatment with denaturing solutions such as urea and guanidine.[11] SpA has been reported to also bind to the variable region of the antibody, specifically to the V_H3-encoded human antibodies.[16-18] During the antibody purification process, impurities are washed away after binding the antibody to the ligand. Subsequently, elution is achieved using a low pH solution. Since SpA's introduction for IgG purification, many improvements have been made to the native affinity ligand through point mutations, most notably, increased stability under alkaline conditions, increased binding capacity, and decreased affinity for the F_{ab} region of the antibody.[14,19,20] All affinity ligands derived from SpA are referred to simply as Protein A (ProA). MabSelect Sure is an alkali stabilized ProA ligand

developed by GE Healthcare that is widely used in downstream processing. This ligand is composed of four copies of an engineered version of the wild type B-domain followed by a C-terminal cysteine.[21]

Allosteric effects after protein binding are defined as any conformational or dynamic changes that are distant from the binding site. Those effects on protein therapeutics[22] could be either reversible or irreversible [23] and both are a potential concern. Any irreversible conformational change could lead to a decrease in efficacy or stability of the drug.[24] Many studies have shown evidence of allosteric effects in proteins and monoclonal antibodies. Studies on variable regions of identical human F_{ab} domains from an IgA1 and an IgG1 showed different antigen affinity and C_H1-C_L and C_H1-V_H linkers and interfaces with different rigidity in the IgA1.[25] This rigidity and affinity difference suggest allosteric effects induced in the paratope by distal differences. Additionally, single point mutations in the CDR region of an IgG1 can result in significant difference in labelling at distal sites in the C_L-C_H1 and C_H1-C_H2 interfaces, as revealed by fast photochemical oxidation of proteins (FPOP), indicating allosteric effects induced in the F_c by changes in the F_{ab}.[26] These studies suggest that allosteric coupling between the F_{ab} and distal elements, such as the F_c in an IgG, might lead to conformational changes. Furthermore, it has been shown that isotype-switch variants of anti-DNA antibodies have different changes in secondary structure upon antigen binding, concluding that antigen binding affinity depends on the constant region being expressed.[27]

More importantly, dynamic light scattering and size exclusion chromatography experiments showed a dramatic reduction in the hydrodynamic radius, from 11.5 nm to 5.6 nm in some cases, of three native IgG1 monoclonal antibodies after elution from a ProA affinity chromatography column. The degree of reduction of the hydrodynamic radius was highly dependent on the ionic strength of the buffer, and was reversible after physiological conditions were restored.[28]

Interestingly, several studies suggest allosteric effects in the F_c of an IgG upon antigen binding. Tryptophan fluorescence showed a change in the conformation of the Fc of an IgG1 upon antigen binding, representative of an interaction between the paratope and the Fc region.[29] Also, binding of protein A and protein G to a mouse IgG was inhibited when the antibody bound to a hapten molecule

showing that conformational changes in the Fc region upon antigen binding are possible.[30] Similar results were later obtained with different antibodies using isothermal titration calorimetry and surface plasmon resonance.[31] Moreover, molecular dynamics simulations showed that antigen binding to an IgG1 caused a large conformational change in the F_{ab} and in the C_H2 domain resulting in increased FcγR binding affinity.[32] Those results were recently confirmed using a combination of several experimental techniques.[33] Concluding that some antigen bindings to human IgG promoted a conformational change in the Fc region that increased binding to low affinity Fcγ receptors. Therefore, there is evidence that antigen binding can cause allosteric effects, alter the Fc and inhibit protein A binding. However, there is no information that indicates that protein A interactions with the Fc can cause allosteric effects in the F_{ab} region and influence antigen binding.

Due to the widespread use of protein A in the purification process of therapeutic antibodies and the lack of knowledge of possible allosteric effects in antibodies during or after interaction with protein A, there is a need to understand these interactions and elucidate any allosteric effects induced in antibodies by protein A. Here, we used hydrogen exchange-mass spectrometry (HX-MS) to probe conformational changes in the NIST monoclonal antibody reference material during interaction with the commercially available protein A affinity ligand MabSelect SuRe, both free in solution and immobilized onto a resin. The NIST monoclonal antibody reference material (RM8671) is a recombinant humanized IgG1κ with low abundance post-translational modifications, high abundance N-terminal pyroglutamination and glycosylation of the heavy chains.[34] This reference material is one of the most well characterized proteins available,[35] making it ideal to be used as a model system in our experiments.

3.2. MATERIALS AND METHODS

3.2.1. Materials

NIST mAb RM8671 was obtained from the National Institute of Standard and Technology (NIST; Gaithersburg, MD) [34] [33] at a concentration of 10 mg/mL in 12.5 mM L-histidine, 12.5 mM L-histidine

HCl, pH 6.0. MabSelect SuRe ligand, MabSelect SuRe resin and Sepharose CL-6B were obtained from GE Healthcare (Chicago, IL). Premium grade tris (2-carboxyethyl) phosphine hydrochloride (TCEP) was purchased from Thermo Scientific (Rockford, IL). Sodium phosphate dibasic (anhydrous), sodium chloride, LC-MS grade water and LC-MS 0.1% formic acid in water were purchased from Fisher Scientific (Hampton, NH). Guanidine hydrochloride and glycine hydrochloride were purchased from Sigma-Aldrich (St. Louis, MO). LC-MS grade acetonitrile containing 0.1% formic acid was obtained from Burdick-Jackson (Muskegon, MI). Deuterium oxide (99+ %D) was obtained from Cambridge Isotope Laboratories (Tewksbury, MA).

3.2.2. Sample Preparation

Stock solutions of NIST mAb reference material and MabSelect SuRe ligand were buffer exchanged into 10 mM sodium phosphate, 150 mM sodium chloride buffer at pH 7.01. Buffer exchange was performed twice using centrifugal filters pre-rinsed with buffer to eliminate any contamination (Amicon Ultra, 0.5 mL, 3 kDa MWCO, MilliporeSigma, Burlington, MA) according to manufacturer's instructions. Samples were stored at 4°C and used within few hours. MabSelect Sure resin and Sepharose CL-6B were washed several times into 10 mM sodium phosphate, 150 mM sodium chloride buffer at pH 7.01. For the in-solution experiment, a working solution of NIST mAb with MabSelect SuRe ligand was prepared by volume to volume mixture at a molar ratio of 1:1 and 2:1 (ProA:mAb) and diluted to a nominal concentration of 16.8 µM (for the NIST mAb and ProA ligand) and incubated for 2 hr at room temperature; the reference state was NIST mAb in solution at a nominal concentration of 16.8 µM. For the resin experiment, 100 µL of MabSelect SuRe resin slurry was added to a concentrated NIST mAb solution and diluted to 160 µL (resulting in a nominal concentration for the NIST mAb of 16.8 µM); the reference state was prepared identically but using Sepharose CL-6B as the resin. Solutions were placed on a LabQuake rotating system and equilibrated at room temperature for 2 hr. NIST mAb concentrations

used during the resin experiments are below the dynamic binding capacity for MabSelct SuRe resin as reported by the manufacturer.

3.2.3. Hydrogen exchange-mass spectrometry

HX labeling for the in-solution experiment was performed using a LEAP Technologies HDX PAL robot (Carrboro, NC) with a customized three-valve configuration as described previously.[36] For NIST mAb and NIST mAb containing MabSelect SuRe ligand in solution experiments, deuterated samples were prepared by diluting 5 µL of the working sample in 50 µL of labeling buffer (10 mM sodium phosphate, 150 mM sodium chloride, pD 7.01) (D_2O). The pD was obtained from pH measurements with a glass electrode, corrected for the deuterium isotope effect (pD = pH + 0.4).[37] Samples were labeled in triplicate for each labeling time (60, 360, 1920, 11100, 63360 s) at 25°C. After labeling, 50 µL of each labeled sample was quenched with 50 µL precooled quench buffer (200 mM glycine, 0.5M TCEP, 3 M guanidine hydrochloride, pH 2.4 in water) at 1°C and held for 5 minutes to improve disulfide bond reduction. Non-deuterated controls were prepared identically, but using 10 mM sodium phosphate, 150 mM sodium chloride, pH 7.01. Immediately after, 85 µL of sample was injected into a temperature-controlled chromatography cabinet connected to an Agilent 1260 Infinity series LC system. Cabinet temperature and equipped LC solvent pre-cooler were maintained at 0°C for all experiments. Injected sample was passed over an immobilized pepsin column (2.1 × 50 mm), prepared in house,[38] at 200 µL min^{-1} for 180 s with 0.1% formic acid in H_2O. The resulting peptic peptides were captured on a ZORBAX 300SB-C8 trap (2.1 × 12.5 mm, 5 µm particles) and washed at 200 µL min^{-1} for 60 s with 0.1% formic acid in H_2O. Desalted peptic peptides were separated on a ZORBAX 300SB-C18 column (2.1 × 50 mm, 3.5 µm particles) with a 12-minute linear gradient of 0.1% formic acid in acetonitrile increasing from 13% to 35% acetonitrile. Peptide masses were subsequently measured with an Agilent 6530 Q-TOF mass spectrometer running in ESI-positive mode. Pepsin column washes were performed between each sample injection during the elution step to minimize peptide carry-over.[36] An independent

secondary gradient on trap and column after elution was used to reduce peptide carryover. All HX experiments were performed consecutively spanning 48 hours.

A similar but manual experimental procedure was followed for samples containing MabSelect SuRe resin or Sepharose CL-6B. Briefly, 6 µL of working sample was diluted in in 50 µL of labeling buffer (10 mM sodium phosphate, 150 mM sodium chloride, pD 7.01) in D_2O. Triplicate samples were labeled for each labeling time (20, 100, 500, 2500, 12500, 62500 s) at 22±2°C. Samples were placed on a LabQuake rotating system during labeling to prevent resin sedimentation. After labeling, 50 µL of each labeled sample was quenched with 50 µL precooled quench buffer (200 mM glycine, 0.5 M TCEP, 3 M guanidine hydrochloride, pH 2.4 in water) at 1°C and held for 5 minutes. Non-deuterated controls were prepared identically, but using 10 mM sodium phosphate, 150 mM sodium chloride, pH 7.01. Immediately after, samples were centrifuged (2,000 g for 30 seconds), the supernatant was removed, and flash frozen in liquid nitrogen. Samples were stored at –70°C until analyzed. Prior to the analysis, samples were thawed at room temperature and placed on the HDX PAL auto sampler for digestion and LC-MS analysis as described above. mAb recovery after elution from MabSelect SuRe resin was 104 ± 3% (triplicate measurements, based on standard BCA assay using the NIST mAb, data not shown).

HX-MS data were analyzed using HDExaminer (v. 2.4, Sierra Analytics, Modesto, CA). All results were manually reviewed and curated. Undeuterated NIST mAb peptic peptides were identified by a combination of data-dependent and targeted CID-MS2 in the QTOF using the same LC gradient. MS2 spectra were matched to the NIST mAb sequence, with fixed modifications, using Agilent BioConfirm B.07. Free MabSelect SuRe in the in-solution experiments caused an interference with some NIST mAb peptic peptides, resulting in 88% sequence coverage for the heavy chain and 65% sequence coverage for the light chain. See **Figure 3.B-1**. Higher sequence coverage was achieved with the experiments involving MabSelect Sure resin, bringing 98% sequence coverage for the heavy chain and 100% sequence coverage for the light chain for the NIST mAb, as shown in **Figure 3.B-2**.

The in-solution and resin data set had pooled standard deviations of 0.11 Da. Differential HX data were tested for significance using the hybrid significance testing criteria method[39] using an in-house Matlab

script. Mean HX differences from labeling replicates were classified as significant when the mean centroid mass difference of each peptide at each labeling time point (ΔD) was higher than a critical value (0.5057 Da for the in-solution and experiment and 0.4263 Da for the resin experiment), and a Welch's two-sample t test had $p < 0.01$. Normalized HX differences (ΔHX) for each peptide were obtained by dividing by the theoretical maximum exchange (number of backbone amide hydrogens in each peptide, excluding the N-terminal amide). The absolute values of the normalized differences were then clustered using k-means clustering with $k = 3$ to define thresholds for strong, moderate, and negligible HX differences as described previously.[40,41] For visualization of the HX observations, a homology model was constructed based on a combination of PBD 5K8A[42] and 5VGP.[43] Peptides with strong or moderate effects as shown by the k-means clustering were mapped onto the homology model. When two overlapping peptides had different clustering, priority was given to the strongest effect. Following HX-MS community standards[43], additional HX details such as: back exchange measurements, all HX-MS uptake plots, and metadata are available online (see Supporting Information in Rincon Pabon et al[10]).

3.3. RESULTS

Hydrogen exchange-mass spectrometry was employed to identify allosteric effects in the NIST mAb induced by interaction with a commercially available protein A ligand. Two separate experiments were completed using the protein A ligand, MabSelect SuRe. The first one utilized the free ligand in solution, in the second one the ligand was attached to a resin. Free mAb in solution and mAb with uncoupled resin were used as reference states, respectively.

3.3.1. ProA binding induces a decrease in backbone flexibility in the CH2 and CH3 regions

HX-MS measurements of NIST mAb bound to MabSelect SuRe in solution (1:1 molar ratio) revealed many regions with protection from deuterium exchange compared to the unbound NIST mAb reference state. **Figure 3.1a** shows representative uptake plots for heavy chain peptides with strong, moderate, and negligible increases in protection from deuterium exchange. Statistical analysis[39] of the differential

HX-MS data (see **Figure 3.2**) identified several peptides that became strongly protected by ProA binding (residues 244-255 in the HC) and moderately protected by ProA binding (residues 238-243, 256-265, 309-321, 337-351 and 426-449 in the HC) in the C_H2 and C_H3 domains of the heavy chain. No significant changes in HX were detected in the light chain.

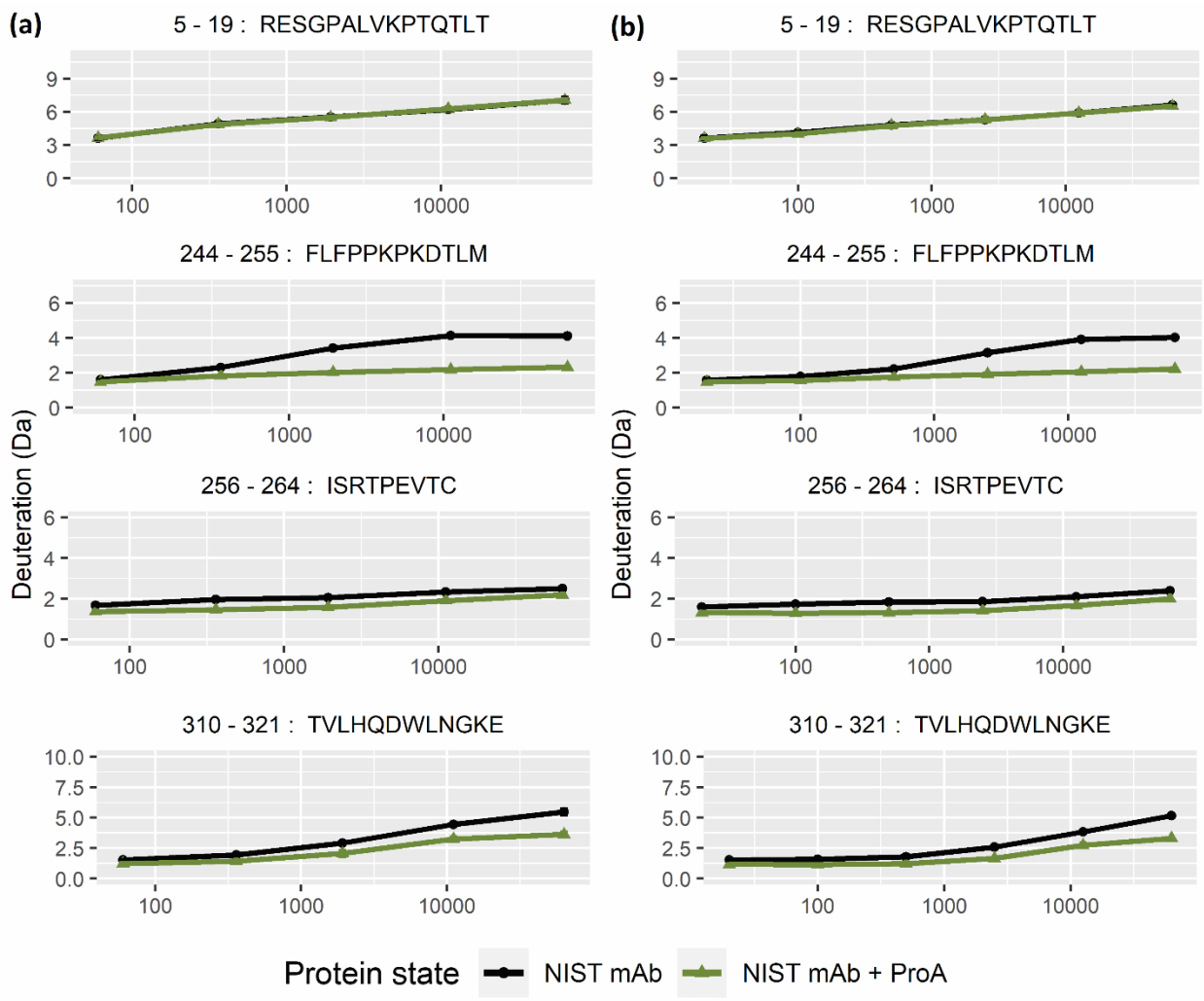

Figure 3.20 Representative uptake plots showing the effect of ProA binding to the NIST mAb. (a) NIST mAb and NIST mAb bound to MabSelect SuRe in solution (1:1 ratio). (b) NIST mAb with Sepharose and NIST mAb bound to MabSelect SuRe resin. Error bars represent the 95% confidence intervals from triplicate measurements.

MabSelect SuRe binds to antibodies through the Fc region,[17] specifically through the region between the C_H2 and the C_H3 domains. Contrary to previously published data,[17] a study by Batch et al. suggested that MabSelect SuRe can also interact with the F_{ab} regions coming from the V_H3 family of antibodies.[44]

While the NIST mAb is not a V_H3 encoded antibody,[45,46] the interactions might still be possible. To examine this possibility, we increased the concentration of the MabSelect SuRe ligand in solution to 2:1 (ProA:mAb) molar ratio to drive the binding equilibrium to favor the bound state. Statistical analysis of the HX-MS data (see **Figure 3.B-4**) from this experiment identified the same protected regions in the C_H2 and C_H3 domains plus an additional peptide in the C_H3 region (residues 414-425), as shown in **Figure 3.4**. The presence of the additional protected peptide in this region is due to a smaller critical value ($|\Delta D| \geq 0.44$ Da) that classifies the HX difference as significant in the 2:1 experiment, but not in the 1:1 experiment. Additionally, 2:1 ProA binding caused a moderate *increase* in flexibility in peptides in the light chain of the F_{ab} region (light chain residues 46-53, 115-124 and 172-180 in the LC) among the CDRL2 and C_L regions (see **Figure 3.B-3**). This increase in HX when ProA binds at 2:1 suggests an allosterically induced increase in backbone flexibility. It is possible that at the 2:1 ratio, two separate ProA molecules each bind to one of the two available Fc sites and that this dual engagement leads to allosteric effects in the F_{ab}. However, more experiments evaluating this hypothesis would be required. It is important to note that **Figure 3.2** and **S3.4** show HX differences in the statistically significant region (black dots) that were subsequently classified as negligible by the *k*-means clustering (see Materials and Methods section). Although the absolute magnitude of the HX effects were significant (horizontal axis of the volcano plots in **Figures 3.2a** and **3.3a**), when the effects were normalized for the number of exchangeable amide hydrogens, the relative HX protection became negligible.

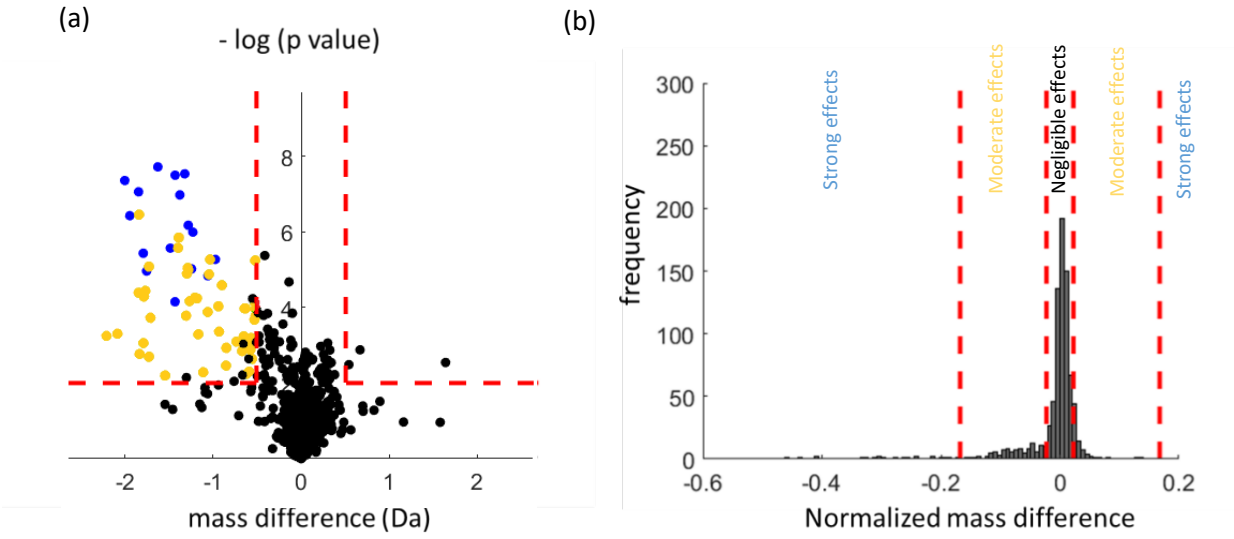

Figure 3.21 Statistical analysis for the MabSelect SuRe in solution (1:1 ratio) experiment. (a) volcano plot for identification of peptides with significant differences and magnitude of the effects. Negligible (black), moderate (yellow) and strong (blue) effects as revealed by k-mean clustering of the data. Red dashed lines in the volcano plot represent significance thresholds (horizontal sig. threshold = 2, vertical sig. threshold = ±0.5057Da) as defined by Hageman et al.[38] Note: black dots above the threshold limits are statistically significant but considered negligible effects since the normalized magnitude is too small. (b) histogram distribution of normalized HX differences (for all peptides at each labeling timepoint) used for the k-means clustering. Normalized differences were clustered into 3 bins, for negligible, moderate, and strong effects. Red dashed lines in the histogram (±0.0225 and ±0.1578) represent the threshold limits for each cluster.

Biophysical characterization of the in-solution antibody-ProA complex is experimentally convenient because there is no interference caused by the resin, but it may not be a realistic model of the interactions between an antibody and ProA immobilized onto a resin. The interaction between immobilized ProA and the antibody is more relevant from a downstream processing perspective. To examine the interactions of the NIST mAb with the MabSelect SuRe resin, we used HX-MS to compare NIST mAb bound to immobilized ProA and the NIST mAb in the presence of unloaded resin. Sepharose is an ideal resin for this control state, since both MabSelect SuRe and Sepharose are agarose matrices with similar physical and chemical properties. **Figure 3.1b** shows representative uptake plots for peptides with strong, moderate, and negligible changes in HX. Statistical analysis for this data set (see **Figure 3.3**) identified several peptides that became strongly protected by ProA binding (residues 244-255 in the HC) and moderately protected (residues 238-243, 256-265, 309-321, 337-351, and 414-449 in the HC) in the C_H2 and C_H3 domains. The regions of protection are consistent with both the 1:1 and 2:1 in-solution HX

measurements. Importantly, unlike 2:1 in-solution experiment, there are no significant *increases* in HX when NIST mAb is bound to immobilized ProA, probably because at low antibody concentrations (<40 mg/mL resin) the most probable binding stoichiometry between an antibody and MabSelect SuRe resin is 1:1.[47]

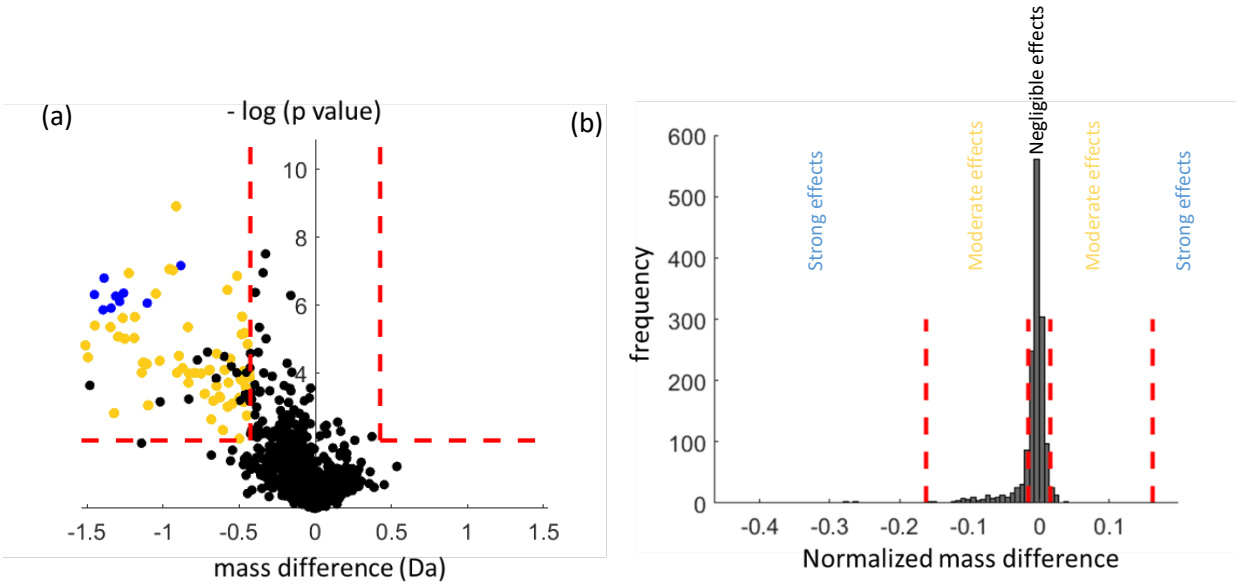

Figure 3.22 Statistical analysis for the MabSelect SuRe resin experiment. (a) volcano plot for identification of peptides with significant differences and magnitude of the effects. Negligible (black), moderate (yellow) and strong (blue) effects as revealed by k-mean clustering of the data. Red dashed lines in the volcano plot represent significance thresholds (horizontal sig. threshold = 2, vertical sig. threshold = ±0.4263Da) as defined by Hageman et al.[38] Note: black dots above the threshold limits are statistically significant but considered negligible effects since the normalized magnitude is too small. (b) histogram distribution of normalized HX differences (for all peptides at each labeling timepoint) used for the k-means clustering. Normalized differences were clustered into 3 bins, for negligible, moderate, and strong effects. Red dashed lines in the histogram (±0.0157 and ±0.1621) represent the threshold limits for each cluster.

3.3.2. All peptides with decreased backbone flexibility contained residues located on the ProA:Fc interface

Figure 3.4 shows the strong and moderate effects on HX of the NIST mAb mapped onto the homology model of the antibody as revealed by the *k*-means clustering. As expected, all the protected residues detected by HX-MS are in the expected ProA binding region, between the C_H2 and C_H3 domains. There is no crystal structure of MabSelect SuRe bound to an antibody, however the crystal structures of complexes of SpA domain B[48,49] and C[50] bound to F_c are available. MabSelect SuRe consists of a

tetramer of a proprietary domain Z that is an engineered analogue of the B domain of SpA.[44,51] Therefore, it is reasonable that the crystal structure of the complex between the SpA B domain and the Fc is a good model of the ProA:NIST mAb complex used in our experiments. **Figure 3.5** compares the protected regions detected by HX-MS with the F_c interface in the antibody-SpA B domain complex obtained by the analysis of crystal structure (PBD 5U4Y[48]) using PDBePISA software.[52] There is good correlation between the interface mapped by X-ray crystallography (red horizontal stripes) and the protected regions detected by HX-MS (blue and yellow peptides). A single peptide, HC 339-351, exhibited slowed hydrogen exchange upon ProA binding. However, this region is not located in the interface and the result is not corroborated by overlapping peptides, suggesting a potential false positive.

Every F_c residue in the SpA B-domain interface was strongly or moderately protected according to the hydrogen exchange data for the resin experiment and altered hydrogen exchange was only detected in a single peptide located away from the interface. These HX-MS results strongly suggest that there are no allosteric effects in the NIST mAb induced by interaction with the protein A ligand. There are a few false negatives, peptides 290-314, 300-328, 310-312, 317-330, 317-331 and 414-431 that cover interfacial residues but were classified as non-significant based on the HX measurements, as shown in **Figure 3.5**. This classification is due to either a high standard deviation for those peptides that render them non-significant based on hybrid significance testing or because the protection was so small compared to other peptides that they were clustered as negligible differences.

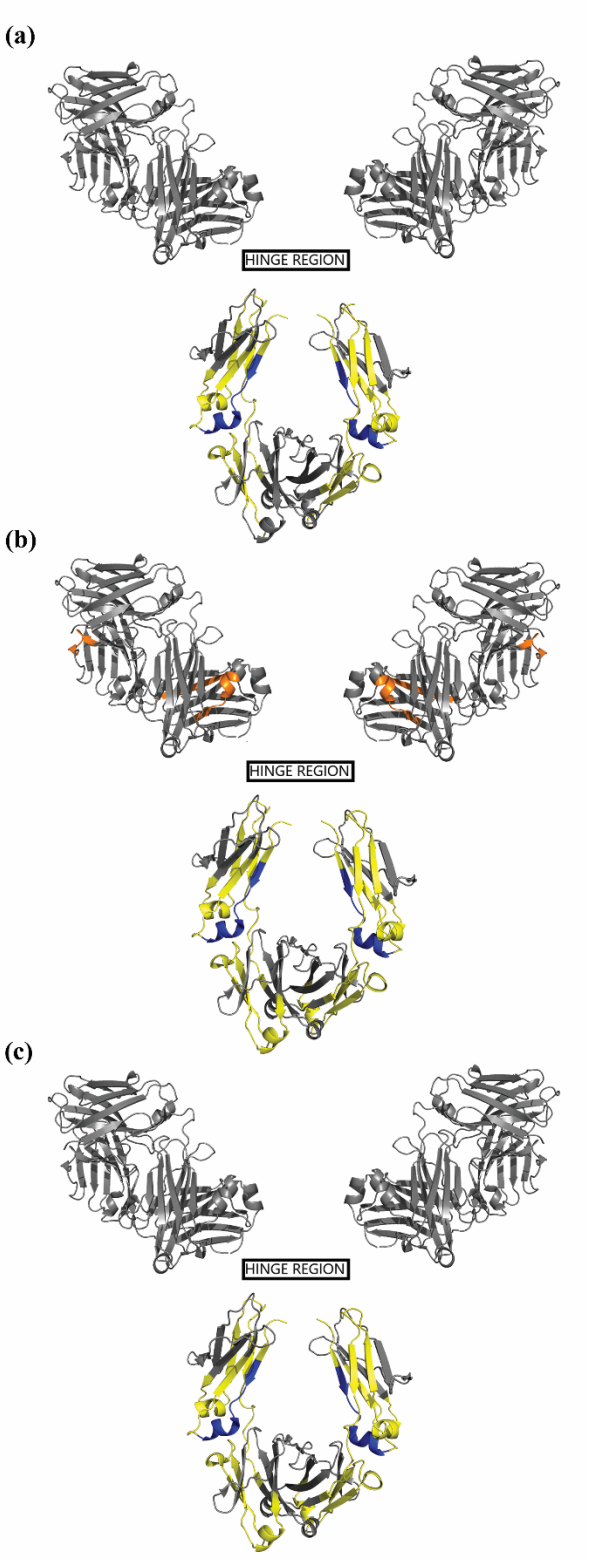

Figure 3.23 HX-MS differences provoked by binding to (a) MabSelect SuRe in solution (1:1 ratio) (b) MabSelect SuRe in solution (2:1 ratio) and (c) MabSelect SuRe resin mapped onto the NIST mAb homology model. Yellow represents moderate protection, blue strong protection and orange deprotection or faster exchange. No changes were detected in the hinge region.

3.4. DISCUSSION

The impact of protein A binding on the higher order structure of an IgG1 as assessed by hydrogen exchange-mass spectrometry was evaluated here. To our knowledge this is the first study assessing allostery in a mAb during interaction with ProA ligand using HX-MS. While studying protein A attached onto a resin is feasible, the HX workflow becomes more difficult because of the need for resin removal (see Materials and Methods). **Figure 3.4** shows that almost identical HX protection results were obtained when NIST mAb was bound to either MabSelect SuRe in solution or attached to a resin. Residues HC 414-425 were moderately protected in the resin experiment but not in the solution experiment. This additional protected region on the Fc was not detected in the solution experiment due to peptide interference/overlap, most likely from intact ProA (see Materials and Methods section). Even though both experiments gave similar results, in-solution ProA might not be a reliable model since there is poor coverage in the light chain. Additional steps to increase the coverage might be needed to get a more convenient model to investigate the interaction between antibodies and ProA. In-solution experiments used both 1:1 and 2:1 molar ratios, these ratios give the relationship of total molecules in solution and do not specify the binding stoichiometry. HX measurements give an ensemble average deuterium uptake between both states weighted by the population of the bound state. **Figure 3.4** shows both Fc chains perturbed when bound to ProA for a better representation regardless of binding stoichiometry.

The segment with strong protection in the C_H2 domain (244-254) has been previously identified as a potential aggregation hotspot in similar IgG1 mAbs.[53] Increase in flexibility in this region have been correlated with point mutations,[54] excipients effects,[55,56] methionine oxidation, [57,58] changes in glycosylation[57,59,60] and to drug conjugation to free cysteine residues.[61] We previously suggested that limiting the flexibility of this region might provide higher thermostability and resistance to aggregation

in IgG1 mAbs.[54] This suggestion is supported by Zhang et al.[62] who demonstrated that ProA interactions with the Fc limit the Fc-Fc interactions between mAbs, thus inhibiting aggregation.

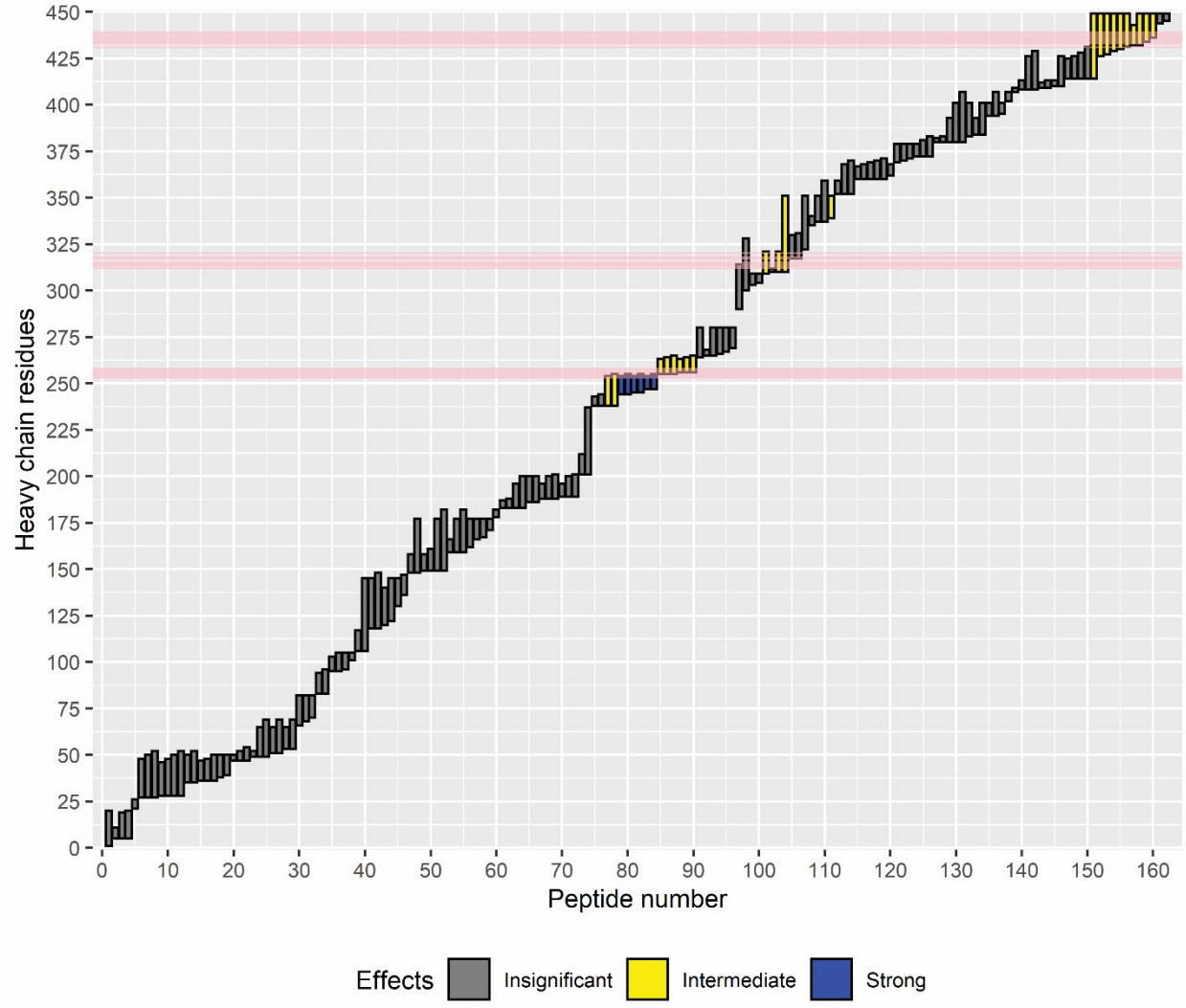

Figure 3.24 Correlation between HX protection in the NIST mAb heavy chain (blue and yellow) for the resin experiment with the SpA B domain interface mapped by X-ray crystallography (PDB 5U4Y48) (red) as defined with a buried surface area > 0 Å2. The vertical axis is the heavy chain residue numbering and the horizontal axis is the peptide number (see peptide list in the SI[10]).

Increase in overall production of biopharmaceutical products has forced a need to work with higher volumes and the use of multiple purification processes, which require high stability of the process and a strict control of the product.[63] With that in mind, it is crucial to eliminate possible alterations to the product during downstream processes. It is possible to have a reversible allosteric unfolding in the

variable domains of the NIST mAb when bound in solution to ProA at a 2:1 molar ratio, however, 2:1 ProA:mAb ratio is unrealistic when considering immobilized ProA, since achieving 2:1 binding would require an extremely high ProA surface coverage on the resin and use well above the recommended dynamic binding ratio.[47] There is no evidence that the Fc-ProA binding causes any reversible allosteric conformational changes when 1:1 ratio ProA:mAb, but lack of coverage in the light chain could hide some effects. In the case of binding to the ProA resin, there is no evidence of reversible allosteric effects. This result indicates that utilizing immobilized ProA affinity ligands to purify monoclonal antibodies in downstream processes does not provoke unfolding in the IgG1 when it is bound to ProA. This result is important because such allosteric unfolding could cause instability or co-purification of contaminants when resin is used. It is important to note that the NIST mAb (RM8671) was produced in murine suspension culture and had undergone biopharmaceutical industry standard upstream and downstream purification processes.[64] With that in mind, the NIST mAb used for our experiments had already been exposed to protein A purification. It is possible that the previous exposure to protein A provoked an irreversible conformational change in the structure that would be undetectable with our measurements. In summary, our study shows many peptides in the C_H2 and C_H3 domains become protected right at the binding site when ProA binds. We are able to rule out reversible allosteric effects in the NIST mAb when ProA attached onto a resin is used. It is probable that these interactions and effects are mAb-specific and can not be extrapolated to other IgGs. However, we would expect that heavily conserved domains in other IgG1s would behave similarly. To further evaluate allosteric effects in mAbs bound to a ProA ligand, it is necessary to extend this work to other mAbs as well with as naïve mAbs that have not been exposed to a protein A affinity medium.

3.5. APPENDIX B

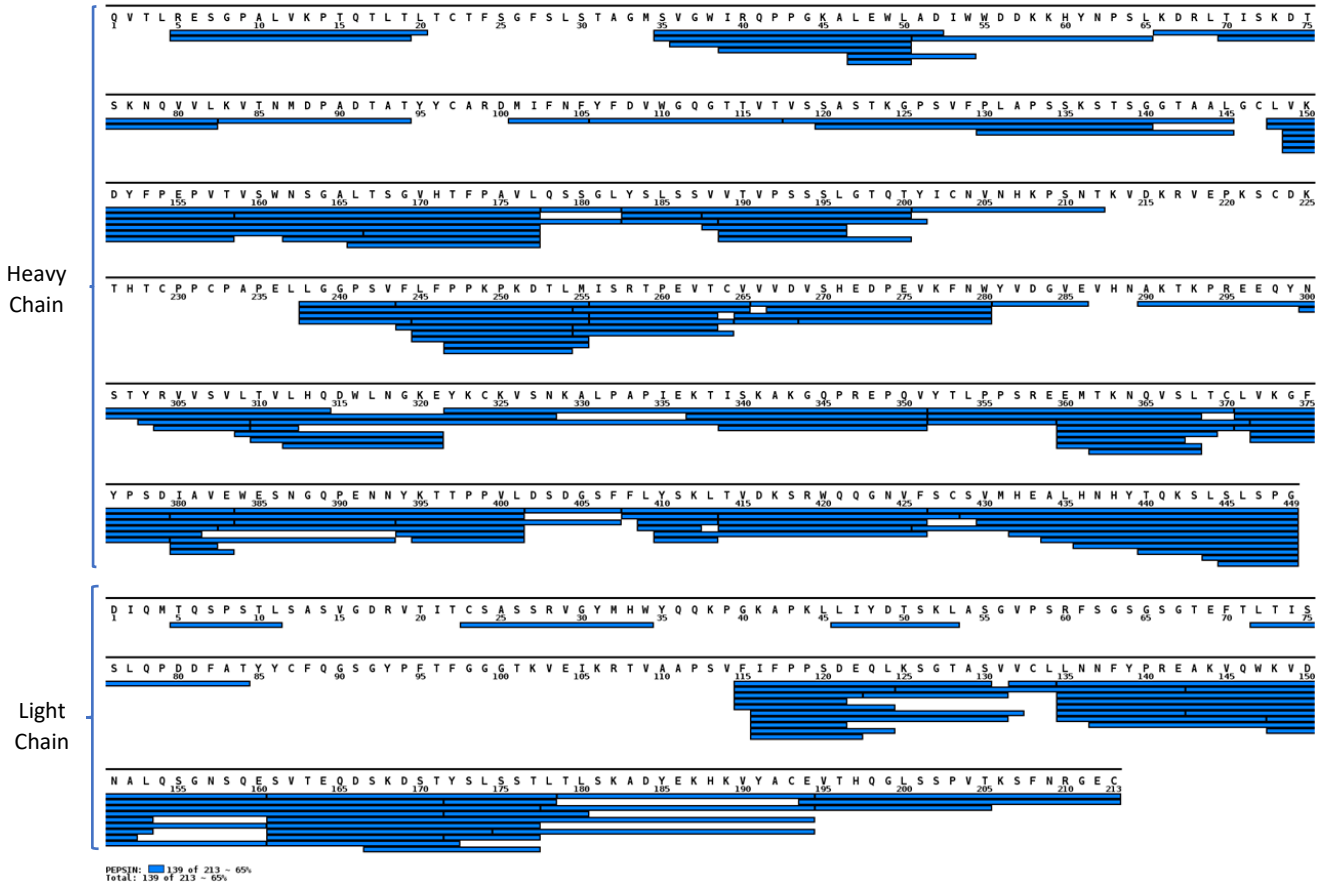

Figure 3.B-1. NIST mAb peptic peptide coverage map for the in-solution MabSelect SuRe experiment.

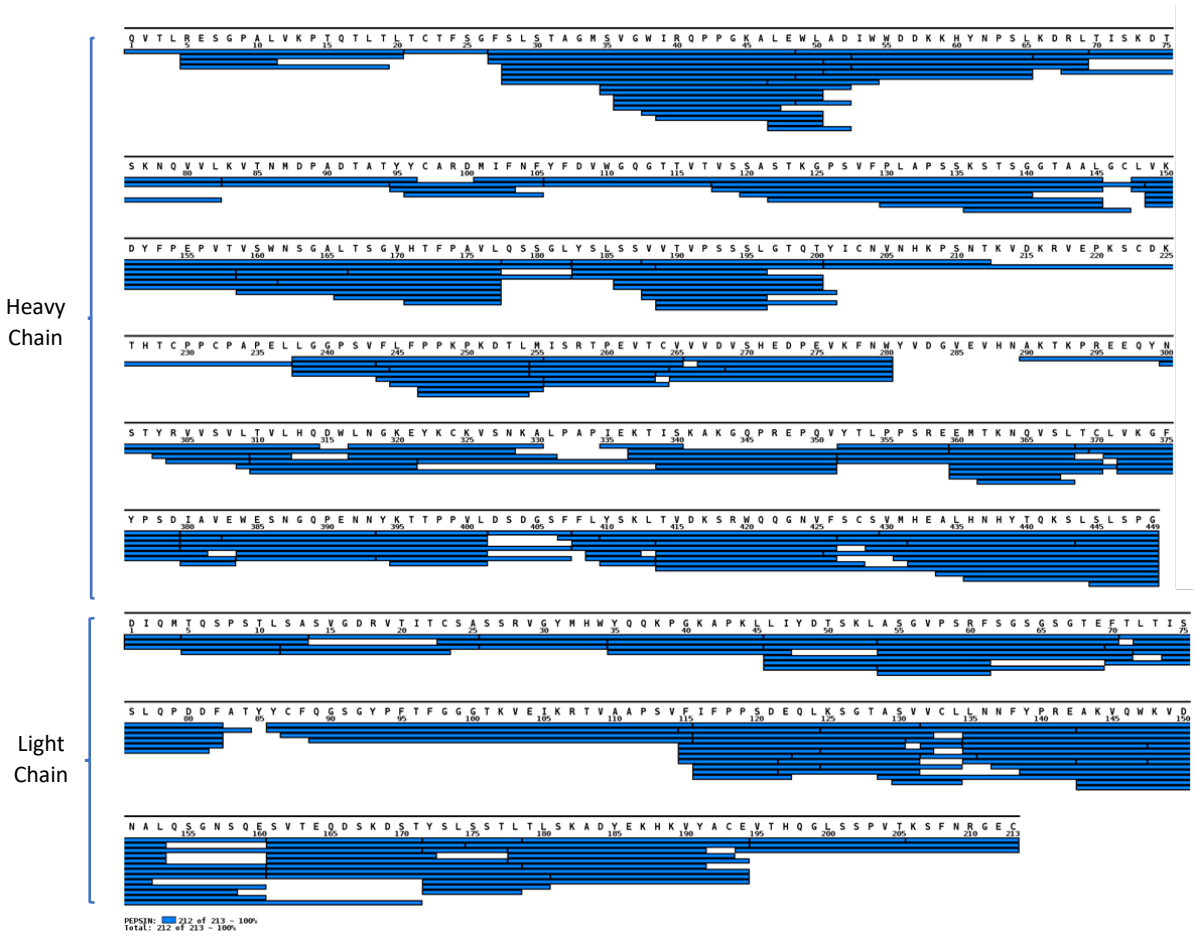

Figure 3.B-2. NIST mAb peptic peptide coverage map for the MabSelect SuRe resin experiment.

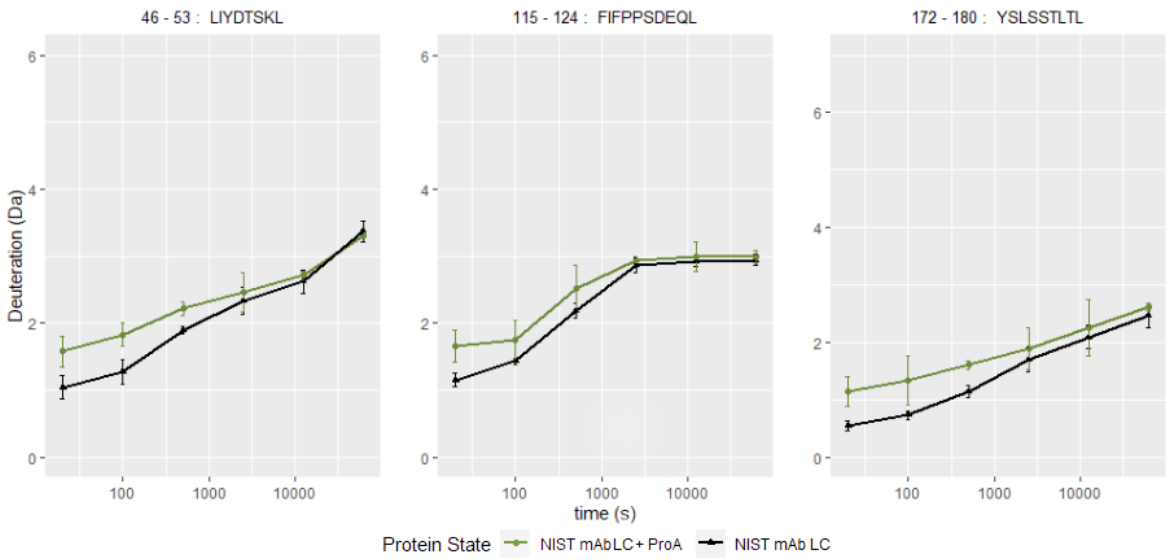

Figure 3.B-3. Uptake plots for light chain peptides with increased flexibility in the in-solution experiment with MabSelect SuRe 2:1 ratio. Error bars represent the 95% confidence interval for triplicate measurements of HX for each time point.

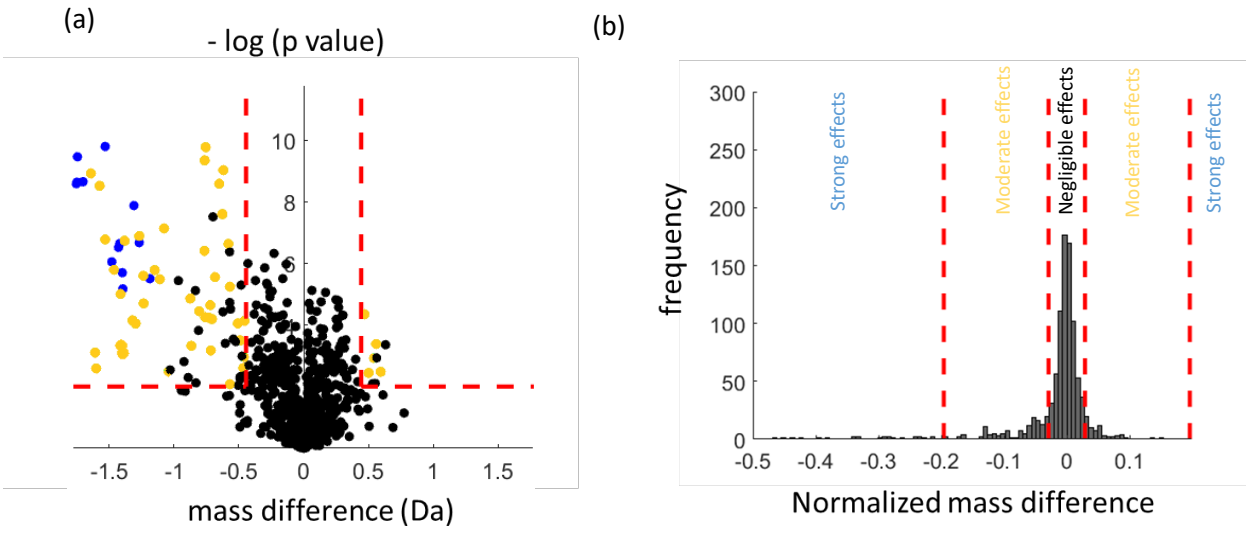

Figure 3.B-4. Statistical analysis for the MabSelect SuRe in solution (2:1 ratio) experiment. (a) volcano plot for identification of peptides with significant differences and magnitude of the effects. Negligible (black), moderate (yellow) and strong (blue) effects as revealed by k-mean clustering of the data. Red dashed lines in the volcano plot represent significance thresholds (horizontal sig. threshold = 2, vertical sig. threshold = ±0.5057Da) as defined by Hageman et al.[38] Note: black dots above the threshold limits are statistically significant but considered negligible effects since the normalized magnitude is too small. (b) histogram distribution of normalized HX differences (for all peptides at each labeling timepoint) used for the k-means clustering. Normalized differences were clustered into 3 bins, for negligible, moderate, and strong effects. Red dashed lines in the histogram (±0.0291 and ±0.1961) represent the threshold limits for each cluster.

	In-solution experiment (1:1 ratio)		In-solution experiment (2:1 ratio)		Resin experiment	
Data Set	**Control**	**mAb+ProA**	**Control**	**mAb+ProA**	**Control**	**mAb+ProA**
HDX reaction details	10 mM Na_2HPO_4, 150 mM sodium chloride, pH_{read} = 6.61, 25 °C	10 mM Na_2HPO_4, 150 mM sodium chloride, pH_{read} = 6.61, 25 °C	10 mM Na_2HPO_4, 150 mM sodium chloride, pH_{read} = 6.61, 25 °C	10 mM Na_2HPO_4, 150 mM sodium chloride, pH_{read} = 6.61, 25 °C	10 mM Na_2HPO_4, 150 mM sodium chloride, pH_{read} = 6.61, 22 °C	10 mM Na_2HPO_4, 150 mM sodium chloride, pH_{read} = 6.61, 22 °C
HDX time course (s)	60, 360, 1920, 11100, 63360	60, 360, 1920, 11100, 63360	20, 100, 500, 2500, 12500, 62500	20, 100, 500, 2500, 12500, 62500	20, 100, 500, 2500, 12500, 62500	20, 100, 500, 2500, 12500, 62500
HDX control samples	none		none		none	
Deuterium recovery (mean / IQR)	65%* / 15.5					
# of Peptides	165	165	159	159	256	256
Sequence coverage	LC 65%, HC 88%	LC 65%, HC 88%	LC 65%, HC 88%	LC 65%, HC 88%	LC 100%, HC 98%	LC 100%, HC 98%
Average peptide length / Redundancy	14/3.5		13.5/3.2		14.4/5.5	
Replicates (biological or technical)	3 (technical)	3 (technical)	4 (technical)	4 (technical)	4 (technical)	4 (technical)
Repeatability (pooled standard deviation)	0.1098 Da		0.1178 Da		0.1134 Da	
Significant differences in HDX (delta HDX > X D)**	0.5057 Da		0.5057 Da		0.4263 Da	

* average deuterium recovery calculated using pGlu-HWSYGLRPG-NH2, RPPGFSPFR, YGGFLR and YPI as model peptides, n=5

**see material and methods for description of significant differences threshold

3.6. REFERENCES

1. Lagasse HA, Alexaki A, Simhadri VL, Katagiri NH, Jankowski W, Sauna ZE, Kimchi-Sarfaty C 2017. Recent advances in (therapeutic protein) drug development. F1000Research 6:113.
2. Singh S, Kumar NK, Dwiwedi P, Charan J, Kaur R, Sidhu P, Chugh VK 2018. Monoclonal Antibodies: A Review. Current clinical pharmacology 13(2):85-99.
3. Mills BJ, Moussa EM, Jameel F. 2020. Chapter 1: Monoclonal Antibodies: Structure, Physicochemical Stability, and Protein Engineering. In Jameel F, Skoug JW, Nesbitt RR, editors. Development of Biopharmaceutical Drug-Device Products, ed., Cham: Springer International Publishing. p 3-26.
4. Elgundi Z, Reslan M, Cruz E, Sifniotis V, Kayser V 2017. The state-of-play and future of antibody therapeutics. Adv Drug Deliv Rev 122:2-19.
5. Ambrogelly A, Gozo S, Katiyar A, Dellatore S, Kune Y, Bhat R, Sun J, Li N, Wang D, Nowak C, Neill A, Ponniah G, King C, Mason B, Beck A, Liu H 2018. Analytical comparability study of recombinant monoclonal antibody therapeutics. MAbs 10(4):513-538.
6. Castelli MS, McGonigle P, Hornby PJ 2019. The pharmacology and therapeutic applications of monoclonal antibodies. Pharmacol Res Perspect 7(6):e00535.
7. Kaplon H, Reichert JM 2018. Antibodies to watch in 2019. MAbs 11(2):219-238.
8. Tsumoto K, Isozaki Y, Yagami H, Tomita M 2019. Future perspectives of therapeutic monoclonal antibodies. Immunotherapy 11(2):119-127.
9. Liu HF, Ma J, Winter C, Bayer R 2010. Recovery and purification process development for monoclonal antibody production. MAbs 2(5):480-499.
10. Rincon Pabon JP, Kochert BA, Liu Y-H, Richardson DD, Weis DD 2021. Protein A does not induce allosteric structural changes in an IgG1 antibody during binding. Journal of Pharmaceutical Sciences.
11. Huse K, Böhme H-J, Scholz GH 2002. Purification of antibodies by affinity chromatography. Journal of Biochemical and Biophysical Methods 51(3):217-231.
12. Urh M, Simpson D, Zhao K. 2009. Chapter 26 Affinity Chromatography: General Methods. In Burgess RR, Deutscher MP, editors. Methods in Enzymology, ed.: Academic Press. p 417-438.
13. Surolia A, Pain D, Islam Khan M 1982. Protein A: nature's universal anti-antibody. Trends in Biochemical Sciences 7(2):74-76.
14. Hober S, Nord K, Linhult M 2007. Protein A chromatography for antibody purification. Journal of Chromatography B 848(1):40-47.

15. Jendeberg L, Nilsson P, Larsson A, Denker P, Uhlén M, Nilsson B, Nygren P-Å 1997. Engineering of Fc1 and Fc3 from human immunoglobulin G to analyse subclass specificity for staphylococcal protein A. Journal of Immunological Methods 201(1):25-34.
16. Ishihara T, Kadoya T, Yoshida H, Tamada T, Yamamoto S 2005. Rational methods for predicting human monoclonal antibodies retention in protein A affinity chromatography and cation exchange chromatography. Structure-based chromatography design for monoclonal antibodies. Journal of chromatography A 1093(1-2):126-138.
17. Ghose S, Allen M, Hubbard B, Brooks C, Cramer SM 2005. Antibody variable region interactions with Protein A: Implications for the development of generic purification processes. Biotechnology and Bioengineering 92(6):665-673.
18. Jansson B, Uhlen M, Nygren PA 1998. All individual domains of staphylococcal protein A show Fab binding. FEMS immunology and medical microbiology 20(1):69-78.
19. Pabst TM, Palmgren R, Forss A, Vasic J, Fonseca M, Thompson C, Wang WK, Wang X, Hunter AK 2014. Engineering of novel Staphylococcal Protein A ligands to enable milder elution pH and high dynamic binding capacity. Journal of chromatography A 1362:180-185.
20. Nilsson B, Moks T, Jansson B, Abrahmsén L, Elmblad A, Holmgren E, Henrichson C, Jones TA, Uhlén M 1987. A synthetic IgG-binding domain based on staphylococcal protein A. Protein Engineering, Design and Selection 1(2):107-113.
21. Heathcare G. 2005. MabSelect SuRe—studies on ligand toxicity, leakage, removal of leached ligand, and sanitization. ed.: Technical note.
22. Yang D, Kroe-Barrett R, Singh S, Roberts CJ, Laue TM 2017. IgG cooperativity - Is there allostery? Implications for antibody functions and therapeutic antibody development. MAbs 9(8):1231-1252.
23. Ascenzi P, Bocedi A, Bolli A, Fasano M, Notari S, Polticelli F 2005. Allosteric modulation of monomeric proteins*. Biochemistry and Molecular Biology Education 33(3):169-176.
24. Wang W, Roberts CJ 2018. Protein aggregation - Mechanisms, detection, and control. International journal of pharmaceutics 550(1-2):251-268.
25. Correa A, Trajtenberg F, Obal G, Pritsch O, Dighiero G, Oppezzo P, Buschiazzo A 2013. Structure of a human IgA1 Fab fragment at 1.55 Å resolution: potential effect of the constant domains on antigen-affinity modulation. Acta Crystallographica Section D: Biological Crystallography 69(3):388-397.
26. Cornwell O, Bond NJ, Radford SE, Ashcroft AE 2019. Long-Range Conformational Changes in Monoclonal Antibodies Revealed Using FPOP-LC-MS/MS. Anal Chem 91(23):15163-15170.

27. Xia Y, Janda A, Eryilmaz E, Casadevall A, Putterman C 2013. The constant region affects antigen binding of antibodies to DNA by altering secondary structure. Molecular Immunology 56(1):28-37.
28. Gagnon P, Nian R, Leong D, Hoi A 2015. Transient conformational modification of immunoglobulin G during purification by protein A affinity chromatography. Journal of Chromatography A 1395:136-142.
29. Schlessinger J, Steinberg IZ, Givol D, Hochman J, Pecht I 1975. Antigen-induced conformational changes in antibodies and their Fab fragments studied by circular polarization of fluorescence. Proc Natl Acad Sci U S A 72(7):2775-2779.
30. Oda M, Kozono H, Morii H, Azuma T 2003. Evidence of allosteric conformational changes in the antibody constant region upon antigen binding. International immunology 15(3):417-426.
31. Sagawa T, Oda M, Morii H, Takizawa H, Kozono H, Azuma T 2005. Conformational changes in the antibody constant domains upon hapten-binding. Molecular Immunology 42(1):9-18.
32. Zhao J, Nussinov R, Ma B 2019. Antigen binding allosterically promotes Fc receptor recognition. MAbs 11(1):58-74.
33. Orlandi C, Deredge D, Ray K, Gohain N, Tolbert W, DeVico AL, Wintrode P, Pazgier M, Lewis GK 2020. Antigen-Induced Allosteric Changes in a Human IgG1 Fc Increase Low-Affinity Fcgamma Receptor Binding. Structure 28(5):516-527 e515.
34. Formolo T, Ly M, Levy M, Kilpatrick L, Lute S, Phinney K, Marzilli L, Brorson K, Boyne M, Davis D. 2015. Determination of the NISTmAb primary structure. State-of-the-art and emerging technologies for therapeutic monoclonal antibody characterization volume 2 Biopharmaceutical characterization: The NISTmAb case study, ed.: ACS Publications. p 1-62.
35. Schiel JE, Davis DL, Borisov OV. 2015. State-of-the-art and emerging technologies for therapeutic monoclonal antibody characterization volume 2. biopharmaceutical characterization: the NISTmAb case study. ed.: ACS Publications.
36. Majumdar R, Manikwar P, Hickey JM, Arora J, Middaugh CR, Volkin DB, Weis DD 2012. Minimizing Carry-Over in an Online Pepsin Digestion System used for the H/D Exchange Mass Spectrometric Analysis of an IgG1 Monoclonal Antibody. Journal of The American Society for Mass Spectrometry 23(12):2140-2148.
37. Glasoe PK, Long FA 1960. Use of Glass Electrodes to Measure Acidities in Deuterium Oxide1,2. The Journal of Physical Chemistry 64(1):188-190.
38. A. Busby S, J. Chalmers M, Griffin P. 2007. Improving digestion efficiency under H/D exchange conditions with activated pepsinogen coupled columns. ed. p 130-139.

39. Hageman TS, Weis DD 2019. Reliable Identification of Significant Differences in Differential Hydrogen Exchange-Mass Spectrometry Measurements Using a Hybrid Significance Testing Approach. Analytical Chemistry 91(13):8008-8016.
40. Angalakurthi SK, Vance DJ, Rong Y, Nguyen CMT, Rudolph MJ, Volkin D, Middaugh CR, Weis DD, Mantis NJ 2018. A Collection of Single-Domain Antibodies that Crowd Ricin Toxin's Active Site. Antibodies (Basel) 7(4):45.
41. Toth RTt, Angalakurthi SK, Van Slyke G, Vance DJ, Hickey JM, Joshi SB, Middaugh CR, Volkin DB, Weis DD, Mantis NJ 2017. High-Definition Mapping of Four Spatially Distinct Neutralizing Epitope Clusters on RiVax, a Candidate Ricin Toxin Subunit Vaccine. Clin Vaccine Immunol 24(12):e00237-00217.
42. Gallagher DT, Karageorgos I, Hudgens JW, Galvin CV 2018. Data on crystal organization in the structure of the Fab fragment from the NIST reference antibody, RM 8671. Data in Brief 16:29-36.
43. Gallagher DT, Galvin CV, Karageorgos I 2018. Structure of the Fc fragment of the NIST reference antibody RM8671. Acta Crystallographica Section F 74(9):524-529.
44. Bach J, Lewis N, Maggiora K, Gillespie AJ, Connell-Crowley L 2015. Differential binding of heavy chain variable domain 3 antigen binding fragments to protein A chromatography resins. Journal of chromatography A 1409:60-69.
45. Schroeder HW, Jr., Hillson JL, Perlmutter RM 1990. Structure and evolution of mammalian VH families. International immunology 2(1):41-50.
46. Silverman GJ, Goldfien RD, Chen P, Mageed RA, Jefferis R, Goni F, Frangione B, Fong S, Carson DA 1988. Idiotypic and subgroup analysis of human monoclonal rheumatoid factors. Implications for structural and genetic basis of autoantibodies in humans. J Clin Invest 82(2):469-475.
47. G LS, Plewka J, Lichtenegger H, Dias-Cabral AC, Jungbauer A, Tscheliessnig R 2019. The pearl necklace model in protein A chromatography: Molecular mechanisms at the resin interface. Biotechnol Bioeng 116(1):76-86.
48. Ultsch M, Braisted A, Maun HR, Eigenbrot C 2017. 3-2-1: Structural insights from stepwise shrinkage of a three-helix Fc-binding domain to a single helix. Protein Engineering, Design and Selection 30(9):619-625.
49. Deisenhofer J 1981. Crystallographic refinement and atomic models of a human Fc fragment and its complex with fragment B of protein A from Staphylococcus aureus at 2.9- and 2.8-.ANG. resolution. Biochemistry 20(9):2361-2370.
50. Deis LN, Wu Q, Wang Y, Qi Y, Daniels KG, Zhou P, Oas TG 2015. Suppression of conformational heterogeneity at a protein–protein interface. Proceedings of the National Academy of Sciences 112(29):9028.

51. Tashiro M, Tejero R, Zimmerman DE, Celda B, Nilsson B, Montelione GT 1997. High-resolution solution NMR structure of the Z domain of staphylococcal protein A. Journal of molecular biology 272(4):573-590.
52. Krissinel E, Henrick K 2007. Inference of macromolecular assemblies from crystalline state. J Mol Biol 372(3):774-797.
53. Noda M, Ishii K, Yamauchi M, Oyama H, Tadokoro T, Maenaka K, Torisu T, Uchiyama S 2019. Identification of IgG1 Aggregation Initiation Region by Hydrogen Deuterium Mass Spectrometry. Journal of pharmaceutical sciences 108(7):2323-2333.
54. Majumdar R, Esfandiary R, Bishop SM, Samra HS, Middaugh CR, Volkin DB, Weis DD 2015. Correlations between changes in conformational dynamics and physical stability in a mutant IgG1 mAb engineered for extended serum half-life. MAbs 7(1):84-95.
55. Majumdar R, Manikwar P, Hickey JM, Samra HS, Sathish HA, Bishop SM, Middaugh CR, Volkin DB, Weis DD 2013. Effects of salts from the Hofmeister series on the conformational stability, aggregation propensity, and local flexibility of an IgG1 monoclonal antibody. Biochemistry 52(19):3376-3389.
56. Manikwar P, Majumdar R, Hickey JM, Thakkar SV, Samra HS, Sathish HA, Bishop SM, Middaugh CR, Weis DD, Volkin DB 2013. Correlating excipient effects on conformational and storage stability of an IgG1 monoclonal antibody with local dynamics as measured by hydrogen/deuterium-exchange mass spectrometry. Journal of pharmaceutical sciences 102(7):2136-2151.
57. Houde D, Peng Y, Berkowitz SA, Engen JR 2010. Post-translational modifications differentially affect IgG1 conformation and receptor binding. Molecular & Cellular Proteomics 9(8):1716-1728.
58. Zhang A, Hu P, MacGregor P, Xue Y, Fan H, Suchecki P, Olszewski L, Liu A 2014. Understanding the conformational impact of chemical modifications on monoclonal antibodies with diverse sequence variation using hydrogen/deuterium exchange mass spectrometry and structural modeling. Analytical chemistry 86(7):3468-3475.
59. Houde D, Arndt J, Domeier W, Berkowitz S, Engen JR 2009. Characterization of IgG1 conformation and conformational dynamics by hydrogen/deuterium exchange mass spectrometry. Analytical chemistry 81(7):2644-2651.
60. Groves K, Cryar A, Cowen S, Ashcroft AE, Quaglia M 2020. Mass Spectrometry Characterization of Higher Order Structural Changes Associated with the Fc-glycan Structure of the NISTmAb Reference Material, RM 8761. J Am Soc Mass Spectrom 31(3):553-564.
61. Pan LY, Salas-Solano O, Valliere-Douglass JF 2014. Conformation and dynamics of interchain cysteine-linked antibody-drug conjugates as revealed by hydrogen/deuterium exchange mass spectrometry. Analytical chemistry 86(5):2657-2664.

62. Zhang J, Topp EM 2012. Protein G, protein A and protein A-derived peptides inhibit the agitation induced aggregation of IgG. Molecular pharmaceutics 9(3):622-628.
63. Singh N, Herzer S. 2018. Downstream Processing Technologies/Capturing and Final Purification. In Kiss B, Gottschalk U, Pohlscheidt M, editors. New Bioprocessing Strategies: Development and Manufacturing of Recombinant Antibodies and Proteins, ed., Cham: Springer International Publishing. p 115-178.
64. Schiel JE, Turner A 2018. The NISTmAb Reference Material 8671 lifecycle management and quality plan. Anal Bioanal Chem 410(8):2067-2078.

4. CHAPTER FOUR: EVALUATION OF STRUCTURAL CHANGES IN A MONOCLONAL ANTIBODY AT DIFFERENT PHs

4.1. INTRODUCTION

Protein therapeutics are revolutionizing the global market of pharmaceutical drugs due to the high specificity, efficacy, and lower risks to develop secondary effects after administration[1,2]. Therapeutic proteins have been used successfully in the treatment of many diseases such as cancers, autoimmune and infectious diseases. The types of therapeutic proteins available for treating such diseases include monoclonal antibodies (mAbs), enzymes, hormones, interleukins, interferons and many more[3]. As of late 2019, more than 570 therapeutic mAbs have been studied in clinical trials[4] and 79 therapeutic mAbs have been approved by the FDA[5]. Seven of the top 10 highest-selling drugs globally in 2019, were protein therapeutics, and five of them antibodies[6], showcasing the importance of this class of therapeutics and their exponential growth in the last decades.

The therapeutic activity of these proteins is governed by their higher-order structures (HOS), loss or change of HOS might decrease or affect the desired therapeutic properties. Protein therapeutics have very complex structures, highly sensitive to external conditions, hence production of these pharmaceuticals is challenging and requires many optimization processes to ensure efficacy, safety and quality[7]. One the biggest concerns is aggregation of the proteins during production, storage, transportation or administration steps[8], since aggregates can lead to loss of efficacy or to possibly develop immunogenicity responses[9]. The success of protein therapeutics is then highly dependent upon delivering the protein in its active form to the site of action. To achieve that goal, special protein formulations are developed that ensure that proteins remains physically, chemically and biologically stable during storage, administration and until reaching the site of action[10]. Formulation optimization is a challenging process that evaluates and improves protein stability by adjusting solution composition. Some of the factors evaluated are temperature, presence of excipients, ionic strength, introduction of co-solvents and many more. Often, formulations are unique for each developed therapeutic protein. A typical antibody formulation is composed of the antibody, a buffer, and a combination of excipients that vary widely. A recent review of formulations of commercially available antibodies showed how variable

these formulations can be[6]: antibody concentrations ranging from 0.012 to 200 mg/mL; pH values from 4.8 to 8.0; buffer concentrations between 0.02 M to 0.1 M; varied non-ionic excipients (such as trehalose or sorbitol); several lyoprotectants for mAbs formulated as solids (such as sucrose or mannitol); tonicity-adjusting agents (most common one is sodium chloride); many surfactants (such as PS20 or PS80), different chelators and more[6]. More importantly, therapeutic antibodies need to be able to withstand changes in pH without permanently affecting their functions. During normal administration, distribution, action, metabolism, and elimination of the mAbs in the human body, they are exposed to a wide range of pH environments from 5.9 to 7.4[11,12]. Thus, after administration they face microenvironments with concentration of hydronium ions (H^+) that can differ more that 30-fold. Although the difference in pH is necessary for the normal metabolism of the drugs (a decrease in pH in the endosomes is responsible for the high affinity binding of the mAbs to the FcRn receptors[12]; a crucial step in antibody recycling), it is imperative to know if there are any structural changes in the antibody after such drastic pH changes.

Hydrogen exchange-mass spectrometry (HX-MS) has emerged as a powerful technique to probe protein dynamics, elucidate structural changes, for formulation development in protein therapeutics, and other applications [13,14]. The effect of pH on antibody stability has been evaluated before[15-17]. It is known that changing the pH can vary the aggregation propensity of a protein, however, little is known about the structural changes provoked by these changes in pH. A clear insight into the structural changes in the antibodies could lead to better understanding of the stability and aggregation mechanisms of antibodies as well as enhanced formulations. Here, we used hydrogen exchange-mass spectrometry (HX-MS) to identify conformational changes in the NIST reference mAb when exposed to different formulation pHs. The range of pH selected, 5-8, for this study encompass the physiological and formulation pHs to which mAbs are usually exposed.

4.2. MATERIALS AND METHODS

4.2.1. Materials

NIST mAb RM8671 was obtained from the National Institute of Standard and Technology (NIST; Gaithersburg, MD) at a concentration of 10 mg/mL in 12.5 mM L-histidine, 12.5 mM L-histidine HCl, pH 6.0. Premium grade tris (2-carboxyethyl) phosphine hydrochloride (TCEP) and bradykinin were purchased from Thermo Scientific (Rockford, IL). Sodium phosphate dibasic (anhydrous), sodium chloride, urea, citric acid (anhydrous), LC-MS grade water and LC-MS 0.1% formic acid in water were purchased from Fisher Scientific (Hampton, NH). LC-MS grade acetonitrile containing 0.1% formic acid was obtained from Burdick-Jackson (Muskegon, MI). Synthetic peptide YPI was purchased from LifeTein (Someset, NJ). Deuterium oxide (99+ %D) was obtained from Cambridge Isotope Laboratories (Tewksbury, MA). Internal exchange reporter compounds TM-65 (5-(methoxycarbonyl)-1,3-dimethylbenzimidazolium) and TM-68[18] (1,3,5-trimethylbenzimidazolium) were a gift from Prof. Miklos Guttman (University of Washington, Seattle, WA).

4.2.2. Sample Preparation

Four stock solutions of NIST mAb reference material were buffer exchanged into 5 mM sodium phosphate, 5 mM sodium citrate, 100 mM sodium chloride buffer with pH values 5.00, 6.00, 7.00 and 8.00 ±0.02. Buffer exchange was performed twice using centrifugal filters pre-rinsed twice with buffer to eliminate contamination (Amicon Ultra, 0.5 mL, 3 kDa MWCO, MilliporeSigma, Burlington, MA) according to manufacturer's instructions. Samples were stored at 4°C and used within a few hours. Working solutions of NIST mAb at different pHs were diluted to a nominal concentration of 16.8 μM. All working solutions contained approximately 7 μM bradykinin, synthetic peptide YPI and internal exchange reporter compounds TM-65 and TM-68.

4.2.3. Hydrogen exchange-mass spectrometry

Hydrogen exchange labeling was performed using a LEAP Technologies HDX PAL robot (Carrboro, NC) with a customized three-valve configuration as described previously[19]. Deuterated samples were

prepared by diluting 5 µL of the working sample in 50 µL of labeling buffer (5 mM sodium phosphate, 5 mM sodium citrate, 100 mM sodium chloride with pD values 5.00, 6.00, 7.00 and 8.00 ±0.02 in D_2O). The pD was obtained from pH measurements with a glass electrode, corrected for the deuterium isotope effect (pD = pH + 0.4)[20]. Samples were labeled in quadruplicate for each labeling time (see **Table 4.1**) at 25°C. After labeling, the HX reaction was quenched with a 1 to 1 dilution with precooled quench buffer (8 M urea, 1.0 M TCEP) to a final pH of 2.5 at 1°C, aspirated 8 times to improve mixing and then held for 500 seconds to enhance disulfide bond reduction. Non-deuterated controls were prepared identically, but using 5 mM sodium phosphate, 5 mM sodium citrate, 100 mM sodium chloride with pH values 5.00, 6.00, 7.00 and 8.00 ±0.02 in H_2O. Immediately after the 500 s hold, 80 µL of sample was injected into a temperature-controlled chromatography cabinet connected to an Agilent 1260 Infinity series liquid chromatography system. Cabinet temperature and equipped liquid chromatography solvent pre-cooler were maintained at 0°C for all experiments. Injected sample was passed over an immobilized pepsin column (2.1 × 100 mm), prepared in house,[21] at 200 µL min^{-1} for 180 s with 0.1% formic acid in H_2O. The resulting peptic peptides were captured on a ZORBAX 300SB-C8 trap (2.1 × 12.5 mm, 5 µm particles) and washed at 200 µL min^{-1} for 60 s with 0.1% formic acid in H_2O. Desalted peptic peptides were separated on a ZORBAX 300SB-C18 column (2.1 × 50 mm, 3.5 µm particles) with a 12-minute linear gradient of 0.1% formic acid in acetonitrile increasing from 13% to 35% acetonitrile. Peptide masses were subsequently measured with an Agilent 6530 Q-TOF mass spectrometer running in ESI-positive mode. Pepsin column washes were performed between each sample injection during the elution step to minimize peptide carry-over.[19] An independent secondary gradient on trap and column after elution was used to reduce peptide carryover.

Table 4.1 HX experiment labeling times

Solution	Experimental labeling times (s)										
pH 5	320	860	3200	8600	32000	60000	86000				
pH 6	32	86	320	860	3200	6000	8600				
pH 7			32	86	320	600	860	3200	10000	32000	86000
pH 8					32	60	86	320	1000	3200	8600

HX-MS data were analyzed using HDExaminer (v. 3.2, Sierra Analytics, Modesto, CA). All results were manually reviewed and curated. Undeuterated NIST mAb peptic peptides were identified by a combination of data-dependent and targeted CID-MS2 in the QTOF using the same liquid chromatography gradient. MS2 spectra were matched to the NIST mAb sequence, with fixed modifications, using Agilent BioConfirm B.07. In-line digestion of the NIST mAb, resulted in 95% sequence coverage for the heavy chain (HC) and 98% sequence coverage for the light chain (LC). See **Figure 4.1**.

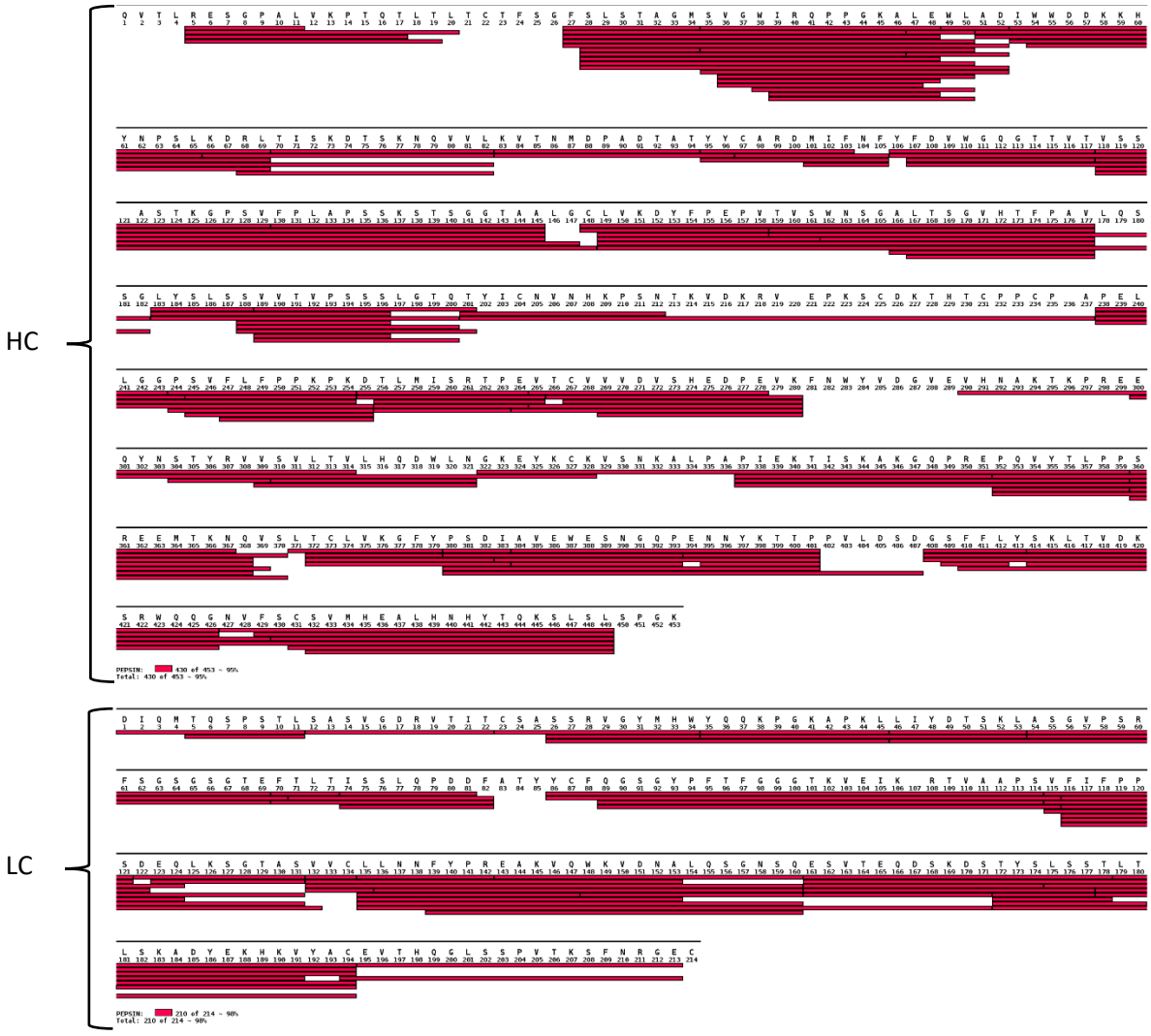

Figure 4.25 NIST mAb peptic peptides coverage map for the hydrogen exchange experiments. Top figure represent the coverage map for the heavy chain (HC) and bottom one for the light chain (LC) of the NIST mAb. Coverage maps were made using MSTools[22].

Correction of experimental labeling times at different pHs to a common reference state was done using equation 4.1 as established before[23,24]:

$$t = t_{\mathrm{ref}} 10^{\Delta \mathrm{pH}} \quad (4.1)$$

Where t is the labeling time at the measured pH, t_{ref} is the equivalent labeling time measured at the selected reference pH, and ΔpH is the difference between the reference state and the measured sample pH values ($\Delta pH = pH_{ref} - pH$).

When two states shared the same labeling times after the mathematical correction using equation 4.1, differential HX ($\Delta D = D - D_{ref}$) data were tested for significance using the hybrid significance testing criteria method[25] using an in-house Matlab script. For all comparisons, the pH 7 dataset was used as the reference state. Mean HX differences from labeling replicates were classified as significant when the absolute value of the mean centroid mass difference of each peptide at each labeling time point ($|\Delta D|$) was higher than a critical value (0.4059 Da) for the pH 5 vs. pH 7 comparison and 0.4275 Da for pH 6 vs. pH 7 comparison), and a Welch's two-sample t test had $p < 0.01$. Normalized HX differences (ΔHX), were obtained by dividing ΔD by number of backbone amide hydrogens in each peptide, excluding the first two residues. The absolute values of the normalized differences were then clustered using k-means clustering with $k = 3$ to define thresholds for strong, intermediate, and negligible HX differences, as described previously[26,27]. Labeling times conversion from the pH 8 experiment to the reference state was done using the ratio of the calculated exchange rates for the IER compounds TM-65 and TM-68 as described previously[18]. To identify HX changes for the pH 8 vs. pH 7 comparison, the areas between uptake curves for each peptide were used (see section 4.3.3 for further details). The area between curves was determined by calculating the area of a spline function based on the experimental data points (see **Figure 4.C-1**) using an in-house R-script (see **Table 4.C-1** in appendix C). Spline functions were integrated from $\log(t)=2.30$ to $\log(t)=4.73$ (first and last labeling time point at pH=8 after empirical correction) using the DescTools R package[28]. Normalized areas between curves were clustered as described above with $k = 3$. For visualization of the HX observations, a homology model was constructed

based on a combination of PBD 5K8A[29] and 5VGP[30]. Only peptides with strong effects identified by the *k*-means clustering were mapped onto the homology model. When two overlapping peptides presented conflicting results (different clustering), priority was given to the strongest effect. Following HX-MS community standards[43], additional HX details such as back exchange measurements and peptide coverage redundancy are available in Appendix C.

4.3. RESULTS

To identify structural changes in the NIST reference mAb when exposed to different formulation pH values, hydrogen exchange-mass spectrometry was used. Since changes in pH inherently change the chemical exchange rate for the experiments, a mathematical correction to the experimental labeling times was performed, as described in the Experimental section[18,23,24]. Four formulation pH values were employed (5, 6, 7 and 8) that encompass all endogenous and formulation pHs that mAb are normally exposed to during production, storage, and administration. In all cases pH 7 was used as the reference state.

4.3.1. Evaluation of the time point conversion using IER compounds

To determine if the mathematical labeling time correction works under the experimental conditions, synthetic peptide YPI and internal exchange reporter compounds TM-65 and TM-68 were used. **Figure 4.2** shows the uptake plot for synthetic peptide YPI[31] at different pH values after all experimental labeling times were corrected using equation 4.1 to the same reference state.

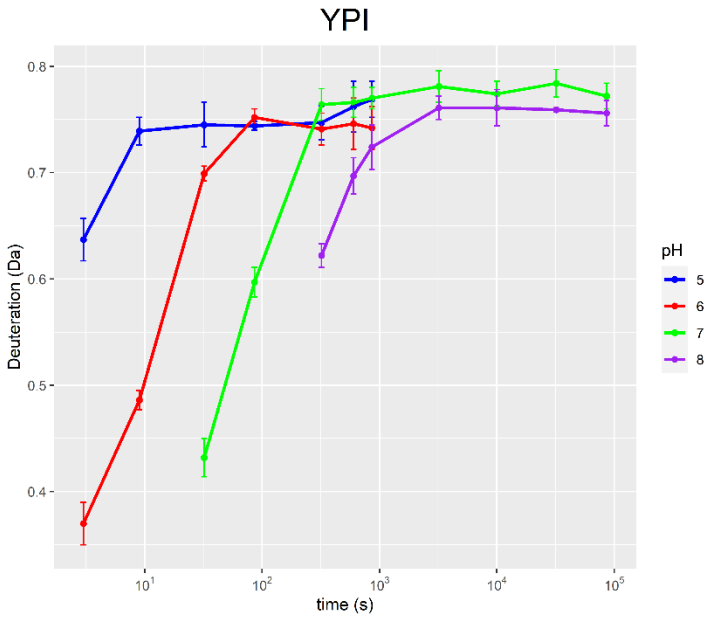

Figure 4.26. Deuterium uptake plot for synthetic peptide YPI measured at different pH. Labeling timepoints have been converted to the reference state (pH =7) using equation 4.1. Error bars represent the 99% confidence interval for quadruplicate measurements of HX at each labeling time.

Figure 4.2 shows very different deuterium uptake kinetics for the synthetic peptide at different pHs after the labeling time correction. These results could indicate that either the mathematical correction used does not work properly, or that the synthetic peptide YPI does not behave ideally and does not work as an internal standard for these HX experiments. YPI has a single amide, located at the C-terminus. C-terminal amides have been previously reported to have a complex pH-dependent exchange[18], this could explain why the deuterium uptake at the same nominal labeling time is so different. Additionally, **Figure 4.2** shows that YPI get fully deuterated at pH 7 in a matter of minutes. That small exchange time window limits the use of YPI as an internal reference compound. To further evaluate if the mathematical correction was working, IER compounds TM-68 and TM-65 were used[18].

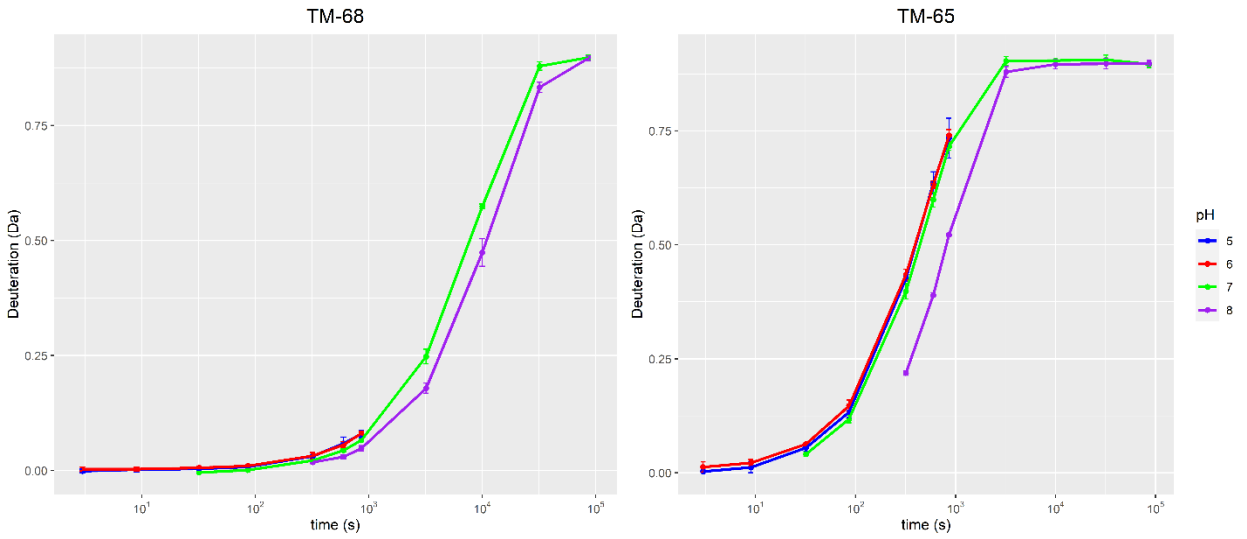

Figure 4.27 Deuterium uptake plots for IER compounds TM-68 and TM-65 measured at different pH values. Labeling timepoints have been converted to the reference state (pH =7) using equation 4.1. Error bars represent the 99% confidence interval for quadruplicate measurements of HX at each labeling time.

Figure 4.3 shows deuterium uptake plots for both IER compounds TM-65 and TM-68 measured at different pH values with labeling times converted to the same reference state by using equation 4.1. For both compounds, experimental data at pH 5, 6 and 7 exhibit almost indistinguishable kinetics. Since the IER compounds do not have secondary structure, the deuterium uptake will only depend on solution conditions and hence overlapping curves demonstrate that the time point conversion used is working properly at those pH values. Interestingly, both IER compounds at pH 8 shows a different behavior, based on pH 8 vs. pH 7 uptake plots using equation 4.1 correction (**Figure 4.3**) pH 8 showed slower corrected exchange compared to the reference state. These results indicate that the mathematical labeling time point conversion at pH 8 is not accurate and should not be used to compare further experiments at that pH value. Murphree et al.[18], used the experimental chemical exchange rate constant average ratio (by fitting the data to a single exponential equation) of both IER compounds to convert the labeling time points. **Figure 4.C-2** shows the fitted curve lines with the calculated exchange rate constants for the pH 7 and pH 8 data sets. The calculated exchange rate ratio for TM-68 is 7.0 while for TM-65 is 5.4. Based on equation 4.1, the expected ratio is 10, however the mean rate constant for both compounds at those pH values is 6.2. That average ratio can now be used as a time point shift factor to convert the labeling timepoints from pH 8 to the reference state as shown in equation 4.2.

$$t_{pH\ 8} = 6.2 t_{\mathrm{ref}} \quad (4.2)$$

NIST mAb labeling times at pH 5 and 6 were converted to the reference time scale by using the mathematical approach while pH 8 used the experimental factor 6.2 to convert labeling times at pH 8 to the reference state. This experimental timepoint conversion, causes a "misalignment" in the HX labeling times, preventing the use of the differential HX statistical analysis, and forcing the use of an alternative method utilizing the area between curves.

Changes in ionic strength can impact the chemical exchange rate constant. The effect on the chemical exchange rate constant depends on the local microenvironments and electrostatic fields of the protein[32]. Hence, changes in ionic strength could positively or negatively affect the exchange depending on the region of the protein. Here, we used a McIlvaine buffer at four different pH values (5, 6, 7 and 8). The McIlvaine buffer is a citric-phosphate buffer, with a buffer range from pH 3 to 8. Mass balance for the ionic species and total ionic strength for the 5 mM sodium phosphate, 5 mM sodium citrate, 100 mM sodium chloride buffer used in the HX experiments at different pH values calculated using Visual MINTEQ v3.1 software (considering Molarity (M) = molality (m) for all solutions used and neglecting the ionic contribution from the strong acid/base used to adjust the pH) is presented in table 4.2.

Table 4.2.Mass balance for ionic species and total ionic strength values for the McIlvaine buffer used in the HX experiments at different pH values.

	pH 5	pH 6	pH 7	pH 8
Ion	Concentration (mM)			
$Citrate^{3-}$	0.487	2.239	3.129	3.261
Cl^{1-}	96.815	96.871	96.915	96.933
H^{1+}	0.013	0.001	0.000	0.000
H_2-$Citrate^{-}$	0.906	0.040	0.001	0.000
$H_2PO_4^{-}$	4.427	3.852	1.659	0.247
H_3-$Citrate_{(aq)}$	0.009	0.000	0.000	0.000
H_3PO_4	0.004	0.000	0.000	0.000
H-$Citrate^{2-}$	3.323	1.500	0.207	0.021
HPO_4^{2-}	0.059	0.518	2.250	3.367
Na^{1+}	106.030	105.010	104.120	103.770
$Na_2HPO_{4(aq)}$	0.001	0.009	0.039	0.058
$Na_2PO_4^{-}$	0.000	0.000	0.000	0.000
Na-$Citrate^{2-}$	0.274	1.220	1.664	1.718

$NaCl_{(aq)}$	3.184	3.129	3.084	3.067
$NaH_2PO_{4(aq)}$	0.485	0.414	0.176	0.026
$NaHPO_4^-$	0.024	0.206	0.876	1.301
$NaOH_{(aq)}$	0.000	0.000	0.000	0.000
$NaPO_4^{2-}$	0.000	0.000	0.000	0.000
OH^-	0.000	0.000	0.000	0.001
PO_4^{3-}	0.000	0.000	0.000	0.000
Ionic Strength:	**0.114**	**0.119**	**0.124**	**0.126**

The calculated range of ionic strength for the buffers used goes from 0.114 to 0.126. However, those calculation do not consider the ionic contribution coming from the strong acid/base used to adjust the pH to the proper value. That contribution could affect the ionic strength calculation, especially for the pH 8 buffer that required higher amount of strong base to reach the desired pH. Nevertheless, we expect the experimental ionic strength of the buffers used for the HX experiments be within 20% of the calculated values shown in Table 4.2. The influence in the chemical exchange rate is expected to be minimal[32], although an increase in ionic strength is likely to contribute to a greater deviation in the HX measurements. **Figure 4.3** shows that the IER compounds at pH 8 have a slower chemical exchange rate compared to the other pH values. It is possible that the increase in ionic strength at pH 8 is responsible for decreasing the chemical exchange rate at pH 8, however the change in the rate constant is big enough that more likely there are additional unidentified sources of deviation in the system. Additional experiments need to be performed to identify them.

4.3.2. Changes in mAb conformation and dynamics at pH below 7

HX-MS measurements of the NIST reference mAb at pH 6 revealed many regions with increased flexibility compared to pH 7 after the time point conversion using equation 4.1 was performed. Statistical analysis for the data set (see **Figure 4.4a**) showed many peptides with intermediate increase in flexibility along the whole structure and nine peptides with strong increase in flexibility (residues 95-105, 238-255, 322-359, 372-382 in the HC). No strong significant changes were identified in the LC. Similarly, HX-MS measurements of the NIST reference mAb at pH 5 revealed many regions with deprotection compared to pH 7 after the time point conversion using equation 4.1 was used. Statistical analysis[25] of

the differential HX-MS data (see **Figure 4.4c**) identified several peptides with strongly increased flexibility at pH 5 (residues 95-105, 238-255 and 309-321 in the HC) and many more with moderately increased flexibility for both the HC and LC. No peptides in the LC showed strong effects. Even though most ΔD differences are not statistically significant, both **Figure 4.4a and 4.4c** show a clear systematic bias towards faster HX at lower pH. This systematic bias emerges because either the pH correction introduced a systematic error or because lowering the pH globally stimulates HX in the NIST mAb.

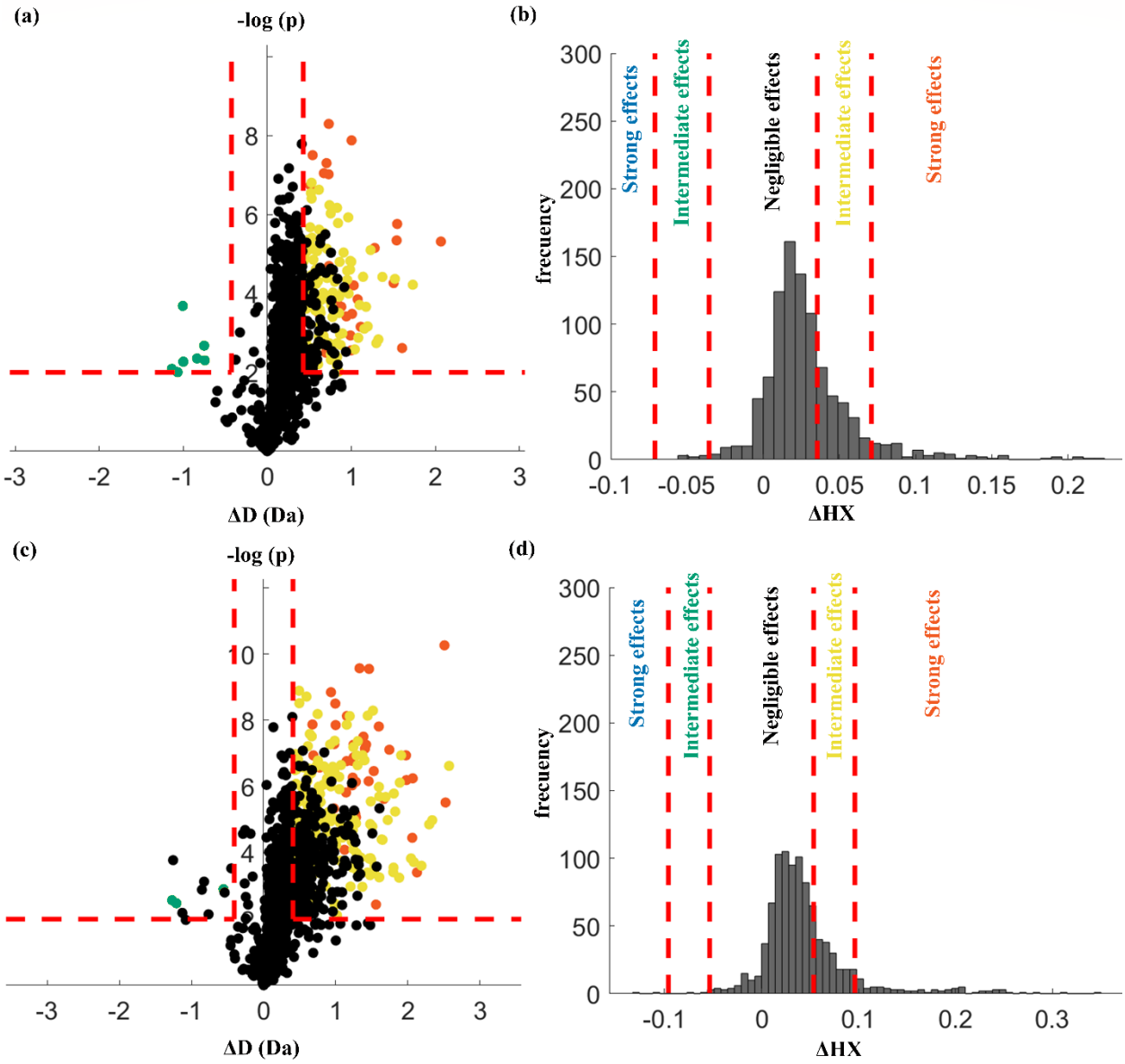

Figure 4.28 Statistical analysis for the NIST mAb at pH 6 and 5 compared to the reference state. (a)(c) Volcano plots for identification of peptides with significant differences and magnitude of the effects at pH 6 and 5 respectively. Negligible (black),

intermediate (green and yellow) and strong (vermillion) effects as revealed by k-means clustering of the data. Red dashed lines in the volcano plot represent significance thresholds (horizontal significance threshold $p < 0.01$, vertical significance threshold $|\Delta D| > 0.4059$ Da for pH 6 data set and >0.4275 Da for pH 5 data set comparison) as defined by Hageman et al.[25] Note: black dots above the threshold limits are statistically significant but considered negligible effects since the normalized magnitude is too small based on the k-means clustering. (b)(d) histograms distribution of normalized HX differences (for all peptides at each labeling timepoint) used for the k-means clustering at pH 6 and 5 respectively. Normalized differences were clustered into 3 bins, for negligible, intermediate, and strong effects. Red dashed lines in the histogram represent the threshold limits for each cluster.

Figure 4.5 shows representative uptake plots for three HC peptides identified as negligible, intermediate, and strong effects by the k-means clustering, the rest of the peptides (see all uptake plots in appendix C). Peptides classified as having negligible and intermediate HX effects are very similar and are difficult to distinguish visually. Equation 4.1 for the mathematical conversion of timescales to a reference state works very well (see **Figure 4.3**) and shows almost indistinguishable kinetics for the IER compounds at pH 5, 6 and 7. Hence the systematic bias toward faster HX most probably arises because lowering the pH indeed stimulates HX in the NIST mAb and not due to introduction of a systematic error from equation 4.1.

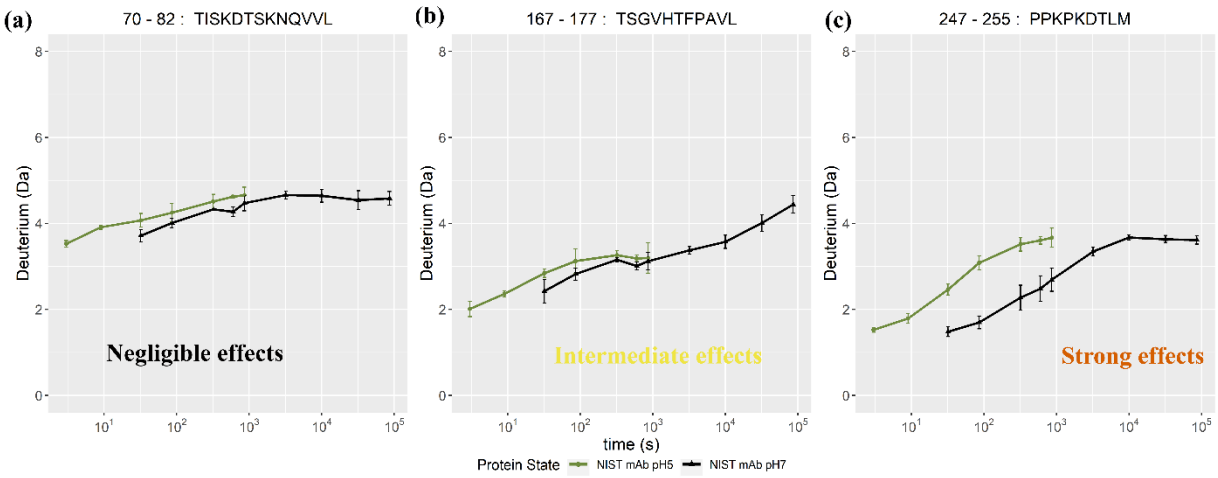

Figure 4.29 Representative uptake plots of the HC peptides showing the effect of lower pH (pH 5) compared to the reference state and the magnitude of the effect as revealed by the k-means clustering. (a) Peptide classified as with negligible effect. (b) Peptide classified as with intermediate effect. (c) Peptide classified as with strong effect. Error bars represent the 99% confidence intervals from quadruplicate measurements. Although all corrected HX labeling times are shown, HX differences were only determined when the HX times overlapped.

Figure 4.6 shows the statistically significant peptides as identified by the hybrid significance testing and the k-means clustering approaches for pH 5 compared to pH 7 (see **Figure 4.C-3** for pH 6 comparison to the reference state). Peptides with increased flexibility (yellow and vermillion bars) are seen along the whole sequence of the mAb, both in the heavy and light chain. Decreasing the pH increased the

flexibility for the whole protein compared to the reference state. However, there are many overlapping peptides in the experiment showing different clustering results (see peptides identified with different effects in the same region of the protein in **Figure 4.6** and **Figure 4.C-3**), and it is challenging to differentiate between them. As seen on **Figure 4.4** a decrease in pH essentially increases the backbone flexibility along the entire mAb. Nevertheless, some of those effects are small and difficult to detect in some peptides.

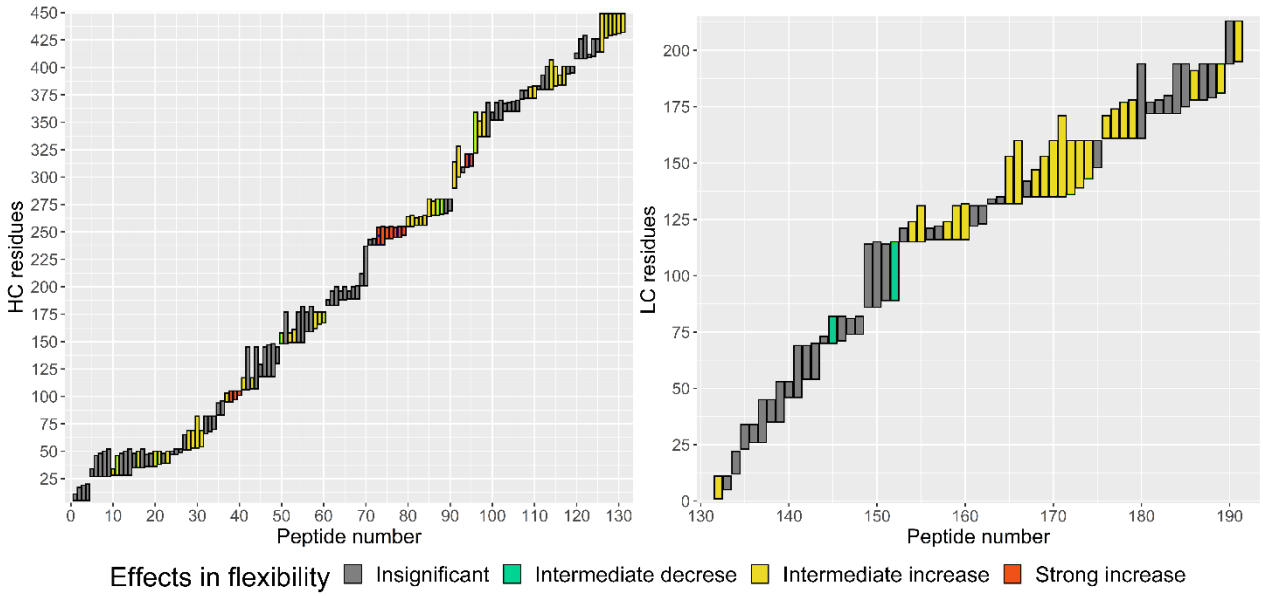

Figure 4.30 Bar plot showing the classification and magnitude of the effects in the peptides measured at pH 5 compared to the reference state by using volcano plots and k-means clustering for the heavy chain (left) and light chain (right). The vertical axis shows the protein residues numbers and the horizontal axis the peptide number.

Strong effects, however, are highly localized and overlapping peptides do not show conflicting. Hence, we will focus on strong effects only, since are the ones that represent the most substantial changes in the NIST mAb when the pH is changed. To be able to identify subtle or intermediate effects using this approach it is necessary to develop stronger statistical tests that consider errors coming from the time point conversion or use a different conversion method (section 4.3.3 use the area between curves to identify HX differences).

Both pH 6 and pH 5 compared to pH 7 showed similar regions strongly deprotected. Residues HC 95-105 located close to and withing the CDRH3 region, residues HC 238-255 C-terminal to the hinge region

and in the C_H2-C_H3 interface and residues HC 310-321 in the C_H2 domain, were strongly deprotected when the pH was decreased. Additional residues HC 372-382 in the C_H3 domain, close to the C_H2-C_H3 interface were also identified as strongly deprotected at pH 6 but not at pH 5 (these residues were classified as intermediately deprotected in the pH 5 experiment). This difference in classification is due to differences in the k-means cluster limits. pH 5 experiments showed bigger effects in general, that moved the k-means clusters bins to higher limits and classifying residues HC 372-382 as intermediately deprotected at pH 5. **Figure 4.9a and b** shows the strongly deprotected regions at pH 6 and 5 mapped onto the homology model. As depicted in the figure, deprotected regions are almost identical between pH 6 and pH 5 experiments (**Figure 4.9a and b**), only a few residues in the C_H3 domain are additionally deprotected in the pH 6 experiment. Statistical analysis comparing pH 6 and pH 5 data sets and manual evaluation of individual uptake plots (data not shown) confirmed that the extent of increased flexibility at pH 5 is larger compared to the pH 6 experiment. Therefore, similar regions are deprotected in the pH 5 and pH 6 experiment, but the effect is bigger and stronger when the pH is decreased to 5.

Overall, data show that the general structure of the antibody is more flexible at pH 6 and 5. Strong increases in flexibility are located mainly next to the hinge region and between the C_H2 and C_H3 domains. Interestingly, a strong increase in flexibility was also seen in residues HC 95-105 in the F_{ab} fragment of the antibody, in the HC CDR3 loop.

4.3.3. Changes in mAb conformation and dynamics at pH 8

Figure 4.3 shows that equation 4.1 cannot be used to convert labeling times from the pH 8 scale to the reference state. Instead, an empirical approach was used: the labeling times are shifted using the average rate ratio of rate constants for HX by the IER compounds TM-65 and TM-68. Experimental labeling times at pH 8 (see table 4.1), were converted to the reference state by dividing them by 6.2 (see equation 4.2) resulting in the following labeling times "misaligned" with pH 7: 198, 372, 533, 1984, 6200, 19840 and 53320 seconds. **Figure 4.7** shows representative uptake plots for representative peptides at pH 8 after the empirical labeling time correction compared to the reference state. For most of the peptides,

uptake plots overlap with the reference state over the full-time window, only a few peptides showed different deuterium uptake behavior.

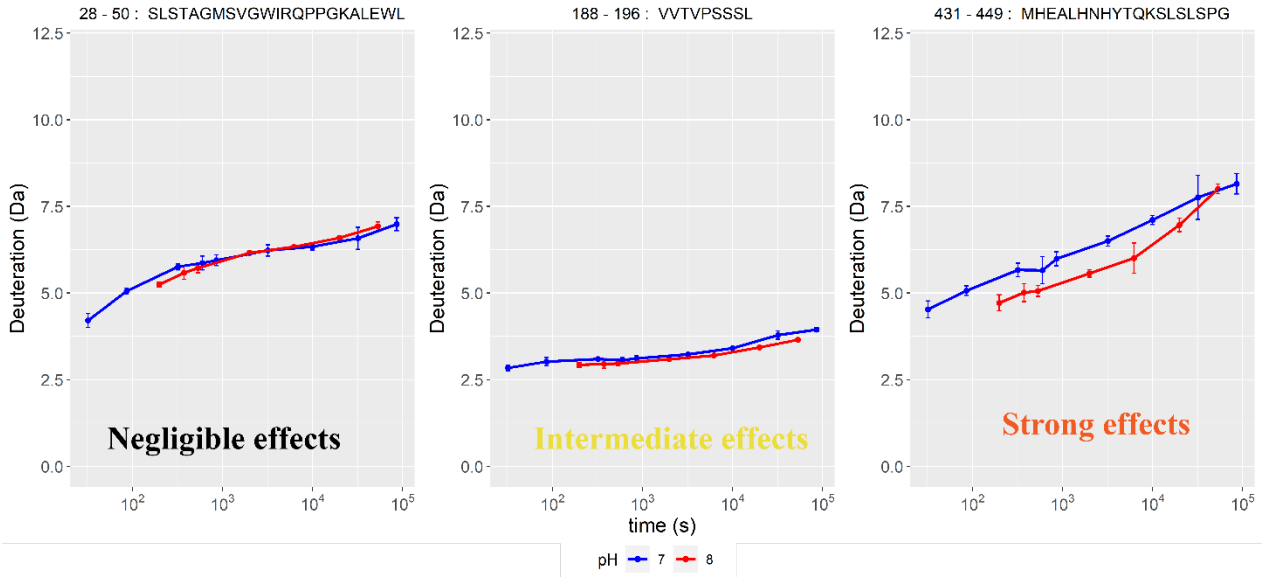

Figure 4.31 Representative uptake plots for HC peptides at pH 8 and pH 7 after the empirical labeling time correction. Error bars represent the 99% confidence intervals from quadruplicate measurements.

Traditional statistical analysis (hybrid significance test) to identify significant differences in the HX data for the pH 8 mAb compared to the pH 7 mAb, could not be performed due to the misalignment of the labeling time points between the two states. Instead, a different approach using the area between the curves was used[33,34]. The area between the uptake curves was calculated, normalized by the number of exchangeable amide hydrogens, and clustered into three bins using k-means clustering to identify negligible, intermediate, and strong effects. To evaluate the performance of this alternative approach, it was first applied to the pH 5 vs the reference state data set (see **Figure 4.C-4**). Although there are few peptides classified with intermediate effects using the hybrid significance test that were classified with negligible effects using the area between curves, both approaches identified the same residues as strongly deprotected except for two residues (HC 95 and 96, see peptide number 38 in **Figure4-C4**). These results provide confidence that the area between curves approach can properly identify strong effects in the data set. By using this approach to compare the pH 8 data versus pH 7 (see **Figure 4.C-5** for the histogram of the areas between curves used for the k-means clustering), eight peptides were identified as strongly

protected as shown in **Figure 4.8** (residues 5-11, 238-243, 431-449 in the HC and 35-81 in the LC). Each uptake plot for the strongly protected peptides was manually reviewed to confirm the classification.

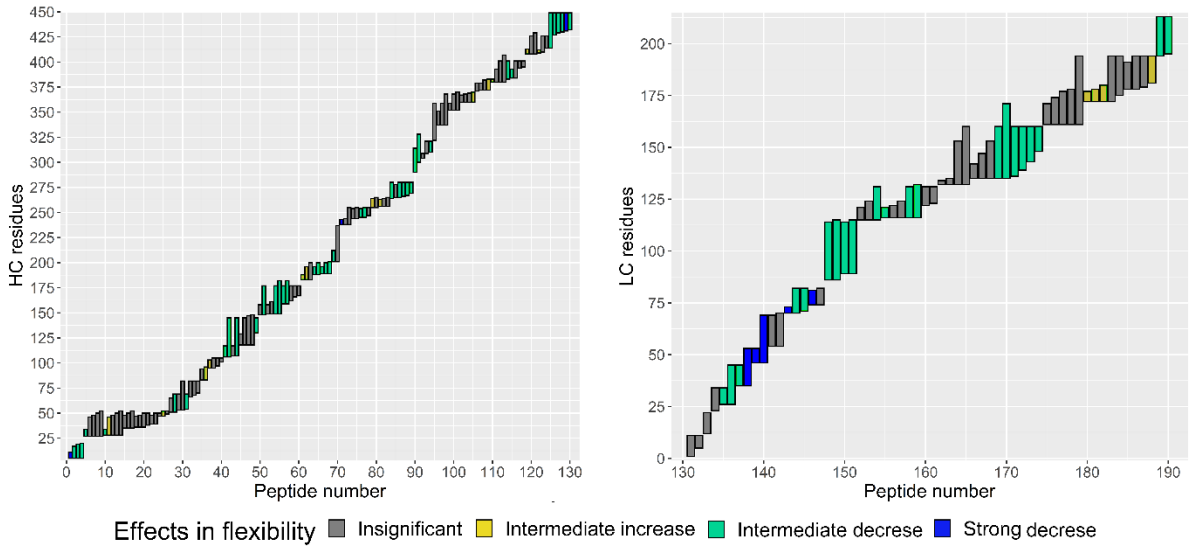

Figure 4.32 Bar plot showing the classification and magnitude of the effects in the peptides measured at pH 8 compared to the reference state by using the area between curves approach for the heavy chain (left) and light chain (right). The vertical axis shows the protein residues numbers and the horizontal axis the peptide number.

Is important to note that there are a few overlapping peptides in the heavy chain showing inconsistent results (see **Figure 4.8** for peptides classified as with intermediate increase (yellow) and peptides with intermediate decrease (light green) in flexibility across the same region). Inconsistent results are only seen with peptides classified with intermediate effects, most probably due to measurement errors and the use of the area between curves approach to identify the substantial changes.

Figure 4.9c shows the strongly protected regions at pH 8 compared to pH 7 mapped onto the homology model. Residues in the C_H2 located next to the hinge region and in the C_H3 located close to the C_H2-C_H3 interface show a strong increase in protection from the hydrogen exchange. Interestingly, there are also a residues strongly protected on the F_{ab} fragment. Specifically, in the CDRL2 and close to the CDRL1.

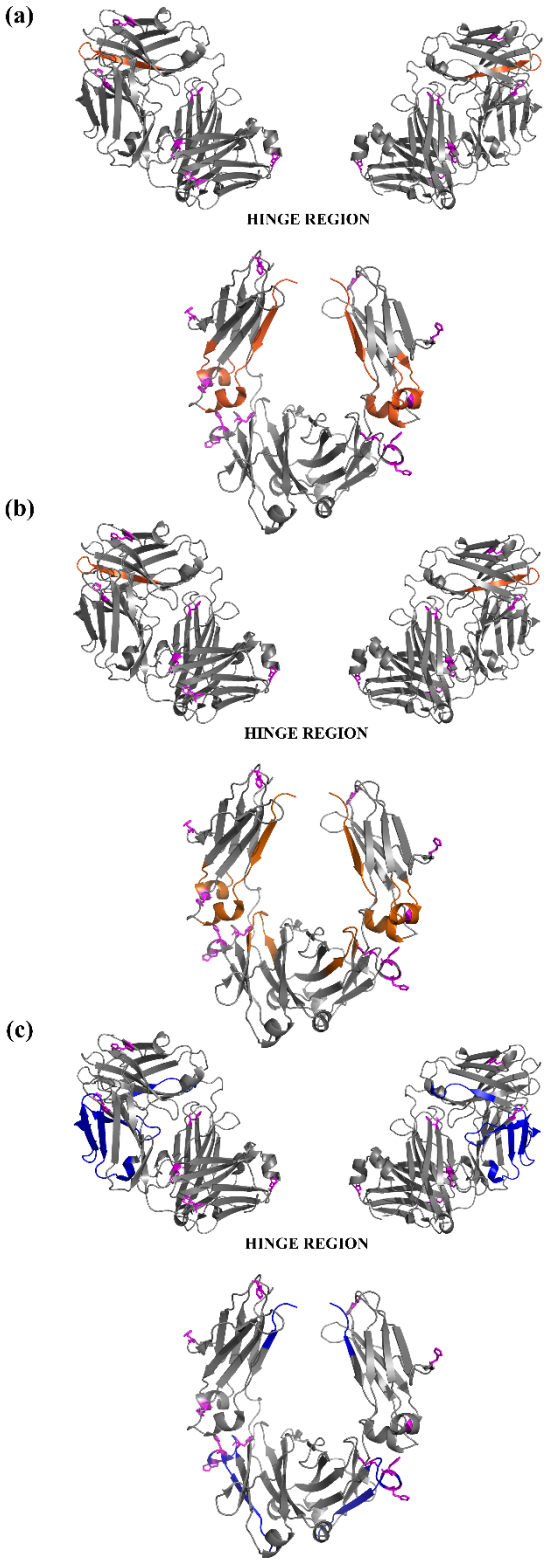

Figure 4.33 HX-MS differences provoked by changing the formulation pH compared to the reference state (pH = 7) mapped onto the homology model for the NIST mAb (PBD 5K8A[29] and 5VGP[30]). (a) pH 5 (b) pH 6 (c) pH 8. Vermillion represents areas with strong deprotection and blue areas with strong protection to deuterium exchange. In magenta Histidine residues.

4.4. DISCUSSION

Identification of changes conformation and dynamics of the NIST mAb after a change in formulation pH by using hydrogen exchange-mass spectrometry was evaluated here. While directly comparing protein states at different pH values is, in principle, simple and easy, changes in solution pH have an inherent influence on the chemical hydrogen exchange rate. Hence, it is necessary to correct for those changes to be able to identify HX differences coming from changes in conformation and dynamics and not from changes in the chemical hydrogen exchange rate. The pH range evaluated here (from pH 5 to pH 8) covers the whole formulation and endogenous pH values that antibodies are normally exposed to during storage, administration, and metabolism. There is limited literature on using HX-MS for identification of conformational changes due to pH changes in a monoclonal antibodies[35]. Here we used HX-MS to identify conformational changes after a change in pH using the NIST reference mAb as a model system.

IER compounds showed that a simple mathematical correction to labeling times is sufficient to correct for the intrinsic changes in the hydrogen exchange rate constant due to pH variation at values 5, 6 and 7 (see **Figure 4.3**). However, pH 8 data set showed an abnormal behavior that did not follow the model. For that case, an empirical correction to the data by using experimental exchange rate constants had to be used[18]. Hydrogen exchange rate constants are highly dependent on temperature and pH but are also influenced to some degree by the ionic strength of the solution[36,37]. All HX experiments presented here, used a McIlvine buffer (citrate-phosphate buffer) that has a buffer range from 3 to 8[38]. Calculated ionic strength values for the buffers used in the experiments ranged from 0.114 to 0.126 M (see Table 4.2). However, those calculation does not consider contributions coming from the strong acid/base used to adjust the pH. Nevertheless, we expect the experimental ionic strength of the buffers be within 20% of the values presented in Table 4.2. Generally, the higher the ionic strength, the stronger the influence in the acid- and base-catalyzed exchange HX rate. The effect could be negative or positive depending on the local electrostatic fields of the protein[36,39]. Although buffer solutions used in the experiments did not

have constant ionic strength values, the difference is expected to be small and the influence in the HX rate should be minimal[32]. However, pH 8 dataset (the one with the highest ionic strength) showed an unusual behavior with a slower chemical exchange rate than expected. Small variations in the ionic strength (0.002 M for the pH 7 and pH 8 comparison, see Table 4.2) are unlikely to explain why the pH 8 data is deviated from the theory. The decrease in the chemical exchange rate constant at pH 8 is more probably affected by other factors not identified here. More experiments are needed to identify possible causes.

For simplicity, all experimental comparisons used pH 7 as the reference state. Statistical analysis of HX data (see **Figure 4.4**) showed a general increase in flexibility along the whole antibody sequence when the pH was decreased to 6 or 5. Specifically, a strong increase in flexibility was seen for peptides in the C_H2 domain close to the hinge region and next to the C_H2-C_H3 interface (see **Figure 4.9a and b**). The structural effect seen here is bigger at pH 5 indicating that the lower the pH, the more dynamic the region becomes. Increases in flexibility in that same region (residues HC 238-255) have been correlated with distal point mutations[40], excipients effects[14,41], distal methionine oxidation[42,43], changes in glycosylation[42,44,45] but more importantly have been identified as a potential aggregation hotspot for IgG1 Abs[46,47]. This suggest that aggregation propensity for the NIST mAb at pH 6 or 5 could be higher compared to pH 7, however many experiments have shown the contrary: at lower pHs (6-5) the stability tends to be greater and aggregation propensity tends to be lower for IgG1 mAbs[48,49]. Xu et al., demonstrated that the NIST mAb was more colloidally stable at pH 6 compared to pH 7 or 8, because at higher pH values there were more attractive protein-protein interactions (PPI)[50]. The isoelectric point of the NIST reference mAb is 9.2[51], hence at higher pH (closer to the isoelectric point), there is less electrostatic repulsion between molecules and therefore more attractive protein-protein interactions[52]. Although at lower pH values protein stability tends to be better for most of the proteins, it is known that stability is buffer-, protein-, pH-, ionic strength-, and cosolute-dependent [53-56]. High pH values favor oxidation and deamidation post-translational modifications, and both modifications also increase the

aggregation propensity[57]. Altogether, the increase in flexibility in that region could change the aggregation propensity and stability of the mAb but that is dependent on other solution conditions.

An additional region in the C_H3 domain, next to the C_H2-C_H3 interface, had a strong increase in flexibility at pH 6 compared to pH 7 but not at pH 5 (that region was classified as with intermediate effect for the pH 5 comparison). This difference in classification is due to different cluster limits in the k-means clustering categorization. However, that region has a notable increase in flexibility at both pH 5 and 6 experiments.

FcRn receptor binds to IgG1 C_H2 and C_H3 domains, specifically to C_H2 residues 252-254, 309-311 and C_H3 residues 434-436.[58] IgG1-FcRn bind at pH 6 with an affinity constant in the nanomolar order but has negligible binding at pH 7.[59] FcRn showed no structural changes between pH 6.5 and 8[60], hence the increase in binding affinity is mainly attributed to increased electrostatic interactions between charged histidines in the Fc domain and the acidic residues in the FcRn[61]. An increase in structural flexibility in the C_H2-C_H3 interface, could also play an important role in the increase in binding affinity as suggested recently[62]. Thorough understanding of the receptor-antibody binding would allow the possible manipulation and improvement of effector functions.[63,64]

Additionally, both pH 6 and 5 showed increased flexibility in the CDRH3 loop when compared to the reference state (**Figure 4.9a and b**). An increase in CDR loop flexibility has been reported to increase antigen binding for specific cases[65], but more recently, a large scale study in CDRH3 loops of thousands of antibodies shows that an increase in rigidity in the CDRH3 loop might be involved in the increase of binding affinity[66]. Nowadays, there is a strong interest in the design of antibodies with decrease affinity at acidic endosomal pH, since such antibodies would release the antigen (e.g., cytokines or toxins) within the endosomes after endocytosis. Releasing the antigen within the endosome would reduce the so called "buffering effect" of antibodies that end up increasing the half-life of the target antigens.[67,68] A clear understanding of the conformational changes within the paratope of an antibody after a pH change can provide valuable information and help in the development of such antibodies.

Recently, Hamuro, et al.[35] evaluated the stability and aggregation propensity of the NIST mAb at different pH values using hydrogen exchange-mass spectrometry and other biophysical techniques. Buffer system and ionic strength conditions for their HDX experiments were different, and regions with increased flexibility were located mainly in the C_H2 and C_H3 domains when comparing pH 5 to pH 7 in the presence of 150 mM NaCl. Similarly, a general increased in flexibility was observed along the whole antibody and residues HC 97-117, 254-255, 261-264, 267-268, 261-264, 267-268, 281-288, 305-309, 318-321, 374-382, 397-401, 431-114 and LC 137-141 showed the highest increase in flexibility at pH 5 compared to pH 7. Curiously, only residues 97-105, 254-255, 309-321 were identified as strongly deprotected by both set of experiments, the rest of the strongly deprotected residues seen by Hamuro, et al.[35] were classified as intermediate effects here (except residues HC 281-288 that were missing in our data set). These discrepancies might be because of different solution conditions and different data analysis approaches.

Changing the pH of the solution can also affect the charge of some amino acid sidechains. Histidine residues, have a pK_a for the side chain of approximately 6. A decrease in pH (≤ 6) will protonate histidine side chains (this protonation is partially responsible for the increase in the Fc-FcRn binding affinity as explain above) and will positively affect (increase) the chemical exchange rate of the amide to its immediate left (towards the N-terminus) and the rate of the amide to the immediate right (towards the C-terminus) as stablished by Bai, et al. and later corrected by Nguyen, et al.[36,69]. Hence, peptides containing histidine residues at pH ≤ 6 will have a higher chemical exchange rate constant compared to the unprotonated histidine peptides. However, only one region (HC 310-321) identified as strongly deprotected by HX-MS for the pH 6 or 5 comparison contain a histidine residue. While having a charged histidine in the region will undoubtedly increase the chemical exchange rate for the neighboring residues, the extent of change seen in the experiments is big enough that it cannot be uniquely attributed to the charged histidines. Likewise, aspartic acid and glutamic acid residues have a pK_a for the side chain of approximately 3.7 and 4.3, respectively. It is possible that at pH 5, those residues became partially

protonated, increasing the chemical exchange rate constant. All the regions identified as strongly deprotected for the pH 6 and 5 comparison to the reference state contain at least one aspartic or glutamic acid residue. Partial protonation of those residues will generate a small change in the uptake plots for those peptides. However, those effects will undoubtfully be small and will not generate the strong increases in flexibility described here. Therefore, all the strong effects described here are attributed to the pH change and not to the small variation in the chemical exchange rates due to possible protonation of the sidechains.

The C_H2-C_H3 interface is a well conserved region among human IgG subclasses. It is mainly stabilized by hydrogen bonds and electrostatic interactions between residues in the C_H2 and C_H3 domains. Specifically, two salt bridges between side chains (K248/E380 and K338/E435), two hydrogen bonds (L251/H435 and K340/Y373) and a hydrophobic "ball in socket" joint are responsible for stabilizing that region[70,71]. The NIST mAb contains 6 histidine residues in the C_H2 and C_H3 domains, some of them (H313, H432, H436 and H438) are within or very close to the C_H2-C_H3 interface (see **Figure 4.9**). We hypothesize that decreasing the pH (hence protonating histidine residues) introduce additional electrostatic interactions to the C_H2-C_H3 interface, that disrupts the region. This destabilization is the one responsible for the increase in flexibility in the region as seen by our HX-MS experiments.

Finally, HX-MS experiments showed that an increase in formulation pH (from 7 to 8) provokes a general increase in rigidity of the structure, more specifically, a strong increase in protection close to the hinge region in the C_H2 domain and in the C_H3 domain close to the C_H2-C_H3 (residues HC 238-243, 431-449) and in a long region in the LC that includes the CDRL2, and residues close to the CDRL1. Interestingly, in this case the residues affected by the pH change in the F_{ab} fragment are different than the ones identified at pH 6 and 5 (see **Figure 4.9**). More importantly, a lack of structural changes in the C_H2 domain close to the C_H2-C_H3 interface as seen with the pH 6 and pH 5 data sets, further supporting our hypothesis that charged histidine residues are responsible for destabilizing that region.

In summary, our study clearly shows conformational or dynamic changes in the NIST mAb when the formulation pH is changed. A decrease in pH below 7 causes regions in the C_H2 domain and next to the C_H2-C_H3 interface to become more flexible while an increase in pH above 7 causes rigidity close to the hinge region in the C_H2 domain, and in the C_H3 domain close to the C_H2-C_H3 interface. This suggests an inverse relation between the pH and the C_H2-C_H3 interface flexibility. Additionally, changes in formulation pH also showed conformational changes in the Fab fragment of the antibody. A decrease in pH caused increased in flexibility in the CDRH3 while an increase in pH caused increase rigidity in the CDRL2 and close to the CDRL1. Changes in pH cause structural changes in very sensitive regions of the antibody and could affect both effector and antigen functions, both effects should be evaluated after a pH change in a case-by-case basis. Although we expect that heavily conserved Fc domains in other IgG1s would behave similarly, it is difficult to predict pH-induced changes in the hypervariable regions. To further evaluate structural changes in other mAbs after a formulation pH change, it is necessary to perform a more systematic work including many other mAbs and compare the regions affected.

4.5. APPENDIX C

Table 4.C-1. In-house R script to identify HX changes for the pH 8 vs. pH 7 comparison. The area between curves was determined by calculating the area of a spline function based on the experimental data points.

```
library(ggplot2) #Load libraries
library(readxl)
library(dplyr)
library(DescTools)
library(Ckmeans.1d.dp)
library(xlsx)

# Manually import data using RStudio import option
# use pH7 and pH8 to name the imported data

logtimr7= c(1.51, 1.93, 2.51, 2.78, 2.93, 3.51, 4.00, 4.51, 4.93) #timepoints in log scale
logtimr8= c(2.30, 2.57, 2.73, 3.30, 3.79, 4.30, 4.73) #timepoints in log scale

onlyaveph7= data.frame(pH7$`Ave 5`, pH7$`Ave 14`, pH7$`Ave 52`, pH7$`Ave 97`, pH7$`Ave
139`, pH7$`Ave 516`, pH7$`Ave 1613`, pH7$`Ave 5161`,pH7$`Ave 13871` ) #data organization
onlyaveph8= data.frame(pH8$`Ave 32`, pH8$`Ave 60`, pH8$`Ave 86`, pH8$`Ave 320`, pH8$`Ave
1000`, pH8$`Ave 3200`, pH8$`Ave 8600`) #data organization

areadif=c(1:pH7$ID) #necessary to avoid error
areadifnorm=c(1:pH7$ID) #necessary to avoid error
areadlogif=c(1:pH7$ID) #necessary to avoid error
areadlognorm=c(1:pH7$ID) #necessary to avoid error

for (i in pH7$ID){
transposedph7=t(onlyaveph7[i,]) # transpose values to a column
transposedph8=t(onlyaveph8[i,]) # transpose values to a column

arealogph7=AUC(logtimr7,transposedph7, method="spline",from=min(2.30),to=max(4.73))
#integrate spline from 32 to 8600
arealogph8=AUC(logtimr8,transposedph8, method="spline",from=min(2.30),to=max(4.73))
#integrate spline from 32 to 8600

areadlogif[i]=arealogph8-arealogph7
areadlognorm[i]=areadlogif[i]/pH7$`Max D`[i]
}

areadlognorm2=abs(areadlognorm)
kmeans2=Ckmeans.1d.dp(areadlognorm2,3) #K-means clustering
export=data.frame(PeptideID=c(1:190),Chain=pH7$Protein,start=pH7$Start,end=pH7$End,maxD=
pH7$`Max D`,arealog=areadlogif,arealogNorm=areadlognorm,Clusterlog=kmeans2$cluster)
write.csv(export,"RESULTSAUCnewlogpH8vs7_3.csv") #export results
```

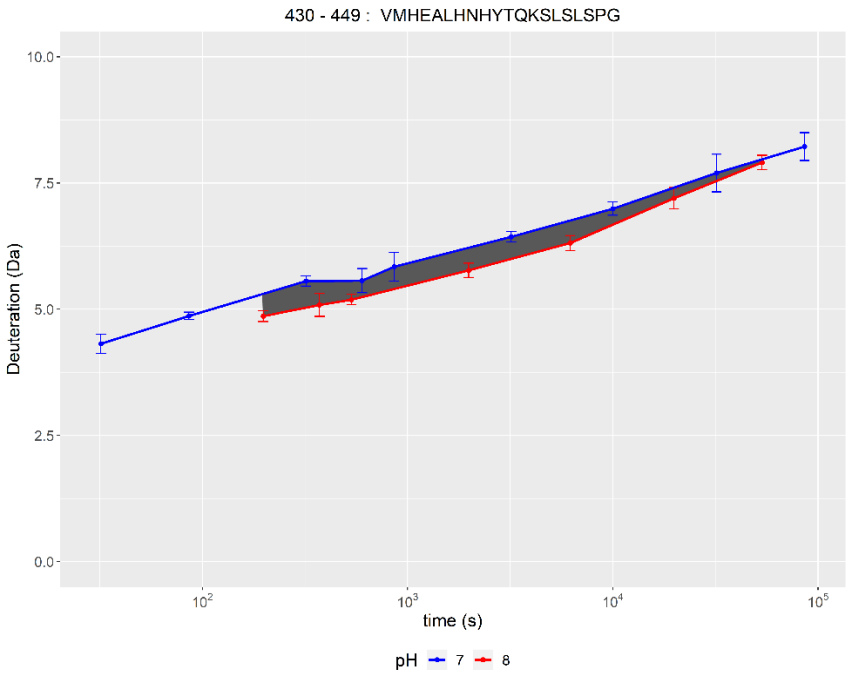

Figure 4.C-1. Representative uptake plot for peptide HC 430-449 at pH 8 and pH 7 after the empirical labeling time correction. Error bars represent the 99% confidence interval from quadruplicate measurements. In dark gray is the calculated area between curves used for k-means clustering of the data set and identify negligible, intermediate, and strong effects (see main text for details).

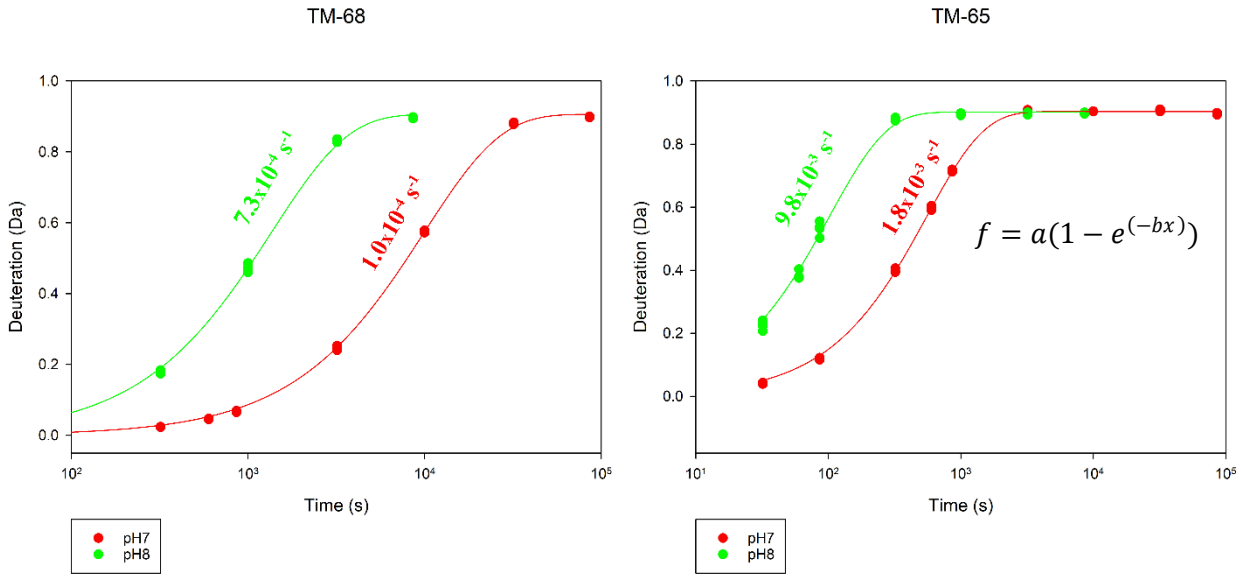

Figure 4.C-2. Deuterium uptake plots for IER compounds TM-65 and TM-68 at pH 7 and pH 8. Solid lines represent the exponential fit. Next to each line are the calculated exchange rate constants (b parameter in the fitted equation) for each compound. Data was fit to a two-parameter single exponential equation using SigmaPlot version 14.0, from Systat Software, Inc., San Jose California USA.

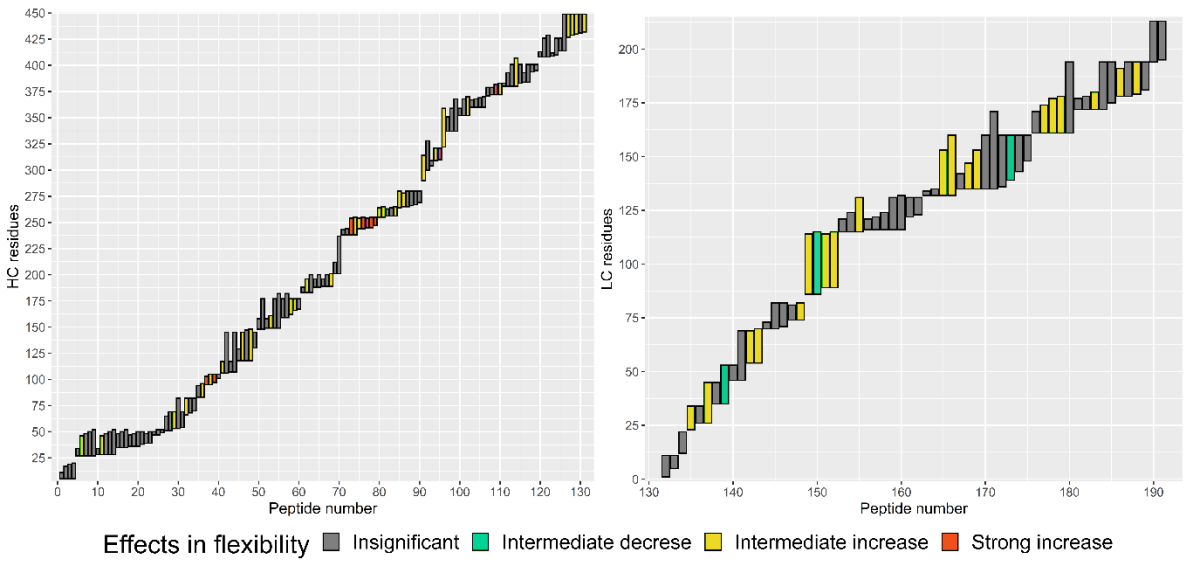

Figure 4.C-3. Bar plot showing the classification and magnitude of the effects in the NIST mAb peptides measured at pH 6 compared to the reference state by using volcano plots and k-means clustering for the heavy chain (left) and light chain (right). The vertical axis shows the protein residues numbers and the horizontal axis the peptide number.

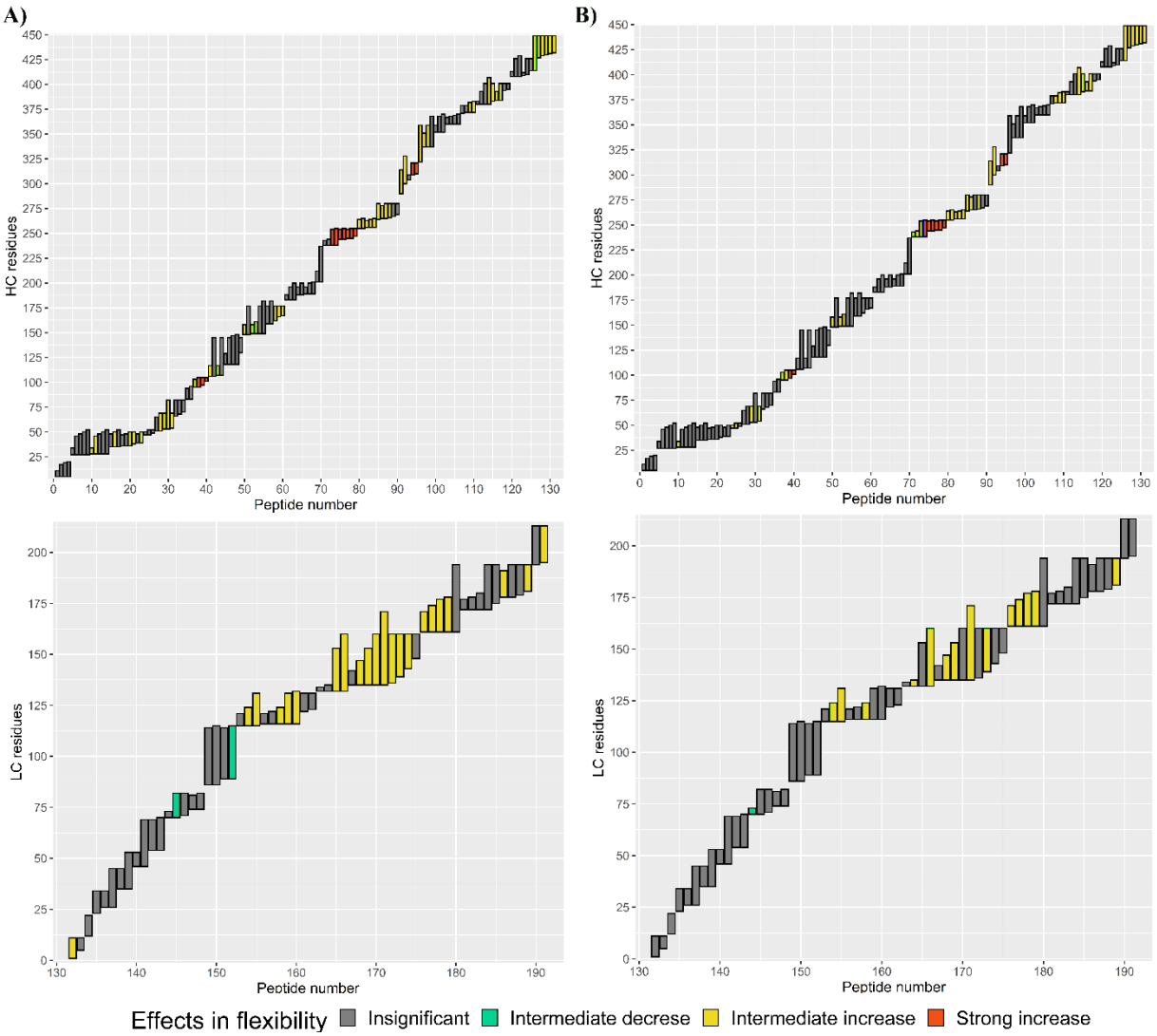

Figure 4.C-4. Bar plot showing the classification and magnitude of the effects in the NIST mAb peptides measured at pH 5 compared to the reference state using two different approaches. (A) classification and magnitude of the effects obtained by using the hybrid significance test and k-means clustering approach. (B) classification and magnitude of the effects obtained by using the area between curves and k-means clustering. See materials and methods section for more information.

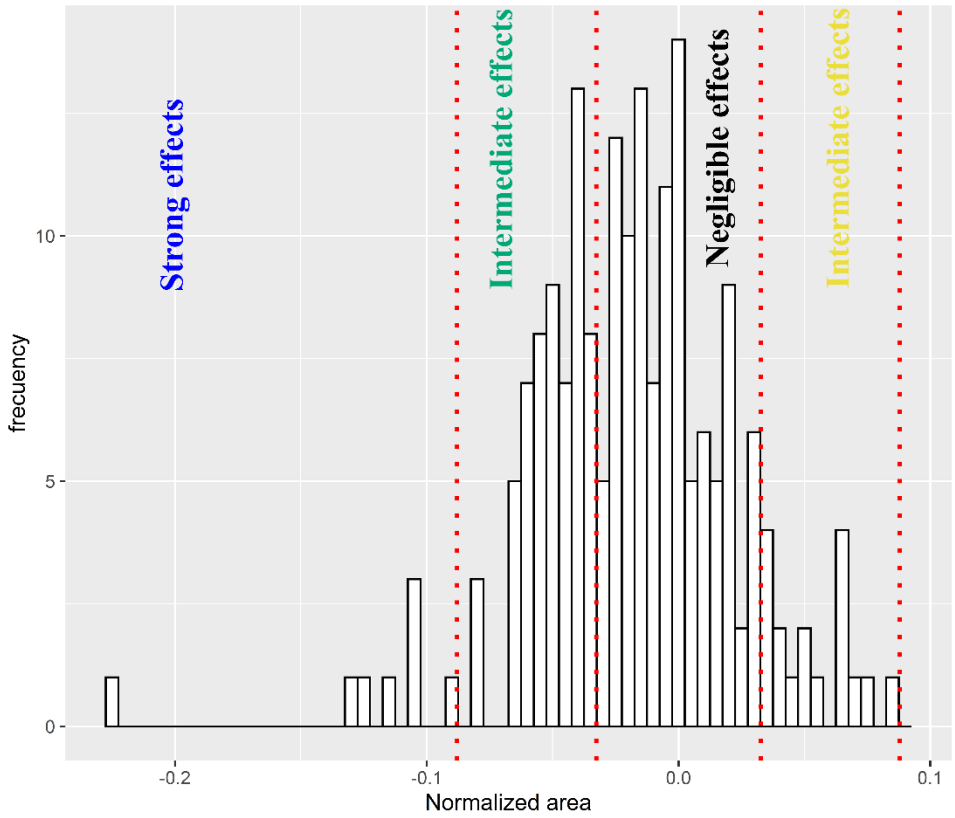

Figure 4.C-5. Histogram distribution of normalized areas between curves used for the k-means clustering in the pH 8 vs reference state comparison. Normalized differences were clustered into 3 bins, for negligible, intermediate, and strong effects. Red dashed lines in the histogram represent the threshold limits for each cluster.

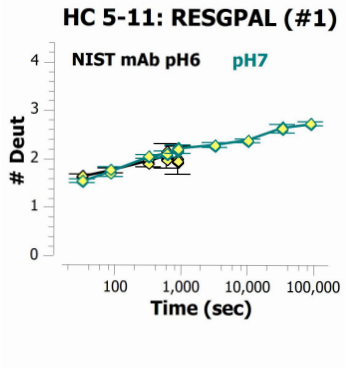
HC 5-11: RESGPAL (#1)
NIST mAb pH6 pH7
Deut
Time (sec)

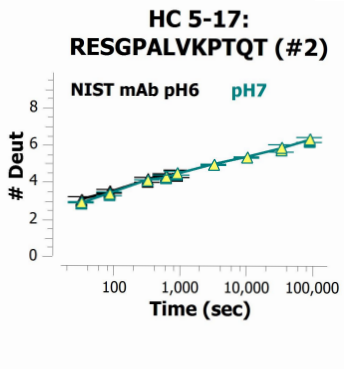
HC 5-17: RESGPALVKPTQT (#2)
NIST mAb pH6 pH7
Deut
Time (sec)

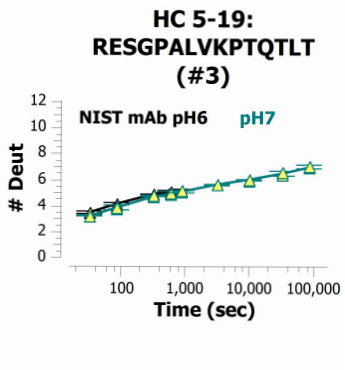
HC 5-19: RESGPALVKPTQTLT (#3)
NIST mAb pH6 pH7
Deut
Time (sec)

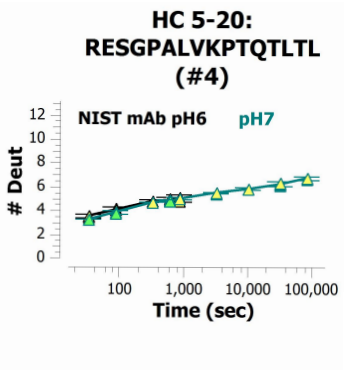
HC 5-20: RESGPALVKPTQTLTL (#4)
NIST mAb pH6 pH7
Deut
Time (sec)

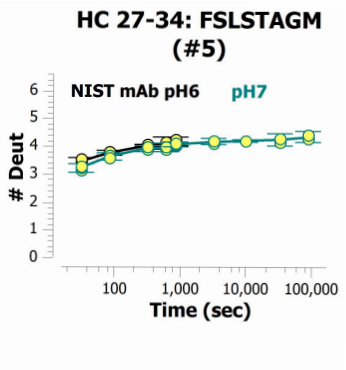
HC 27-34: FSLSTAGM (#5)
NIST mAb pH6 pH7
Deut
Time (sec)

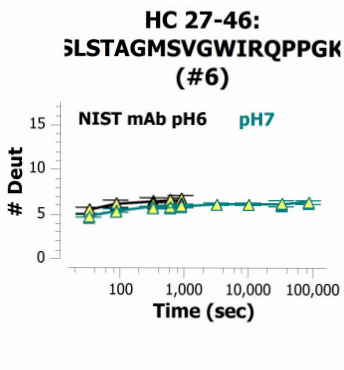
HC 27-46: SLSTAGMSVGWIRQPPGK (#6)
NIST mAb pH6 pH7
Deut
Time (sec)

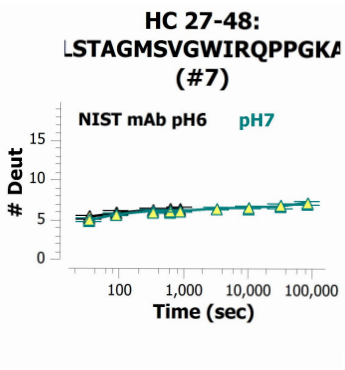
HC 27-48: LSTAGMSVGWIRQPPGKA (#7)
NIST mAb pH6 pH7
Deut
Time (sec)

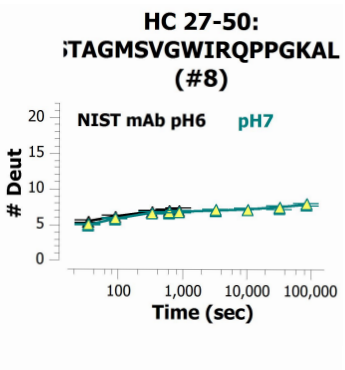
HC 27-50: STAGMSVGWIRQPPGKAL (#8)
NIST mAb pH6 pH7
Deut
Time (sec)

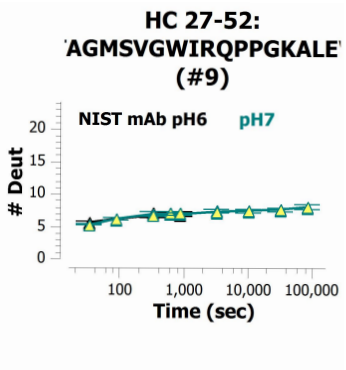
HC 27-52: AGMSVGWIRQPPGKALE (#9)
NIST mAb pH6 pH7
Deut
Time (sec)

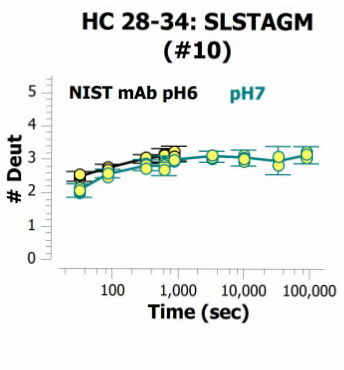
HC 28-34: SLSTAGM (#10)
NIST mAb pH6 pH7
Deut
Time (sec)

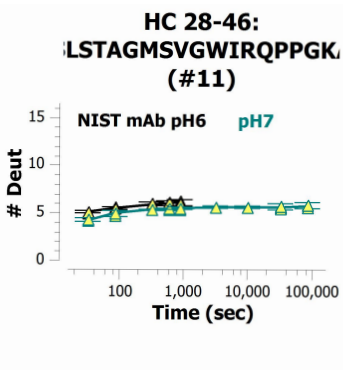
HC 28-46: LSTAGMSVGWIRQPPGK (#11)
NIST mAb pH6 pH7
Deut
Time (sec)

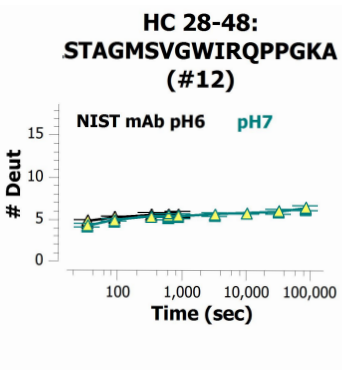
HC 28-48: STAGMSVGWIRQPPGKA (#12)
NIST mAb pH6 pH7
Deut
Time (sec)

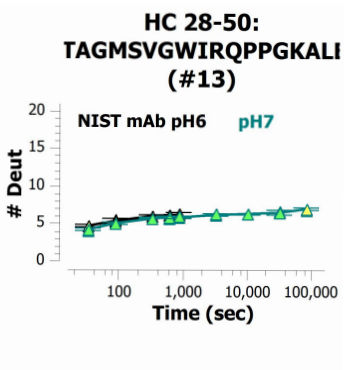
HC 28-50: TAGMSVGWIRQPPGKALI (#13)
NIST mAb pH6 pH7
Deut
Time (sec)

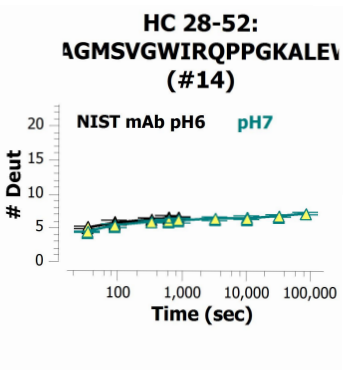
HC 28-52: AGMSVGWIRQPPGKALEV (#14)
NIST mAb pH6 pH7
Deut
Time (sec)

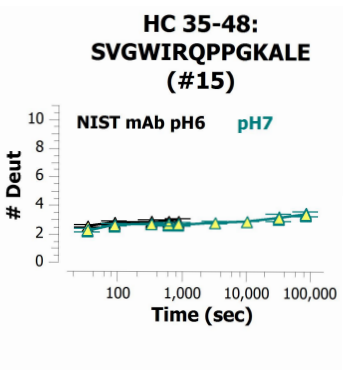
HC 35-48: SVGWIRQPPGKALE (#15)
NIST mAb pH6 pH7
Deut
Time (sec)

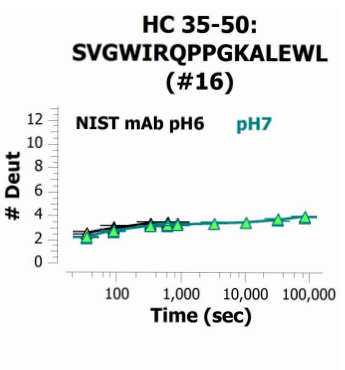
HC 35-50: SVGWIRQPPGKALEWL (#16)
NIST mAb pH6 pH7
Deut
Time (sec)

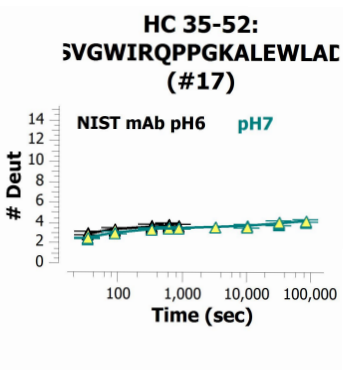
HC 35-52: SVGWIRQPPGKALEWLAD (#17)
NIST mAb pH6 pH7
Deut
Time (sec)

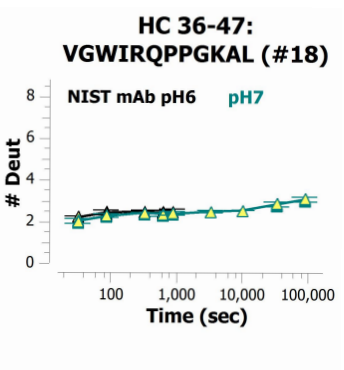
HC 36-47: VGWIRQPPGKAL (#18)
NIST mAb pH6 pH7
Deut
Time (sec)

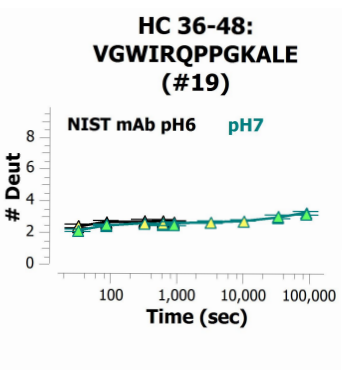
HC 36-48: VGWIRQPPGKALE (#19)
NIST mAb pH6 pH7
Deut
Time (sec)

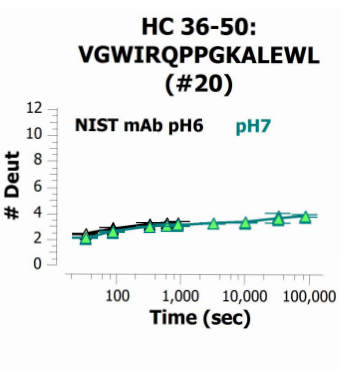
HC 36-50: VGWIRQPPGKALEWL (#20)
NIST mAb pH6 pH7
Deut
Time (sec)

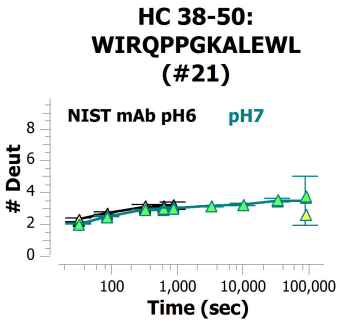
HC 38-50: WIRQPPGKALEWL (#21)
NIST mAb pH6 pH7
Deut
Time (sec)

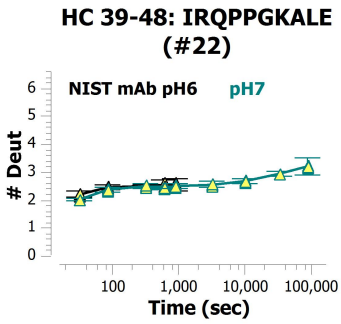
HC 39-48: IRQPPGKALE (#22)
NIST mAb pH6 pH7
Deut
Time (sec)

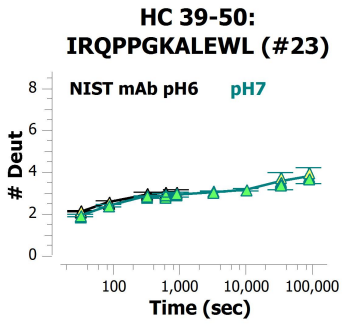
HC 39-50: IRQPPGKALEWL (#23)
NIST mAb pH6 pH7
Deut
Time (sec)

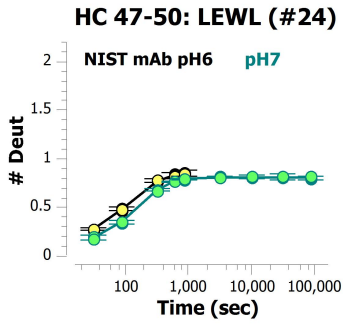
HC 47-50: LEWL (#24)
NIST mAb pH6 pH7
Deut
Time (sec)

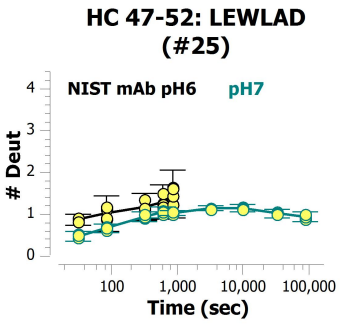
HC 47-52: LEWLAD (#25)
NIST mAb pH6 pH7
Deut
Time (sec)

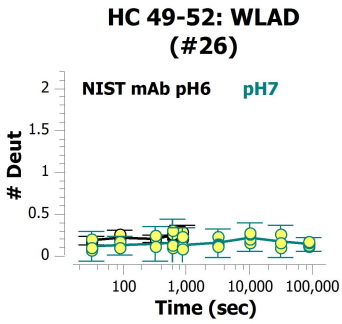
HC 49-52: WLAD (#26)
NIST mAb pH6 pH7
Deut
Time (sec)

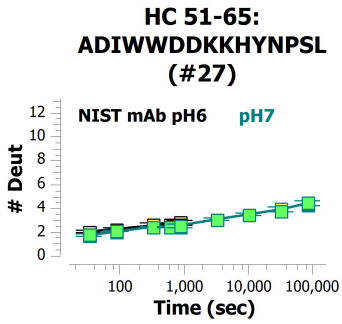
HC 51-65: ADIWWDDKKHYNPSL (#27)
NIST mAb pH6 pH7
Deut
Time (sec)

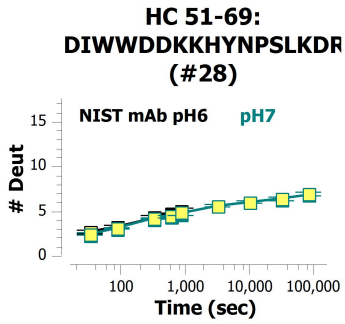
HC 51-69: DIWWDDKKHYNPSLKDR (#28)
NIST mAb pH6 pH7
Deut
Time (sec)

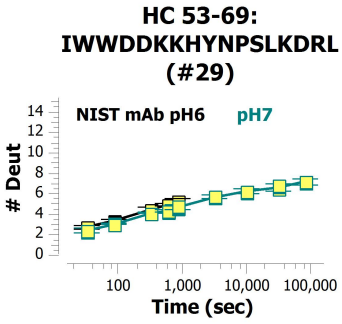
HC 53-69: IWWDDKKHYNPSLKDRL (#29)
NIST mAb pH6 pH7
Deut
Time (sec)

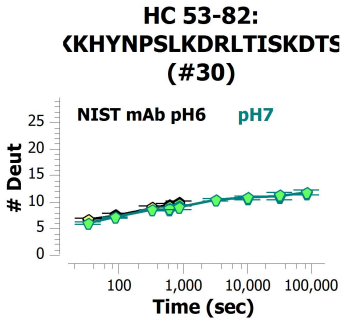
HC 53-82: (KHYNPSLKDRLTISKDTS (#30)
NIST mAb pH6 pH7
Deut
Time (sec)

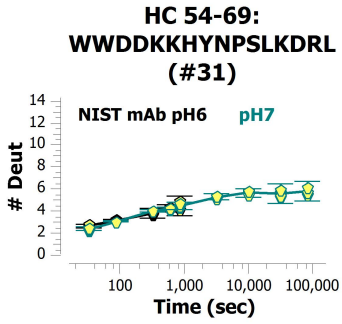
HC 54-69: WWDDKKHYNPSLKDRL (#31)
NIST mAb pH6 pH7
Deut
Time (sec)

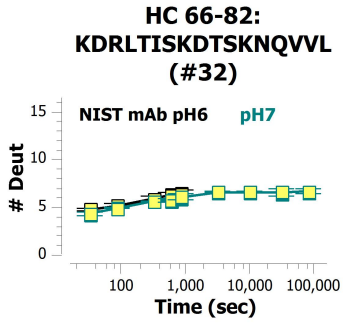
HC 66-82: KDRLTISKDTSKNQVVL (#32)
NIST mAb pH6 pH7
Deut
Time (sec)

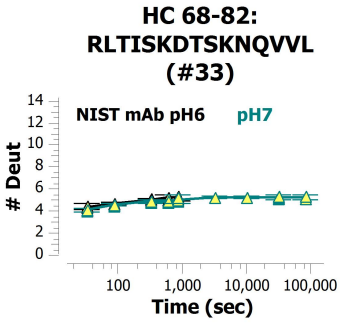
HC 68-82: RLTISKDTSKNQVVL (#33)
NIST mAb pH6 pH7
Deut
Time (sec)

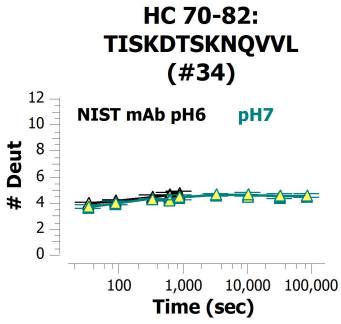
HC 70-82: TISKDTSKNQVVL (#34)
NIST mAb pH6 pH7
Deut
Time (sec)

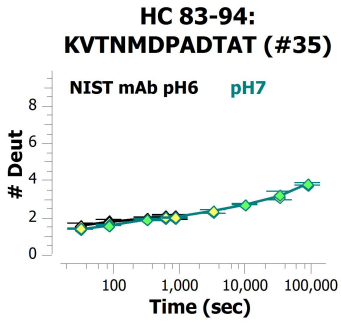
HC 83-94: KVTNMDPADTAT (#35)
NIST mAb pH6 pH7
Deut
Time (sec)

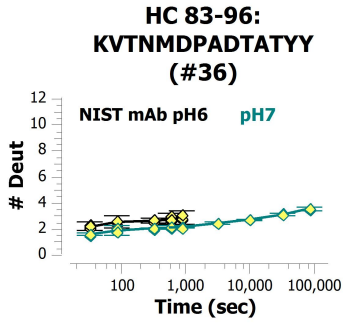
HC 83-96: KVTNMDPADTATYY (#36)
NIST mAb pH6 pH7
Deut
Time (sec)

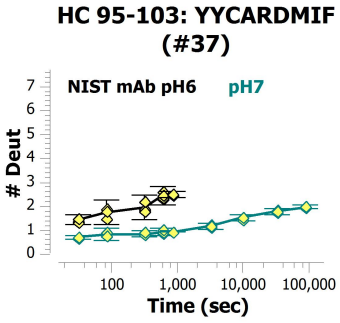
HC 95-103: YYCARDMIF (#37)
NIST mAb pH6 pH7
Deut
Time (sec)

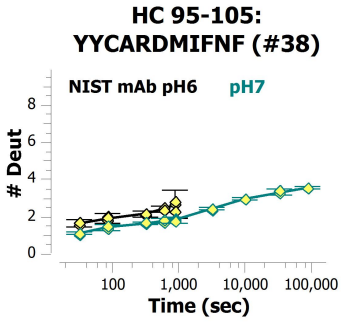
HC 95-105: YYCARDMIFNF (#38)
NIST mAb pH6 pH7
Deut
Time (sec)

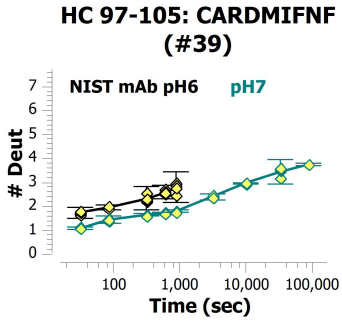
HC 97-105: CARDMIFNF (#39)
NIST mAb pH6 pH7
Deut
Time (sec)

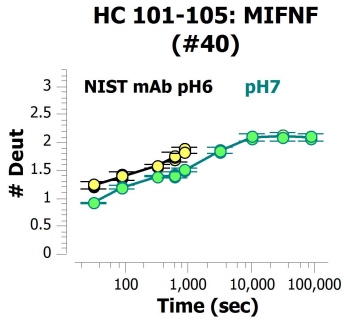
HC 101-105: MIFNF (#40)
NIST mAb pH6 pH7
Deut
Time (sec)

HC 106-117: YFDVWGQGTTVT (#41)

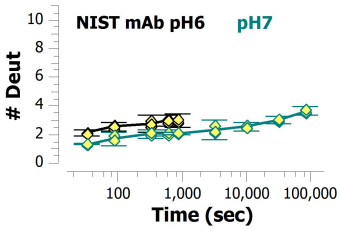

HC 106-145: VTVSSASTKGPSVFPLAPS (#42)

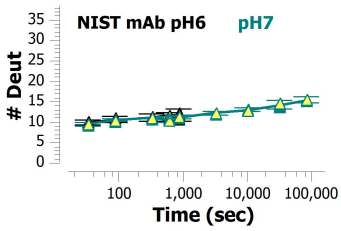

HC 107-117: FDVWGQGTTVT (#43)

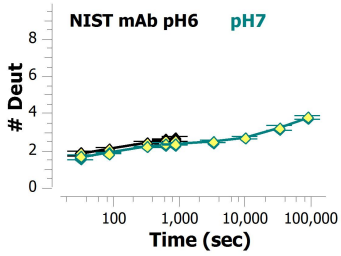

HC 107-145: TVSSASTKGPSVFPLAPS (#44)

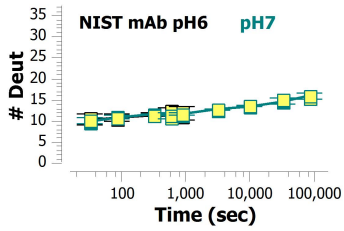

HC 118-129: VSSASTKGPSVF (#45)

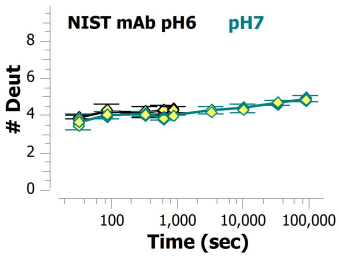

HC 118-145: TKGPSVFPLAPSSKSTSG (#46)

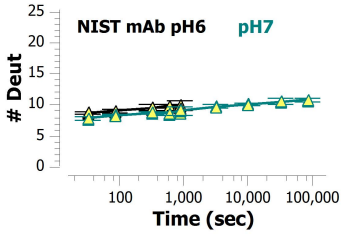

HC 118-147: KGPSVFPLAPSSKSTSGG (#47)

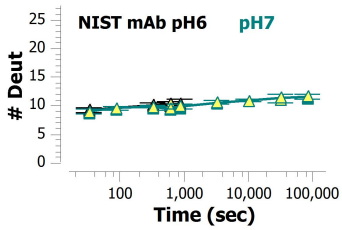

HC 118-148: KGPSVFPLAPSSKSTSGGT (#48)

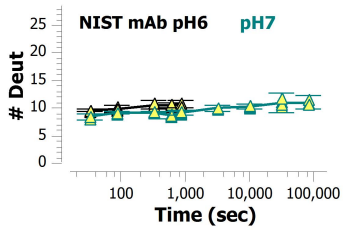

HC 130-145: PLAPSSKSTSGGTAAL (#49)

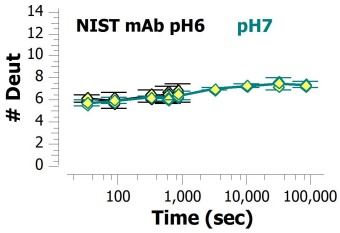

HC 148-158: LVKDYFPEPVT (#50)

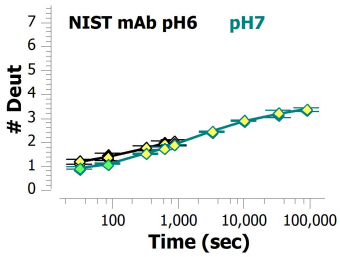

HC 148-177: PEPVTVSWNSGALTSGVH (#51)

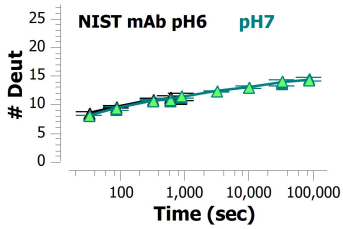

HC 149-158: VKDYFPEPVT (#52)

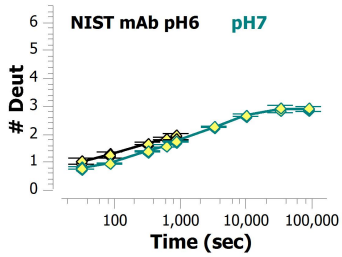

HC 149-161: VKDYFPEPVTVSW (#53)

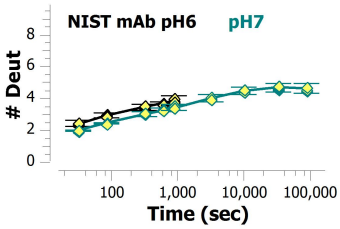

HC 149-177: PEPVTVSWNSGALTSGVH (#54)

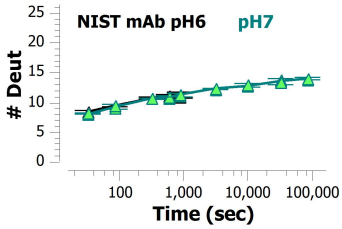

HC 149-182: VTVSWNSGALTSGVHTFP (#55)

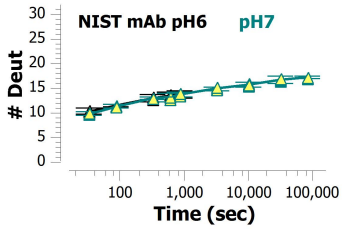

HC 159-177: SWNSGALTSGVHTFPAV (#56)

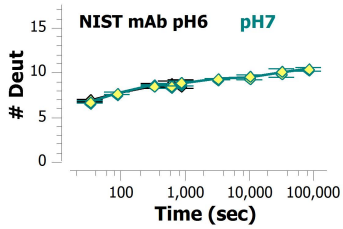

HC 159-182: NSGALTSGVHTFPAVLQS (#57)

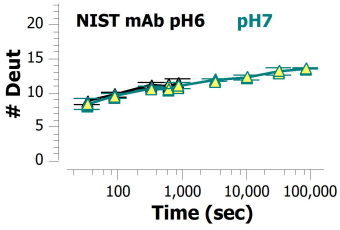

HC 162-177: NSGALTSGVHTFPAVL (#58)

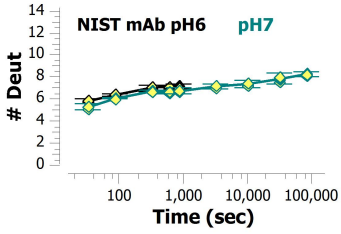

HC 166-177: LTSGVHTFPAVL (#59)

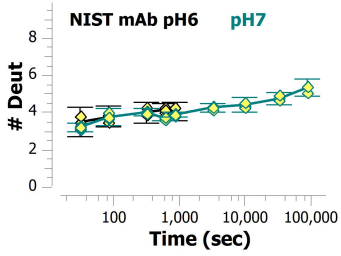

HC 167-177: TSGVHTFPAVL (#60)

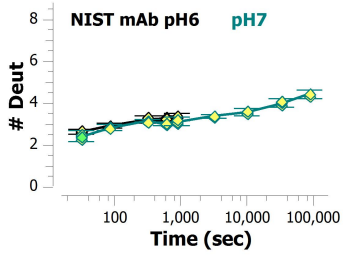

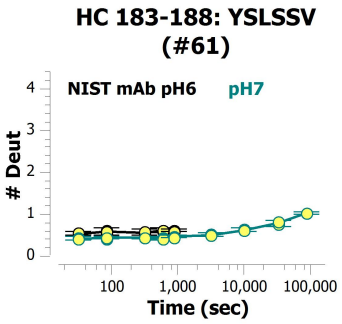
HC 183-188: YSLSSV (#61)
NIST mAb pH6
pH7
Deut
Time (sec)

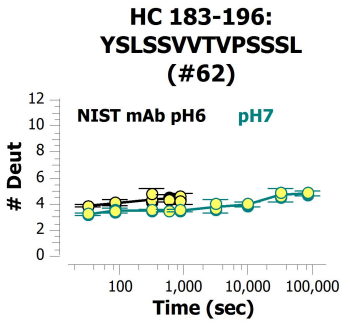
HC 183-196: YSLSSVVTVPSSSL (#62)
NIST mAb pH6
pH7
Deut
Time (sec)

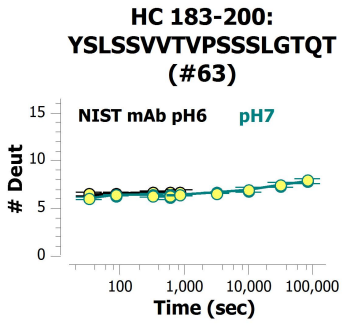
HC 183-200: YSLSSVVTVPSSSLGTQT (#63)
NIST mAb pH6
pH7
Deut
Time (sec)

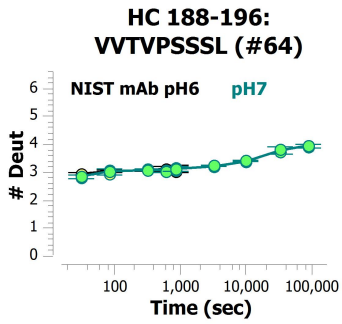
HC 188-196: VVTVPSSSL (#64)
NIST mAb pH6
pH7
Deut
Time (sec)

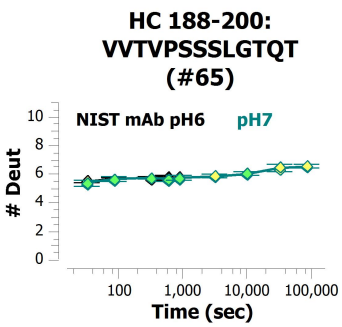
HC 188-200: VVTVPSSSLGTQT (#65)
NIST mAb pH6
pH7
Deut
Time (sec)

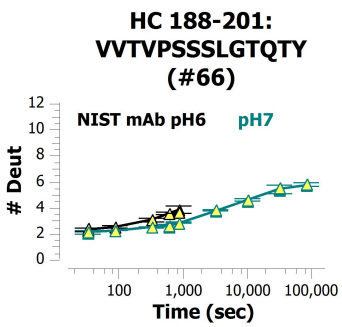
HC 188-201: VVTVPSSSLGTQTY (#66)
NIST mAb pH6
pH7
Deut
Time (sec)

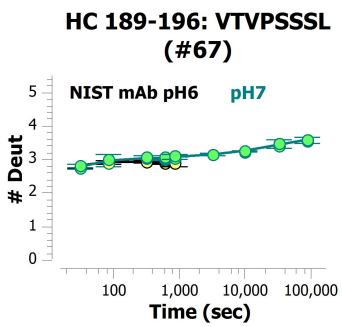
HC 189-196: VTVPSSSL (#67)
NIST mAb pH6
pH7
Deut
Time (sec)

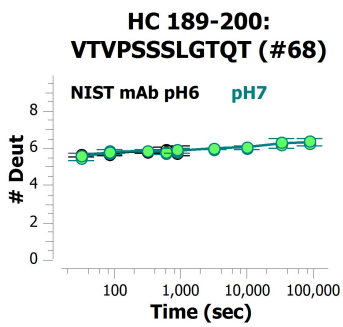
HC 189-200: VTVPSSSLGTQT (#68)
NIST mAb pH6
pH7
Deut
Time (sec)

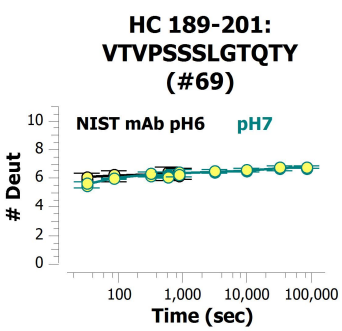
HC 189-201: VTVPSSSLGTQTY (#69)
NIST mAb pH6
pH7
Deut
Time (sec)

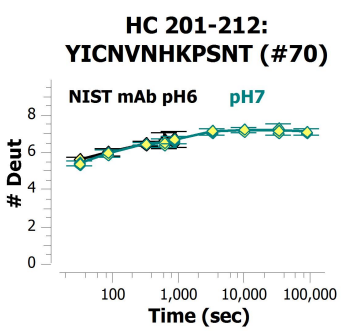
HC 201-212: YICNVNHKPSNT (#70)
NIST mAb pH6
pH7
Deut
Time (sec)

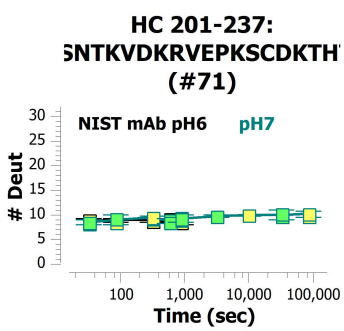
HC 201-237: SNTKVDKRVEPKSCDKTH (#71)
NIST mAb pH6
pH7
Deut
Time (sec)

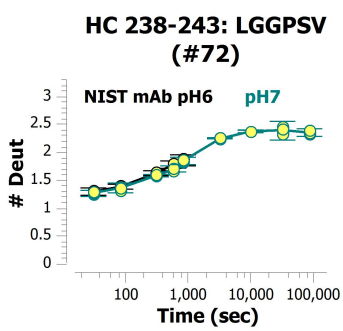
HC 238-243: LGGPSV (#72)
NIST mAb pH6
pH7
Deut
Time (sec)

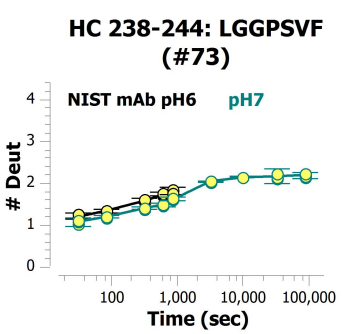
HC 238-244: LGGPSVF (#73)
NIST mAb pH6
pH7
Deut
Time (sec)

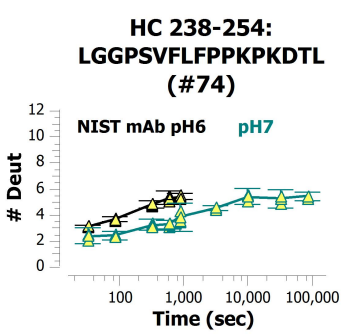
HC 238-254: LGGPSVFLFPPKPKDTL (#74)
NIST mAb pH6
pH7
Deut
Time (sec)

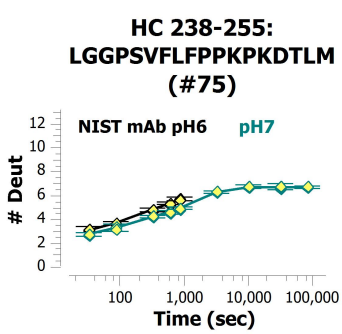
HC 238-255: LGGPSVFLFPPKPKDTLM (#75)
NIST mAb pH6
pH7
Deut
Time (sec)

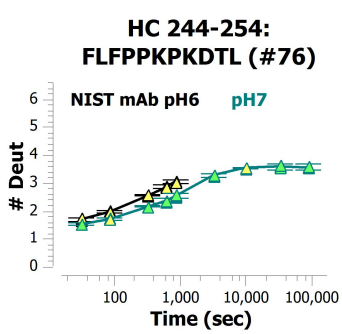
HC 244-254: FLFPPKPKDTL (#76)
NIST mAb pH6
pH7
Deut
Time (sec)

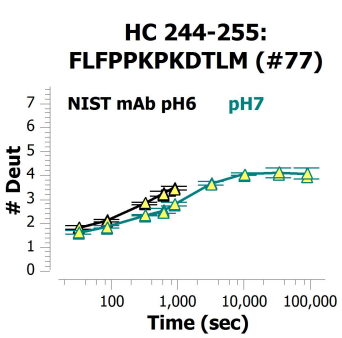
HC 244-255: FLFPPKPKDTLM (#77)
NIST mAb pH6
pH7
Deut
Time (sec)

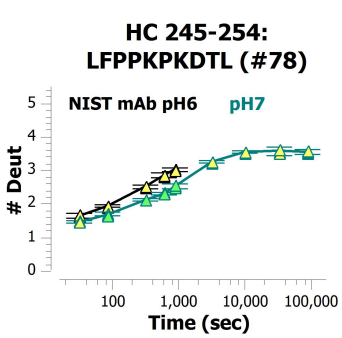
HC 245-254: LFPPKPKDTL (#78)
NIST mAb pH6
pH7
Deut
Time (sec)

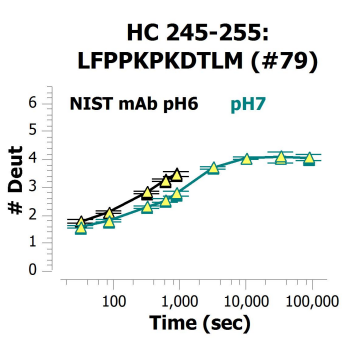
HC 245-255: LFPPKPKDTLM (#79)
NIST mAb pH6
pH7
Deut
Time (sec)

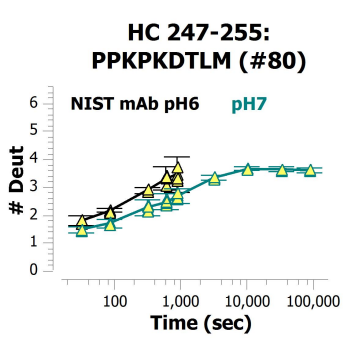
HC 247-255: PPKPKDTLM (#80)
NIST mAb pH6
pH7
Deut
Time (sec)

HC 255-264: MISRTPEVTC (#81)

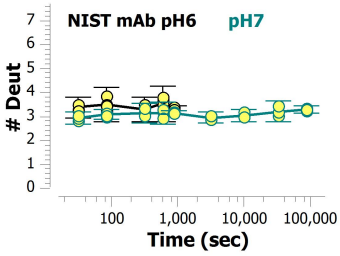

HC 255-265: MISRTPEVTCV (#82)

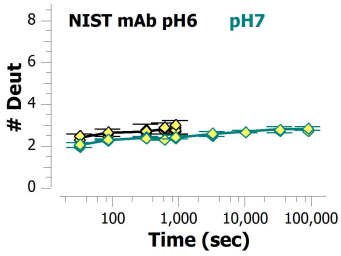

HC 256-263: ISRTPEVT (#83)

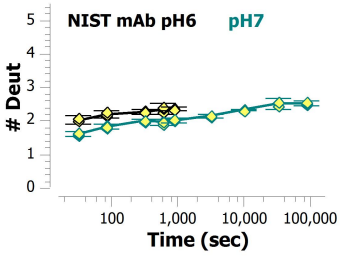

HC 256-264: ISRTPEVTC (#84)

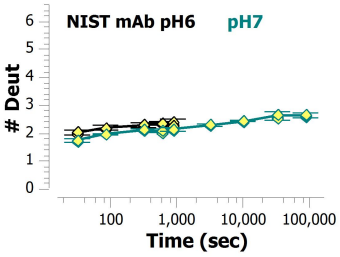

HC 256-265: ISRTPEVTCV (#85)

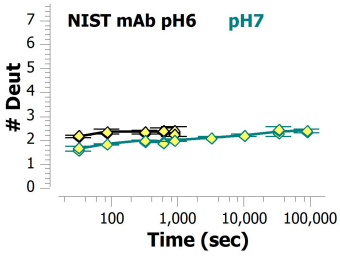

HC 264-280: CVVVDVSHEDPEVKFNW (#86)

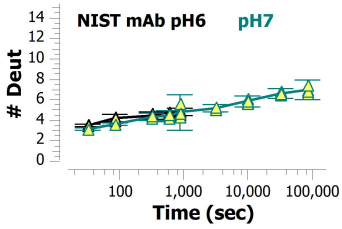

HC 265-278: VVVDVSHEDPEVKF (#87)

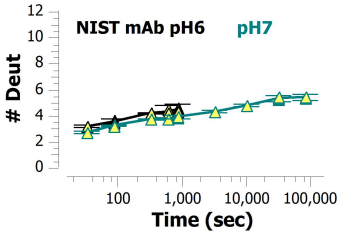

HC 265-280: VVVDVSHEDPEVKFNW (#88)

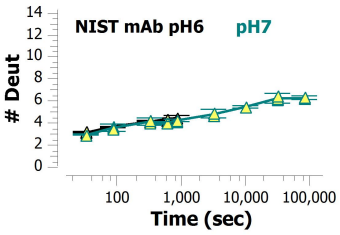

HC 266-280: VVDVSHEDPEVKFNW (#89)

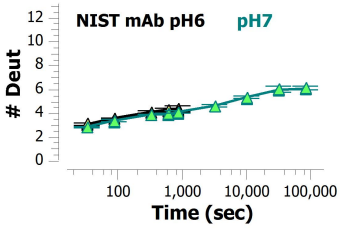

HC 267-280: VDVSHEDPEVKFNW (#90)

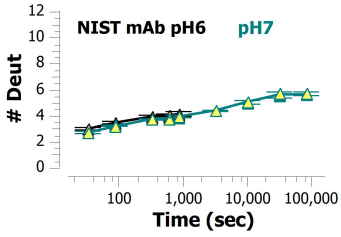

HC 269-280: VSHEDPEVKFNW (#91)

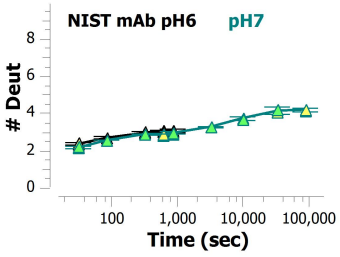

HC 290-314: PREEQYN*STYRVVSVLT (#92)

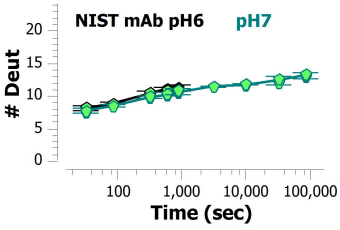

HC 300-328: /VSVLTVLHQDWLNGKEY (#93)

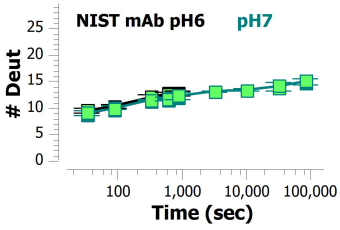

HC 304-309: RVVSVL (#94)

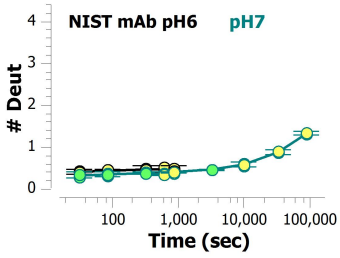

HC 309-321: LTVLHQDWLNGKE (#95)

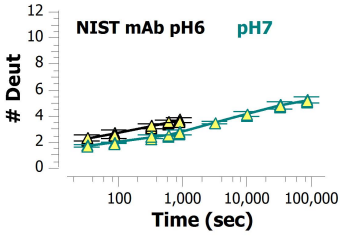

HC 310-321: TVLHQDWLNGKE (#96)

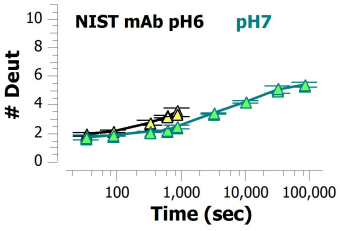

HC 322-359: _PAPIEKTISKAKGQPREP (#97)

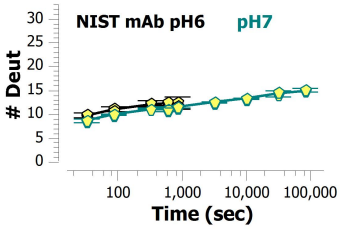

HC 337-351: KTISKAKGQPREPQV (#98)

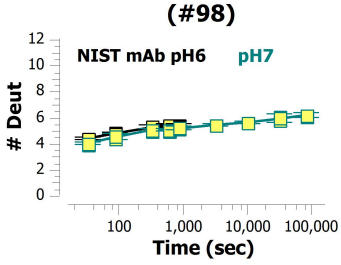

HC 337-359: [SKAKGQPREPQVYTLPPS (#99)

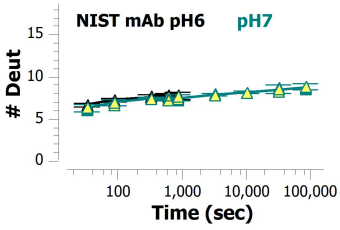

HC 337-368: GQPREPQVYTLPPSREEM (#100)

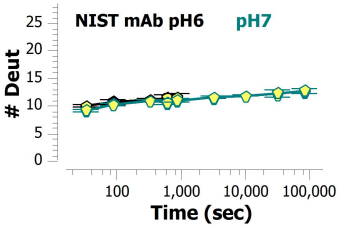

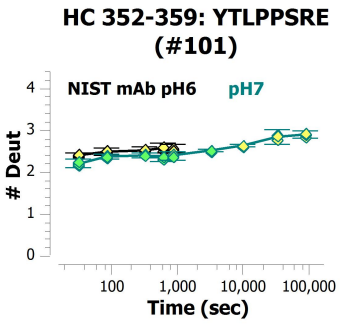
HC 352-359: YTLPPSRE (#101)
NIST mAb pH6
pH7
Deut
Time (sec)

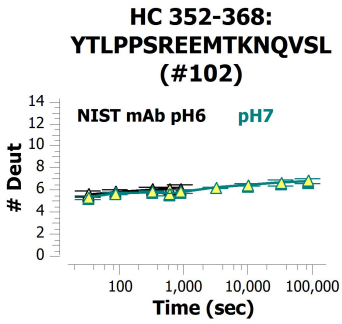
HC 352-368: YTLPPSREEMTKNQVSL (#102)
NIST mAb pH6
pH7
Deut
Time (sec)

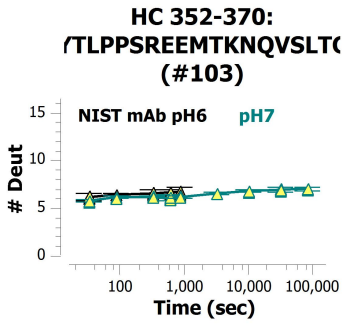
HC 352-370: /TLPPSREEMTKNQVSLTC (#103)
NIST mAb pH6
pH7
Deut
Time (sec)

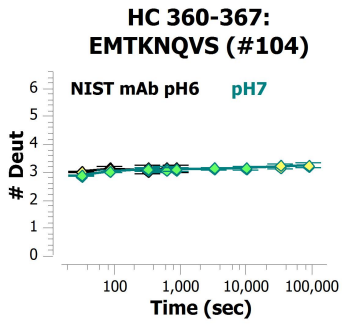
HC 360-367: EMTKNQVS (#104)
NIST mAb pH6
pH7
Deut
Time (sec)

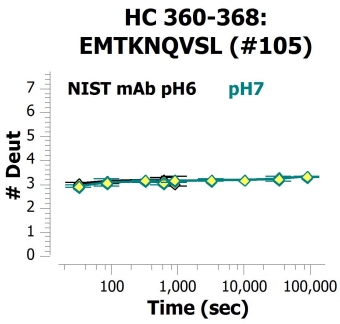
HC 360-368: EMTKNQVSL (#105)
NIST mAb pH6
pH7
Deut
Time (sec)

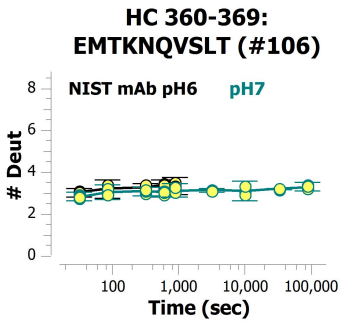
HC 360-369: EMTKNQVSLT (#106)
NIST mAb pH6
pH7
Deut
Time (sec)

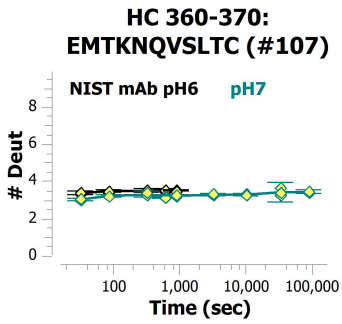
HC 360-370: EMTKNQVSLTC (#107)
NIST mAb pH6
pH7
Deut
Time (sec)

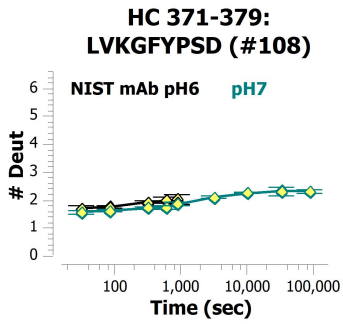
HC 371-379: LVKGFYPSD (#108)
NIST mAb pH6
pH7
Deut
Time (sec)

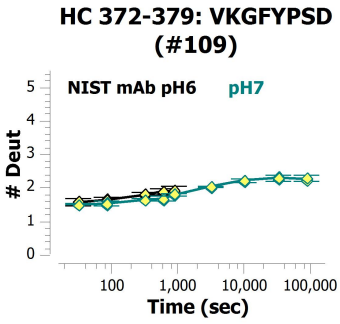
HC 372-379: VKGFYPSD (#109)
NIST mAb pH6
pH7
Deut
Time (sec)

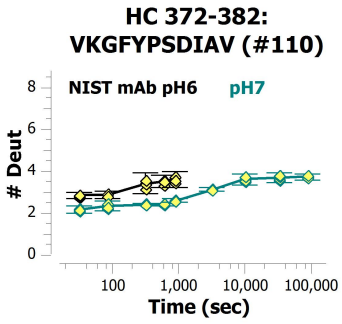
HC 372-382: VKGFYPSDIAV (#110)
NIST mAb pH6
pH7
Deut
Time (sec)

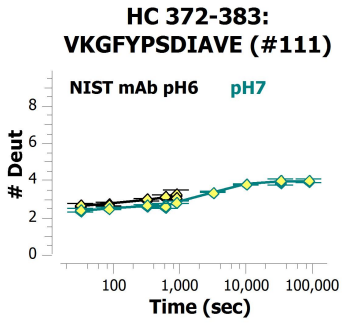
HC 372-383: VKGFYPSDIAVE (#111)
NIST mAb pH6
pH7
Deut
Time (sec)

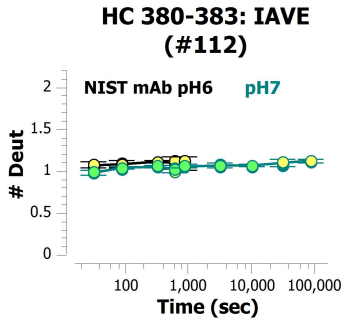
HC 380-383: IAVE (#112)
NIST mAb pH6
pH7
Deut
Time (sec)

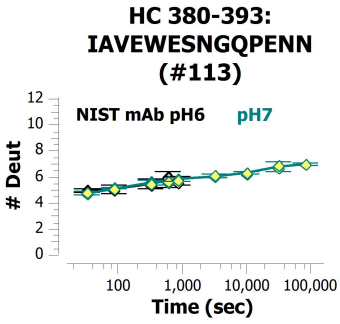
HC 380-393: IAVEWESNGQPENN (#113)
NIST mAb pH6
pH7
Deut
Time (sec)

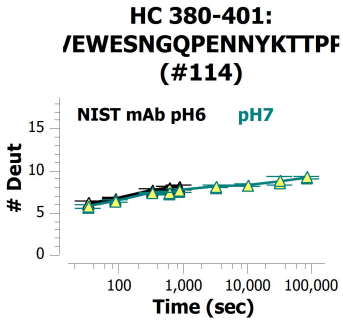
HC 380-401: /EWESNGQPENNYKTTPF (#114)
NIST mAb pH6
pH7
Deut
Time (sec)

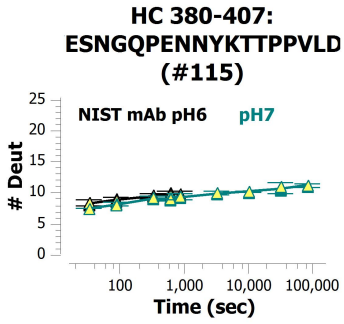
HC 380-407: ESNGQPENNYKTTPPVLD (#115)
NIST mAb pH6
pH7
Deut
Time (sec)

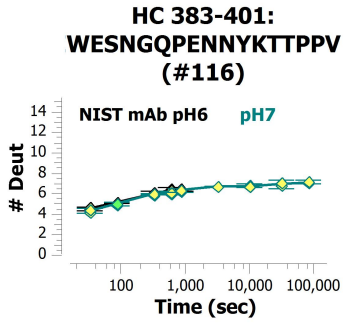
HC 383-401: WESNGQPENNYKTTPPV (#116)
NIST mAb pH6
pH7
Deut
Time (sec)

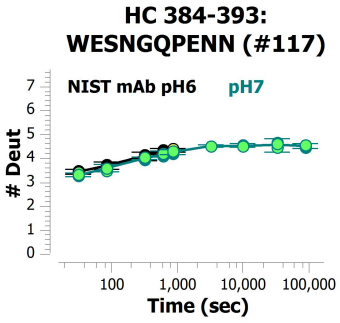
HC 384-393: WESNGQPENN (#117)
NIST mAb pH6
pH7
Deut
Time (sec)

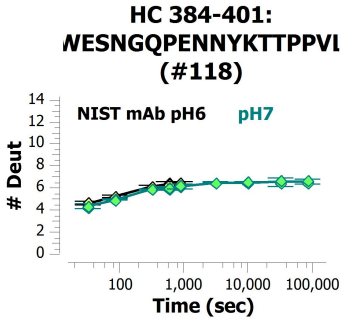
HC 384-401: WESNGQPENNYKTTPPVI (#118)
NIST mAb pH6
pH7
Deut
Time (sec)

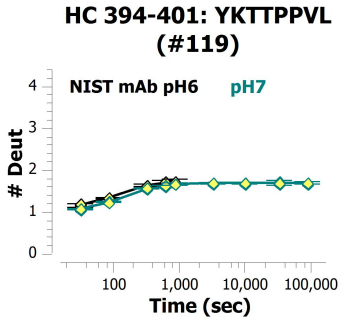
HC 394-401: YKTTPPVL (#119)
NIST mAb pH6
pH7
Deut
Time (sec)

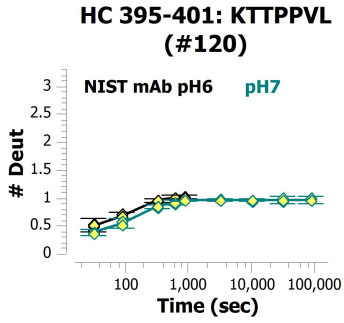
HC 395-401: KTTPPVL (#120)
NIST mAb pH6
pH7
Deut
Time (sec)

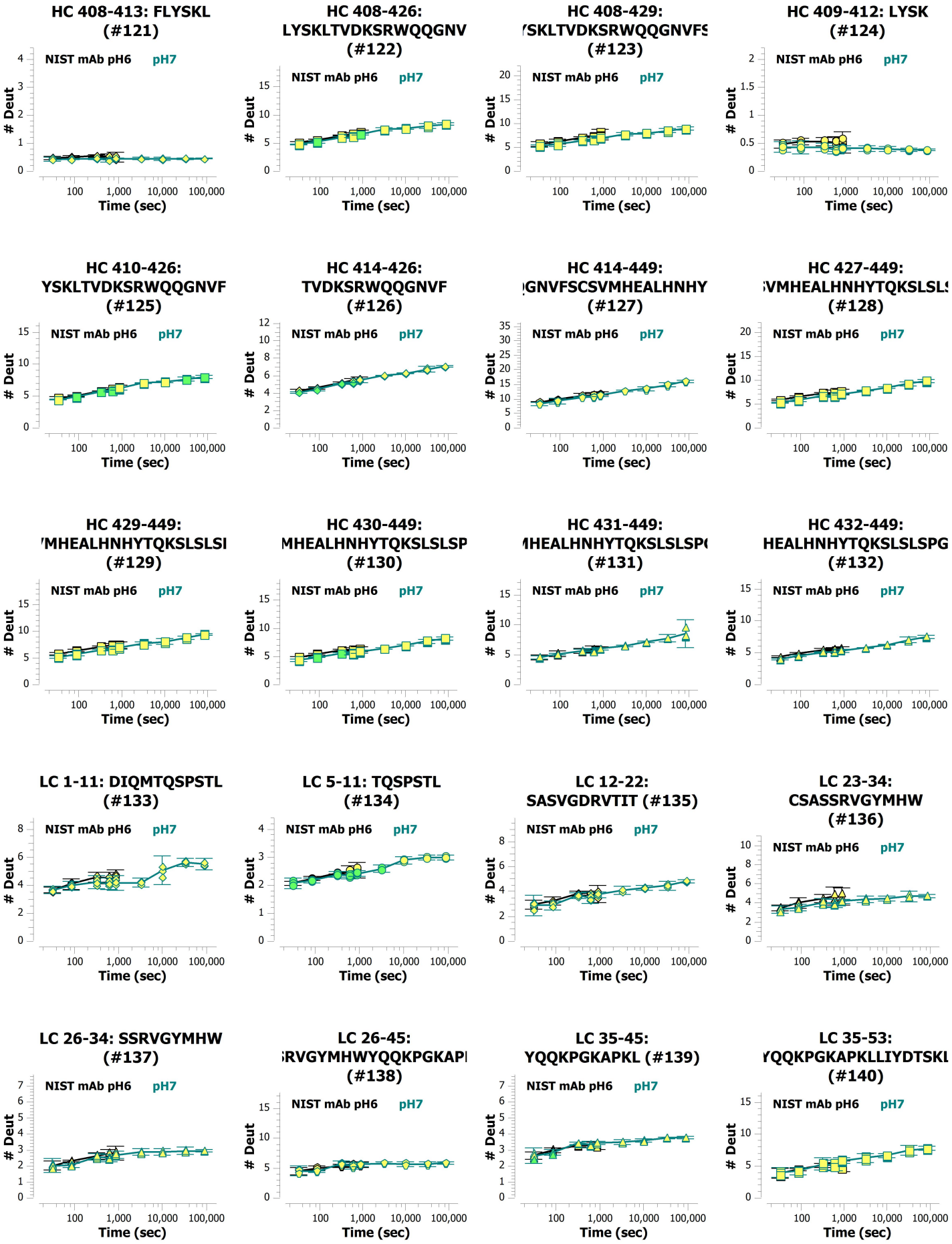
HC 408-413: FLYSKL (#121)
HC 408-426: LYSKLTVDKSRWQQGNV (#122)
HC 408-429: SKLTVDKSRWQQGNVFS (#123)
HC 409-412: LYSK (#124)
HC 410-426: YSKLTVDKSRWQQGNVF (#125)
HC 414-426: TVDKSRWQQGNVF (#126)
HC 414-449: GNVFSCSVMHEALHNHY (#127)
HC 427-449: VMHEALHNHYTQKSLSL (#128)
HC 429-449: MHEALHNHYTQKSLSLS (#129)
HC 430-449: MHEALHNHYTQKSLSLSP (#130)
HC 431-449: HEALHNHYTQKSLSLSP (#131)
HC 432-449: HEALHNHYTQKSLSLSPG (#132)
LC 1-11: DIQMTQSPSTL (#133)
LC 5-11: TQSPSTL (#134)
LC 12-22: SASVGDRVTIT (#135)
LC 23-34: CSASSRVGYMHW (#136)
LC 26-34: SSRVGYMHW (#137)
LC 26-45: RVGYMHWYQQKPGKAP (#138)
LC 35-45: YQQKPGKAPKL (#139)
LC 35-53: YQQKPGKAPKLLIYDTSK (#140)
NIST mAb pH6
pH7
Deut
Time (sec)
100
1,000
10,000
100,000

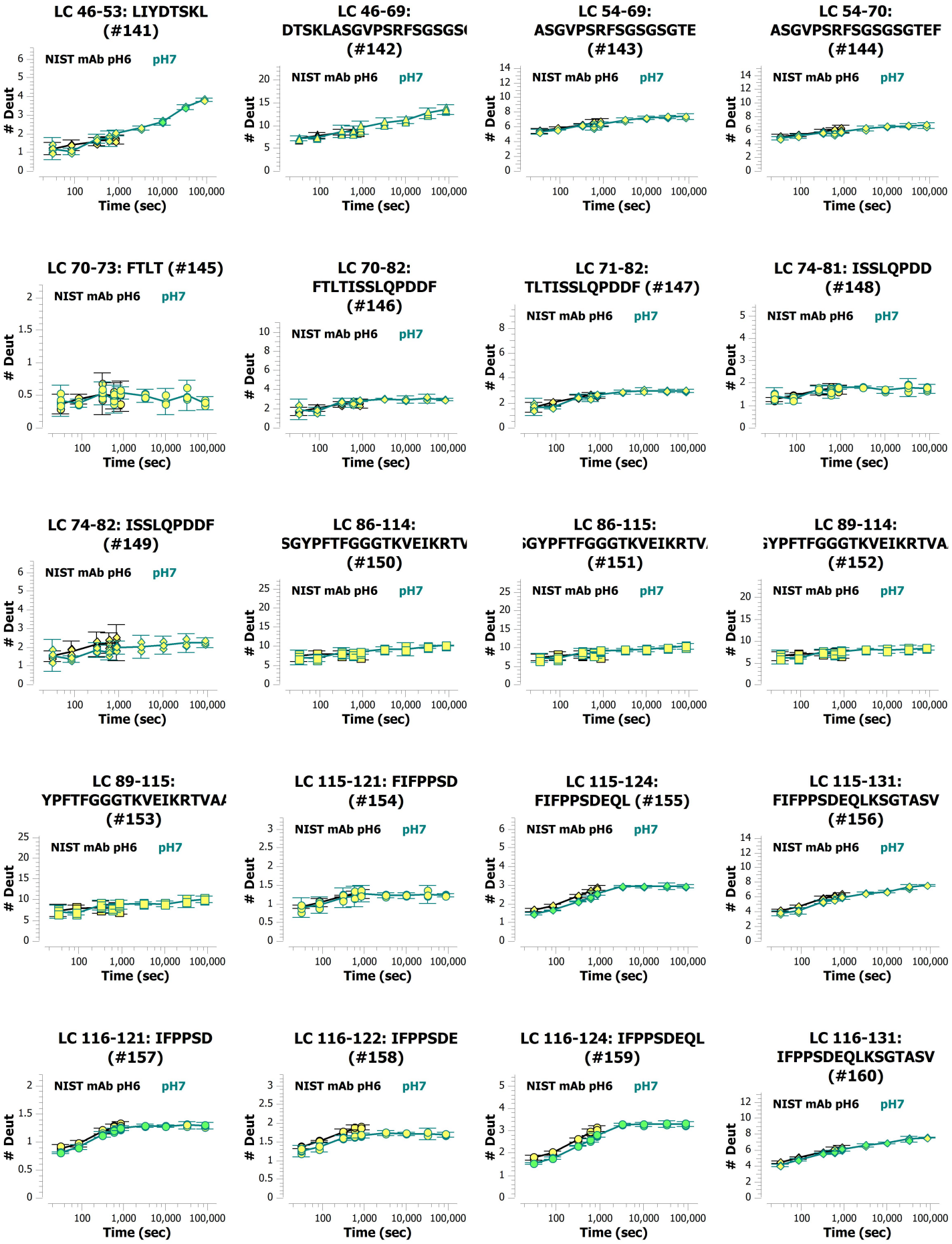
LC 46-53: LIYDTSKL (#141)
LC 46-69: DTSKLASGVPSRFSGSGS((#142)
LC 54-69: ASGVPSRFSGSGSGTE (#143)
LC 54-70: ASGVPSRFSGSGSGTEF (#144)
LC 70-73: FTLT (#145)
LC 70-82: FTLTISSLQPDDF (#146)
LC 71-82: TLTISSLQPDDF (#147)
LC 74-81: ISSLQPDD (#148)
LC 74-82: ISSLQPDDF (#149)
LC 86-114: SGYPFTFGGGTKVEIKRTV (#150)
LC 86-115: GYPFTFGGGTKVEIKRTV. (#151)
LC 89-114: YPFTFGGGTKVEIKRTVA (#152)
LC 89-115: YPFTFGGGTKVEIKRTVA/ (#153)
LC 115-121: FIFPPSD (#154)
LC 115-124: FIFPPSDEQL (#155)
LC 115-131: FIFPPSDEQLKSGTASV (#156)
LC 116-121: IFPPSD (#157)
LC 116-122: IFPPSDE (#158)
LC 116-124: IFPPSDEQL (#159)
LC 116-131: IFPPSDEQLKSGTASV (#160)
NIST mAb pH6
pH7
Deut
Time (sec)
100
1,000
10,000
100,000

LC 116-132: IFPPSDEQLKSGTASVV (#161)

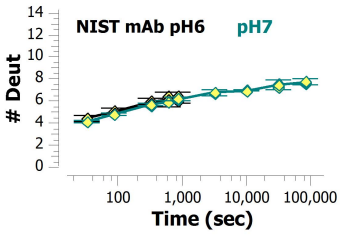

LC 122-131: EQLKSGTASV (#162)

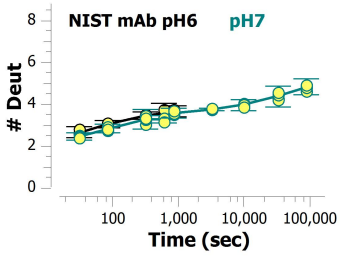

LC 123-131: QLKSGTASV (#163)

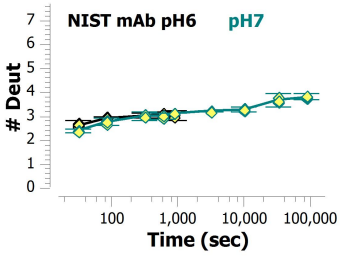

LC 132-134: VCL (#164)

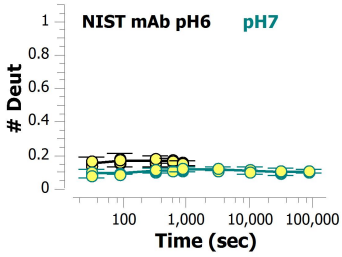

LC 132-135: VCLL (#165)

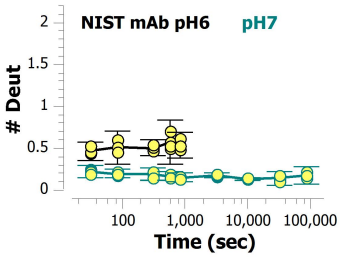

LC 132-153: LNNFYPREAKVQWKVDN (#166)

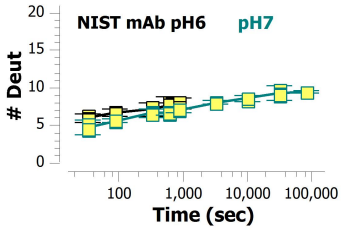

LC 132-160: FYPREAKVQWKVDNALQ (#167)

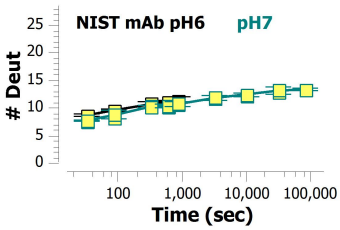

LC 135-142: LNNFYPRE (#168)

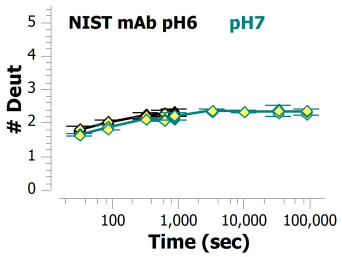

LC 135-147: LNNFYPREAKVQW (#169)

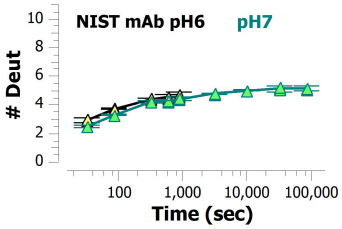

LC 135-153: NNFYPREAKVQWKVDNA (#170)

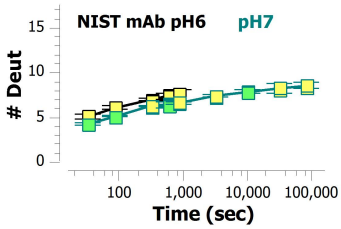

LC 135-160: PREAKVQWKVDNALQSC (#171)

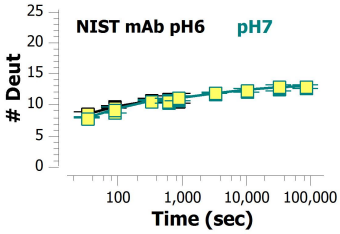

LC 135-171: VQWKVDNALQSGNSQES (#172)

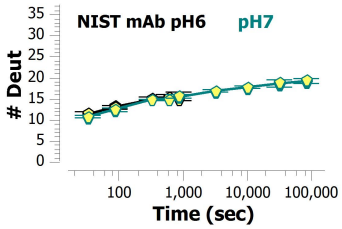

LC 136-160: PREAKVQWKVDNALQSG (#173)

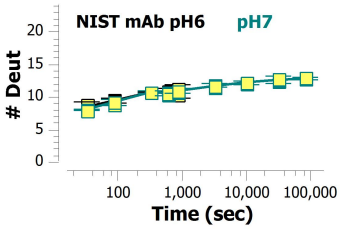

LC 139-160: EAKVQWKVDNALQSGNS (#174)

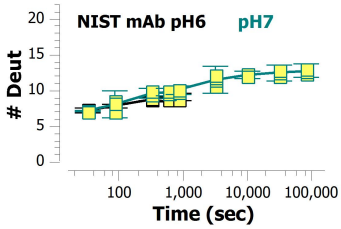

LC 143-160: AKVQWKVDNALQSGNSQI (#175)

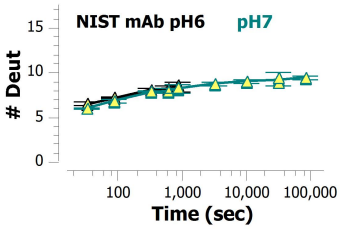

LC 148-160: KVDNALQSGNSQE (#176)

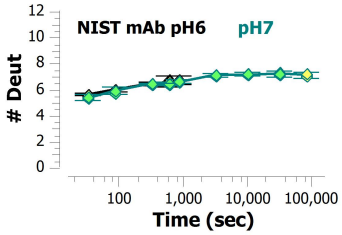

LC 161-171: SVTEQDSKDST (#177)

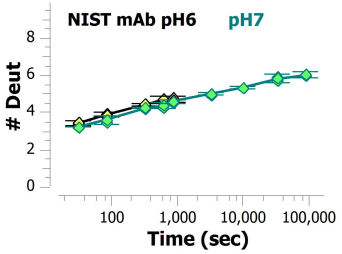

LC 161-174: SVTEQDSKDSTYSL (#178)

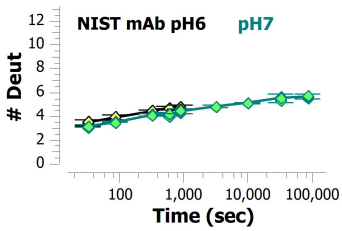

LC 161-177: SVTEQDSKDSTYSLSST (#179)

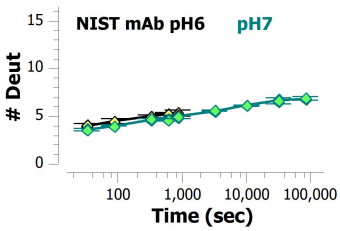

LC 161-178: SVTEQDSKDSTYSLSSTL (#180)

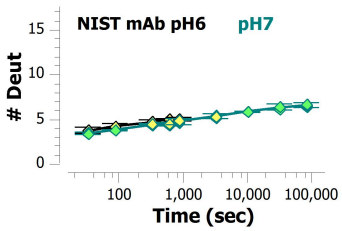

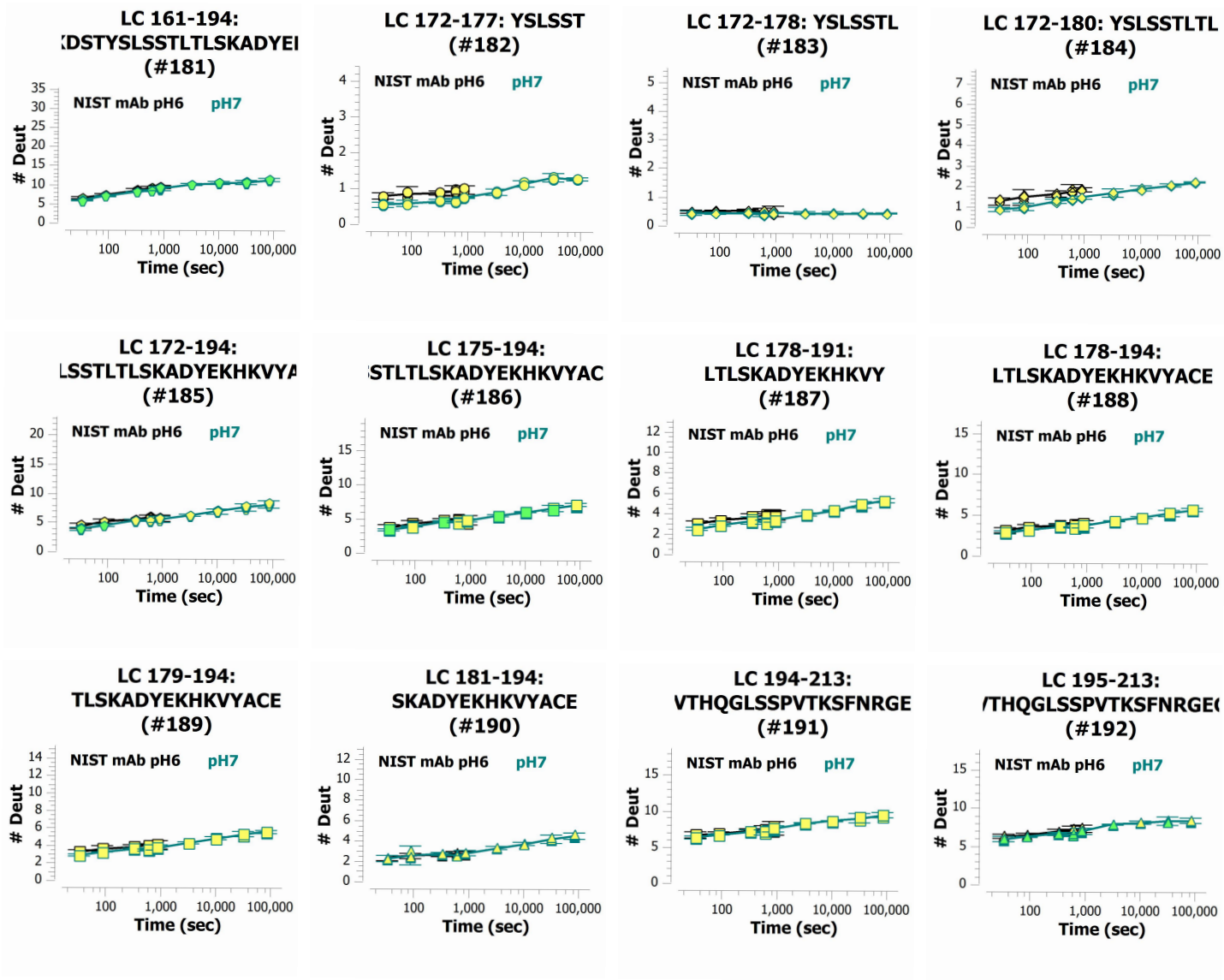

Figure 4.C-6. Deuterium uptake plots for the NIST mAb peptic peptides at pH 7 and pH 6 after timepoint labeling correction using equation 4.1.

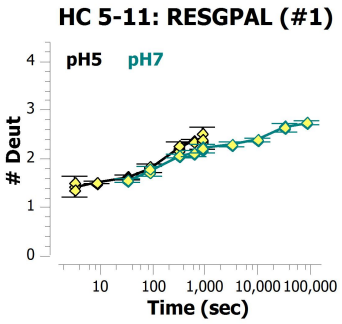
HC 5-11: RESGPAL (#1)
pH5 pH7
Deut
Time (sec)

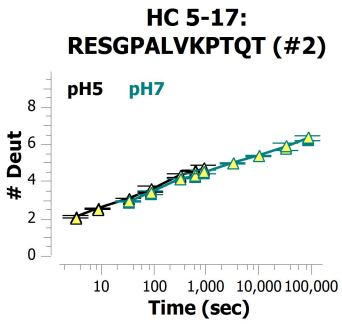
HC 5-17: RESGPALVKPTQT (#2)
pH5 pH7
Deut
Time (sec)

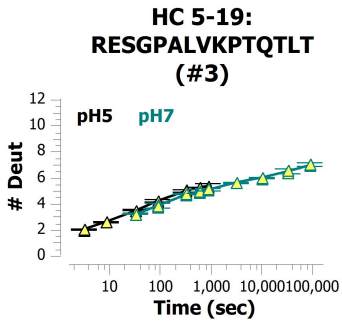
HC 5-19: RESGPALVKPTQTLT (#3)
pH5 pH7
Deut
Time (sec)

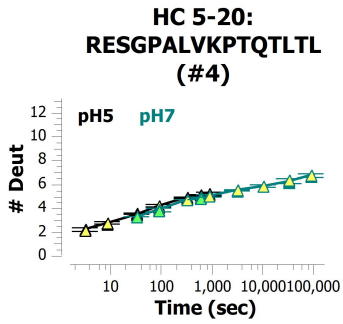
HC 5-20: RESGPALVKPTQTLTL (#4)
pH5 pH7
Deut
Time (sec)

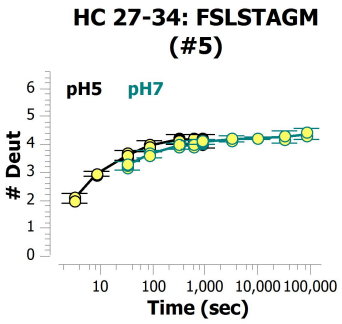
HC 27-34: FSLSTAGM (#5)
pH5 pH7
Deut
Time (sec)

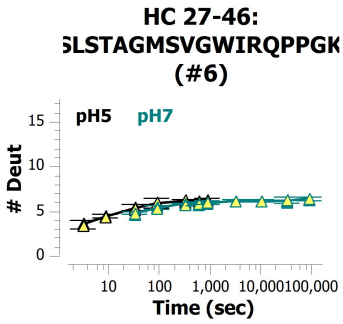
HC 27-46: SLSTAGMSVGWIRQPPGK (#6)
pH5 pH7
Deut
Time (sec)

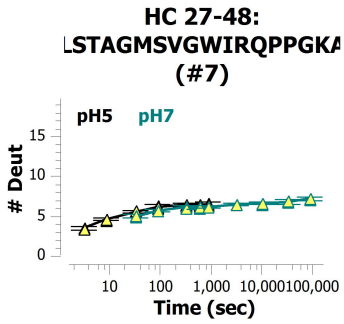
HC 27-48: LSTAGMSVGWIRQPPGKA (#7)
pH5 pH7
Deut
Time (sec)

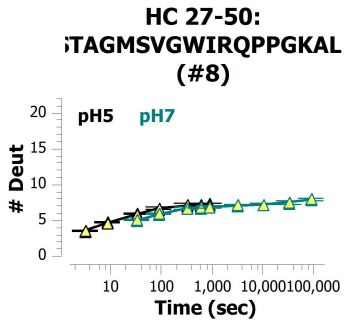
HC 27-50: STAGMSVGWIRQPPGKAL (#8)
pH5 pH7
Deut
Time (sec)

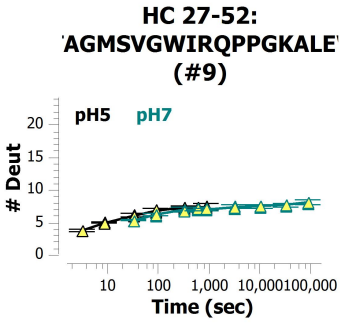
HC 27-52: TAGMSVGWIRQPPGKALE (#9)
pH5 pH7
Deut
Time (sec)

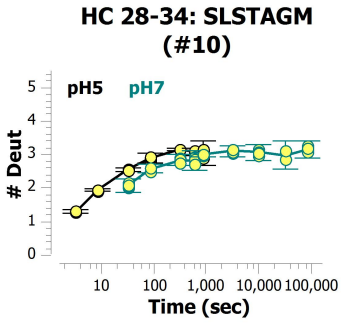
HC 28-34: SLSTAGM (#10)
pH5 pH7
Deut
Time (sec)

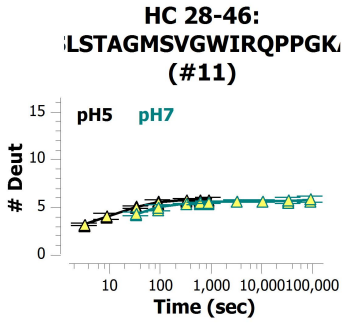
HC 28-46: LSTAGMSVGWIRQPPGK (#11)
pH5 pH7
Deut
Time (sec)

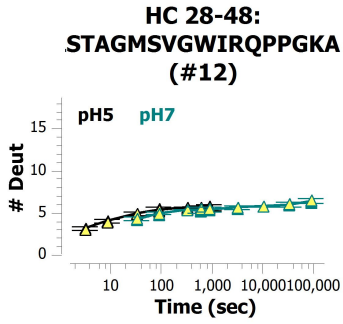
HC 28-48: STAGMSVGWIRQPPGKA (#12)
pH5 pH7
Deut
Time (sec)

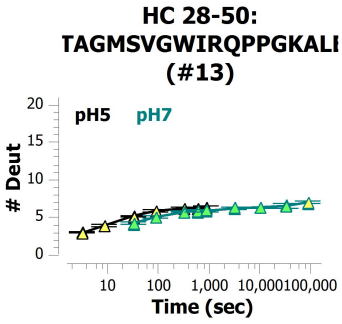
HC 28-50: TAGMSVGWIRQPPGKALI (#13)
pH5 pH7
Deut
Time (sec)

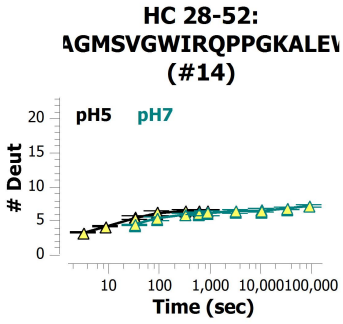
HC 28-52: AGMSVGWIRQPPGKALEV (#14)
pH5 pH7
Deut
Time (sec)

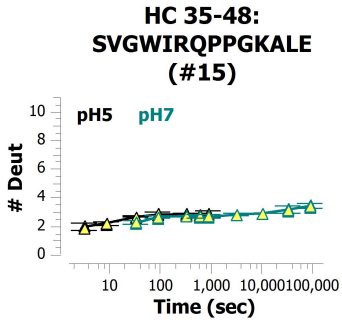
HC 35-48: SVGWIRQPPGKALE (#15)
pH5 pH7
Deut
Time (sec)

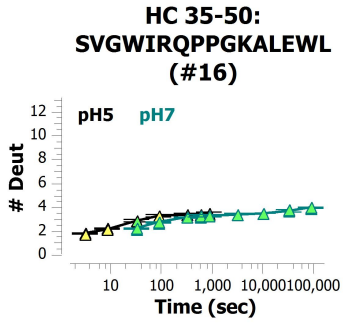
HC 35-50: SVGWIRQPPGKALEWL (#16)
pH5 pH7
Deut
Time (sec)

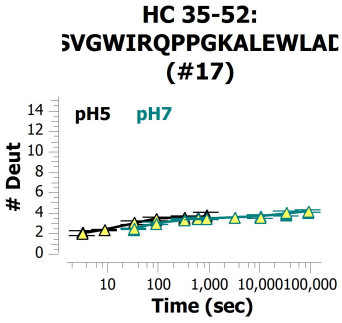
HC 35-52: SVGWIRQPPGKALEWLAD (#17)
pH5 pH7
Deut
Time (sec)

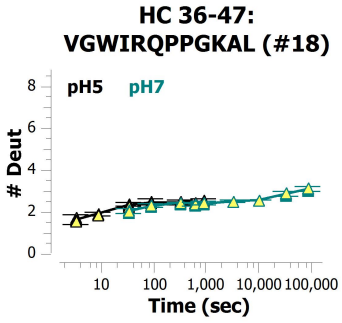
HC 36-47: VGWIRQPPGKAL (#18)
pH5 pH7
Deut
Time (sec)

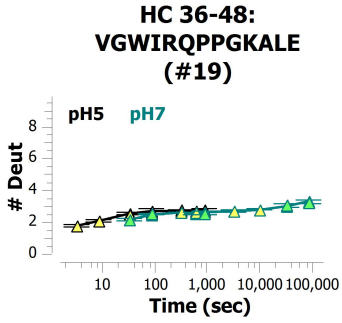
HC 36-48: VGWIRQPPGKALE (#19)
pH5 pH7
Deut
Time (sec)

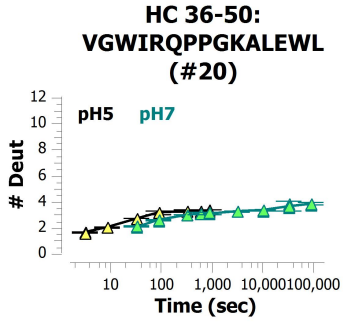
HC 36-50: VGWIRQPPGKALEWL (#20)
pH5 pH7
Deut
Time (sec)

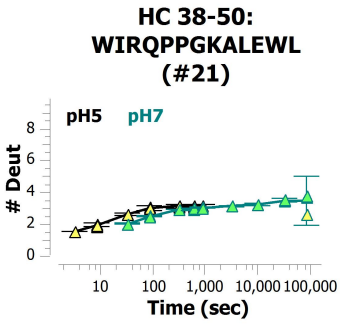
HC 38-50: WIRQPPGKALEWL (#21)
pH5 pH7
Deut
Time (sec)

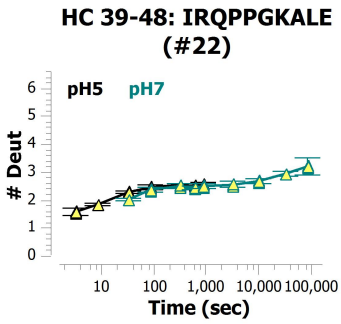
HC 39-48: IRQPPGKALE (#22)
pH5 pH7
Deut
Time (sec)

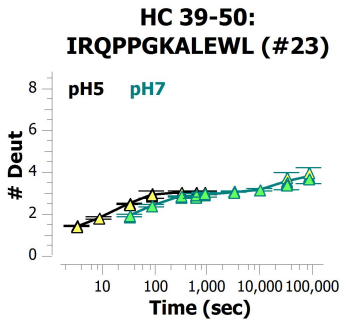
HC 39-50: IRQPPGKALEWL (#23)
pH5 pH7
Deut
Time (sec)

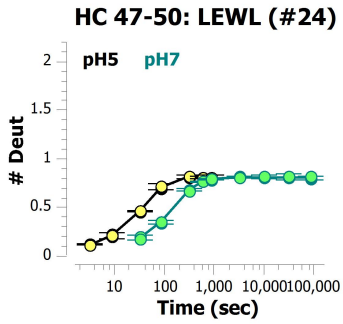
HC 47-50: LEWL (#24)
pH5 pH7
Deut
Time (sec)

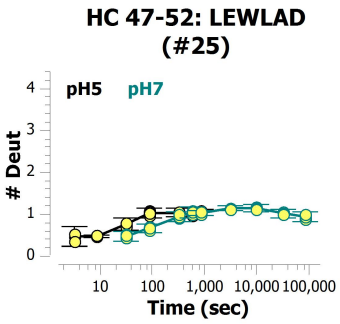
HC 47-52: LEWLAD (#25)
pH5 pH7
Deut
Time (sec)

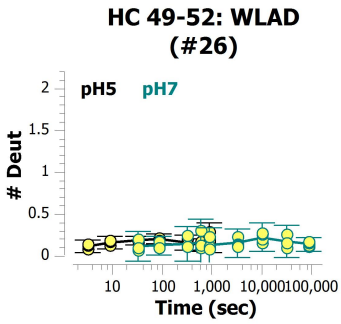
HC 49-52: WLAD (#26)
pH5 pH7
Deut
Time (sec)

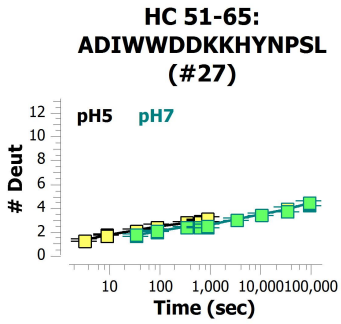
HC 51-65: ADIWWDDKKHYNPSL (#27)
pH5 pH7
Deut
Time (sec)

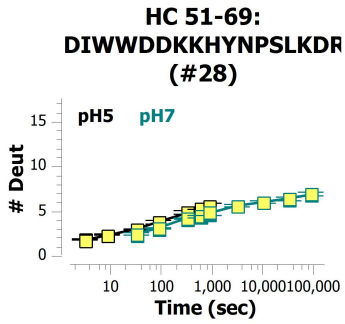
HC 51-69: DIWWDDKKHYNPSLKDR (#28)
pH5 pH7
Deut
Time (sec)

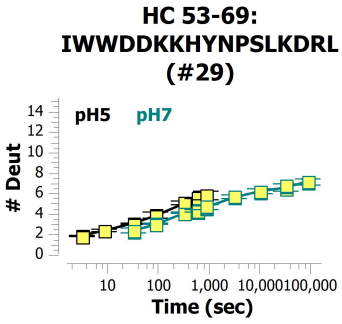
HC 53-69: IWWDDKKHYNPSLKDRL (#29)
pH5 pH7
Deut
Time (sec)

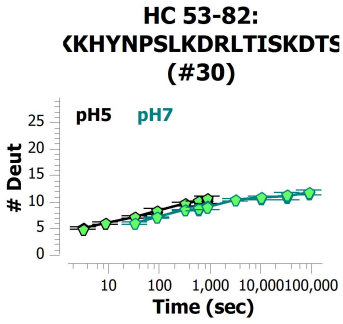
HC 53-82: (KHYNPSLKDRLTISKDTS (#30)
pH5 pH7
Deut
Time (sec)

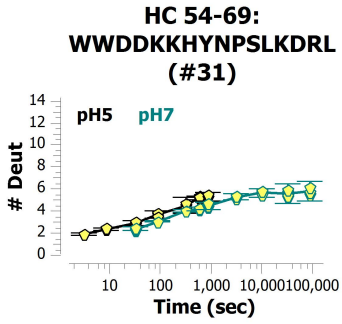
HC 54-69: WWDDKKHYNPSLKDRL (#31)
pH5 pH7
Deut
Time (sec)

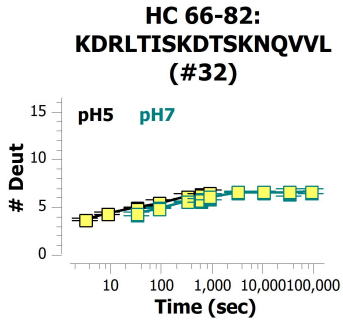
HC 66-82: KDRLTISKDTSKNQVVL (#32)
pH5 pH7
Deut
Time (sec)

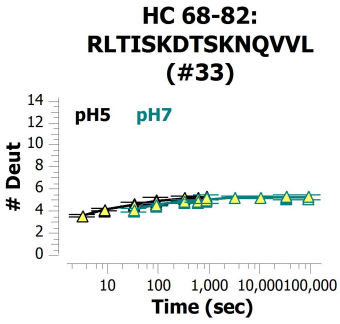
HC 68-82: RLTISKDTSKNQVVL (#33)
pH5 pH7
Deut
Time (sec)

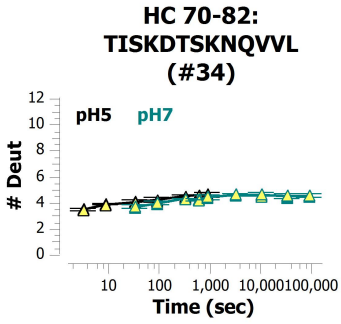
HC 70-82: TISKDTSKNQVVL (#34)
pH5 pH7
Deut
Time (sec)

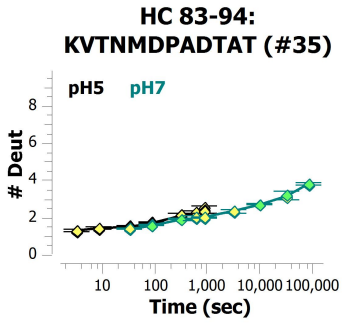
HC 83-94: KVTNMDPADTAT (#35)
pH5 pH7
Deut
Time (sec)

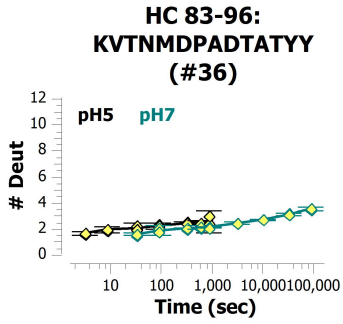
HC 83-96: KVTNMDPADTATYY (#36)
pH5 pH7
Deut
Time (sec)

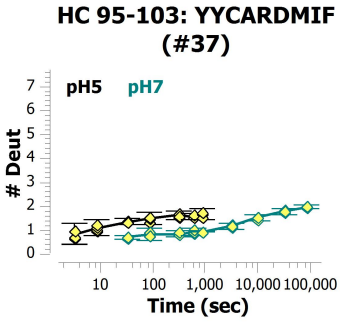
HC 95-103: YYCARDMIF (#37)
pH5 pH7
Deut
Time (sec)

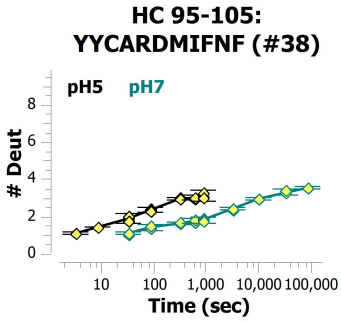
HC 95-105: YYCARDMIFNF (#38)
pH5 pH7
Deut
Time (sec)

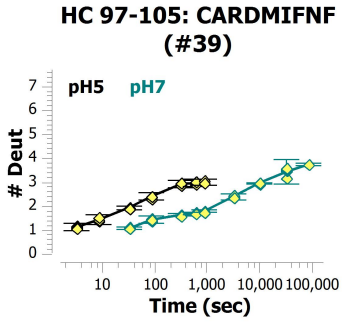
HC 97-105: CARDMIFNF (#39)
pH5 pH7
Deut
Time (sec)

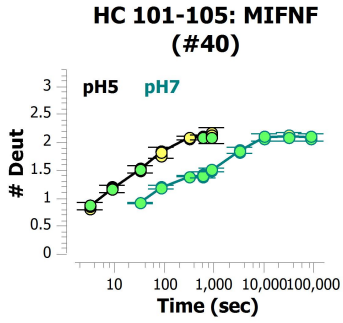
HC 101-105: MIFNF (#40)
pH5 pH7
Deut
Time (sec)

HC 106-117: YFDVWGQGTTVT (#41)

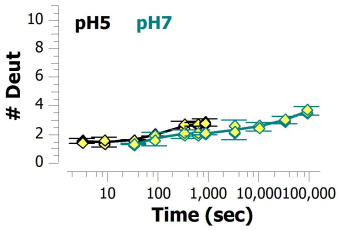

HC 106-145: VTVSSASTKGPSVFPLAPS (#42)

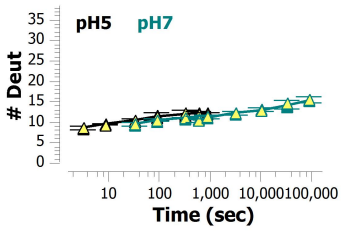

HC 107-117: FDVWGQGTTVT (#43)

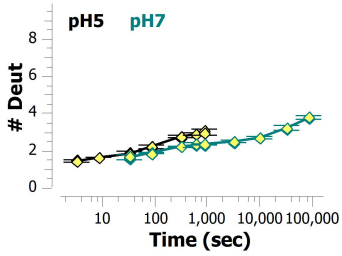

HC 107-145: TVSSASTKGPSVFPLAPS (#44)

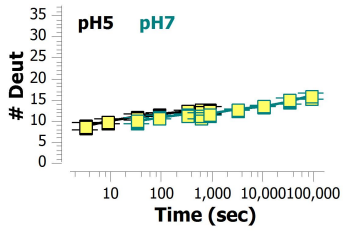

HC 118-129: VSSASTKGPSVF (#45)

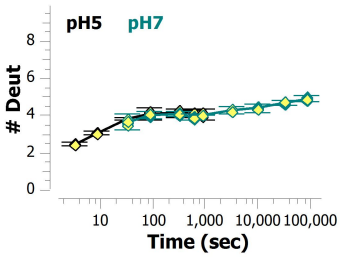

HC 118-145: TKGPSVFPLAPSSKSTSG (#46)

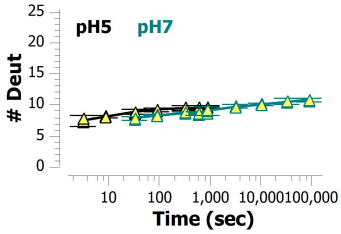

HC 118-147: KGPSVFPLAPSSKSTSGG (#47)

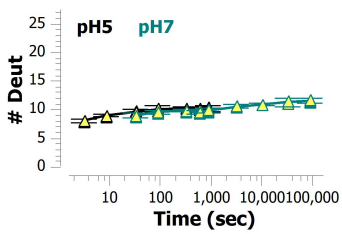

HC 118-148: KGPSVFPLAPSSKSTSGGT (#48)

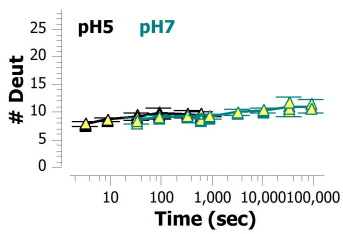

HC 130-145: PLAPSSKSTSGGTAAL (#49)

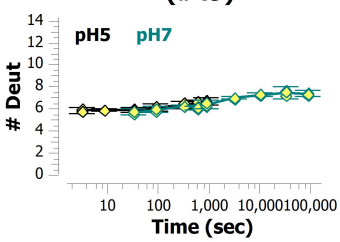

HC 148-158: LVKDYFPEPVT (#50)

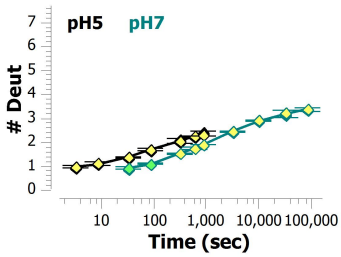

HC 148-177: PEPVTVSWNSGALTSGVH (#51)

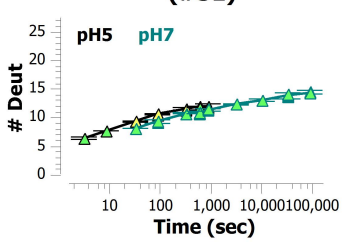

HC 149-158: VKDYFPEPVT (#52)

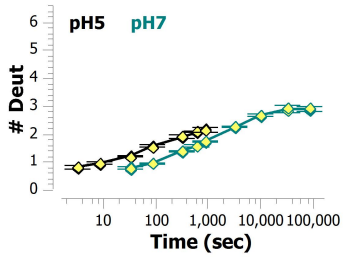

HC 149-161: VKDYFPEPVTVSW (#53)

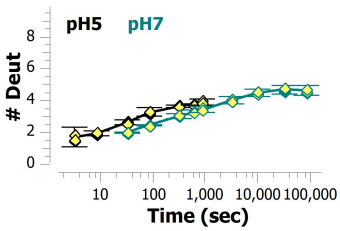

HC 149-177: PEPVTVSWNSGALTSGVH (#54)

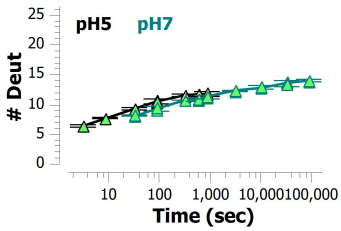

HC 149-182: VTVSWNSGALTSGVHTFP (#55)

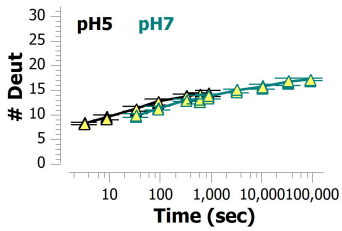

HC 159-177: SWNSGALTSGVHTFPAV (#56)

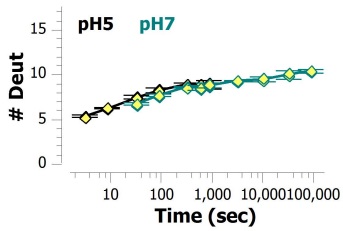

HC 159-182: NSGALTSGVHTFPAVLQS (#57)

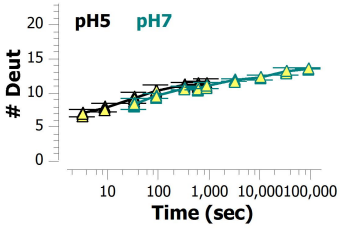

HC 162-177: NSGALTSGVHTFPAVL (#58)

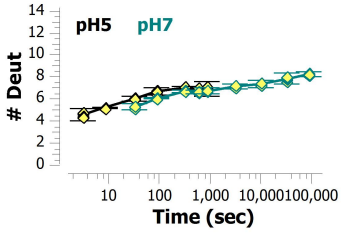

HC 166-177: LTSGVHTFPAVL (#59)

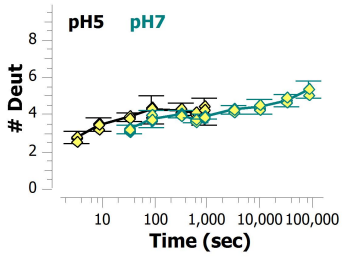

HC 167-177: TSGVHTFPAVL (#60)

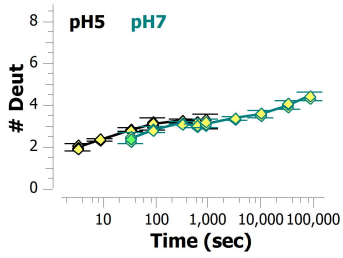

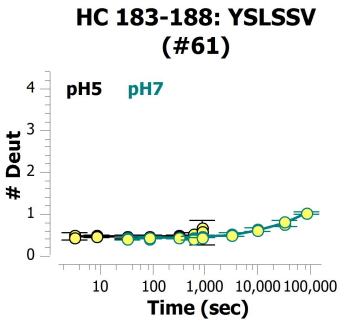
HC 183-188: YSLSSV (#61)
pH5 pH7
Deut
Time (sec)

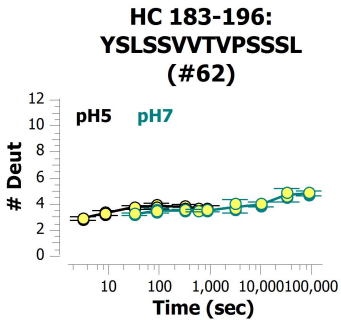
HC 183-196: YSLSSVVTVPSSSL (#62)
pH5 pH7
Deut
Time (sec)

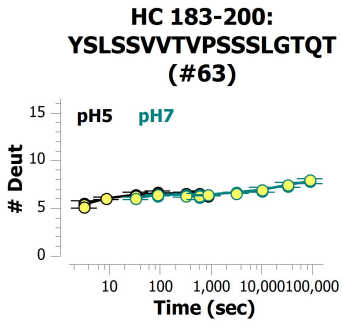
HC 183-200: YSLSSVVTVPSSSLGTQT (#63)
pH5 pH7
Deut
Time (sec)

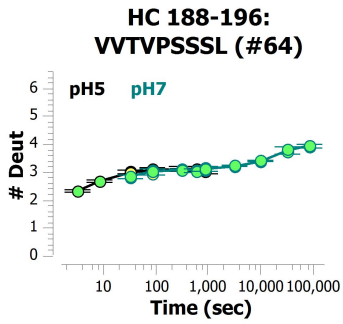
HC 188-196: VVTVPSSSL (#64)
pH5 pH7
Deut
Time (sec)

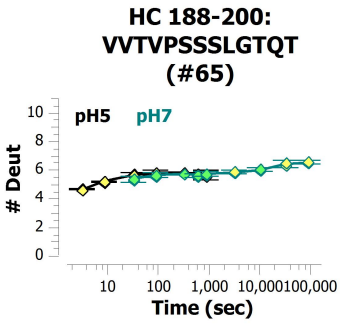
HC 188-200: VVTVPSSSLGTQT (#65)
pH5 pH7
Deut
Time (sec)

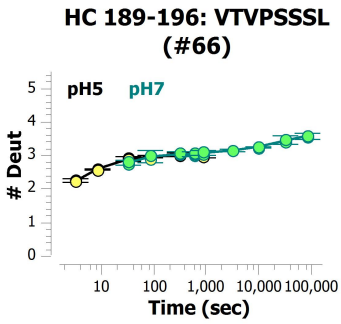
HC 189-196: VTVPSSSL (#66)
pH5 pH7
Deut
Time (sec)

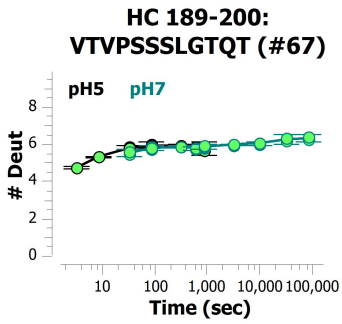
HC 189-200: VTVPSSSLGTQT (#67)
pH5 pH7
Deut
Time (sec)

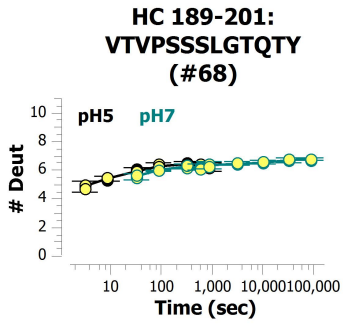
HC 189-201: VTVPSSSLGTQTY (#68)
pH5 pH7
Deut
Time (sec)

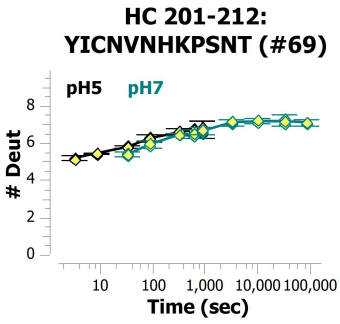
HC 201-212: YICNVNHKPSNT (#69)
pH5 pH7
Deut
Time (sec)

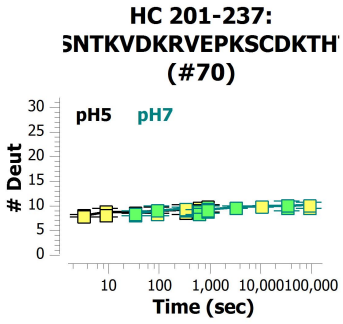
HC 201-237: SNTKVDKRVEPKSCDKTH (#70)
pH5 pH7
Deut
Time (sec)

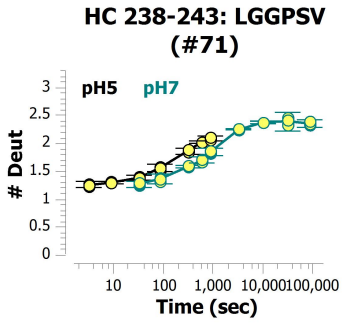
HC 238-243: LGGPSV (#71)
pH5 pH7
Deut
Time (sec)

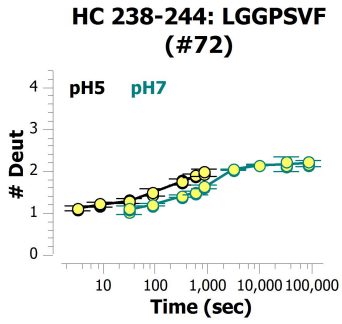
HC 238-244: LGGPSVF (#72)
pH5 pH7
Deut
Time (sec)

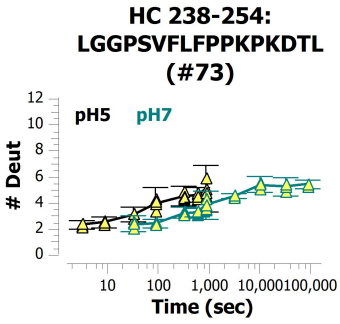
HC 238-254: LGGPSVFLFPPKPKDTL (#73)
pH5 pH7
Deut
Time (sec)

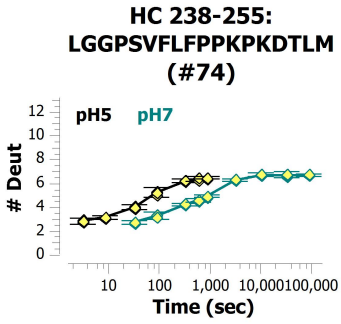
HC 238-255: LGGPSVFLFPPKPKDTLM (#74)
pH5 pH7
Deut
Time (sec)

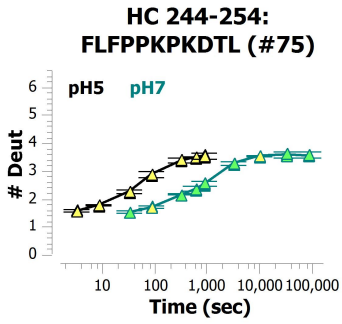
HC 244-254: FLFPPKPKDTL (#75)
pH5 pH7
Deut
Time (sec)

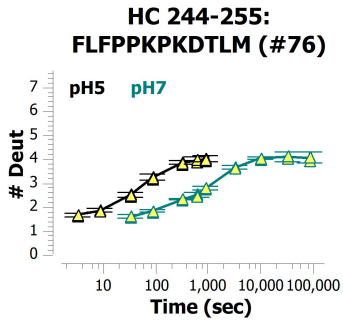
HC 244-255: FLFPPKPKDTLM (#76)
pH5 pH7
Deut
Time (sec)

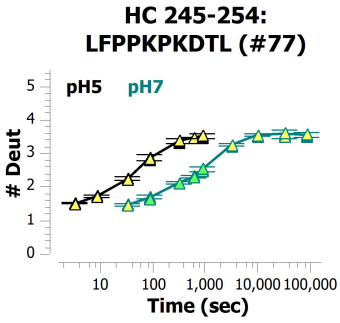
HC 245-254: LFPPKPKDTL (#77)
pH5 pH7
Deut
Time (sec)

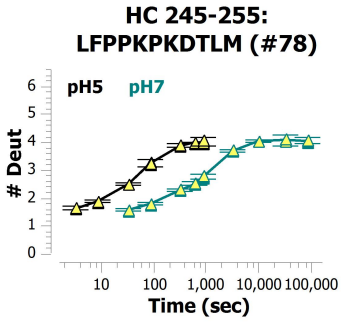
HC 245-255: LFPPKPKDTLM (#78)
pH5 pH7
Deut
Time (sec)

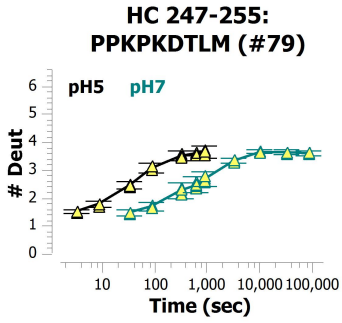
HC 247-255: PPKPKDTLM (#79)
pH5 pH7
Deut
Time (sec)

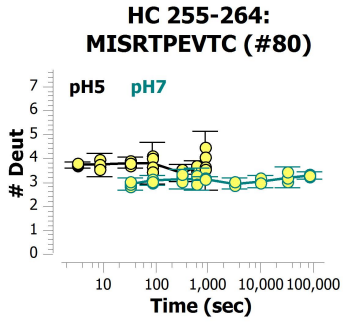
HC 255-264: MISRTPEVTC (#80)
pH5 pH7
Deut
Time (sec)

HC 255-265: MISRTPEVTCV (#81)

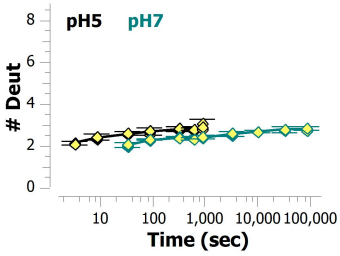

HC 256-263: ISRTPEVT (#82)

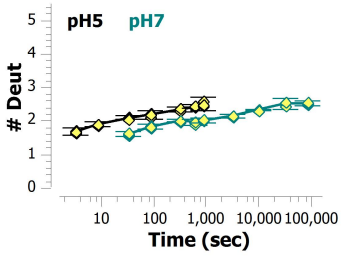

HC 256-264: ISRTPEVTC (#83)

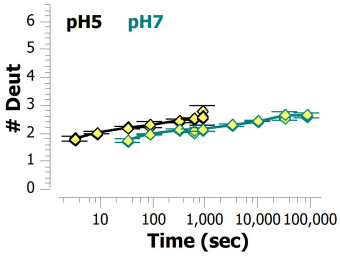

HC 256-265: ISRTPEVTCV (#84)

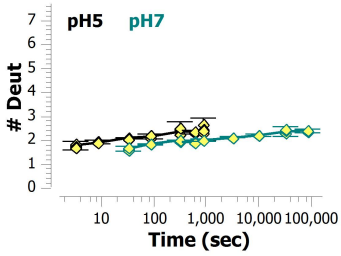

HC 264-280: CVVVDVSHEDPEVKFNW (#85)

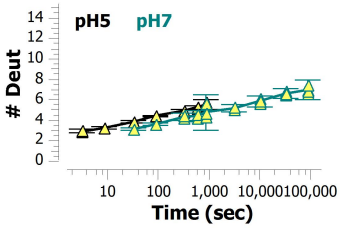

HC 265-278: VVVDVSHEDPEVKF (#86)

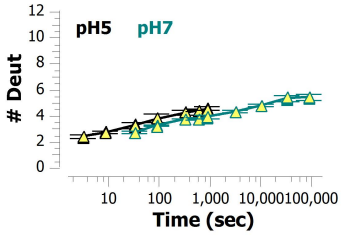

HC 265-280: VVVDVSHEDPEVKFNW (#87)

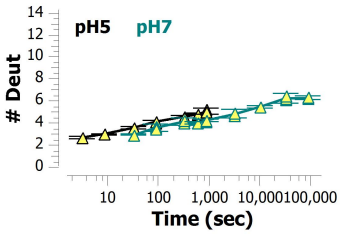

HC 266-280: VVDVSHEDPEVKFNW (#88)

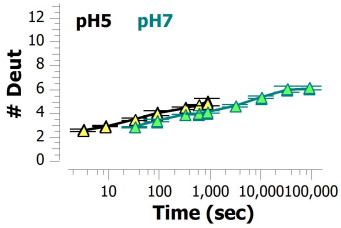

HC 267-280: VDVSHEDPEVKFNW (#89)

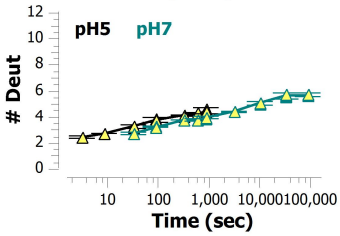

HC 269-280: VSHEDPEVKFNW (#90)

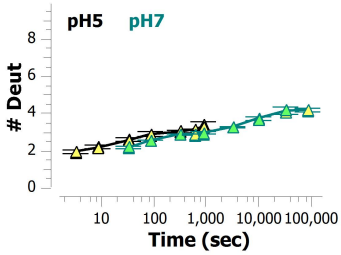

HC 290-314: PREEQYN*STYRVVSVLT (#91)

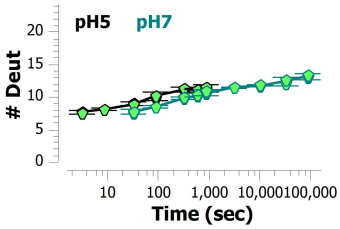

HC 300-328: VSVLTVLHQDWLNGKEY (#92)

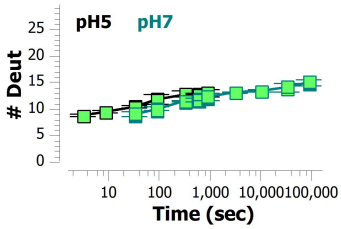

HC 304-309: RVVSVL (#93)

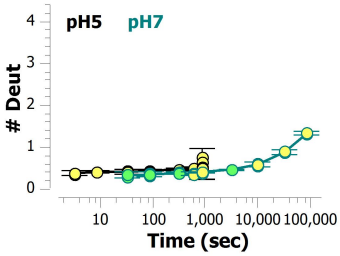

HC 309-321: LTVLHQDWLNGKE (#94)

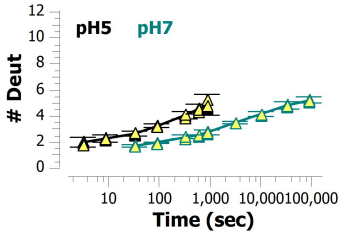

HC 310-321: TVLHQDWLNGKE (#95)

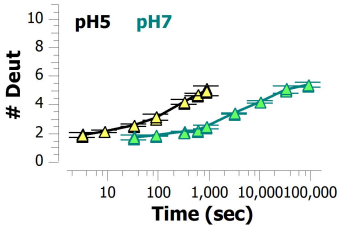

HC 322-359: LPAPIEKTISKAKGQPREP (#96)

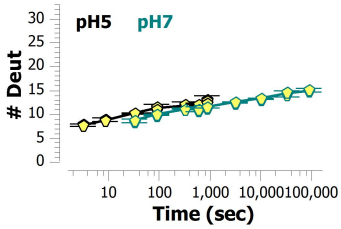

HC 337-351: KTISKAKGQPREPQV (#97)

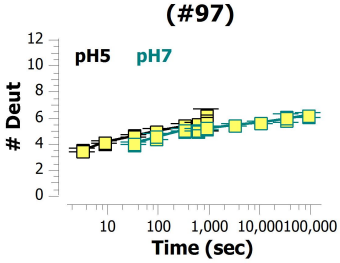

HC 337-359: ISKAKGQPREPQVYTLPPS (#98)

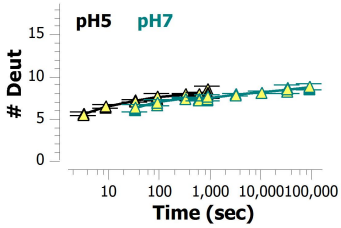

HC 337-368: GQPREPQVYTLPPSREEM (#99)

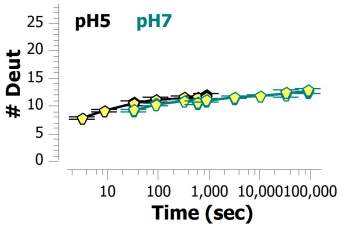

HC 352-359: YTLPPSRE (#100)

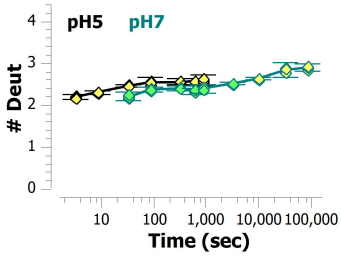

HC 352-368: YTLPPSREEMTKNQVSL (#101)

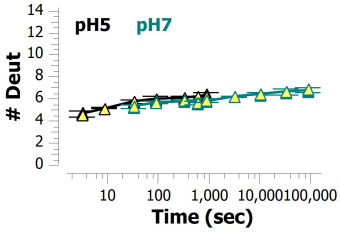

HC 352-370: /TLPPSREEMTKNQVSLTC (#102)

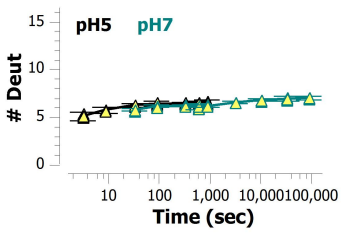

HC 360-367: EMTKNQVS (#103)

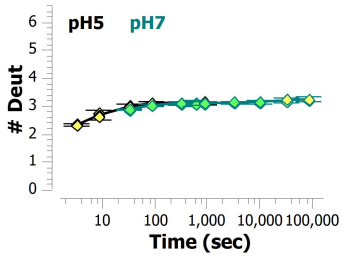

HC 360-368: EMTKNQVSL (#104)

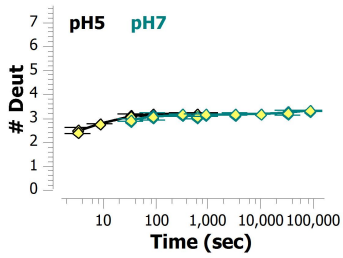

HC 360-369: EMTKNQVSLT (#105)

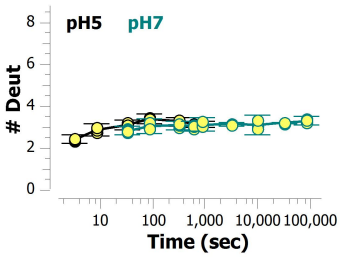

HC 360-370: EMTKNQVSLTC (#106)

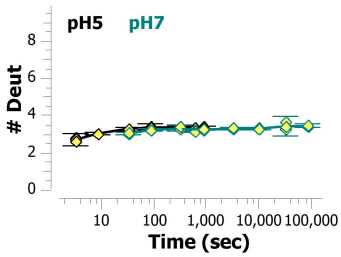

HC 371-379: LVKGFYPSD (#107)

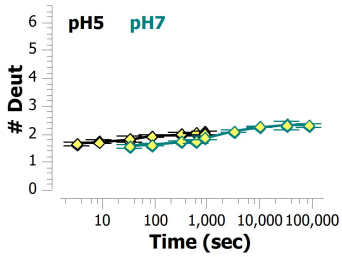

HC 372-379: VKGFYPSD (#108)

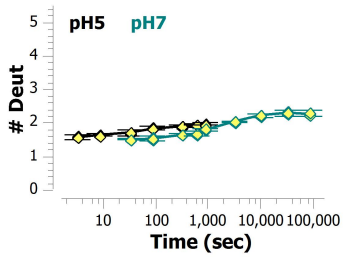

HC 372-382: VKGFYPSDIAV (#109)

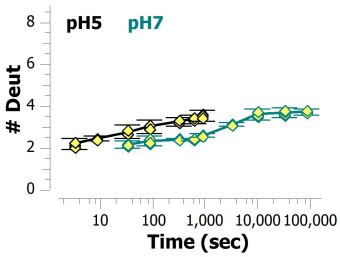

HC 372-383: VKGFYPSDIAVE (#110)

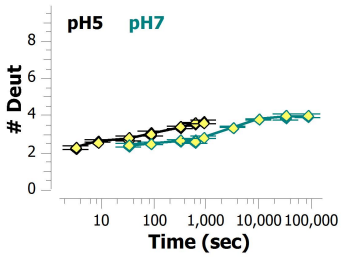

HC 380-383: IAVE (#111)

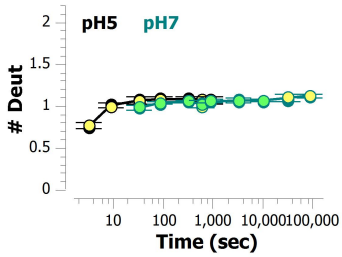

HC 380-393: IAVEWESNGQPENN (#112)

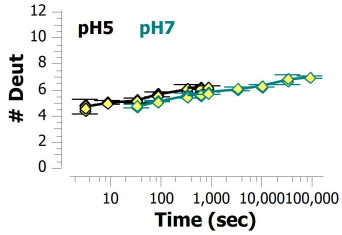

HC 380-401: /EWESNGQPENNYKTTPF (#113)

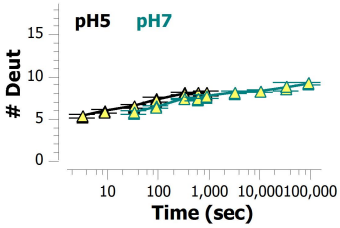

HC 380-407: ESNGQPENNYKTTPPVLD (#114)

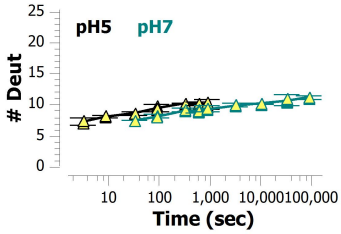

HC 383-401: WESNGQPENNYKTTPPV (#115)

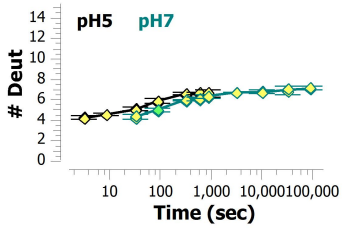

HC 384-393: WESNGQPENN (#116)

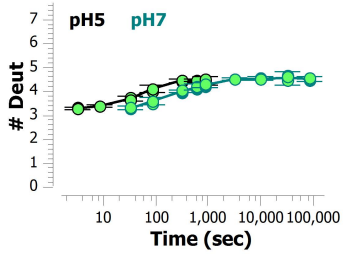

HC 384-401: WESNGQPENNYKTTPPVI (#117)

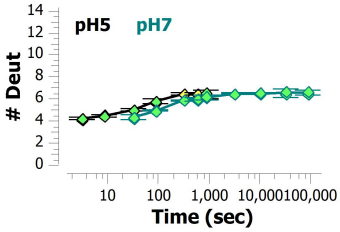

HC 394-401: YKTTPPVL (#118)

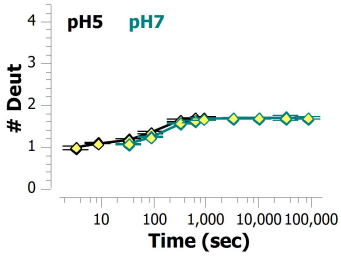

HC 395-401: KTTPPVL (#119)

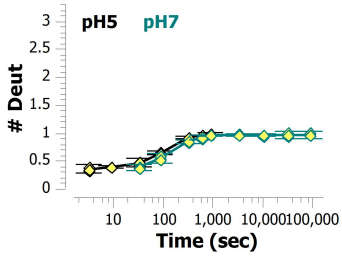

HC 408-413: FLYSKL (#120)

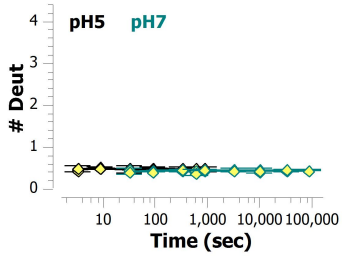

HC 408-426: LYSKLTVDKSRWQQGNV (#121)

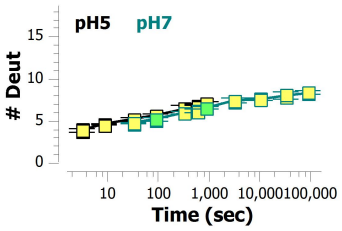

HC 408-429: YSKLTVDKSRWQQGNVFS (#122)

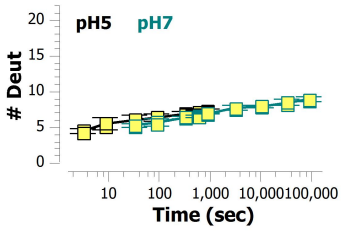

HC 409-412: LYSK (#123)

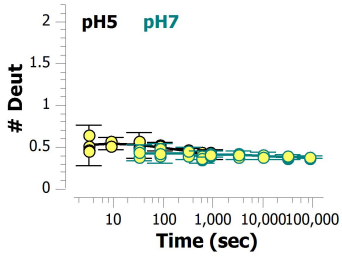

HC 410-426: YSKLTVDKSRWQQGNVF (#124)

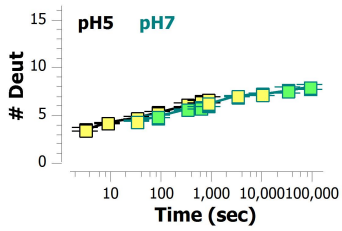

HC 414-426: TVDKSRWQQGNVF (#125)

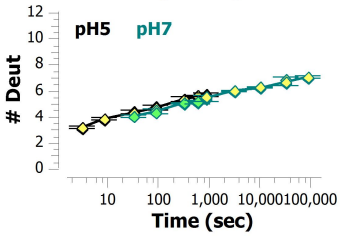

HC 414-449: GNVFSCSVMHEALHNHY (#126)

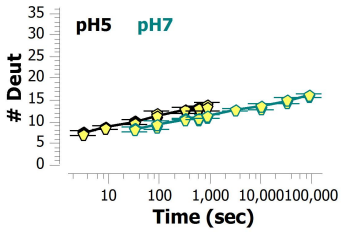

HC 427-449: VMHEALHNHYTQKSLSLS (#127)

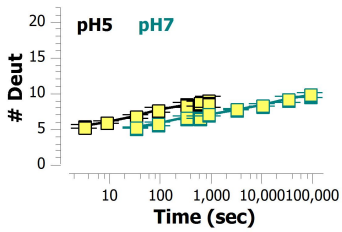

HC 429-449: MHEALHNHYTQKSLSLSI (#128)

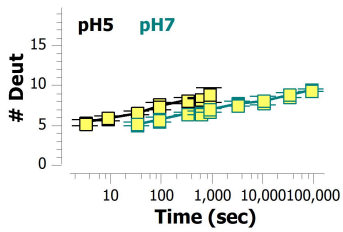

HC 430-449: MHEALHNHYTQKSLSLSP (#129)

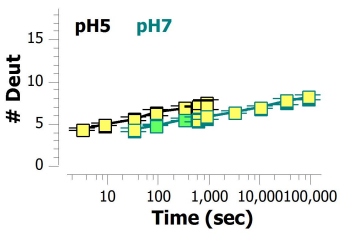

HC 431-449: HEALHNHYTQKSLSLSP((#130)

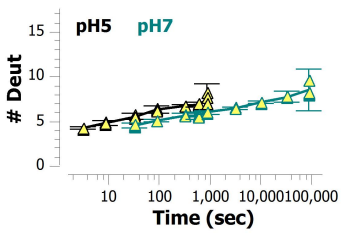

HC 432-449: HEALHNHYTQKSLSLSPG (#131)

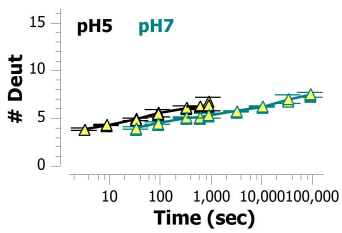

LC 1-11: DIQMTQSPSTL (#132)

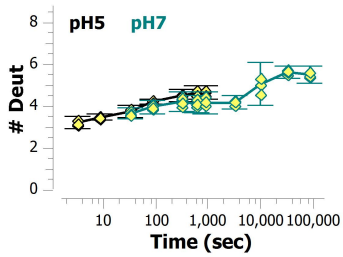

LC 5-11: TQSPSTL (#133)

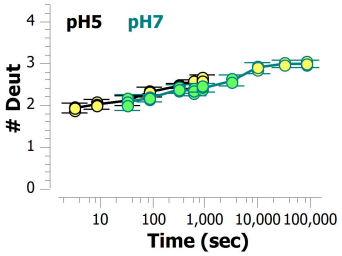

LC 12-22: SASVGDRVTIT (#134)

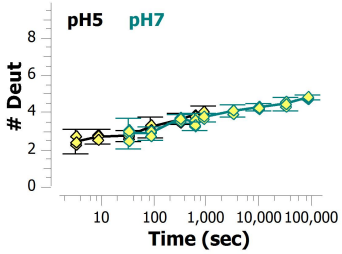

LC 23-34: CSASSRVGYMHW (#135)

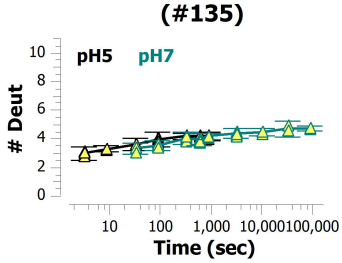

LC 26-34: SSRVGYMHW (#136)

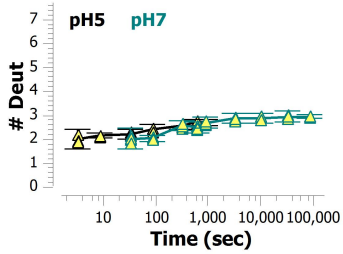

LC 26-45: RVGYMHWYQQKPGKAP (#137)

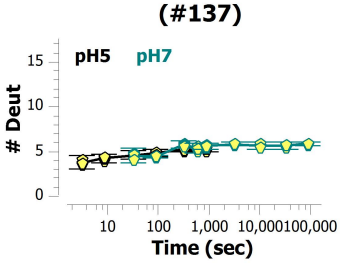

LC 35-45: YQQKPGKAPKL (#138)

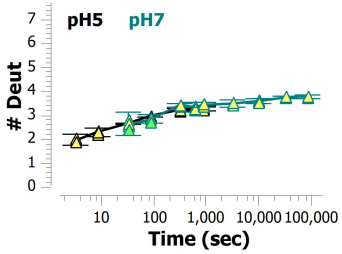

LC 35-53: YQQKPGKAPKLLIYDTSK (#139)

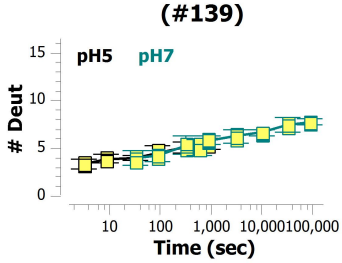

LC 46-53: LIYDTSKL (#140)

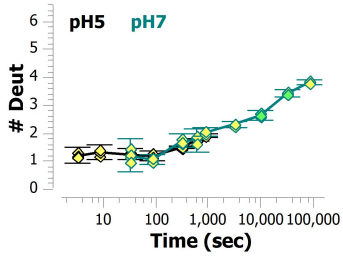

LC 46-69: DTSKLASGVPSRFSGSGS((#141)

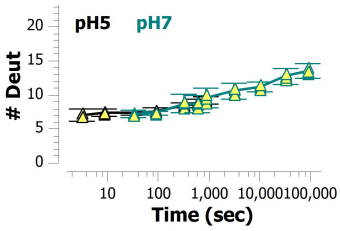

LC 54-69: ASGVPSRFSGSGSGTE (#142)

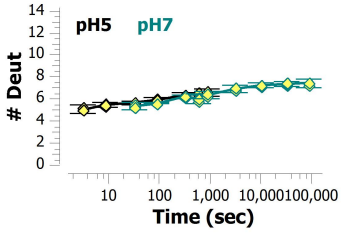

LC 54-70: ASGVPSRFSGSGSGTEF (#143)

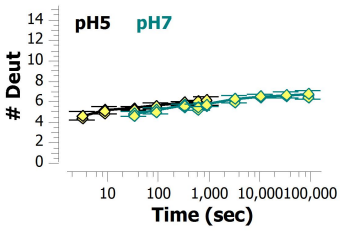

LC 70-73: FTLT (#144)

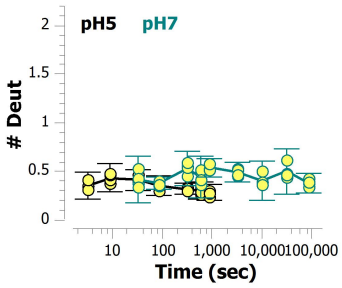

LC 70-82: FTLTISSLQPDDF (#145)

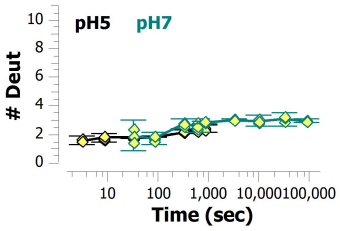

LC 71-82: TLTISSLQPDDF (#146)

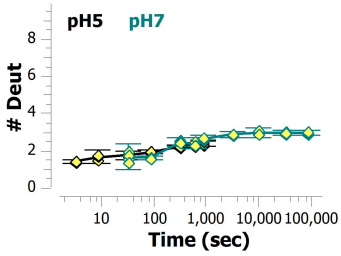

LC 74-81: ISSLQPDD (#147)

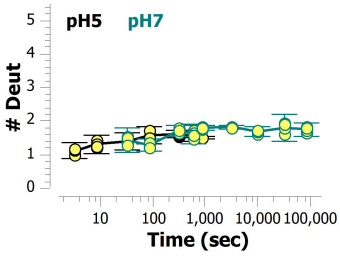

LC 74-82: ISSLQPDDF (#148)

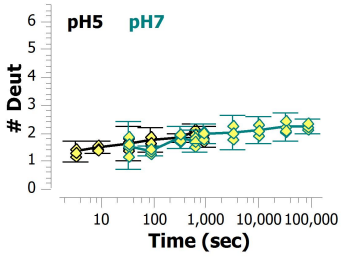

LC 86-114: SGYPFTFGGGTKVEIKRTV (#149)

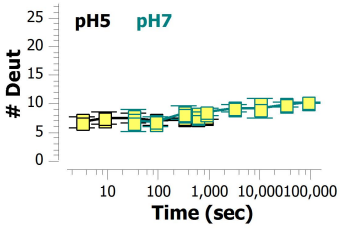

LC 86-115: GYPFTFGGGTKVEIKRTV (#150)

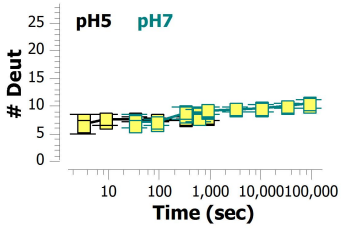

LC 89-114: YPFTFGGGTKVEIKRTVA (#151)

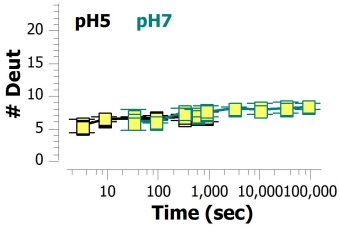

LC 89-115: YPFTFGGGTKVEIKRTVA (#152)

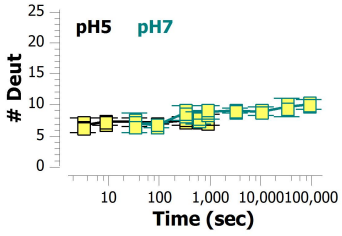

LC 115-121: FIFPPSD (#153)

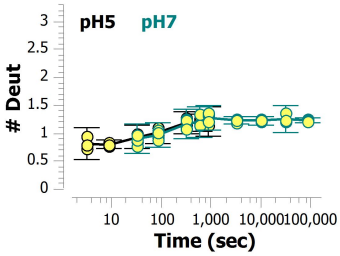

LC 115-124: FIFPPSDEQL (#154)

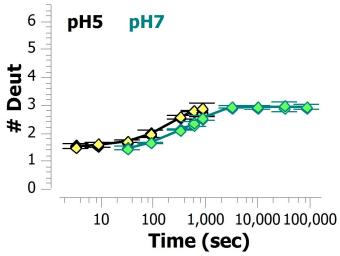

LC 115-131: FIFPPSDEQLKSGTASV (#155)

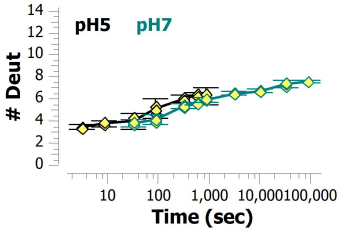

LC 116-121: IFPPSD (#156)

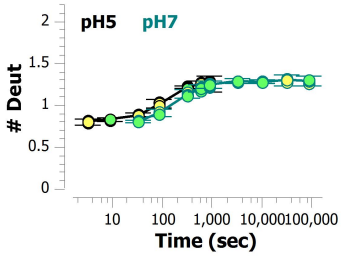

LC 116-122: IFPPSDE (#157)

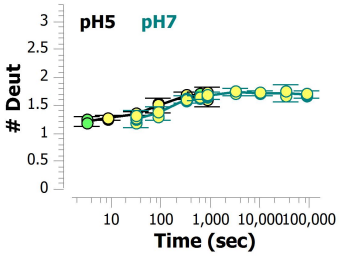

LC 116-124: IFPPSDEQL (#158)

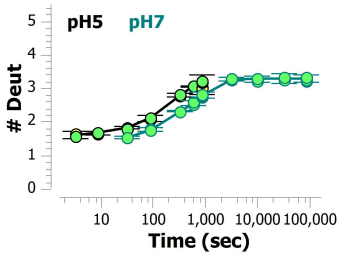

LC 116-131: IFPPSDEQLKSGTASV (#159)

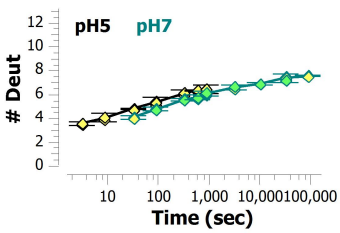

LC 116-132: IFPPSDEQLKSGTASVV (#160)

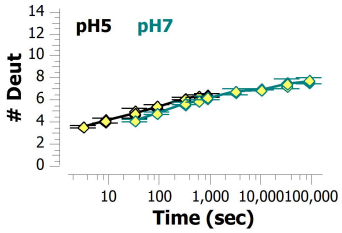

LC 122-131: EQLKSGTASV (#161)

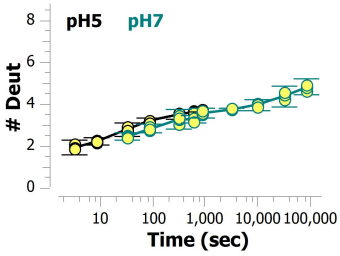

LC 123-131: QLKSGTASV (#162)

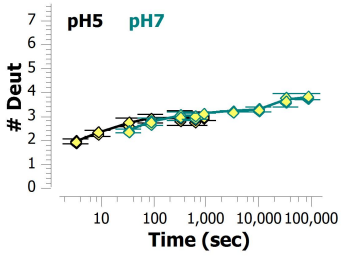

LC 132-134: VCL (#163)

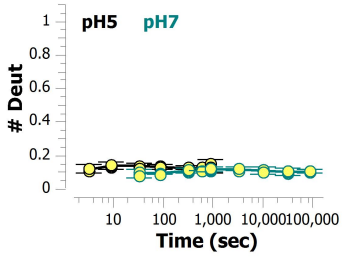

LC 132-135: VCLL (#164)

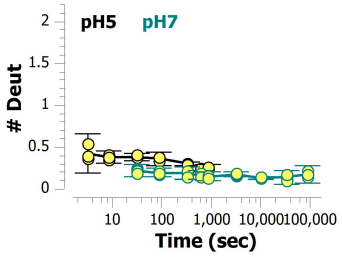

LC 132-153: .LNNFYPREAKVQWKVDN (#165)

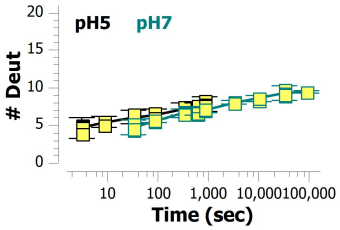

LC 132-160: FYPREAKVQWKVDNALQ (#166)

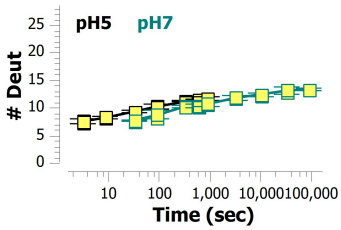

LC 135-142: LNNFYPRE (#167)

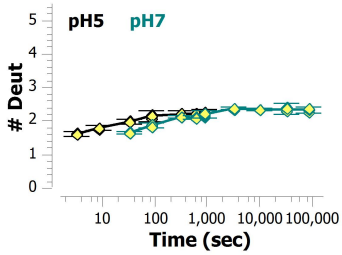

LC 135-147: LNNFYPREAKVQW (#168)

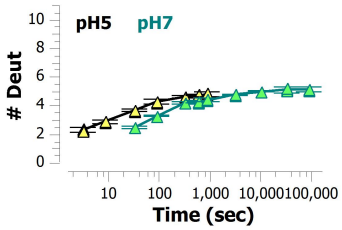

LC 135-153: NNFYPREAKVQWKVDNA (#169)

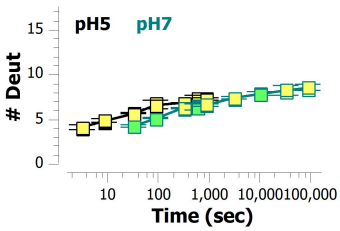

LC 135-160: 'PREAKVQWKVDNALQSC (#170)

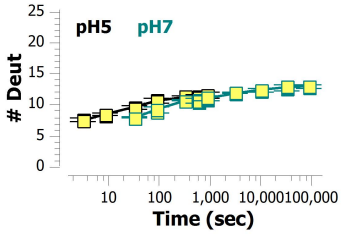

LC 135-171: VQWKVDNALQSGNSQES (#171)

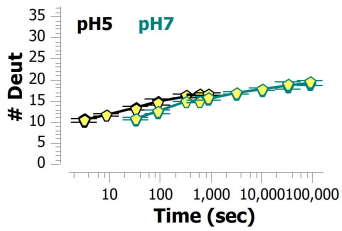

LC 136-160: PREAKVQWKVDNALQSG (#172)

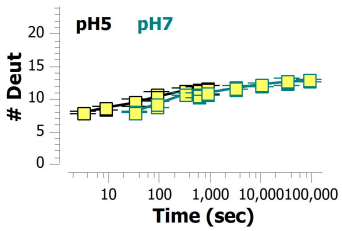

LC 139-160: EAKVQWKVDNALQSGNS (#173)

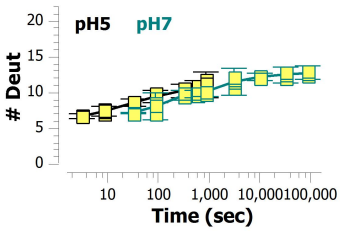

LC 143-160: AKVQWKVDNALQSGNSQ (#174)

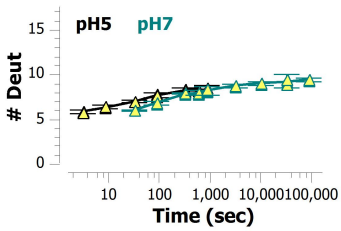

LC 148-160: KVDNALQSGNSQE (#175)

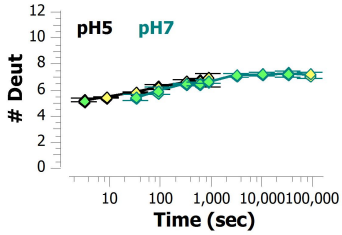

LC 161-171: SVTEQDSKDST (#176)

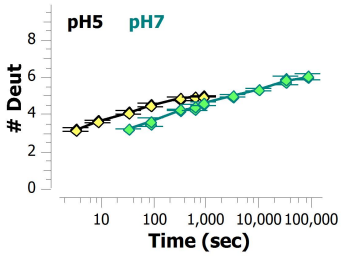

LC 161-174: SVTEQDSKDSTYSL (#177)

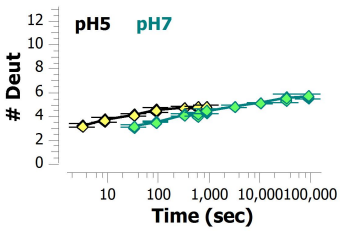

LC 161-177: SVTEQDSKDSTYSLSST (#178)

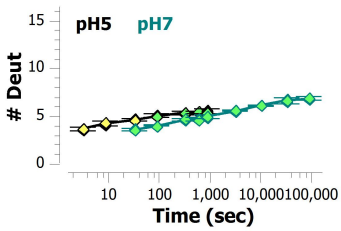

LC 161-178: SVTEQDSKDSTYSLSSTL (#179)

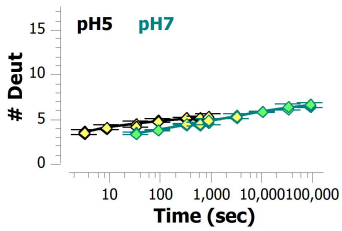

LC 161-194: DSTYSLSSTLTLSKADYEI (#180)

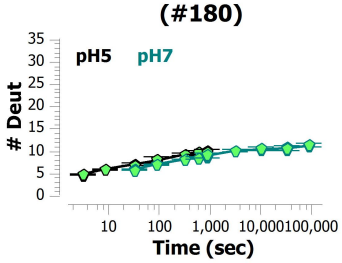

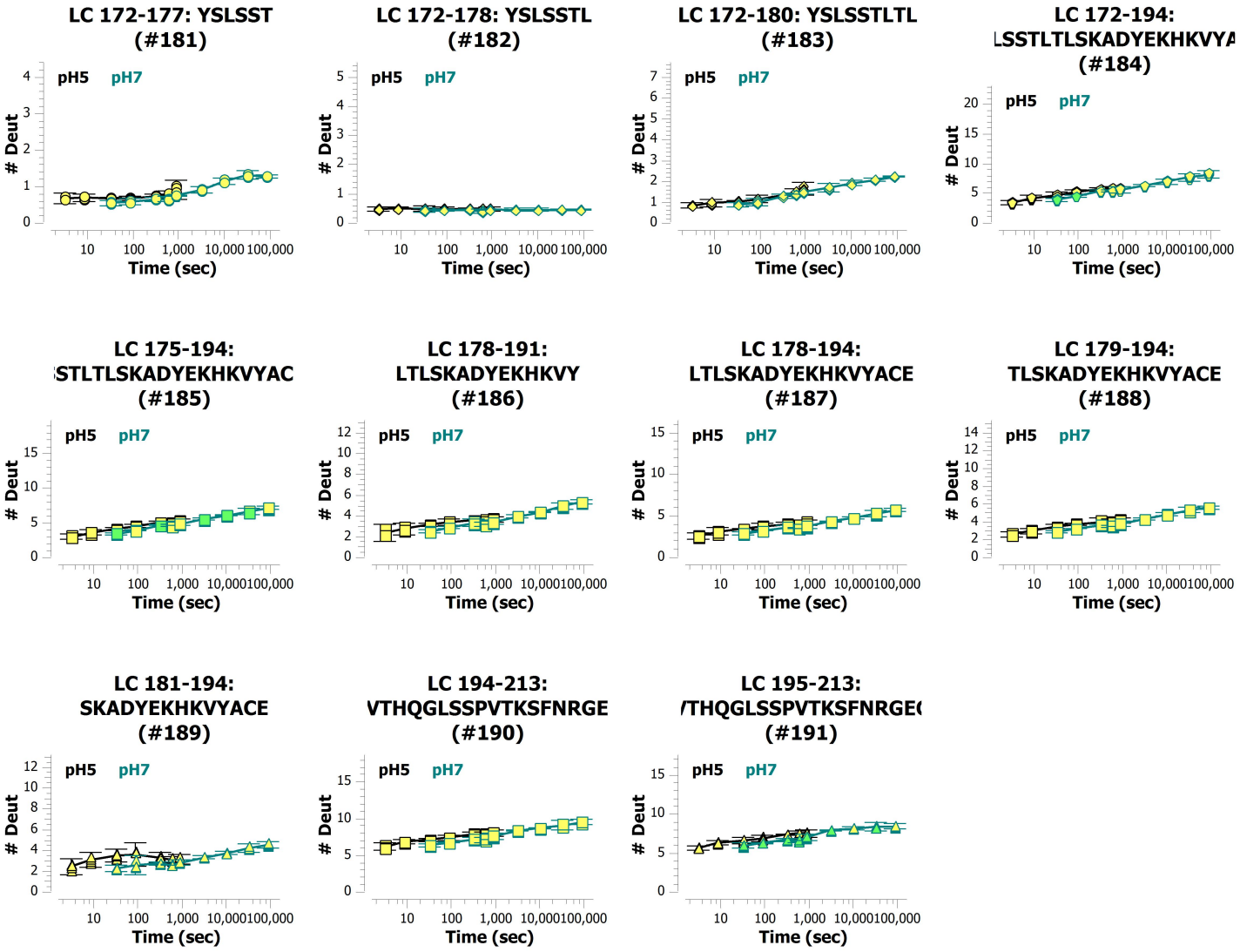

Figure 4.C-7. Deuterium uptake plots for NIST mAb peptic peptides at pH7 and pH 5 after timepoint labeling correction using equation 4.1.

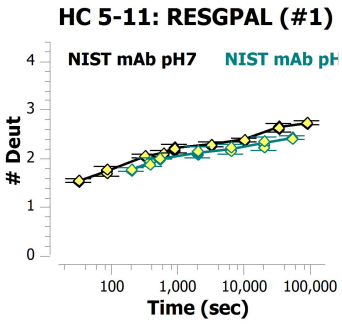
HC 5-11: RESGPAL (#1)
NIST mAb pH7
NIST mAb pH
Deut
Time (sec)

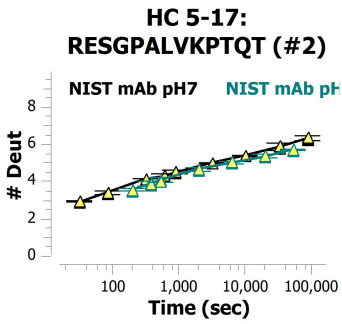
HC 5-17: RESGPALVKPTQT (#2)
NIST mAb pH7
NIST mAb pH
Deut
Time (sec)

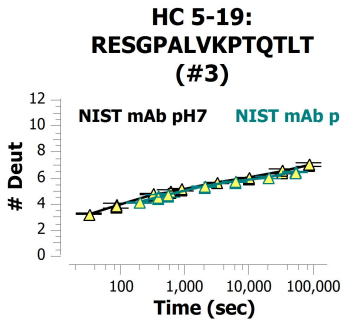
HC 5-19: RESGPALVKPTQTLT (#3)
NIST mAb pH7
NIST mAb p
Deut
Time (sec)

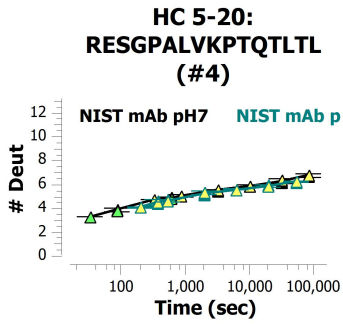
HC 5-20: RESGPALVKPTQTLTL (#4)
NIST mAb pH7
NIST mAb p
Deut
Time (sec)

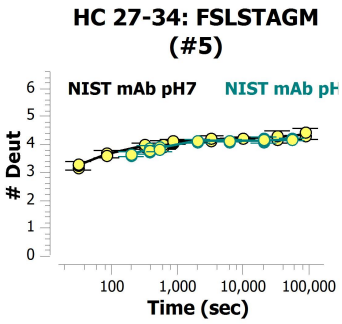
HC 27-34: FSLSTAGM (#5)
NIST mAb pH7
NIST mAb pH
Deut
Time (sec)

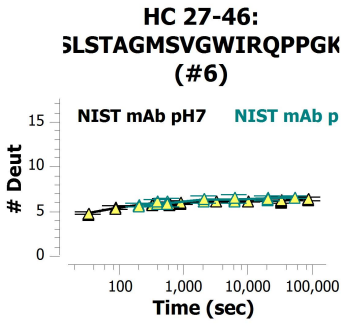
HC 27-46: SLSTAGMSVGWIRQPPGK (#6)
NIST mAb pH7
NIST mAb p
Deut
Time (sec)

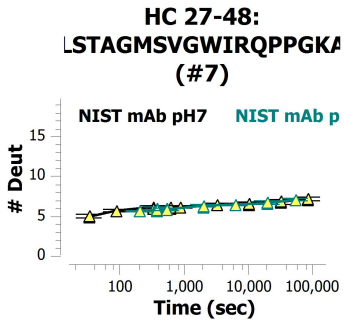
HC 27-48: LSTAGMSVGWIRQPPGKA (#7)
NIST mAb pH7
NIST mAb p
Deut
Time (sec)

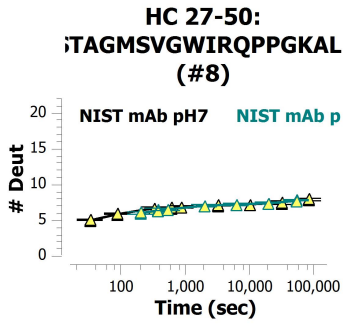
HC 27-50: STAGMSVGWIRQPPGKAL (#8)
NIST mAb pH7
NIST mAb p
Deut
Time (sec)

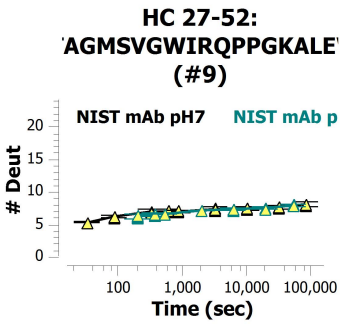
HC 27-52: TAGMSVGWIRQPPGKALE (#9)
NIST mAb pH7
NIST mAb p
Deut
Time (sec)

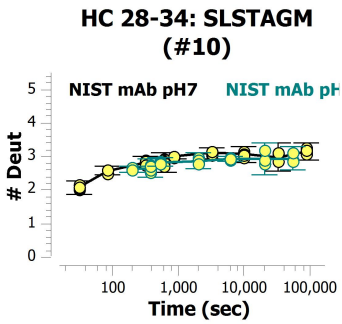
HC 28-34: SLSTAGM (#10)
NIST mAb pH7
NIST mAb pH
Deut
Time (sec)

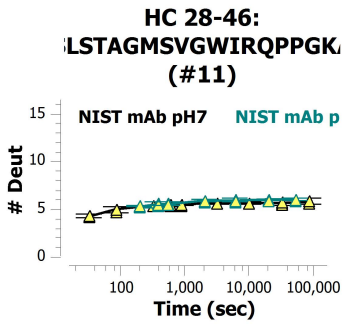
HC 28-46: LSTAGMSVGWIRQPPGK (#11)
NIST mAb pH7
NIST mAb p
Deut
Time (sec)

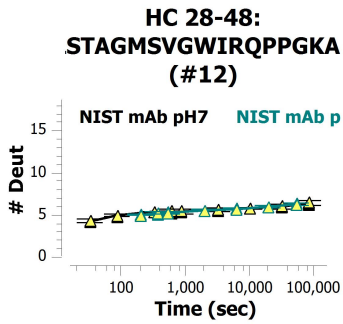
HC 28-48: STAGMSVGWIRQPPGKA (#12)
NIST mAb pH7
NIST mAb p
Deut
Time (sec)

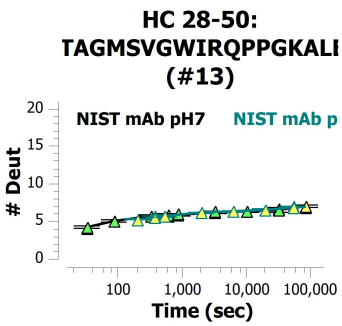
HC 28-50: TAGMSVGWIRQPPGKALI (#13)
NIST mAb pH7
NIST mAb p
Deut
Time (sec)

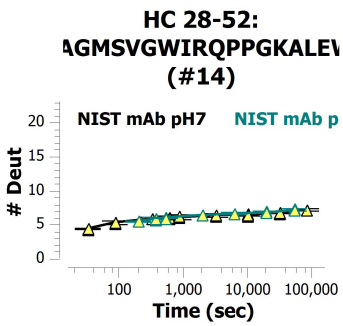
HC 28-52: AGMSVGWIRQPPGKALEV (#14)
NIST mAb pH7
NIST mAb p
Deut
Time (sec)

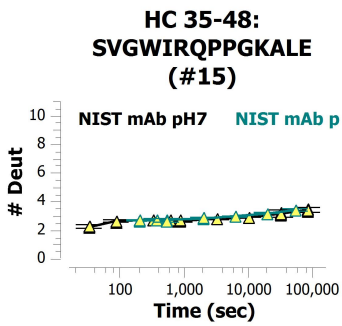
HC 35-48: SVGWIRQPPGKALE (#15)
NIST mAb pH7
NIST mAb p
Deut
Time (sec)

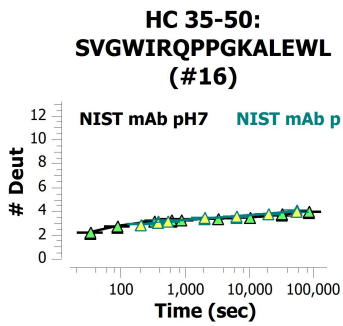
HC 35-50: SVGWIRQPPGKALEWL (#16)
NIST mAb pH7
NIST mAb p
Deut
Time (sec)

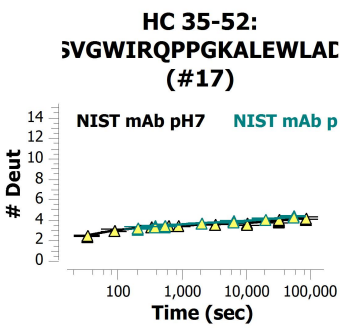
HC 35-52: SVGWIRQPPGKALEWLAD (#17)
NIST mAb pH7
NIST mAb p
Deut
Time (sec)

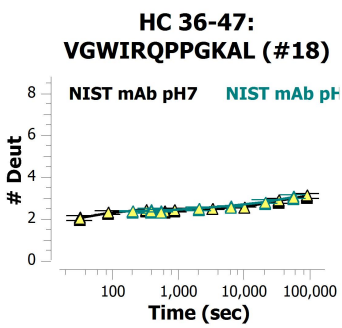
HC 36-47: VGWIRQPPGKAL (#18)
NIST mAb pH7
NIST mAb pH
Deut
Time (sec)

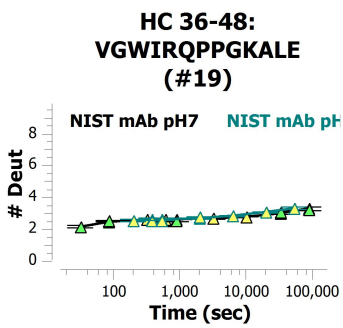
HC 36-48: VGWIRQPPGKALE (#19)
NIST mAb pH7
NIST mAb pH
Deut
Time (sec)

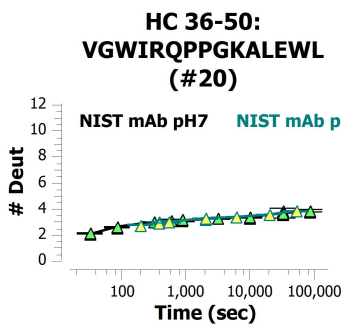
HC 36-50: VGWIRQPPGKALEWL (#20)
NIST mAb pH7
NIST mAb p
Deut
Time (sec)

HC 38-50: WIRQPPGKALEWL (#21)

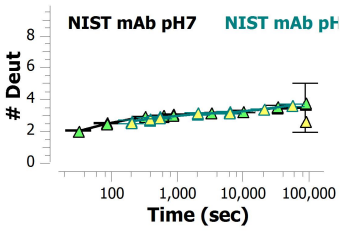

HC 39-48: IRQPPGKALE (#22)

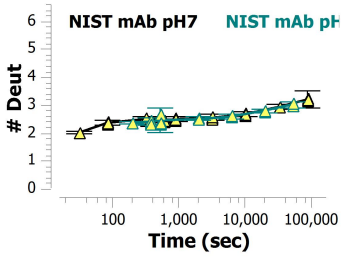

HC 39-50: IRQPPGKALEWL (#23)

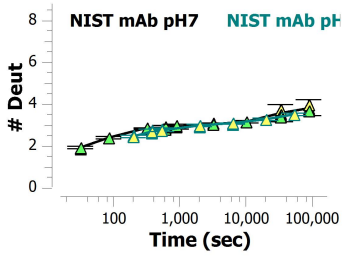

HC 47-50: LEWL (#24)

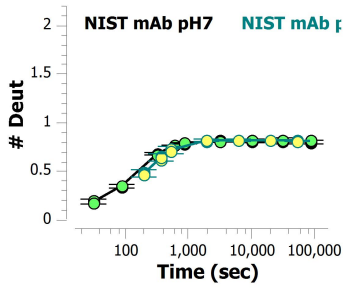

HC 47-52: LEWLAD (#25)

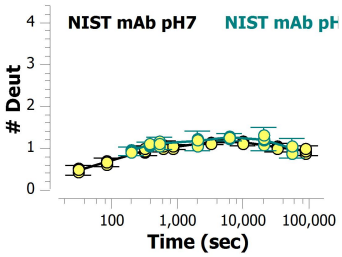

HC 49-52: WLAD (#26)

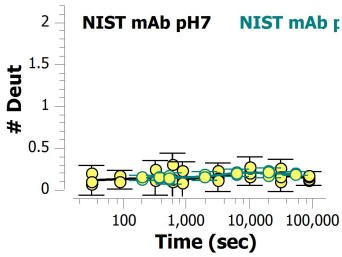

HC 51-65: ADIWWDDKKHYNPSL (#27)

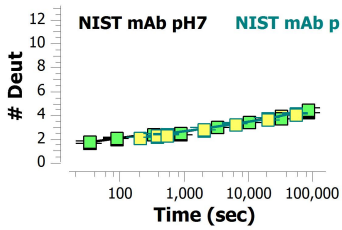

HC 51-69: DIWWDDKKHYNPSLKDR (#28)

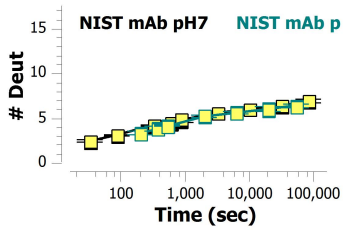

HC 53-69: IWWDDKKHYNPSLKDRL (#29)

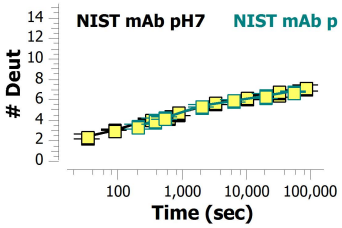

HC 53-82: (KHYNPSLKDRLTISKDTS (#30)

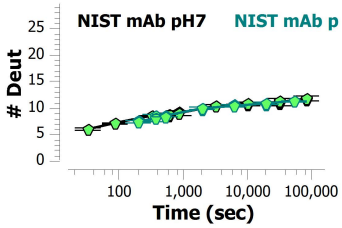

HC 54-69: WWDDKKHYNPSLKDRL (#31)

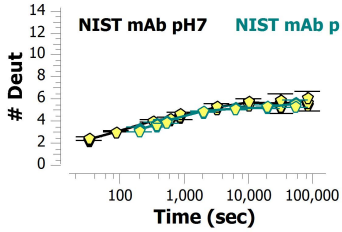

HC 66-82: KDRLTISKDTSKNQVVL (#32)

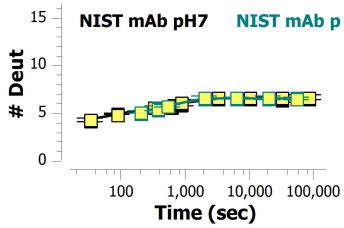

HC 68-82: RLTISKDTSKNQVVL (#33)

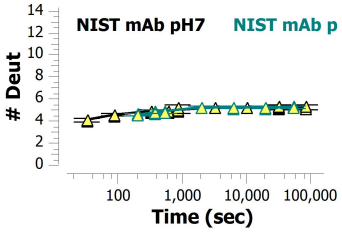

HC 70-82: TISKDTSKNQVVL (#34)

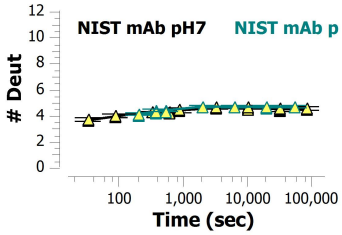

HC 83-94: KVTNMDPADTAT (#35)

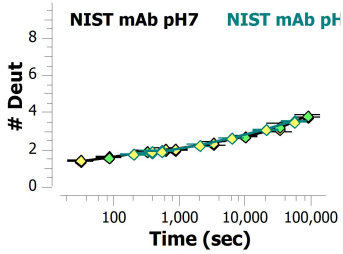

HC 83-96: KVTNMDPADTATYY (#36)

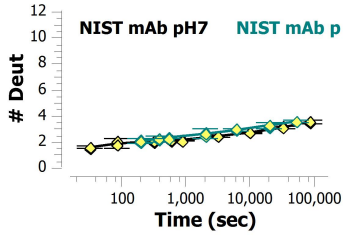

HC 95-103: YYCARDMIF (#37)

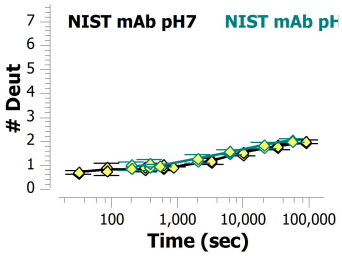

HC 95-105: YYCARDMIFNF (#38)

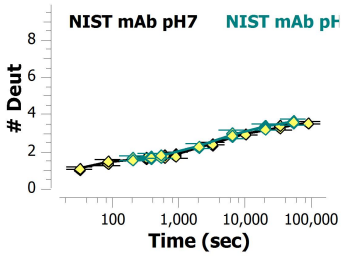

HC 97-105: CARDMIFNF (#39)

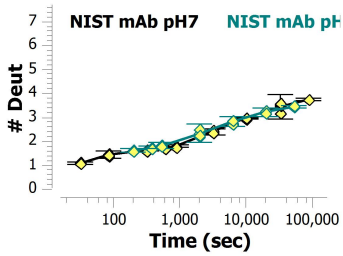

HC 101-105: MIFNF (#40)

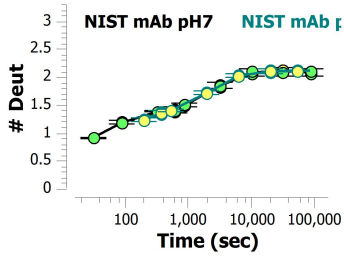

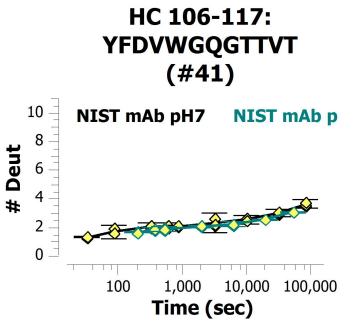
HC 106-117:
YFDVWGQGTTVT
(#41)
NIST mAb pH7
NIST mAb p
Deut
Time (sec)

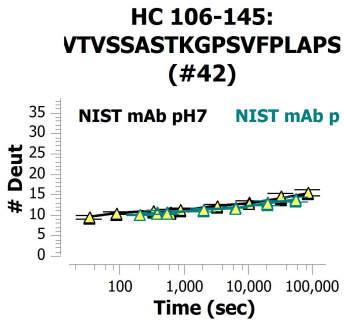
HC 106-145:
VTVSSASTKGPSVFPLAPS
(#42)
NIST mAb pH7
NIST mAb p
Deut
Time (sec)

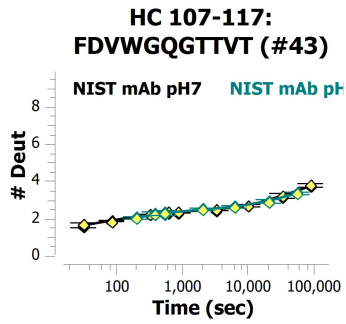
HC 107-117:
FDVWGQGTTVT (#43)
NIST mAb pH7
NIST mAb pH
Deut
Time (sec)

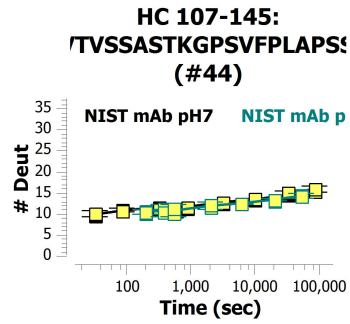
HC 107-145:
TVSSASTKGPSVFPLAPS
(#44)
NIST mAb pH7
NIST mAb p
Deut
Time (sec)

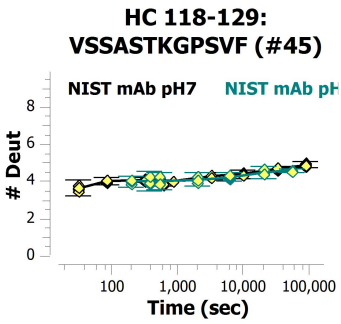
HC 118-129:
VSSASTKGPSVF (#45)
NIST mAb pH7
NIST mAb pH
Deut
Time (sec)

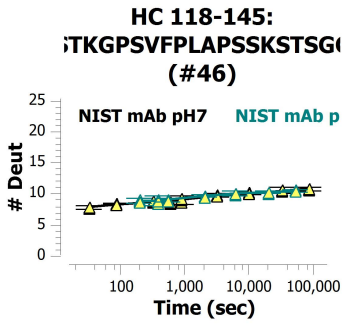
HC 118-145:
TKGPSVFPLAPSSKSTSG
(#46)
NIST mAb pH7
NIST mAb p
Deut
Time (sec)

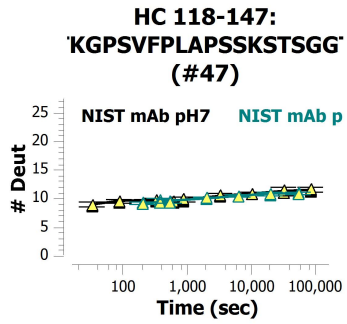
HC 118-147:
KGPSVFPLAPSSKSTSGG
(#47)
NIST mAb pH7
NIST mAb p
Deut
Time (sec)

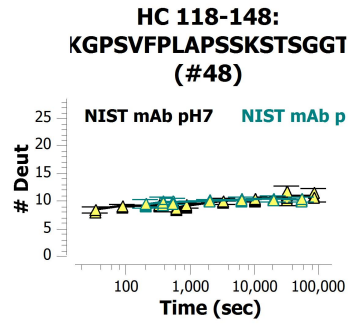
HC 118-148:
KGPSVFPLAPSSKSTSGGT
(#48)
NIST mAb pH7
NIST mAb p
Deut
Time (sec)

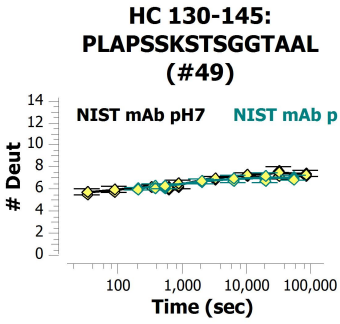
HC 130-145:
PLAPSSKSTSGGTAAL
(#49)
NIST mAb pH7
NIST mAb p
Deut
Time (sec)

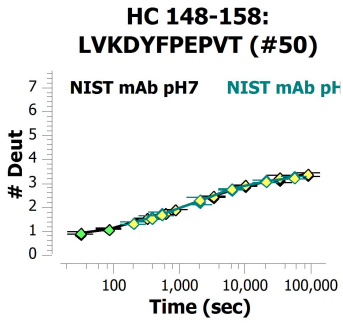
HC 148-158:
LVKDYFPEPVT (#50)
NIST mAb pH7
NIST mAb pH
Deut
Time (sec)

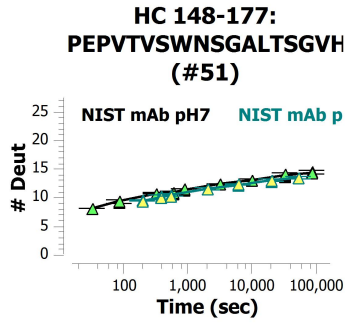
HC 148-177:
PEPVTVSWNSGALTSGVH
(#51)
NIST mAb pH7
NIST mAb p
Deut
Time (sec)

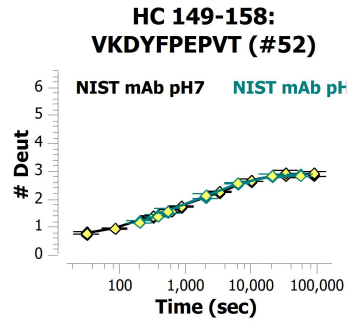
HC 149-158:
VKDYFPEPVT (#52)
NIST mAb pH7
NIST mAb pH
Deut
Time (sec)

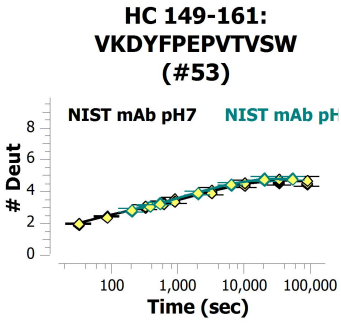
HC 149-161:
VKDYFPEPVTVSW
(#53)
NIST mAb pH7
NIST mAb pH
Deut
Time (sec)

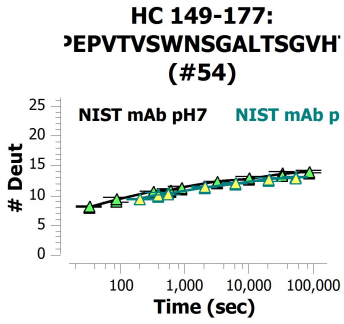
HC 149-177:
PEPVTVSWNSGALTSGVH
(#54)
NIST mAb pH7
NIST mAb p
Deut
Time (sec)

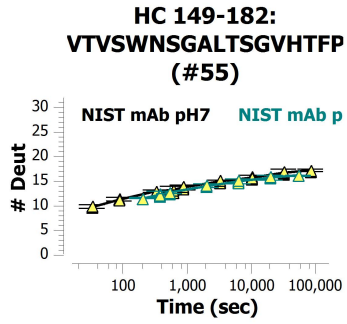
HC 149-182:
VTVSWNSGALTSGVHTFP
(#55)
NIST mAb pH7
NIST mAb p
Deut
Time (sec)

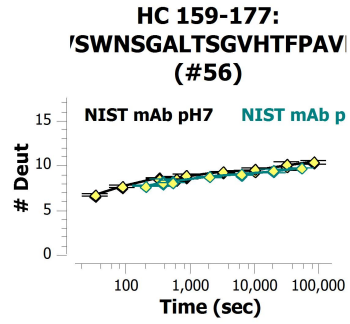
HC 159-177:
SWNSGALTSGVHTFPAV
(#56)
NIST mAb pH7
NIST mAb p
Deut
Time (sec)

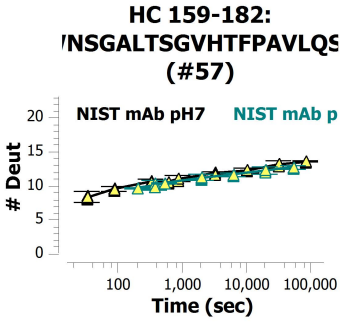
HC 159-182:
NSGALTSGVHTFPAVLQS
(#57)
NIST mAb pH7
NIST mAb p
Deut
Time (sec)

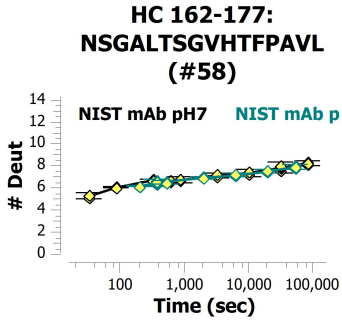
HC 162-177:
NSGALTSGVHTFPAVL
(#58)
NIST mAb pH7
NIST mAb p
Deut
Time (sec)

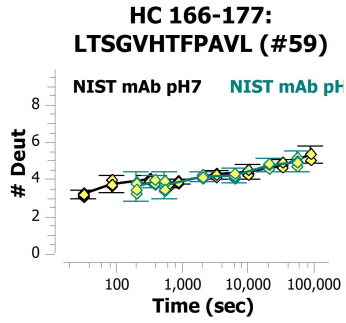
HC 166-177:
LTSGVHTFPAVL (#59)
NIST mAb pH7
NIST mAb pH
Deut
Time (sec)

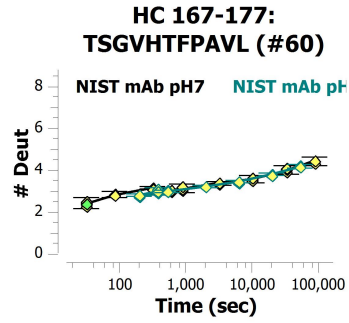
HC 167-177:
TSGVHTFPAVL (#60)
NIST mAb pH7
NIST mAb pH
Deut
Time (sec)

HC 183-188: YSLSSV (#61)

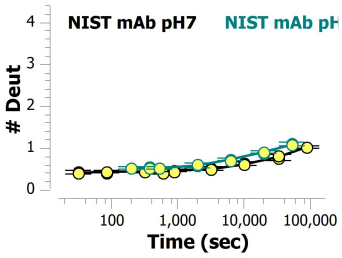

HC 183-196: YSLSSVVTVPSSSL (#62)

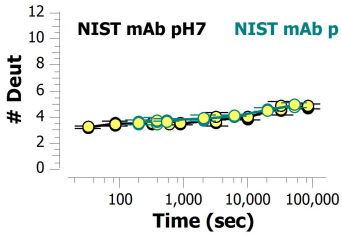

HC 183-200: YSLSSVVTVPSSSLGTQT (#63)

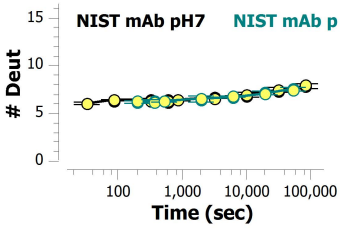

HC 188-196: VVTVPSSSL (#64)

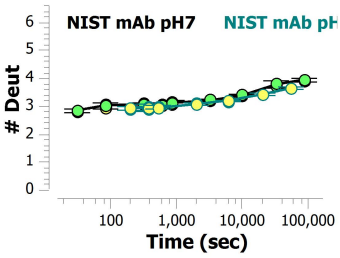

HC 188-200: VVTVPSSSLGTQT (#65)

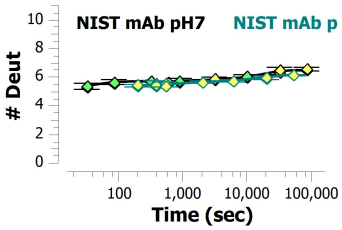

HC 188-201: VVTVPSSSLGTQTY (#66)

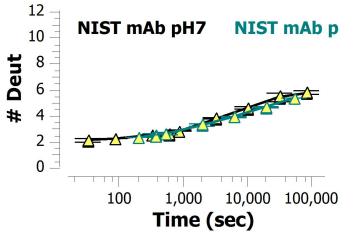

HC 189-196: VTVPSSSL (#67)

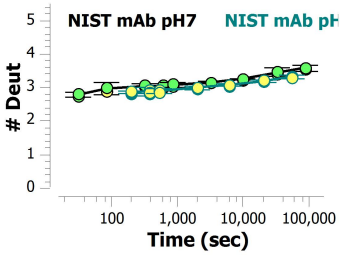

HC 189-200: VTVPSSSLGTQT (#68)

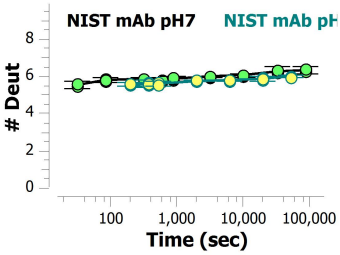

HC 189-201: VTVPSSSLGTQTY (#69)

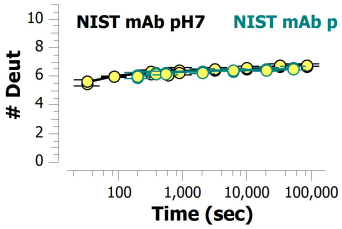

HC 201-212: YICNVNHKPSNT (#70)

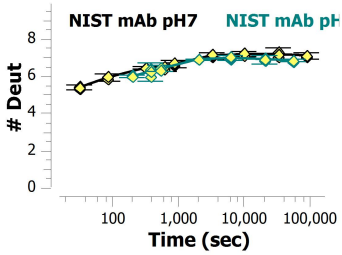

HC 201-237: SNTKVDKRVEPKSCDKTH (#71)

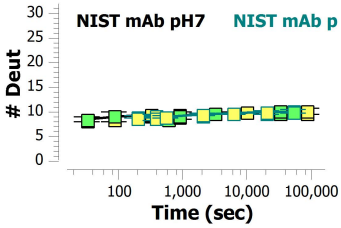

HC 238-243: LGGPSV (#72)

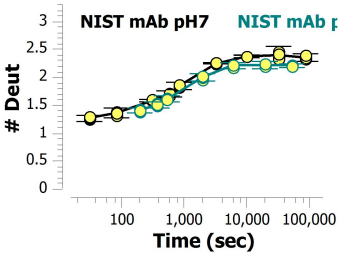

HC 238-244: LGGPSVF (#73)

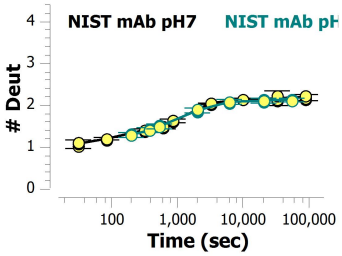

HC 238-255: LGGPSVFLFPPKPKDTLM (#74)

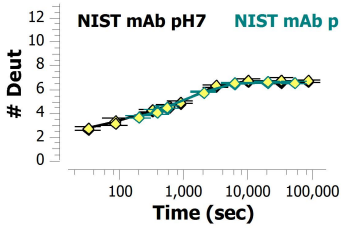

HC 244-254: FLFPPKPKDTL (#75)

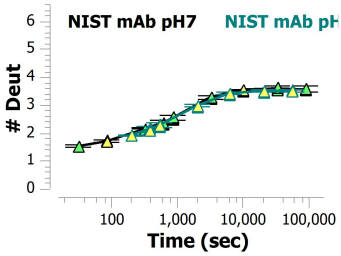

HC 244-255: FLFPPKPKDTLM (#76)

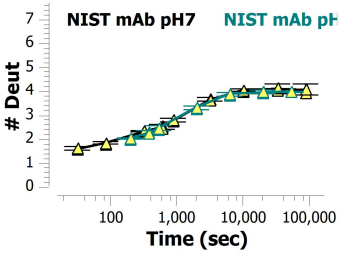

HC 245-254: LFPPKPKDTL (#77)

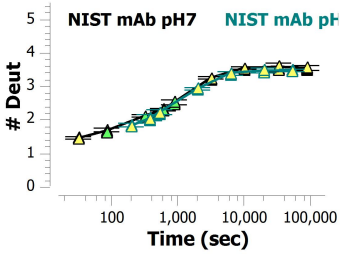

HC 245-255: LFPPKPKDTLM (#78)

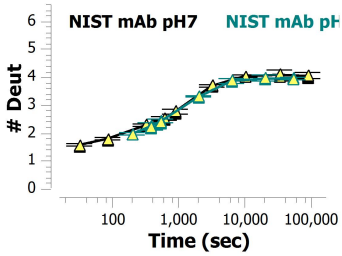

HC 247-255: PPKPKDTLM (#79)

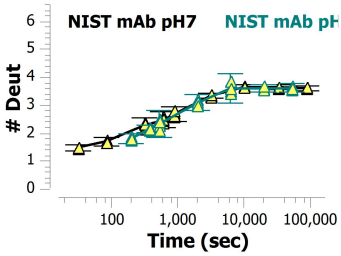

HC 255-264: MISRTPEVTC (#80)

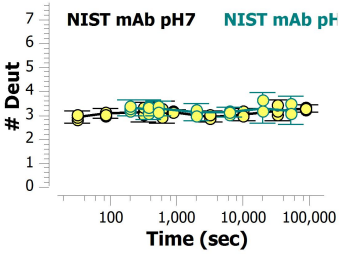

HC 255-265: MISRTPEVTCV (#81)

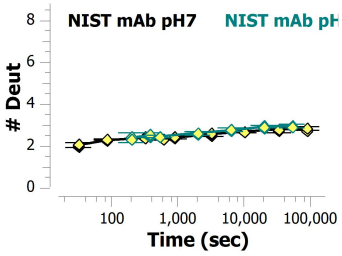

HC 256-263: ISRTPEVT (#82)

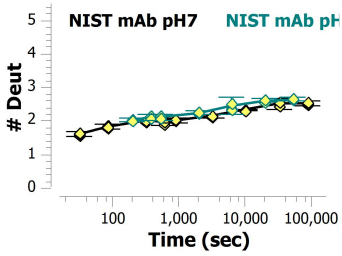

HC 256-264: ISRTPEVTC (#83)

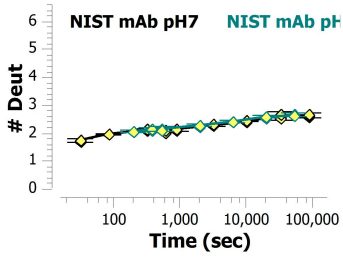

HC 256-265: ISRTPEVTCV (#84)

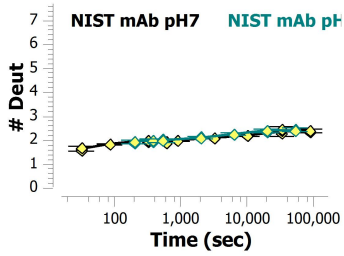

HC 264-280: CVVVDVSHEDPEVKFNW (#85)

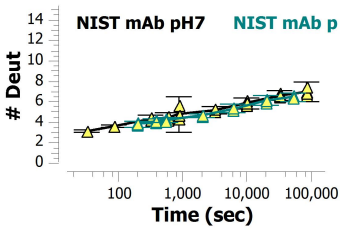

HC 265-278: VVVDVSHEDPEVKF (#86)

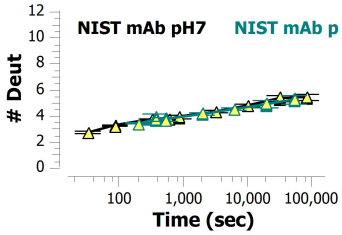

HC 265-280: VVVDVSHEDPEVKFNW (#87)

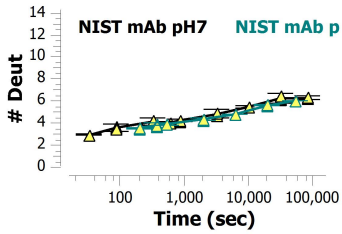

HC 266-280: VVDVSHEDPEVKFNW (#88)

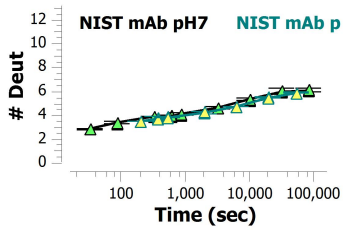

HC 267-280: VDVSHEDPEVKFNW (#89)

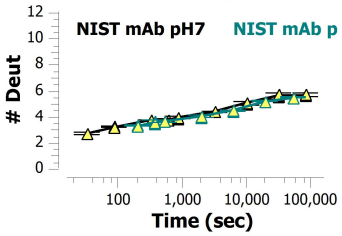

HC 269-280: VSHEDPEVKFNW (#90)

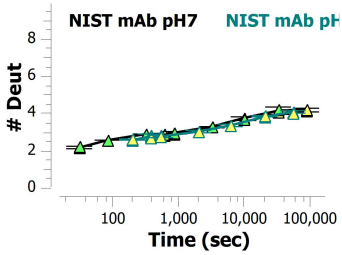

HC 290-314: PREEQYN*STYRVVSVLT (#91)

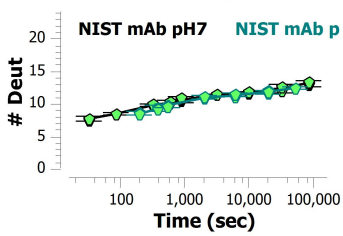

HC 300-328: /VSVLTVLHQDWLNGKEY (#92)

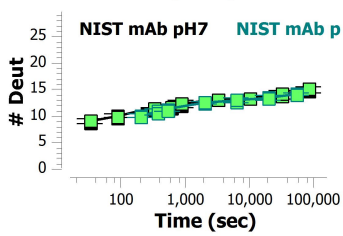

HC 304-309: RVVSVL (#93)

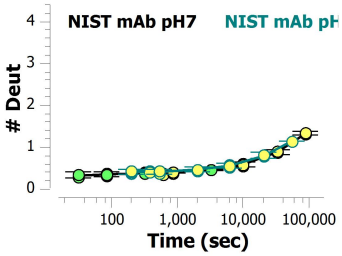

HC 309-321: LTVLHQDWLNGKE (#94)

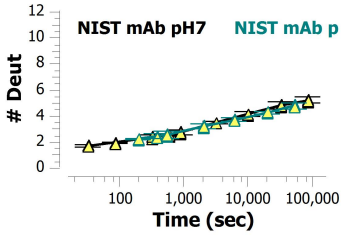

HC 310-321: TVLHQDWLNGKE (#95)

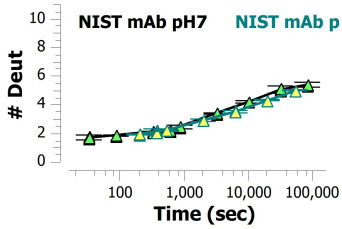

HC 322-359: -PAPIEKTISKAKGQPREP((#96)

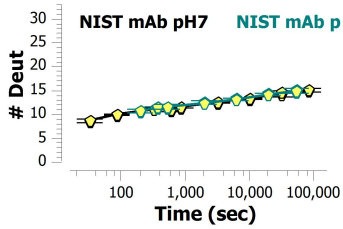

HC 337-351: KTISKAKGQPREPQV (#97)

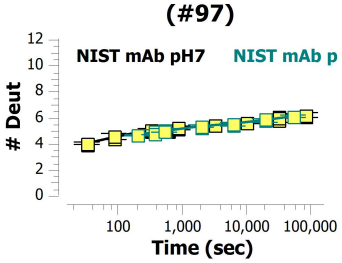

HC 337-359: [SKAKGQPREPQVYTLPPS (#98)

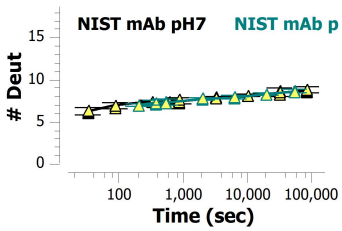

HC 337-368: GQPREPQVYTLPPSREEM (#99)

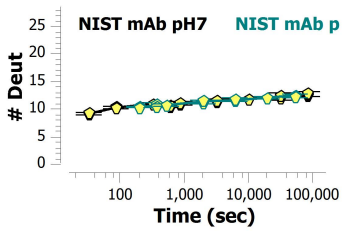

HC 352-359: YTLPPSRE (#100)

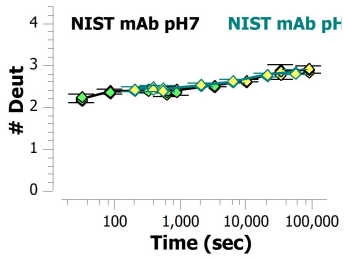

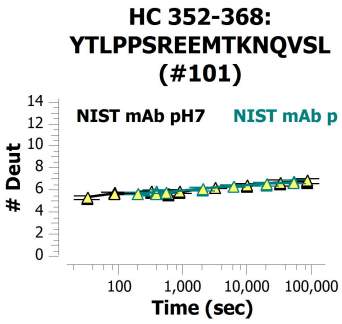
HC 352-368: YTLPPSREEMTKNQVSL (#101)
NIST mAb pH7
NIST mAb p
Deut
Time (sec)

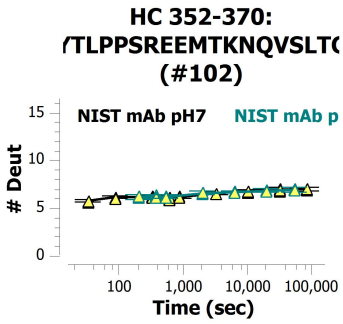
HC 352-370: /TLPPSREEMTKNQVSLTC (#102)
NIST mAb pH7
NIST mAb p
Deut
Time (sec)

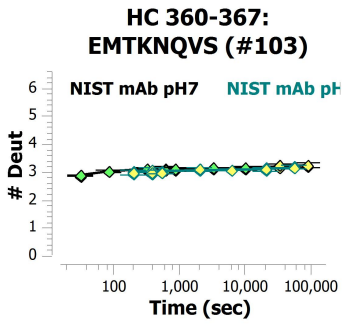
HC 360-367: EMTKNQVS (#103)
NIST mAb pH7
NIST mAb pH
Deut
Time (sec)

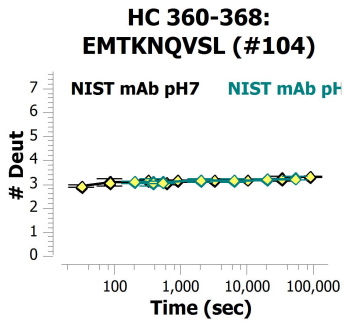
HC 360-368: EMTKNQVSL (#104)
NIST mAb pH7
NIST mAb pH
Deut
Time (sec)

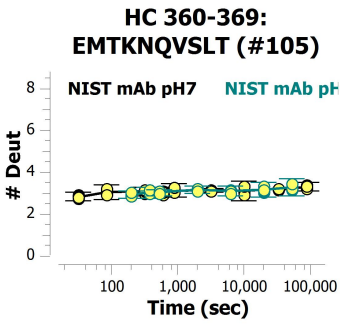
HC 360-369: EMTKNQVSLT (#105)
NIST mAb pH7
NIST mAb pH
Deut
Time (sec)

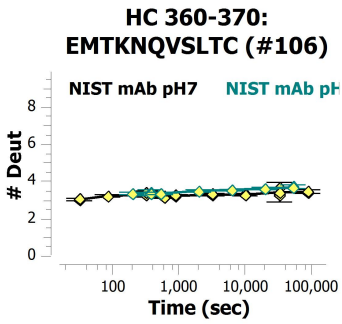
HC 360-370: EMTKNQVSLTC (#106)
NIST mAb pH7
NIST mAb pH
Deut
Time (sec)

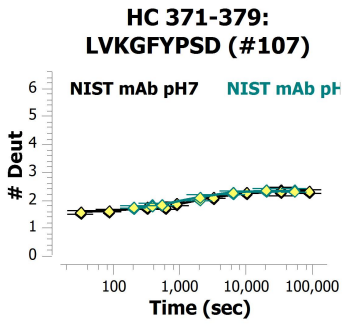
HC 371-379: LVKGFYPSD (#107)
NIST mAb pH7
NIST mAb pH
Deut
Time (sec)

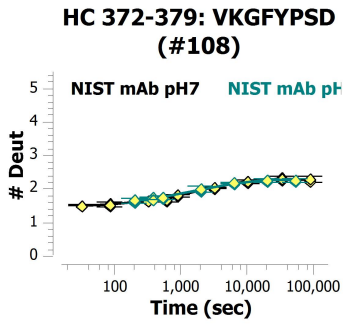
HC 372-379: VKGFYPSD (#108)
NIST mAb pH7
NIST mAb pH
Deut
Time (sec)

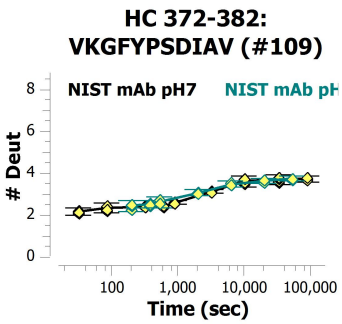
HC 372-382: VKGFYPSDIAV (#109)
NIST mAb pH7
NIST mAb pH
Deut
Time (sec)

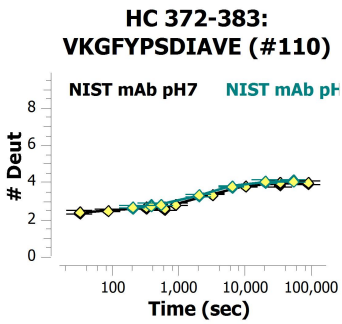
HC 372-383: VKGFYPSDIAVE (#110)
NIST mAb pH7
NIST mAb pH
Deut
Time (sec)

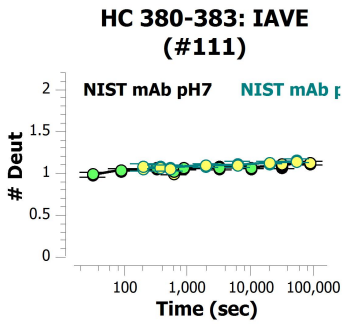
HC 380-383: IAVE (#111)
NIST mAb pH7
NIST mAb p
Deut
Time (sec)

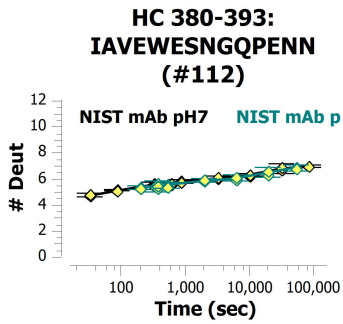
HC 380-393: IAVEWESNGQPENN (#112)
NIST mAb pH7
NIST mAb p
Deut
Time (sec)

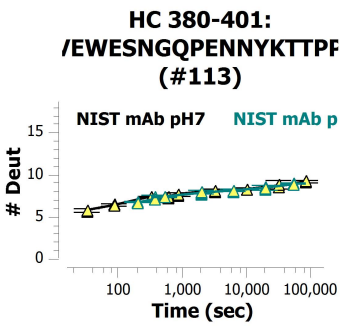
HC 380-401: /EWESNGQPENNYKTTPF (#113)
NIST mAb pH7
NIST mAb p
Deut
Time (sec)

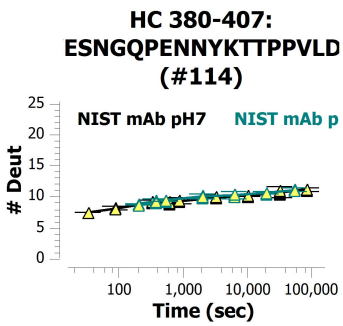
HC 380-407: ESNGQPENNYKTTPPVLD (#114)
NIST mAb pH7
NIST mAb p
Deut
Time (sec)

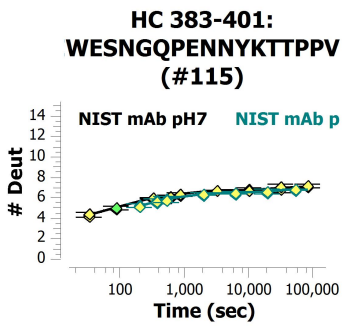
HC 383-401: WESNGQPENNYKTTPPV (#115)
NIST mAb pH7
NIST mAb p
Deut
Time (sec)

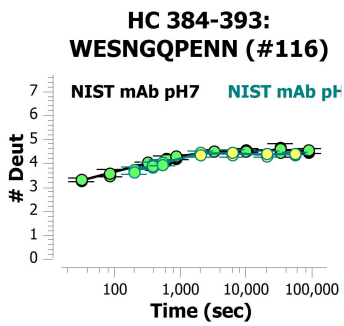
HC 384-393: WESNGQPENN (#116)
NIST mAb pH7
NIST mAb pH
Deut
Time (sec)

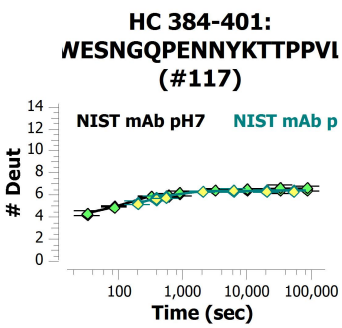
HC 384-401: WESNGQPENNYKTTPPVI (#117)
NIST mAb pH7
NIST mAb p
Deut
Time (sec)

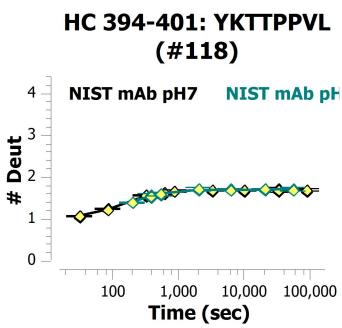
HC 394-401: YKTTPPVL (#118)
NIST mAb pH7
NIST mAb pH
Deut
Time (sec)

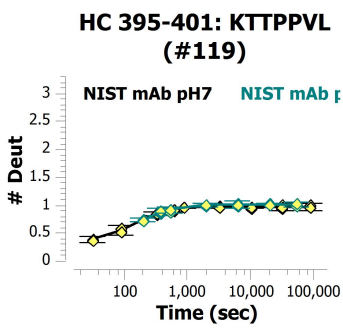
HC 395-401: KTTPPVL (#119)
NIST mAb pH7
NIST mAb p
Deut
Time (sec)

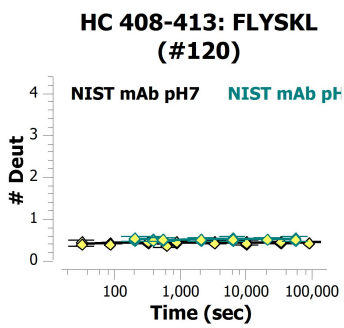
HC 408-413: FLYSKL (#120)
NIST mAb pH7
NIST mAb pH
Deut
Time (sec)

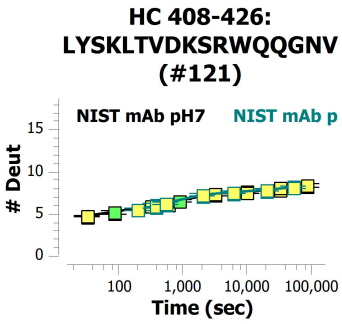
HC 408-426: LYSKLTVDKSRWQQGNV (#121)
NIST mAb pH7
NIST mAb p
Deut
Time (sec)

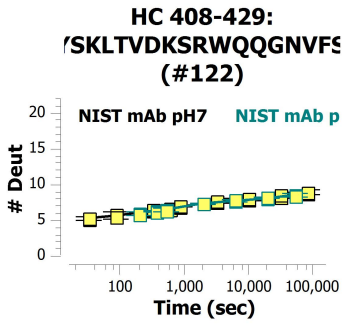
HC 408-429: SKLTVDKSRWQQGNVFS (#122)
NIST mAb pH7
NIST mAb p
Deut
Time (sec)

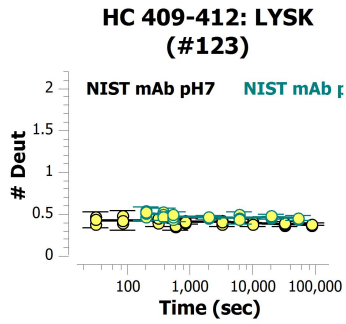
HC 409-412: LYSK (#123)
NIST mAb pH7
NIST mAb p
Deut
Time (sec)

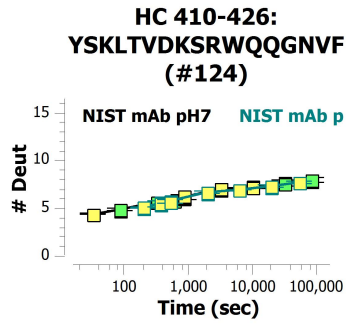
HC 410-426: YSKLTVDKSRWQQGNVF (#124)
NIST mAb pH7
NIST mAb p
Deut
Time (sec)

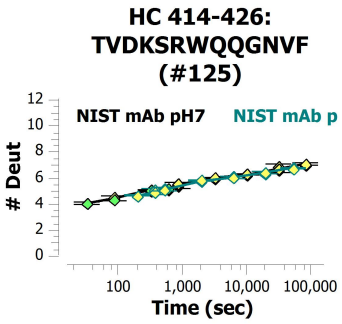
HC 414-426: TVDKSRWQQGNVF (#125)
NIST mAb pH7
NIST mAb p
Deut
Time (sec)

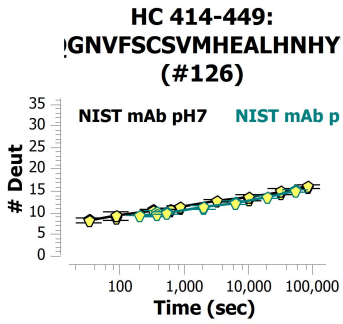
HC 414-449: GNVFSCSVMHEALHNHY (#126)
NIST mAb pH7
NIST mAb p
Deut
Time (sec)

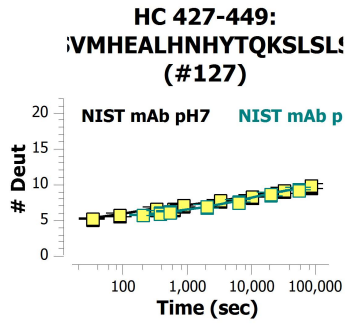
HC 427-449: VMHEALHNHYTQKSLSL (#127)
NIST mAb pH7
NIST mAb p
Deut
Time (sec)

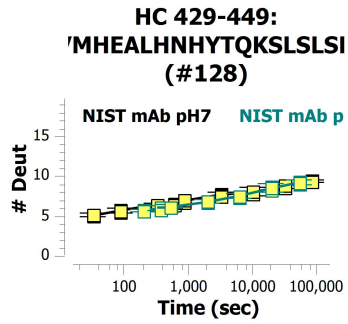
HC 429-449: MHEALHNHYTQKSLSLSI (#128)
NIST mAb pH7
NIST mAb p
Deut
Time (sec)

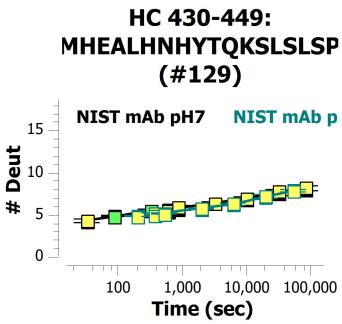
HC 430-449: MHEALHNHYTQKSLSLSP (#129)
NIST mAb pH7
NIST mAb p
Deut
Time (sec)

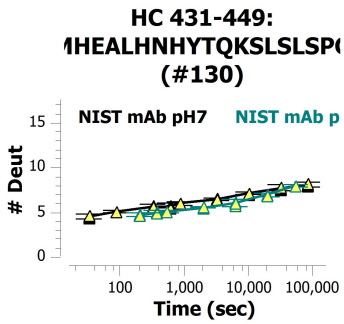
HC 431-449: HEALHNHYTQKSLSLSP((#130)
NIST mAb pH7
NIST mAb p
Deut
Time (sec)

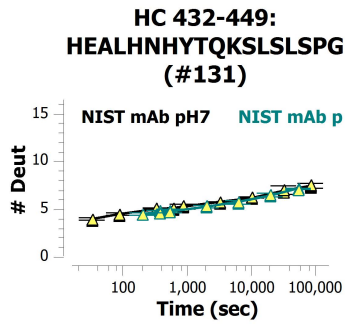
HC 432-449: HEALHNHYTQKSLSLSPG (#131)
NIST mAb pH7
NIST mAb p
Deut
Time (sec)

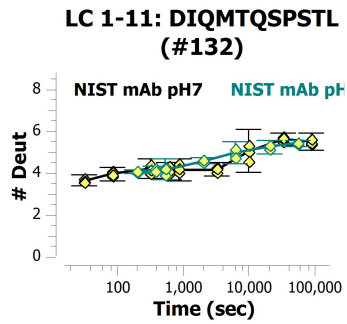
LC 1-11: DIQMTQSPSTL (#132)
NIST mAb pH7
NIST mAb pH
Deut
Time (sec)

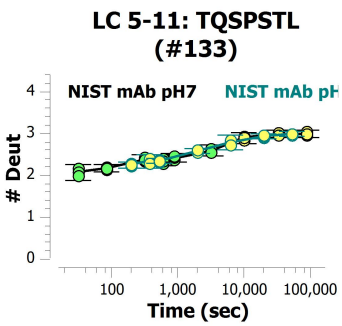
LC 5-11: TQSPSTL (#133)
NIST mAb pH7
NIST mAb pH
Deut
Time (sec)

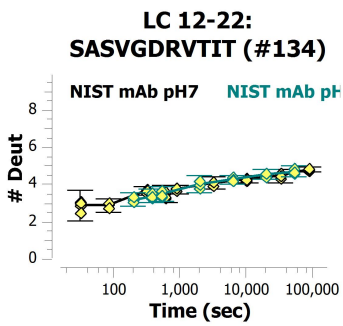
LC 12-22: SASVGDRVTIT (#134)
NIST mAb pH7
NIST mAb pH
Deut
Time (sec)

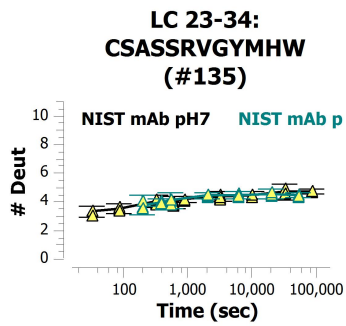
LC 23-34: CSASSRVGYMHW (#135)
NIST mAb pH7
NIST mAb p
Deut
Time (sec)

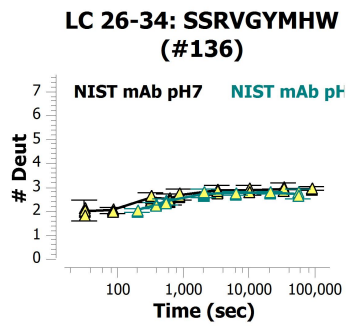
LC 26-34: SSRVGYMHW (#136)
NIST mAb pH7
NIST mAb pH
Deut
Time (sec)

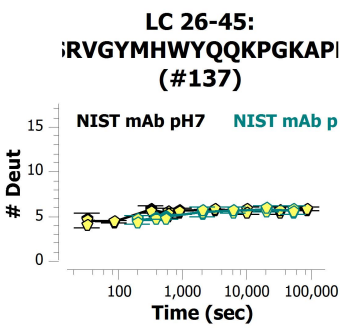
LC 26-45: RVGYMHWYQQKPGKAP (#137)
NIST mAb pH7
NIST mAb p
Deut
Time (sec)

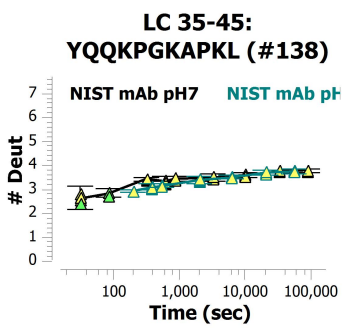
LC 35-45: YQQKPGKAPKL (#138)
NIST mAb pH7
NIST mAb pH
Deut
Time (sec)

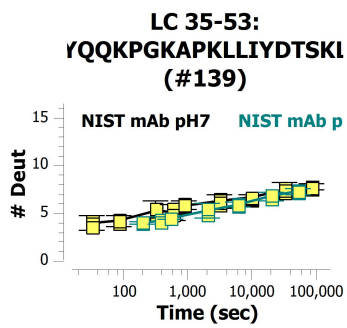
LC 35-53: YQQKPGKAPKLLIYDTSKL (#139)
NIST mAb pH7
NIST mAb p
Deut
Time (sec)

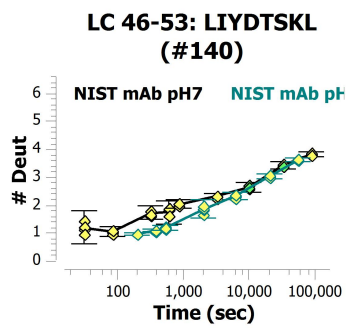
LC 46-53: LIYDTSKL (#140)
NIST mAb pH7
NIST mAb pH
Deut
Time (sec)

LC 46-69: DTSKLASGVPSRFSGSGS((#141)

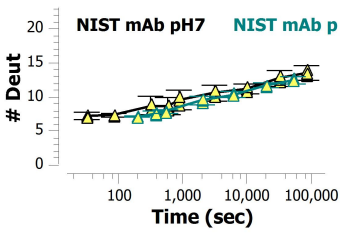

LC 54-69: ASGVPSRFSGSGSGTE (#142)

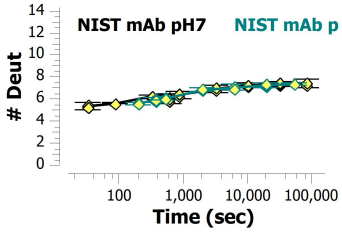

LC 54-70: ASGVPSRFSGSGSGTEF (#143)

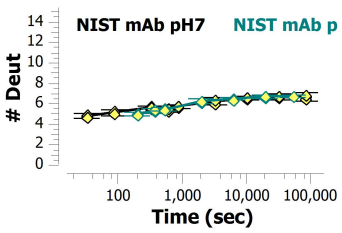

LC 70-73: FTLT (#144)

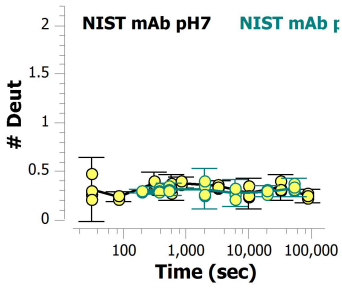

LC 70-82: FTLTISSLQPDDF (#145)

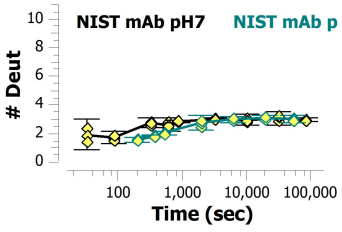

LC 71-82: TLTISSLQPDDF (#146)

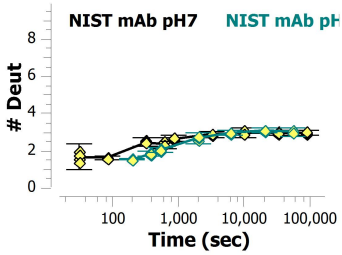

LC 74-81: ISSLQPDD (#147)

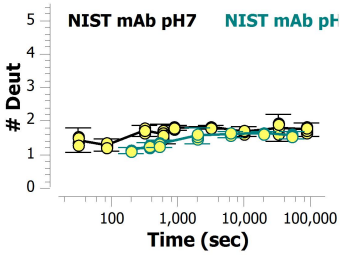

LC 74-82: ISSLQPDDF (#148)

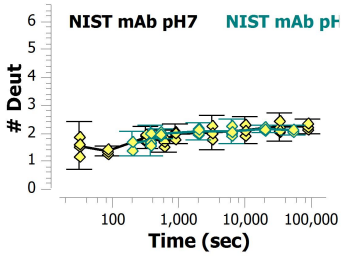

LC 86-114: SGYPFTFGGGTKVEIKRTV (#149)

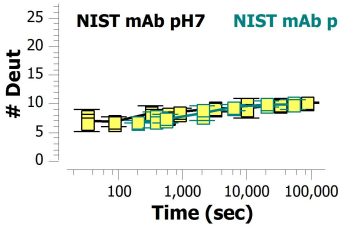

LC 86-115: GYPFTFGGGTKVEIKRTV (#150)

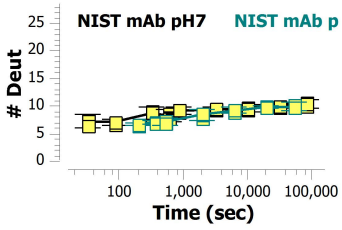

LC 89-114: YPFTFGGGTKVEIKRTVA (#151)

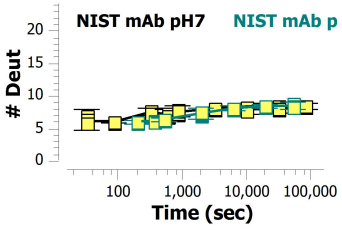

LC 89-115: YPFTFGGGTKVEIKRTVAA (#152)

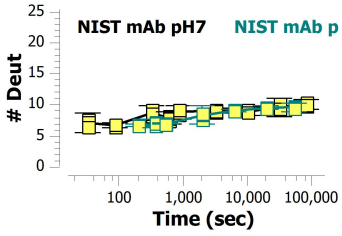

LC 115-121: FIFPPSD (#153)

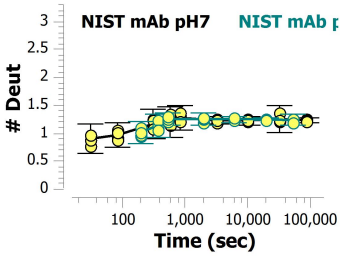

LC 115-124: FIFPPSDEQL (#154)

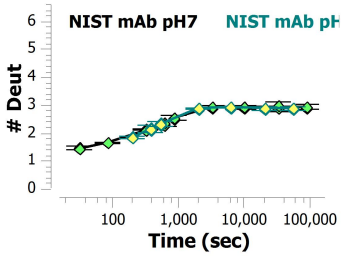

LC 115-131: FIFPPSDEQLKSGTASV (#155)

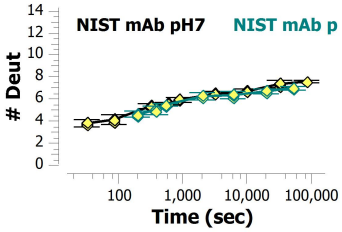

LC 116-121: IFPPSD (#156)

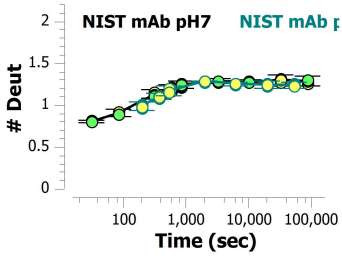

LC 116-122: IFPPSDE (#157)

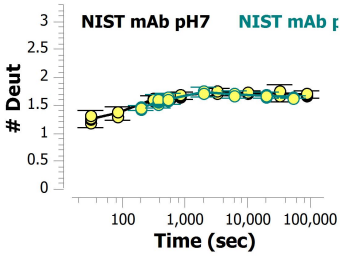

LC 116-124: IFPPSDEQL (#158)

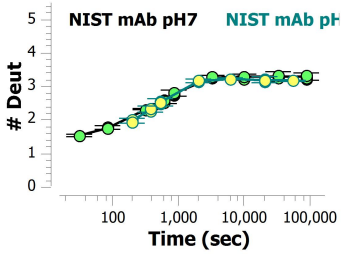

LC 116-131: IFPPSDEQLKSGTASV (#159)

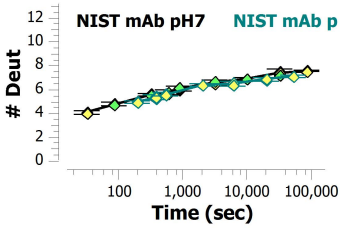

LC 116-132: IFPPSDEQLKSGTASVV (#160)

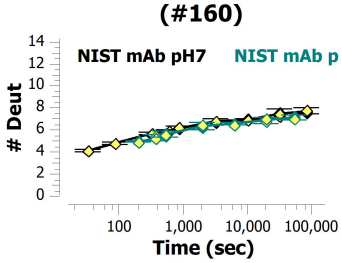

LC 122-131: EQLKSGTASV (#161)

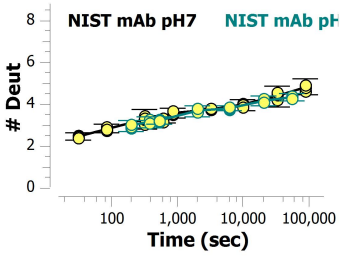

LC 123-131: QLKSGTASV (#162)

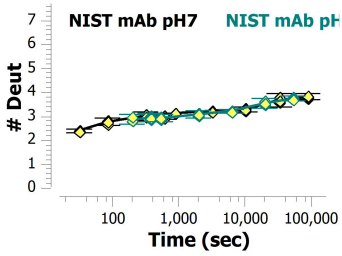

LC 132-134: VCL (#163)

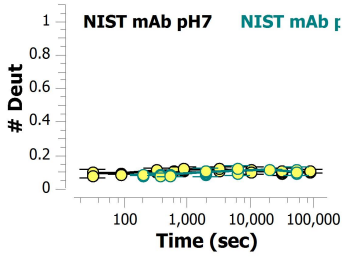

LC 132-135: VCLL (#164)

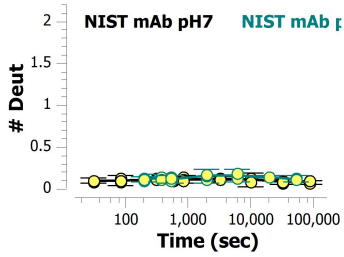

LC 132-153: .LNNFYPREAKVQWKVDN (#165)

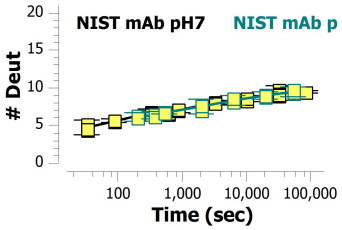

LC 132-160: FYPREAKVQWKVDNALQ (#166)

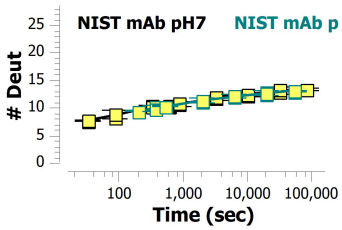

LC 135-142: LNNFYPRE (#167)

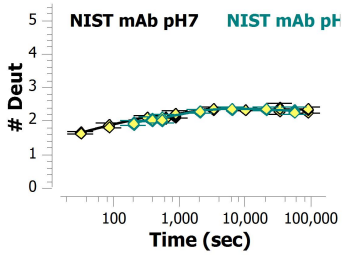

LC 135-147: LNNFYPREAKVQW (#168)

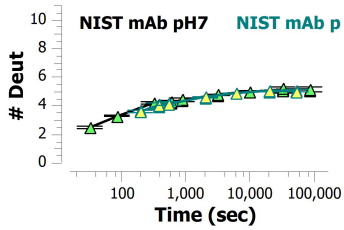

LC 135-153: NNFYPREAKVQWKVDNA (#169)

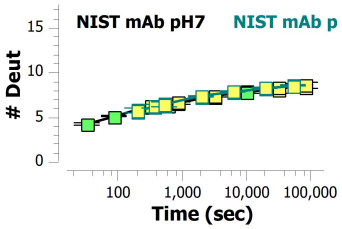

LC 135-160: 'PREAKVQWKVDNALQSC (#170)

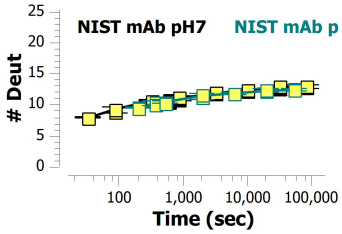

LC 135-171: VQWKVDNALQSGNSQES (#171)

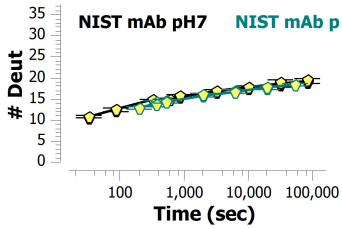

LC 136-160: PREAKVQWKVDNALQSG (#172)

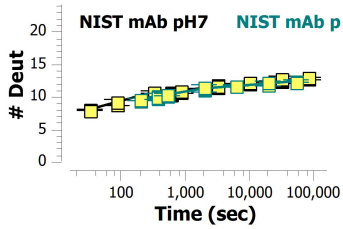

LC 139-160: EAKVQWKVDNALQSGNS (#173)

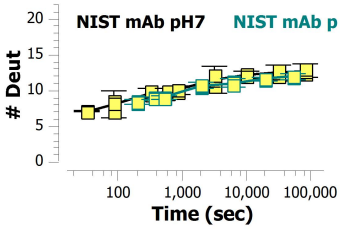

LC 143-160: AKVQWKVDNALQSGNSQ (#174)

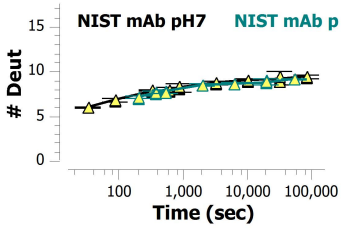

LC 148-160: KVDNALQSGNSQE (#175)

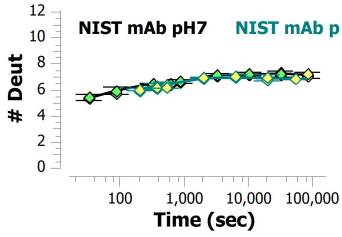

LC 161-171: SVTEQDSKDST (#176)

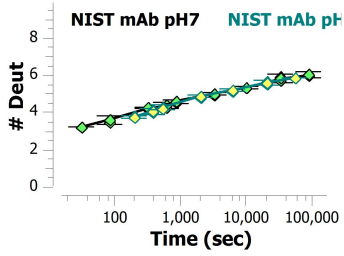

LC 161-174: SVTEQDSKDSTYSL (#177)

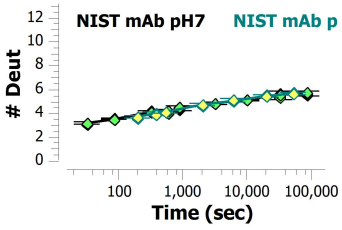

LC 161-177: SVTEQDSKDSTYSLSST (#178)

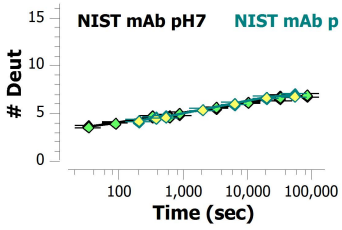

LC 161-178: SVTEQDSKDSTYSLSSTL (#179)

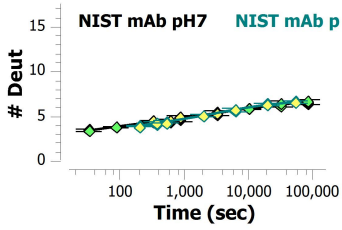

LC 161-194: IDSTYSLSSTLTLSKADYEI (#180)

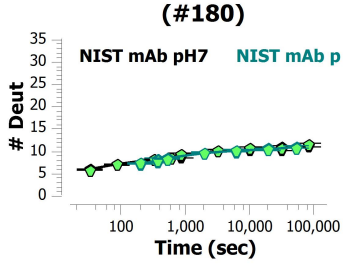

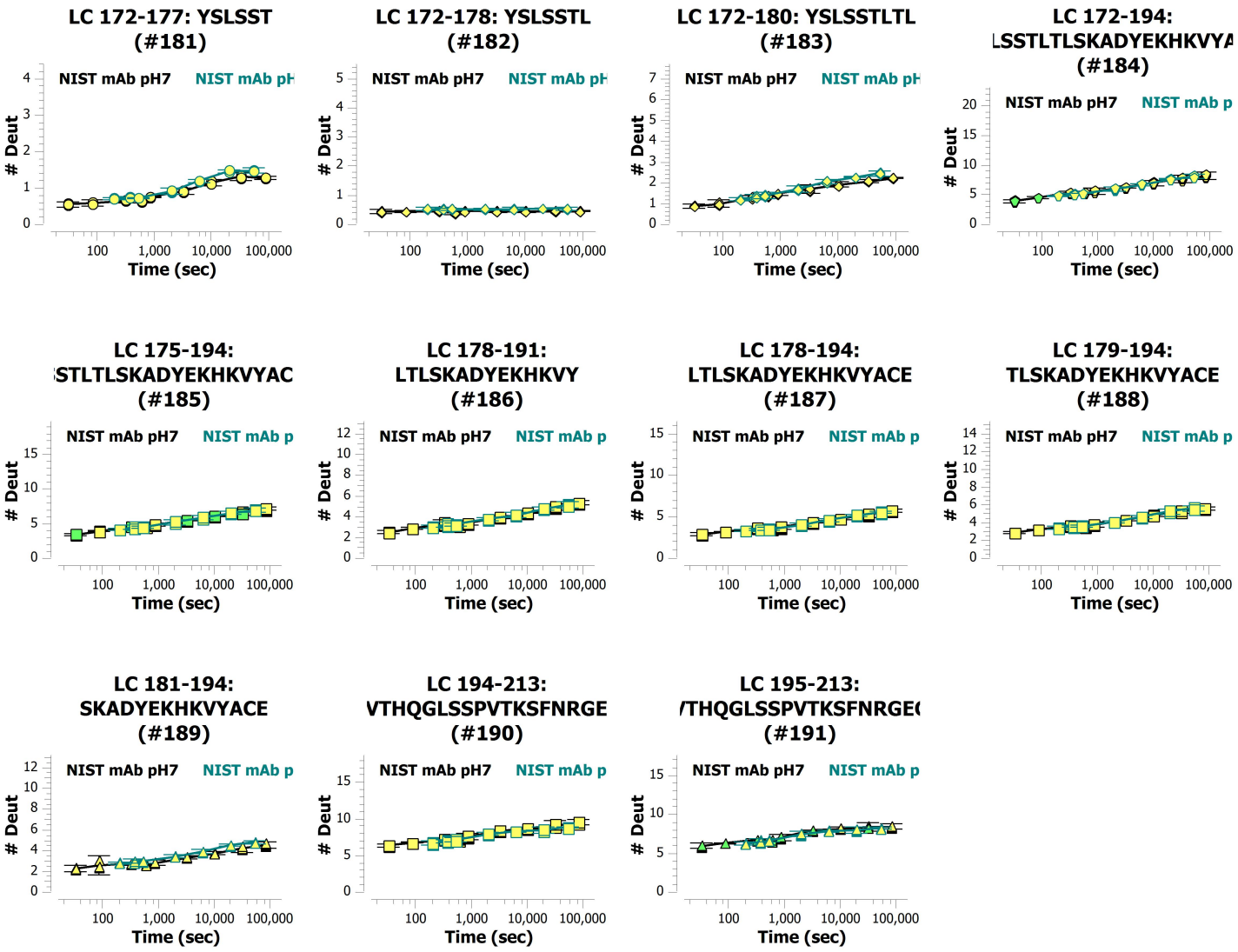

Figure 4.C-8. Deuterium uptake plots for NIST mAb peptic peptides at pH 7 and pH 8 after timepoint labeling correction using equation 4.2.

Data Set	Control (pH 7)	pH 5	pH 6	pH 8
HDX reaction details	5 mM Na_2HPO_4, 5 mM $C_6H_8O_7$, 100 mM sodium chloride pH_{read} = 6.62, 25 °C	5 mM Na_2HPO_4, 5 mM $C_6H_8O_7$, 100 mM sodium chloride pH_{read} = 4.62, 25 °C	5 mM Na_2HPO_4, 5 mM $C_6H_8O_7$, 100 mM sodium chloride pH_{read} = 5.60, 25 °C	5 mM Na_2HPO_4, 5 mM $C_6H_8O_7$, 100 mM sodium chloride pH_{read} = 7.58, 25 °C
HDX time course (s)	32, 86, 320, 600, 860, 3200, 10000, 32000, 86000	320, 860, 3200, 8600, 32000, 60000, 86000	32, 86, 320, 860, 3200, 6000, 8600	32, 60, 86, 320, 1000, 3200, 8600
HDX control samples	pGlu-HWSYGLRPG-NH2, RPPGFSPFR, YGGFLR, YGGFL, DRVYIHPF and YPI used as model peptides			
Deuterium recovery (mean / IQR)	63%* / 7.7			
# of Peptides	191	191	191	191
Sequence coverage	LC 98%, HC 95%			
Average peptide length /Redundancy	15.6/4.4			
Replicates (biological or technical)	4 (technical)			
Repeatability (pooled standard deviation)	Control	0.1082 Da	0.1137 Da	See main text for details
Significant differences in HDX (delta HDX > XD)**	Control	0.4059	0.4275	

* average deuterium recovery calculated using pGlu-HWSYGLRPG-NH2, RPPGFSPFR, YGGFLR, YGGFL, DRVYIHPF and YPI as model peptides, n=5

**see material and methods for description of significant differences threshold

4.6. REFERENCES

1. Dimitrov DS 2012. Therapeutic proteins. Methods in molecular biology (Clifton, NJ) 899:1-26.
2. Lagasse HA, Alexaki A, Simhadri VL, Katagiri NH, Jankowski W, Sauna ZE, Kimchi-Sarfaty C 2017. Recent advances in (therapeutic protein) drug development. F1000Research 6:113.
3. Patil S, Narvekar A, Puranik A, Jain R, Dandekar P. 2019. Formulation of Therapeutic Proteins: Strategies for Developing Oral Protein Formulations. Innovative Dosage Forms, ed. p 391-432.
4. Kaplon H, Reichert JM 2019. Antibodies to watch in 2019. MAbs 11(2):219-238.
5. Lu R-M, Hwang Y-C, Liu IJ, Lee C-C, Tsai H-Z, Li H-J, Wu H-C 2020. Development of therapeutic antibodies for the treatment of diseases. Journal of Biomedical Science 27(1):1.
6. Strickley RG, Lambert WJ 2021. A Review of Formulations of Commercially Available Antibodies. Journal of Pharmaceutical Sciences.
7. Frokjaer S, Otzen DE 2005. Protein drug stability: a formulation challenge. Nat Rev Drug Discov 4(4):298-306.
8. Wang W, Roberts CJ. 2010. Aggregation of Therapeutic Proteins. ed.: Wiley.
9. Chennamsetty N, Voynov V, Kayser V, Helk B, Trout BL 2009. Design of therapeutic proteins with enhanced stability. Proc Natl Acad Sci U S A 106(29):11937-11942.
10. Shahrokh Z. 1997. Developing Pharmaceutical Protein Formulations: Assumptions and Analytical Tools. Therapeutic Protein and Peptide Formulation and Delivery, ed.: American Chemical Society. p 1-28.
11. Klaus T, Deshmukh S 2021. pH-responsive antibodies for therapeutic applications. Journal of Biomedical Science 28(1):11.
12. Ryman JT, Meibohm B 2017. Pharmacokinetics of Monoclonal Antibodies. CPT Pharmacometrics Syst Pharmacol 6(9):576-588.
13. Majumdar R, Middaugh CR, Weis DD, Volkin DB 2015. Hydrogen-deuterium exchange mass spectrometry as an emerging analytical tool for stabilization and formulation development of therapeutic monoclonal antibodies. Journal of pharmaceutical sciences 104(2):327-345.
14. Manikwar P, Majumdar R, Hickey JM, Thakkar SV, Samra HS, Sathish HA, Bishop SM, Middaugh CR, Weis DD, Volkin DB 2013. Correlating excipient effects on conformational and storage stability of an IgG1 monoclonal antibody with local dynamics as measured by hydrogen/deuterium-exchange mass spectrometry. Journal of pharmaceutical sciences 102(7):2136-2151.
15. Roy S, Henderson I, Nayar R, Randolph TW, Carpenter JF 2008. Effect of pH on stability of recombinant botulinum serotype A vaccine in aqueous solution and during storage of freeze-dried formulations. Journal of pharmaceutical sciences 97(12):5132-5146.

16. Le Basle Y, Chennell P, Tokhadze N, Astier A, Sautou V 2020. Physicochemical Stability of Monoclonal Antibodies: A Review. Journal of Pharmaceutical Sciences 109(1):169-190.
17. Sjuts H, Schreuder H, Engel CK, Bussemer T, Gokarn Y 2020. Matching pH values for antibody stabilization and crystallization suggest rationale for accelerated development of biotherapeutic drugs. Drug Dev Res 81(3):329-337.
18. Murphree TA, Vorauer C, Brzoska M, Guttman M 2020. Imidazolium Compounds as Internal Exchange Reporters for Hydrogen/Deuterium Exchange by Mass Spectrometry. Analytical Chemistry 92(14):9830-9837.
19. Majumdar R, Manikwar P, Hickey JM, Arora J, Middaugh CR, Volkin DB, Weis DD 2012. Minimizing Carry-Over in an Online Pepsin Digestion System used for the H/D Exchange Mass Spectrometric Analysis of an IgG1 Monoclonal Antibody. Journal of The American Society for Mass Spectrometry 23(12):2140-2148.
20. Glasoe PK, Long FA 1960. Use of Glass Electrodes to Measure Acidities in Deuterium Oxide1,2. The Journal of Physical Chemistry 64(1):188-190.
21. A. Busby S, J. Chalmers M, Griffin P. 2007. Improving digestion efficiency under H/D exchange conditions with activated pepsinogen coupled columns. ed. p 130-139.
22. Kavan D, Man P 2011. MSTools—Web based application for visualization and presentation of HXMS data. International Journal of Mass Spectrometry 302(1):53-58.
23. Schinkel JE, Downer NW, Rupley JA 1985. Hydrogen exchange of lysozyme powders. Hydration dependence of internal motions. Biochemistry 24(2):352-366.
24. Coales SJ, E SY, Lee JE, Ma A, Morrow JA, Hamuro Y 2010. Expansion of time window for mass spectrometric measurement of amide hydrogen/deuterium exchange reactions. Rapid Communications in Mass Spectrometry 24(24):3585-3592.
25. Hageman TS, Weis DD 2019. Reliable Identification of Significant Differences in Differential Hydrogen Exchange-Mass Spectrometry Measurements Using a Hybrid Significance Testing Approach. Analytical Chemistry 91(13):8008-8016.
26. Angalakurthi SK, Vance DJ, Rong Y, Nguyen CMT, Rudolph MJ, Volkin D, Middaugh CR, Weis DD, Mantis NJ 2018. A Collection of Single-Domain Antibodies that Crowd Ricin Toxin's Active Site. Antibodies (Basel) 7(4):45.
27. Toth RTt, Angalakurthi SK, Van Slyke G, Vance DJ, Hickey JM, Joshi SB, Middaugh CR, Volkin DB, Weis DD, Mantis NJ 2017. High-Definition Mapping of Four Spatially Distinct Neutralizing Epitope Clusters on RiVax, a Candidate Ricin Toxin Subunit Vaccine. Clin Vaccine Immunol 24(12):e00237-00217.

28. 2021. DescTools: Tools for Descriptive Statistics. R package version 0.99.41. Andri et mult al S https://cran.r-project.org/package=DescTools.
29. Gallagher DT, Karageorgos I, Hudgens JW, Galvin CV 2018. Data on crystal organization in the structure of the Fab fragment from the NIST reference antibody, RM 8671. Data in Brief 16:29-36.
30. Gallagher DT, Galvin CV, Karageorgos I 2018. Structure of the Fc fragment of the NIST reference antibody RM8671. Acta Crystallographica Section F 74(9):524-529.
31. Toth RT, Mills BJ, Joshi SB, Esfandiary R, Bishop SM, Middaugh CR, Volkin DB, Weis DD 2017. Empirical Correction for Differences in Chemical Exchange Rates in Hydrogen Exchange-Mass Spectrometry Measurements. Analytical Chemistry 89(17):8931-8941.
32. Christoffersen M, Bolvig S, Tüchsen E 1996. Salt Effects on the Amide Hydrogen Exchange of Bovine Pancreatic Trypsin Inhibitor. Biochemistry 35(7):2309-2315.
33. Hvidt A, Wallevik K 1972. Conformational changes in human serum albumin as revealed by hydrogen-deuterium exchange studies. J Biol Chem 247(5):1530-1535.
34. Mazur SJ, Weber DP 2017. The Area Between Exchange Curves as a Measure of Conformational Differences in Hydrogen-Deuterium Exchange Mass Spectrometry Studies. J Am Soc Mass Spectrom 28(5):978-981.
35. Hamuro Y, Derebe MG, Venkataramani S, Nemeth JF 2021. The Effects of Intramolecular and Intermolecular Electrostatic Repulsions on the Stability and Aggregation of NISTmAb Revealed by HDX-MS, DSC and NanoDSF. Protein Sci.
36. Bai Y, Milne JS, Mayne L, Englander SW 1993. Primary structure effects on peptide group hydrogen exchange. Proteins 17(1):75-86.
37. Molday R, Englander S, Kallen R 1972. Primary structure effects on peptide group hydrogen exchange. Biochemistry 11(2):150-158.
38. McIlvaine TC 1921. A BUFFER SOLUTION FOR COLORIMETRIC COMPARISON. Journal of Biological Chemistry 49(1):183-186.
39. Jensen PF, Rand KD. 2016. Hydrogen Exchange. Hydrogen Exchange Mass Spectrometry of Proteins, ed. p 1-17.
40. Majumdar R, Esfandiary R, Bishop SM, Samra HS, Middaugh CR, Volkin DB, Weis DD 2015. Correlations between changes in conformational dynamics and physical stability in a mutant IgG1 mAb engineered for extended serum half-life. MAbs 7(1):84-95.
41. Majumdar R, Manikwar P, Hickey JM, Samra HS, Sathish HA, Bishop SM, Middaugh CR, Volkin DB, Weis DD 2013. Effects of salts from the Hofmeister series on the conformational stability, aggregation propensity, and local flexibility of an IgG1 monoclonal antibody. Biochemistry 52(19):3376-3389.

42. Houde D, Peng Y, Berkowitz SA, Engen JR 2010. Post-translational modifications differentially affect IgG1 conformation and receptor binding. Molecular & Cellular Proteomics 9(8):1716-1728.
43. Zhang A, Hu P, MacGregor P, Xue Y, Fan H, Suchecki P, Olszewski L, Liu A 2014. Understanding the conformational impact of chemical modifications on monoclonal antibodies with diverse sequence variation using hydrogen/deuterium exchange mass spectrometry and structural modeling. Analytical chemistry 86(7):3468-3475.
44. Houde D, Arndt J, Domeier W, Berkowitz S, Engen JR 2009. Characterization of IgG1 conformation and conformational dynamics by hydrogen/deuterium exchange mass spectrometry. Analytical chemistry 81(7):2644-2651.
45. Groves K, Cryar A, Cowen S, Ashcroft AE, Quaglia M 2020. Mass Spectrometry Characterization of Higher Order Structural Changes Associated with the Fc-glycan Structure of the NISTmAb Reference Material, RM 8761. J Am Soc Mass Spectrom 31(3):553-564.
46. Noda M, Ishii K, Yamauchi M, Oyama H, Tadokoro T, Maenaka K, Torisu T, Uchiyama S 2019. Identification of IgG1 Aggregation Initiation Region by Hydrogen Deuterium Mass Spectrometry. Journal of pharmaceutical sciences 108(7):2323-2333.
47. Chennamsetty N, Voynov V, Kayser V, Helk B, Trout BL 2009. Design of therapeutic proteins with enhanced stability. Proceedings of the National Academy of Sciences 106(29):11937-11942.
48. Ishikawa T, Ito T, Endo R, Nakagawa K, Sawa E, Wakamatsu K 2010. Influence of pH on heat-induced aggregation and degradation of therapeutic monoclonal antibodies. Biol Pharm Bull 33(8):1413-1417.
49. Ito T, Tsumoto K 2013. Effects of subclass change on the structural stability of chimeric, humanized, and human antibodies under thermal stress. Protein Science 22(11):1542-1551.
50. Xu AY, Castellanos MM, Mattison K, Krueger S, Curtis JE 2019. Studying Excipient Modulated Physical Stability and Viscosity of Monoclonal Antibody Formulations Using Small-Angle Scattering. Molecular Pharmaceutics 16(10):4319-4338.
51. Turner A, Schiel JE 2018. Qualification of NISTmAb charge heterogeneity control assays. Anal Bioanal Chem 410(8):2079-2093.
52. Chi EY, Krishnan S, Randolph TW, Carpenter JF 2003. Physical stability of proteins in aqueous solution: mechanism and driving forces in nonnative protein aggregation. Pharmaceutical research 20(9):1325-1336.
53. James S, McManus JJ 2012. Thermal and Solution Stability of Lysozyme in the Presence of Sucrose, Glucose, and Trehalose. The Journal of Physical Chemistry B 116(34):10182-10188.

54. Sudrik C, Cloutier T, Pham P, Samra HS, Trout BL 2017. Preferential interactions of trehalose, L-arginine.HCl and sodium chloride with therapeutically relevant IgG1 monoclonal antibodies. MAbs 9(7):1155-1168.
55. Wen L, Zheng X, Wang X, Lan H, Yin Z 2017. Bilateral Effects of Excipients on Protein Stability: Preferential Interaction Type of Excipient and Surface Aromatic Hydrophobicity of Protein. Pharmaceutical research 34(7):1378-1390.
56. Arora J, Joshi SB, Middaugh CR, Weis DD, Volkin DB 2017. Correlating the Effects of Antimicrobial Preservatives on Conformational Stability, Aggregation Propensity, and Backbone Flexibility of an IgG1 mAb. Journal of Pharmaceutical Sciences 106(6):1508-1518.
57. Usami A, Ohtsu A, Takahama S, Fujii T 1996. The effect of pH, hydrogen peroxide and temperature on the stability of human monoclonal antibody. Journal of pharmaceutical and biomedical analysis 14(8-10):1133-1140.
58. Martin WL, West AP, Jr., Gan L, Bjorkman PJ 2001. Crystal structure at 2.8 A of an FcRn/heterodimeric Fc complex: mechanism of pH-dependent binding. Mol Cell 7(4):867-877.
59. Raghavan M, Bonagura VR, Morrison SL, Bjorkman PJ 1995. Analysis of the pH Dependence of the Neonatal Fc Receptor/Immunoglobulin G Interaction Using Antibody and Receptor Variants. Biochemistry 34(45):14649-14657.
60. Vaughn DE, Bjorkman PJ 1998. Structural basis of pH-dependent antibody binding by the neonatal Fc receptor. Structure 6(1):63-73.
61. Stapleton NM, Einarsdóttir HK, Stemerding AM, Vidarsson G 2015. The multiple facets of FcRn in immunity. Immunol Rev 268(1):253-268.
62. Walters BT, Jensen PF, Larraillet V, Lin K, Patapoff T, Schlothauer T, Rand KD, Zhang J 2016. Conformational Destabilization of Immunoglobulin G Increases the Low pH Binding Affinity with the Neonatal Fc Receptor. J Biol Chem 291(4):1817-1825.
63. Presta LG 2008. Molecular engineering and design of therapeutic antibodies. Current Opinion in Immunology 20(4):460-470.
64. Saunders KO 2019. Conceptual Approaches to Modulating Antibody Effector Functions and Circulation Half-Life. Frontiers in Immunology 10(1296).
65. Krol M, Roterman I, Drozd A, Konieczny L, Piekarska B, Rybarska J, Spolnik P, Stopa B 2006. The increased flexibility of CDR loops generated in antibodies by Congo red complexation favors antigen binding. J Biomol Struct Dyn 23(4):407-416.
66. Jeliazkov JR, Sljoka A, Kuroda D, Tsuchimura N, Katoh N, Tsumoto K, Gray JJ 2018. Repertoire Analysis of Antibody CDR-H3 Loops Suggests Affinity Maturation Does Not Typically Result in Rigidification. Front Immunol 9:413.

67. Devanaboyina SC, Lynch SM, Ober RJ, Ram S, Kim D, Puig-Canto A, Breen S, Kasturirangan S, Fowler S, Peng L, Zhong H, Jermutus L, Wu H, Webster C, Ward ES, Gao C 2013. The effect of pH dependence of antibody-antigen interactions on subcellular trafficking dynamics. MAbs 5(6):851-859.
68. Carol E, Foote J 2005. Antibody buffering of a ligand in vivo. Proceedings of the National Academy of Sciences 102(1):40-44.
69. Nguyen D, Mayne L, Phillips MC, Walter Englander S 2018. Reference Parameters for Protein Hydrogen Exchange Rates. Journal of the American Society for Mass Spectrometry 29(9):1936-1939.
70. Teplyakov A, Zhao Y, Malia TJ, Obmolova G, Gilliland GL 2013. IgG2 Fc structure and the dynamic features of the IgG CH2-CH3 interface. Mol Immunol 56(1-2):131-139.
71. Hanson QM, Barb AW 2015. A perspective on the structure and receptor binding properties of immunoglobulin G Fc. Biochemistry 54(19):2931-2942.

5. CHAPTER FIVE: SUMMARY AND FUTURE DIRECTIONS

5.1. SUMMARY

In Chapter 2 of this dissertation, we used HX-MS experiments to identify conformational changes in a single chain variable fragment used as a protein switch. A W-to-G point mutation in the core of the scFv showed a decrease in the activity of the protein. Our results support the model of chemical rescue of the structure, where the structure and activity of the protein is restored by the addition of a small molecule (indole). Statistical analysis of HDX data showed that the WT and W-to-G scFv have very different structures. However, rescued protein (after the addition of indole) have a very similar HDX behavior compared to the WT scFv. Only minor differences were seen, right at the binding site of the fluorescein. Those differences could explain why the rescued protein does not have the same binding affinity as the wild-type scFv.

In Chapter 3 we used HX-MS to identify possible allosteric effects in the NIST reference mAb during interaction with a commercially available protein A ligand (ProA), both free in solution and attached onto a resin. Statistical analysis of the HDX data, showed allosteric effects in the NIST mAb when in-solution protein A was used at a 2:1 ProA:mAb ratio, specifically allosteric effects in the Fab region were identified. These effects were no longer seen when the molar ratio was decrease to a 1:1 ratio. Although the use of in solution ProA has advantages for the HDX experiments, most pharmaceutical processes use ProA attached onto a resin. When ProA attached to a resin was employed for the HDX experiments, only peptides right at the binding site showed strong protection against hydrogen exchange. These experiments, rule out reversible allosteric effects in the NIST mAb during interaction with a commercially available protein A attached to a resin.

Following results of Chapter 3, in Chapter 4 we used HX-MS to identify conformational changes in the NIST mAb after changing the formulation pH. We used four different pH values ranging from 5 to 8 that encompass all physiological and formulation pH values. HDX data showed that decreasing the pH of the solution induce a strong increase in flexibility in the C_H2 domain and parts of the C_H2-C_H3 interface in the NIST mAb. We hypothesize that these increase in flexibility is provoked by new

electrostatic interactions by protonated histidine residues that disrupt the stability of the region. An increase in pH showed the contrary, a strong decrease in flexibility close to the hinge region and in the C_H3 domain. Importantly, both an increase or decrease in the formulation pH cause conformational changes critical regions of F_{ab} domain of the antibody. Specifically, in the CDRH3 when the pH is decreased and CDRL2 when the pH is increased.

5.2. FUTURE DIRECTIONS

Chapter 2 showed evidence that the chemical rescue of structure by the addition of a small molecule works and could be further developed to be applied to protein therapeutics. The current model uses high concentrations of indole to rescue the structure. It is known that those high concentration of indole are toxic for the human body. Hence, it is necessary to develop protein switches that do not involve the use of indole. Initial approaches using two mutations and less toxic rescue agents are already under development. When available, HX-MS experiments can be used again to check and validate if the rescued protein switch has a similar structure to the one wild-type variant.

Affinity chromatography with protein A ligands is the most common technique in the pharmaceutical industry for purification of monoclonal antibodies. It is imperative to know if the use of such ligands alter or change and the extent of the change if any. Chapter 3 of this dissertation ruled out reversible allosteric effects in the NIST mAb, however irreversible effects were not discarded since the NIST mAb was previously exposed to protein A in the initial purification process. To rule out irreversible allosteric effects, experiments with a naïve mAb that has not been exposed to protein A need to be performed. Additionally, although our results shown no allosteric effects in the NIST mAb, and we would expect that heavily conserved domains in other antibodies behave similar, this must be confirmed. Further experiments using different mAbs would be needed to get a general picture of allosteric effects due to interaction with protein A in monoclonal antibodies.

Conformational changes in protein therapeutics are a big concern. Pharmaceutical industries spend a long-time developing suitable formulations for protein therapeutics. Formulations are designed to guarantee efficacy, stability, and safety of protein therapeutics until administration. Chapter 4 experiments showed that a change in pH in the formulation buffer (either increase or decrease), provokes conformational changes in the Fc and Fab fragments of the antibody. The effect of these changes in flexibility on effector functions and antigen binding still need to be evaluated. Furthermore, like described above, we used a model system for our experiment (NIST mAb). We would expect that heavily conserved domains in other antibodies behave similarly, however this must be confirmed. Chapter 4 identified conformational changes in CDR regions of the NIST mAb. This regions are not conserved on other antibodies, and it is difficult to generalize those conformational changes to other antibodies. A more systematic study including many antibodies need to be done to be able to take a broad view on the effect of pH in antibody structure. It is important to remember that antibodies are exposed to a wide range of pH values during administration, metabolism and during the normal antibody recycling process in the human body. As seen here, a change in pH provokes conformational changes, however, reversibility of the changes is still not known. To address that, experiments with mAbs that have been exposed to pH changes and returned to the initial pH should be performed. Finally, NIST mAb peptides and IER compounds showed an unusual behavior at pH = 8. Experimental data did not follow the traditional model for labeling times correction. Although an empirical correction was performed, more experiments are needed to identify why at high pH values the data behaves differently.